GEOCHEMISTRY AND GEOCHRONOLOGY OF THE IGNEOUS SUITE ASSOCIATED WITH THE KELIAN EPITHERMAL GOLD DEPOSIT, INDONESIA

Bambang Tjahjono Setiabudi

A thesis submitted for the degree of Doctor of Philosophy
of the Australian National University

July 2001

The work presented in this thesis was carried out while I was a full-time student at the Research School of Earth Sciences, The Australian National University, between August 1997 and July 2001. Except where noted in the text, the research described here is my own. This research has also been refined and immensely improved by the input of many people who are mentioned in the acknowledgements. No part of this thesis has been submitted to any other university or similar institution.

Bambang Tjahjono Setiabudi

ACKNOWLEDGEMENTS

This dissertation could not have been completed without the support and help of many people from various institutions. I would like to thank and acknowledge them for their assistance and efforts during the research project. This PhD study was financially supported by the Australian Sponsored Training Scholarships organised by the Australian Agency for International Development (AusAID). The logistical and financial supports during the fieldworks in the Kelian gold mine and regional prospects were provided by PT. Kelian Equatorial Mining (KEM), Rio Tinto Indonesia (RTI) and the Research School of Earth Sciences (RSES), ANU.

First of all, I would like to thank Ian H. Campbell, my chief supervisor, for the guidance, instruction and supervision throughout my course of study. Ian has given the largest influence in this work. His encouragement, insights and enthusiasm are greatly appreciated.

I wish to thank J. Michael Palin (my adviser) and John Mavrogenes (my supervisor) for their advices and supervision during the research and preparation of this thesis. Michael Palin has helped in the field of U-Th-Pb zircon geochronology, particularly in the development of data reduction procedures for U-Th-Pb zircon dating. John Mavrogenes has read manuscripts of the following chapters, criticized and given many suggestions in which improvements might be made. John Mavrogenes has also encouraged and supervised me during the preliminary analysis of melt inclusions.

I am particularly grateful to Charlotte Allen for her invaluable help in many things and for her expertise in analytical geochemistry. Charlotte Allen has assisted in numerous analytical sessions, especially whole-rock geochemical analysis using both excimer laser-mode and solution-mode inductively coupled plasma mass spectrometer. I also thank Charlotte for helping me in the PGE sample preparation in the Clean Lab, and also for running analyses and dating zircon samples of the Kelian tuff and Han and Plata andesites.

I would like to thank Theo van Leeuwen, John Baldwin and Steve Hunt of Rio Tinto for their supports and encouragement in the early stages of this work, particularly during the establishment of the field projects. Theo has established this project and given permission to join the RTI exploration team at Ritan, Muyup, Han and Batu Utul. John

Baldwin was the Chief Geologist and Exploration Manager during my 5-year assignment at the Kelian Gold Mine. John introduced me to the geology of Kelian, Magerang-Imang and Nakan.

I am also indebted to the exploration and mine geologists of PT. Kelian Equatorial Mining and Rio Tinto Exploration for their guidance, discussions and logistical supports. These people are Greg Hartshorn for supervising the entire fieldwork in Kalimantan; Tulus Butar-Butar for his assistance during the fieldwork in the Kelian, Magerang-Imang, Muyup, Ritan, Han and Batu Utul areas; Brendan Howard and Roger Norris for their help and supervision during the fieldwork at Ritan; KEM's geologists: Yudi Nurcahyana, Ewa Rappe and Seno Aji for their help during the fieldwork at the Kelian Gold Mine. Special thanks are due to my field assistant, Santukius and my exploration team at Kelian for their boundless help and friendship.

All the laboratory experiments and analyses have been made possible with the assistance of several experts from the Research School of Earth Sciences, ANU. I wish to thank Bill Hibberson and Dean Scott for helping in the high-temperature furnace laboratory works; Barbara Fairchild for introducing me to the glass fusion technique, sample preparation and ICP-MS data reduction for trace elements, PGE and gold analysis; Les Kinsley and Mike Shelley for their help and advice in the Laser-ICP-MS lab works; Shane Paxton, John Mya and Shally for their help in whole-rock sample preparation and zircon mineral separation; Nick Ware for his help in the electron microprobe analysis; Shally Stowe for the use of Scanning Electron Microscope at RSBS; Graham Mortimer for providing spikes solution and assisting in chemical works in the clean lab. I also acknowledge Ulrich Sennf for the X-Ray Fluorescent analysis and John Vickers for preparing thin sections and polished sections at the Department of Geology, ANU. Many thanks to Ross Wylde-Browne and Duncan Bolt for giving technical support, backing up data and fixing computer problems.

The arguments and interpretation presented in this thesis have much benefited from many productive discussions over the last four years with a number of geologists and geochemists. Steve Eggins gave many suggestions in the ELA-ICPMS analysis and interpretation of trace element geochemistry, provided trace element data for boninites and read the drafts of chapters; Candace Martin helped in data reduction and discussion on the Platinum Group Element and gold analysis; Robert Loucks has provided copies of relevant papers and suggestions on the trace element geochemistry; Thanks to David Green and Stephen Cox for the advice and discussion during the course of this study. Special thanks

are also due to Bruce Rohrlach for introducing me to Canvas software, Julian Ballard for helping with Kaleidagraph, zirconology and geochemical modeling. There are also numerous PhD students and friends at RSES who have helped me in various ways and shared good times; they include Christ Heath, Allistar Hacks, Linda Henley, Heather Scott-Gagan, Lois Taylor and Mike Gagan.

I am indebted to the Directorate of Mineral Resources; in particular Kingking Margawidjaja, Abdurrochman and Koswara Yudhawinata for their supports.

During this study, I have had great times with many friends from the Indonesian Embassy, the Indonesian Postgraduate Student Association and the Indonesian Moslem Student Association; in particular Aria Jalil, Akhdiyat Kartamiharja, Wahdiyudhi, Marpudin Azis, Abrar Yusuf, Teddy Mantoro, A. Kusworo and Edwin Arifin. I acknowledge their helps and supports.

Finally, the most important factor for finishing this job has been undoubtedly the support and encouragement of the "Setiabudi family". My deepest thanks go to Ninuk 'mademoiselle' Sundarsih, Aussie 'dreamcast' Bhaskoro and Dio 'pokemon' Pramudya Bumi for their patience and confidence.

This thesis is dedicated to all of the geologists who worked very hard at Kelian during the exploration period, especially Basuki, Yusuf Laleno and Sihotang of the Directorate of Mineral Resources.

ABSTRACT

The Kelian gold deposit, located 250 km west of the provincial capital of Samarinda, East Kalimantan, is Indonesia's principal gold producer. The deposit is an intrusive-related low sulphidation system, situated within the Central Kalimantan Continental Arc, which consists of andesitic to rhyolitic volcanics and intrusives of Miocene age. Hydrothermal activity produced extensive brecciation, porphyry- to epithermal-style alteration and gold and base metals mineralisation. The nature of genetic relations is the main aspect of this study and is approached through the geochemical evolution of the calc-alkaline suites in relation to the metallic mineralisation.

Geochemical evolution in the Miocence calc-alkaline suites from the Kalimantan volcanic arc exhibit two distinctive trends of magmatic differentiation The first trend is defined by a series of "productive" igneous suites such as Kelian, Muyup and Ritan, and is a "typical" calc-alkaline series characterised by low Mg, moderate K, relatively high Ti and Al and depletion in Cr and Sc. The second trend is defined by the chemical variations of the Magerang-Imang and Nakan suites which have remarkably high concentrations of MgO. Major and trace element geochemistry of the high Mg andesites from Magerang-Imang and Nakan is comparable with that of low-Ca type-2 boninites. The Kelian Igneous Complex is characterised by positive Zr and Hf anomalies in the trace element patterns which is uncommon for calc-alkaline subduction zone magmas. The chemical diversity in the Magerang-Imang and Nakan suite might have been generated by a combined wallrock assimilation and fractional crystallisation process involving a parental basaltic magma and a Zr-rich cumulate. It is suggested that the Magerang-Imang and Nakan high Mg andesites were fed by magma chambers that formed deep in the crust, and were emplaced into pre-existing intrusions of felsic composition that formed as part of the Kelian Igneous Complex cycle. The shallow level stocks at Magerang-Imang and Nakan were generated by intrusions that melted the walls and roofs of related, but pre-existing intrusions, and extracted abundant xenocrystic zircons during the assimilation process.

This study represents the first Platinum Group Element data for a fractionated suite of calc-alkaline andesite. The technique developed in this study represents a breakthrough in our ability to monitor important ore elements in felsic igneous system. The PGE distribution patterns in the Magerang-Imang hornblende andesite are sub-parallel to each other over a range of concentrations that vary by about a factor of 20.

All the Magerang-Imang samples are depleted in Ru, Ir and Os concentrations relative to Re, Pd, Pt and Rh concentrations and have Pd/Ir values of 15 to 54 and Ru/Ir ~1. The PGE concentrations decrease with increasing SiO_2, showing that they are depleted by fractional crystallisation. Gold is depleted by an order of magnitude and relative to Re and Pd. The low concentration of gold in the igneous rocks associated with the Kelian gold deposit is unexpected. Most metal deposits are found in association with rocks that are already enriched in the metal of interest. It is therefore surprising to find a major gold deposit in host rocks that are depleted in Au. It is also interesting that Au and PGE ratios change little during fractionation. This is surprising because it implies either that the partition coefficients for the PGEs into the sulphides are similar, which seems unlikely, or that Au and the PGEs are not being depleted by simple equilibrium fractional crystallisation of sulphide. Alternatively, the gold and PGE fractionation are due to the assimilation of crustal material. This appears to be the most plausible process for the gradual depletion of Au and all of the PGE at Kelian. It is suggested that simple dilution with crustal material that contains no Au or PGE is the most likely process that will decrease the abundance of all of the PGE equally.

Zircon U-Th-Pb isotope dates were determined in situ using excimer laser ablation ICP-MS. The two different bodies of the Magerang hornblende andesite yielded a single age of 19.38 $\pm$ 0.12 Ma and 19.62 $\pm$ 0.21 Ma, while the Nakan andesite gave an age of 20.01$\pm$ 0.15 Ma. The Central Andesite porphyry at Kelian gave 3 populations of U-Pb zircon dates: 21.2 $\pm$ 0.32 Ma, 20.5 $\pm$ 0.12 Ma and 19.7 $\pm$ 0.12 Ma. The youngest date (19.7 Ma) is interpreted as the emplacement age and the two older zircon populations represent the age of inherited zircons coming from the previous thermal event that affected the source region of the andesite. The U-Pb zircon dating for the Runcing Rhyolite porphyry also yielded 3 distinctive date populations: the youngest date of zircon population (19.3 $\pm$ 0.1 Ma) is interpreted as the emplacement age and the other two populations (20.0 $\pm$ 0.2 Ma and 20.8 $\pm$ 0.1 Ma) represent the ages of inherited zircons.

The emplacement age of the Magerang-Imang andesite implies that the high-sulphidation Cu-Au mineralisation at Magerang is younger than the low-sulphidation Au deposit at Kelian. The Kelian and Magerang andesites have a relatively short interval of emplacement ages suggesting that the duration of magmatism and related epithermal mineralisation in the larger Kelian region was between 0.5 – 1 Ma. During this period, the magmatic-hydrothermal system has produced 2 distinctive types of epithermal

mineralisation: firstly, low-sulphidation Au deposit at Kelian and secondly high-sulphidation Cu-Au mineralisation at Magerang-Imang.

Detrital zircons from the Mahakam and Kelian rivers were dated to obtain the overall duration of volcanism in the region. These zircons are dominated by Pliocene, Miocene, Cretaceous, Triassic, Permian and Carboniferous zircons. The youngest detrital zircon from the Kelian river gave an age of 1.7 $\pm$ 0.1 Ma and the oldest one gave an age of 373 Ma. Within the Tertiary zircon population, there are age spectra peaks at Pliocene (from 1.7 Ma to 2.8 Ma) and Miocene (from 15.8 Ma to 21.7 Ma). The Cretaceous zircon population ranges from 67.6 to 126.3 Ma and peaks at 105 Ma. The gold mineralisation at Kelian occurs toward the end of the Miocene volcanism and took place locally within the Kelian region as this Miocene volcanism is not recorded in the zircon component from the larger Mahakam river.

The two large inheritance populations in both the Central Andesite and Runcing Rhyolite lie within the time range of the Kelian igneous complex as defined by the Kelian River detrital zircons. They must be derived from crustal intrusions that formed as part of the Kelian cycle. It is suggested that both the Kelian Andesite and Runcing Rhyolite were fed by 2 magma chambers that formed deep in the crust, each of which were long lived. The magma chambers that fed the Kelian Andesite and Runcing Rhyolite were emplaced into pre-existing intrusions of similar composition that formed as part of the Kelian igneous complex. The abundance of xenocrystic zircons in both units suggests that these earlier intrusions were still hot, or perhaps even partially molten, at the time of magma emplacement. That is the shallow level stocks and diatremes at Kelian were fed by nested, cannibalistic intrusions deep in the crust that melted the walls and roofs of related, but pre-existing intrusions, and inherited abundant xenocrystic zircons in the process. Both the Kelian Andesite and the Runcing Rhyolite have two populations of inherited zircons, which indicate that the pre-existing intrusions formed in two distinct episodes, 0.7 to 0.8 m.y. apart. The difference between the emplacement age and the age of the oldest of the inherited zircon populations shows that this cannibalistic activity took place over 1.5 m.y. The interval of magmatic activity in these chambers corresponds to the period of peak activity in the Kelian igneous complex as defined by the detrital zircons.

TABLE OF CONTENTS

Chapter 1

INTRODUCTION

The occurrences of several major gold deposits in addition to significant Cu-Au mineralisation in the volcanic corridor of the Central Kalimantan Arc have been targeted for scientific research. Previous work has mainly focused on regional tectonics and exploration geology. In contrast, there has been little effort to understand the ore forming systems in the Kalimantan gold belt. In particular, the link between the metallic deposits and volcanism has not been convincingly resolved. The nature of genetic relations is the main aspect of this study and is approached through the geochemical evolution of the intermediate-felsic igneous rocks in relation to the metallic mineralisation.

The genesis of the Kelian gold deposit has never been clearly resolved. The interpretation of the ore forming process is speculative due to the lack of laboratory-based research. There are three possibilities regarding the ore genesis of the Kelian gold deposit. First, the gold mineralisation involved meteoric fluids driven by heat sourced from a high-level intrusion. Gold and other metals were mainly derived from tuff, volcaniclastic sandstone and carbonaceous siltstone. The Kelian andesite porphyry might have provided some metals. Second, the gold mineralisation at Kelian has been controlled by phreatomagmatic processes that have formed the Runcing maar-diatreme complex (Sillitoe, 1993a). The maar-diatreme was possibly generated in relation to the Runcing rhyolite magmatism. The Runcing diatreme contains fragments of fine-grained felsic igneous rocks derived from a high-level porphyry body at depth. This suggests that gold was deposited by hydrothermal fluids derived from a rhyolite porphyry and that there is no genetic link with the andesite porphyry at Kelian. The third possibility is that the gold mineralisation is genetically related to a specific event in the evolution of the andesite porphyry intrusions. Gold has been concentrated by fractionation processes before and during the emplacement of andesite porphyries.

1.1 Objectives of this study

Although the Kelian gold deposit contains features of a porphyry type environment, the chemical process of mineralisation and emplacement of the andesite intrusions are not clear. It is therefore possible to test whether the gold mineralisation was formed by a hydrothermal fluid system driven by the late stage andesite magmatism or by processes related to the phreatomagmatic rhyolite activity as part of a maar-diatreme complex. Igneous suites of the Kelian region and immediate prospects such as Han, Plata, Muyup and Ritan will be studied utilising analytical geochemistry and geochronology to resolve these questions.

The principle objectives of this study are to document the geochemical evolution of the calc alkaline igneous suite associated with the gold mineralisation and show its variation through time. The project was carried out at a regional scale centred on the Kelian Gold Mine and surrounding prospects. The aim is to test the hypothesis that there is a genetic link between the mineralisation and the evolution of the igneous rocks. Selected drill core and outcrop samples were analysed for major elements by X-ray fluorescence (XRF), trace elements by Excimer Laser Ablation Inductively Coupled Plasma Mass Spectrometer (ELA-ICP-MS) and noble metals by isotope dilution ICPMS methods. If there is a direct magmatic link between gold and the igneous porphyries in the Kelian region, gold must be concentrated by fractional crystallisation and this can only occur if the parent magma that gave rise to the Kelian andesite became vapour saturated before it became sulfide saturated. Special emphasis will therefore be placed on the chalcophile elements, copper, gold, rhenium and platinum-group elements (PGE) to see if there is evidence of sulfide saturation. Alternatively, Kelian may be interpreted as an epithermal deposit involving a meteoric-hydrothermal system driven by heat from high-level intrusions and having no direct, magmatic fluid component.

The behaviour of platinum group elements (Pd, Pt, Rh, Ru, Ir and Os) is a particular focus of the study for two reasons. Firstly, the PGE partition more strongly into sulfides than Au, with extreme partition coefficients, possibly in excess of 10^5 (Keays and Campbell, 1981; Campbell and Barnes, 1984; Bezmen et al., 1994). Thus, PGE are more sensitive indicators of sulfide fractionation than Cu and Au. The ELA-ICP-MS has been used to analyse the primary igneous phases in the rocks to identify any minerals that are

fractionating chalcophile elements. Secondly, the PGE are more resistant to mobilisation by hydrothermal fluids than Au or Cu, and more likely to record primary igneous values. If there is fractional differentiation, the PGE concentrations are dropped significantly with the increasing silica content.

In order to resolve the temporal and genetic relations between calc-alkaline magmatism and hydrothermal mineralisation at Kelian, this study attempts to determine absolute ages of the various igneous rocks using the U-Th-Pb zircon dating method by excimer laser ablation ICP-MS. It also aims to examine possible magmatic links between the low-sulfidation gold deposit at Kelian and the high-sulfidation gold-copper mineralisation at Magerang-Imang, a prospect located 4 km NW of the Kelian Mine.

1.2 Scopes of this study

This study aims to document the geochemical characteristics of the least altered intrusive and volcanic rocks in the Kelian Gold Mine and surrounding prospects including Magerang, Muyup, Ritan, Plata and Han areas. The effects of alteration on the chemistry of the wall rocks in the Kelian Gold Mine are also investigated as part of this study.

Selected samples of intrusive rocks as well as detrital zircons were dated by the U-Pb zircon ELA-ICP-MS method in order to constrain the timing of the chemical evolution of the igneous suite. In addition, detrital zircons from the Mahakam and Kelian rivers were dated to constrain the overall duration of magmatism in the region.

Platinum group elements, gold and rhenium have been analysed in samples from the highly altered host rocks of the Kelian deposit and from two adjacent prospects that show only little evidence of alteration: the hornblende phyric Magerang-Imang suite and the pyroxene phyric Nakan suite. This PGE study is used to evaluate a possible hypothesis that the Kelian deposit formed because the parent magma that gave rise to the Kelian andesites became vapour saturated before it became sulfide saturated. If this happens, gold and the PGE are expected to concentrate in the parent magma chamber whereas if the chamber becomes sulfide saturated first, Au and the PGE may be stripped from the magma before it becomes vapour saturated and unavailable to form a magmatic-hydrothermal deposit. Variations in the PGE concentration in a fractionated suite of

andesites may therefore provide a method to distinguish between ore-bearing and barren igneous suites, where ore-bearing suites concentrate PGE with increased fractionation whereas barren suites do not.

1.3 Thesis Organisation

In order to achieve the above objectives, this study will be subdivided as follows:

Chapter 1: Introduction; to define the research topics, background, objectives and methodology.

Chapter 2: An overview of the characteristic features of epithermal ore systems with special reference to the Kelian gold deposit and regional prospects; to provide tectonic and geological aspects of epithermal mineralisation and to describe the geology and mineralisation of the research areas.

Chapter 3: Major and trace element geochemistry of the calc-alkaline igneous suite associated with the Kelian gold deposit; to describe the chemical characteristics of the igneous rocks, wall rock alteration and mineralisation, tectonic significance and genesis of primary magmas as inferred from trace element geochemistry; to establish a genetic link between the variably fractionated igneous rocks in the region.

Chapter 4: Geochemical model of rare earth elements in the Kelian Igneous Complex; to identify the cumulus phases responsible for the geochemical evolution of the igneous suite in the Kelian region.

Chapter 5: Platinum-group elements (PGE), Re and Au geochemistry; to document the characteristics of noble metals in the igneous suite and their distribution on both regional and local/district scales and to evaluate the behaviour of the PGE, Re and Au during fractional crystallisation and hydrothermal mineralisation.

Chapter 6: Geochronology of the andesite-rhyolite suites of the Kelian Igneous Complex and regional prospects; to present age data for the igneous rocks, to constrain the timing of magmatic-volcanic events, and to relate the chemical evolution of the igneous suite to the gold mineralisation.

Chapter 7: Summary and Conclusions; a brief summary of the main conclusions from this study, particularly on the geochemical evolution and geochronology of the igneous

suite associated with the gold mineralisation. The future work is proposed including stable isotope analysis, radiogenic isotope dating of the mineralisation events and melt inclusion analysis to study the characteristics of trace elements and metals and the ore forming conditions, especially the magmatic processes related to the development of the Runcing Rhyolite and the diatreme complex.

1.4 Field Research

The Kelian gold deposit is located in the nearby Kelian River, a tributary of the Mahakan River, which is situated approximately 250 km west of the provincial capital of Samarinda, East Kalimantan (Figure 1.1). The area can be reached in 7 hours by speedboat from Samarinda or 70 minutes by helicopter from Balikpapan. The deposit is currently being mined as an open pit using drill and blast techniques and heavy equipment by PT. Kelian Equatorial Mining.

This study was commenced in September 1997 and the field project was established by the Research School of Earth Sciences, Australian National University, Kelian Equatorial Mining (KEM) and Rio Tinto Indonesia (RTI). The first session of field work was conducted in the Kelian, Muyup and Ritan areas during the period of 22 September 1997 to 26 November 1997. The second field work was conducted in the Kelian Gold Mine and the regional prospects such as Han and Batu Utul during the period of 6 November 1999 to 6 December 1999. The study was financially assisted by the Australian Agency for International Development (AusAID) and the Research School of Earth Sciences (RSES), ANU. During the field work, domestic transport, logistics and accommodation were supported by RTI and KEM.

The field work at Kelian accomplished a review of the regional geology of the greater Kelian areas (Kelian Regional) including the areas of Magerang, Sopandua, Imang and Nakan, observation of the mine pit geology, sampling and documentation of exploration drill cores and pit exposures. The author worked for KEM and RTI in the Kelian Gold Mine and regional exploration programs from 1991 to 1995. All samples were collected from outcrops, exploration drill cores and pit exposures.

The field work in the Ritan and Muyup prospects was jointly carried out and supported by the regional follow-up exploration team of RTI. This included geological mapping and rock-chip sampling, particularly in the mineralisation area of Mejuk and local mine area at Muyup. All the samples of Ritan and Muyup were collected from surface exposures as no drill core samples were available.

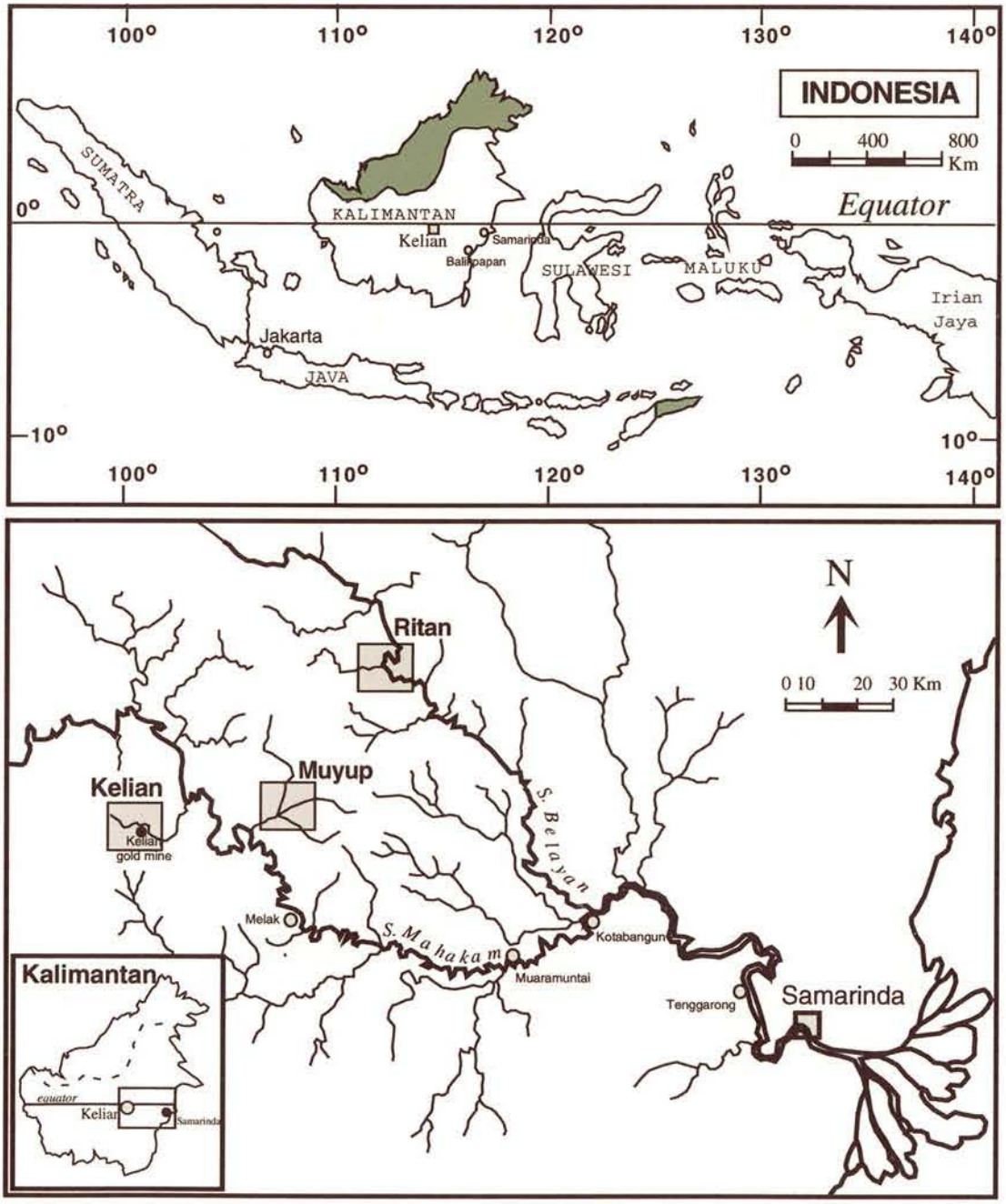

Figure 1.1: Location map of the study area

Plate 1.1 : View looking north over the East Prampus Pit, the Kelian Gold Mine. The west wall of barren, propylitic andesite (left), the Runcing Rhyolite (top centre), and pyroclastic and volcaniclastic units (right).

Plate 1.2: On the north wall of the East Prampus Pit. Pyroclastics are intruded by basaltic dykes of Pleistocene age.

Plate 1.3: Sharp contact between tuff and the Runcing muddy breccia diatreme on the north eastern part of the East Prampus Pit.

Plate 1.4: The barren, propylitic andesite on the west wall of the East Prampus Pit

Chapter 2
OVERVIEW OF THE CHARACTERISTICS OF EPITHERMAL MINERALISATION WITH SPECIAL REFERENCE TO THE KELIAN GOLD DEPOSIT AND REGIONAL PROSPECTS

2.1 Introduction

Studies of major gold deposits and geothermal systems have greatly improved our understanding of ore geology and the geochemistry of epithermal systems. As a result, classification, genetic models and interpretation of the epithermal-type deposits have been refined. This extensive research has also established well-defined geological and geochemical frameworks in which many aspects of ore genesis may be reviewed. This chapter summarises general characteristics of epithermal gold deposits in volcanic terranes and presents the Kelian gold deposit, Kelian Regional, Muyup and Ritan prospects as case studies.

The term *epithermal* was originally proposed as a class of hydrothermal deposits formed by ascending hot waters near the surface in or near volcanic rocks at relatively low temperature and pressure (Lindgren, 1922, 1933). Epithermal deposits generally emplaced at a shallow depth; commonly less than 1500 metres (Schmith, 1950). Several authors have attempted to review the use of the term *epithermal* and restrict its use to the deposits having textural and mineralogical characteristics of a low temperature of formation; from 100°C to 320°C, typically 170°C to 280°C, from dominantly meteoric hydrothermal fluids (White and Hedenquist, 1990; Henley, 1991 and White et al., 1995). Gold and silver are the most valuable ore elements in epithermal ore deposits. They may also contain minor amounts of iron and base-metal sulfides, tellurium and mercury. The ores occur with quartz, carbonates, barite and clays as veins, breccia filling, stock-works and disseminations.

There have been at least three ways to classify epithermal deposits in volcanic terranes:

1. Classification based on hydrothermal vein and alteration minerals (Hayba et al., 1985; Heald et al., 1987):

i. adularia-sericite type (e.g. Creede, Eureka, Guanajuato, Round Mountain districts)

ii. acid-sulfate type (e.g. Summitville, Goldfield, Red Mountain and Julcani districts)

This classification was derived from the detailed evaluation of characteristics of the Au-Ag vein deposits in the North America. It has been slightly modified into adularia-sericite (illite) type and alunite-kaolinite-pyrophillite type (Berger and Henley, 1989). The adularia-sericite assemblage indicates the fluid chemistry of near neutral pH, whereas the alunite-kaolinite indicates the acid pH - fluids. The Kelian and Muyup gold deposits can be assigned to the adularia-sericite (illite)-type deposits, while the Magerang-Imang, Plata and Ritan gold mineralisation are of the alunite-kaolinite-pyrophyllite-type.

2. Classification based on the redox state of the sulfur present in the hydrothermal fluid (White and Hedenquist, 1990):

i. low sulfidation type

ii. high sulfidation type

This classification was proposed by Hedenquist (1987) to distinguish deposits which can not be grouped using diagnostic minerals (e.g. adularia, base-metals and sulfide contents). In general, low sulfidation-type deposits display an alteration assemblage of quartz-adularia-sericite (illite)-pyrite, in contrast to high sulfidation-type deposits which are commonly characterised by an alteration assemblage of alunite-kaolinite-pyrophyllite. Low sulfidation refers to the lowest oxidation state of sulfur (-2) which commonly occurs in near-neutral geothermal systems, while high sulfidation refers to the high oxidation states of sulfur (+4, +6) which is commonly present as SO_2 or sulfate (SO_4^{2}) in volcanic hydrothermal discharge. The low sulfidation type may be subdivided into three different sub-types (Sillitoe, 1993b): sulfide-poor associated with sub-alkalic rhyolitic rocks; sulfide-poor associated with alkalic rocks; and sulfide- (and base-metal) rich associated with sub-alkalic andesitic to rhyodacitic rocks. The Kelian and Muyup gold deposits are representatives of low sulfidation epithermal mineralisation, while the Magerang-Imang and Ritan prospects are of the high sulfidation type.

3. Classification based on genetic (conceptual) models:

i. epithermal vein model as proposed by Buchanan (1981)

ii. hot-springs and open vein deposition models as proposed by Berger and Eimon (1983)

Genetic concepts for epithermal mineralisation (White et al., 1971) involve convection cells of meteoric and late magmatic water circulating through volcanic and sedimentary sequences, where water becomes heated, ascends until boiling causes precipitation of metals and minerals. The epithermal vein model emphasises the importance of the level of boiling at a particular depth under hydrostatic conditions. The vertical extent may vary, depending on the irregularities of paleotopography, structures, isothermic and isobaric conditions, but typically within a range of 300-400 m. The hot-spring model is assigned to deposits formed by very hot solution at or near surface which is characterised by intense silicification and brecciation, adularia-sericite vein alteration, hydrothermal breccias and low-temperature clay alteration. In contrast, the open vein deposition types form at greater depth than the hot-spring type and are characterised by large tonnage of high-grade ore, high base-metal contents and less brecciation. The open vein system may be subdivided into a stacked-cell convection system and a closed-cell convection system.

2.2 Characteristic Features of Epithermal-Type Ore Deposits

The emplacement of epithermal deposits is temporally and spatially related to the extensional tectonic setting and magmatic activity at convergent plate boundaries above subduction zones. The deposits are generally found in areas with well-developed tensional fracture systems or structures related to large-scale volcanic collapse (Panteleyev, 1986, Sillitoe, 1993b). Both adularia-sericite and acid-sulfate types form in similar tectonic settings. Adularia-sericite type deposits occur in the back-arc regions where more potassic and silicic magmatic activities occur within areas of extensional faulting (Berger and Henley, 1989). Kaolinite-alunite types are more likely related to changes in magmatic compositions. Most of the Western United States deposits are associated with structurally complex volcanic domes, particularly along the margins of felsic caldera (Hayba et al., 1985). However, it was thought that calderas are not a pre-requisite for the formation of epithermal deposits since only a few calderas of the Western United States are mineralised. Ore mineralisation commonly occurs near the end of volcanism. This

indicates that hydrothermal processes resulting in ore deposition may result from volcanism, most likely during the waning stages.

Most epithermal gold - silver deposits form in Tertiary volcanic rocks such as subaerial pyroclastics and near-surface intrusions. Older epithermal deposits are less common due to either erosional or metamorphic processes. Heald et al. (1987) have distinguished geological characteristics of 16 major deposits of North and South America into 2 different types; adularia-sericite and acid-sulfate types. Adularia-sericite types have various compositions of host rocks ranging from rhyolite to andesite. They may form in several lithologies within a deposit. Acid-sulfate-type deposits such as Goldfield, Summitville in Colorado and Red Mountain in Nevada are more commonly associated with porphyritic, rhyodacitic rocks. Ore deposition is possibly genetically related to the host rock as indicated by the age of mineralisation which is very close (less than 0.5 Ma) to the formation age of the host rock. The field characteristics of epithermal deposits are listed in Table 2.1.

In terms of mineralogy, adularia-sericite (low sulfidation) types are characterised by the vein assemblage of quartz+adularia+sericite+rhodochrosite+hematite. Wall rock alteration, dominantly sericitic (illite-smectite), borders a silicified zone near vein and grades outward into propylitic alteration. The presence of chlorite, selenite and fluorite are also characteristic of this type. In contrast, the typical minerals in acid-sulfate (high sulfidation) type deposits are assemblages of enargite+pyrite$\pm$covellite. The ore is typically associated with advanced argillic (kaolinite-alunite) alteration. The kaolinite alteration grades outward into argillic and silicic alteration. Alunite may be developed in adularia-sericite types as a supergene mineral in which case it is not related to the ore-forming processes. Precious-metals occur as native gold, native silver, electrum, silver sulfides and silver sulfosalts, with varying silver to gold ratios. Low sulfidation type deposits generally have high silver to gold ratios. However, some high sulfidation type deposits such as Julcani, Mexico; Red Mountain, Nevada and Lake City, Utah also show high silver to gold production ratios (>10) (Heald et al., 1987).

The adularia-sericite or low sulfidation type is generated from near neutral, sulfur-poor, reduced fluids, whereas the acid-sulfate or high sulfidation type is generated from acid, sulfur-rich, oxidised fluids. Fluid salinities range from 0 to 13 eq. wt% NaCl with the limited data on acid-sulfate types showing a wider range of 5 to 24 eq. wt% NaCl. These deposits are interpreted to have formed at palaeodepths of 300 to 1400 metres.

Table 2.1

Characteristics of epithermal deposits

(From Sillitoe, 1993b)

	High Sulfidation (Acid-Sulfate)	**Low Sulfidation (Adularia-Sericite)**
Host rocks	Mainly andesite - rhyodacite	Andesite - rhyodacite - rhyolite
Alteration zone	Areally extensive (commonly several km^2) and visually prominent	Commonly restricted and visually subtle
Key proximal alteration minerals	Crystalline alunite; pyrophyllite at deeper levels	Sericite or illite±adularia; roscoelite (V-mica) in deposits associated with alkalic rocks; chlorite in few cases
Quartz gangue	Fine-grained, massive, mainly replacement origin; residual, slaggy ("vuggy") quartz commonly hosts ore	Chalcedony and/or quartz displaying crustiform, colloform, bladed, cockade and carbonate-replacement textures; open-space filling
Carbonate gangue	Absent	Ubiquitous, commonly manganoan
Other gangue	Barite widespread with ore; native sulfur commonly fills open spaces	Barite and/or fluorite present locally; barite commonly above ore
abundance	10-90 vol.%, mainly fine-grained, partly laminated pyrite	1-20 vol.%, but typically <5 vol.%, predominantly pyrite
Key species	Cu sulfosalts (enargite, luzonite) and Cu + Cu-Fe sulfides (chalcocite, covellite, bornite) common; generally later than pyrite	Sphalerite, galena and tetrahedrite common; Cu present mainly as chalcopyrite
Metals present	Cu, Au, As (Ag, Pb)	Au and/or Ag (Zn, Pb, Cu)
Metals present locally	Bi, Sb, Mo, Sn, Zn, Te (Hg)	Mo, Sb, As (Te, Se, Hg)

Boiling, oxidation and fluid mixing processes are considered as the effective mechanism for ore deposition. Sources of fluids are predominantly meteoric water with possibly minor amounts of magmatic water. The ore and gangue minerals are deposited mostly as vein or breccia filling with banded, crustiform, vuggy, colloform textures.

2.3 Genetic Models

Epithermal mineralisation occurs in hydrothermal convecting systems where meteoric water circulates deeply into volcanic or sedimentary piles. As the fluid becomes heated, metals, sulfur, chloride and other rock components become soluble. The mineralising fluid rises through fractures, reacts with wall-rocks and precipitates ore and gangue minerals as veins and breccia filling, as well as disseminations. Effective fluid conduits may be provided by high- and low-angle faults, volcanic ring fractures, coarse pyroclastic or volcaniclastic rocks, and hydrothermal breccias (Sillitoe, 1993b). The genetic model for vein-type deposits (Buchanan, 1981; Figure 2.1) emphasises the relation of ore deposition with oxidation and boiling due to decreased pressure. Precious-metals are likely deposited at and above the boiling zone, while base-metal sulfides mostly form below and at the boiling level. Boiling and mineralisation commonly occur periodically and result in distinctive, layered and banded ore textures. Boiling causes separation of volatiles such as SO_2 and H_2S into liquid and vapour. Progressive boiling results in increasing pH, salinity and oxygen fugacity in the remaining liquid. This condition allows precipitation of silver minerals along with quartz, carbonates, sericite and adularia. The loss of CO_2 and H_2S also increases the activity of S^{2-} and HS^-, which in turn leads to the formation of thiocomplexes with gold and other metals. This is true in some situations, but the more important point is that boiling causes a loss of sulfur from the system, which results in deposition of gold. Gold is precipitated in the upper part or nearer the palaeosurface in a highly oxidised environment where the thiocomplexes are destabilised by oxidation.

Boiling of the solution results in loss of complexing agent for gold, pH increase and oxidation, all of which favour gold deposition. The possible exchange reactions involved in the precipitation of gold from solution as a bisulfide complex are :

Boiling : $Au(HS)_2^- + \frac{1}{2} H_2 + H^+ = Au + 2 H_2S$

$HCO_3^- + H^+ = H_2O + CO_2$

Oxidation : $Au(HS)_2^- + \frac{1}{2} H_2O + 15/4\ O_2 = Au + 2 H_2S + \frac{1}{4} O_2$

pH increase : $Au(HS)_2^- + \frac{1}{2} H_2O = Au + 2 HS^- + H^+ + \frac{1}{4} O_2$

pH decrease : $Au(HS)_2^- + H^+ + \frac{1}{2} H_2O = Au + 2 H_2S + \frac{1}{4} O_2$

Pyrite precipitation : $Fe^{2+} + 2\ Au(HS)_2^- = 2\ Au + FeS_2 + 2\ H^+ + 2\ HS^-$

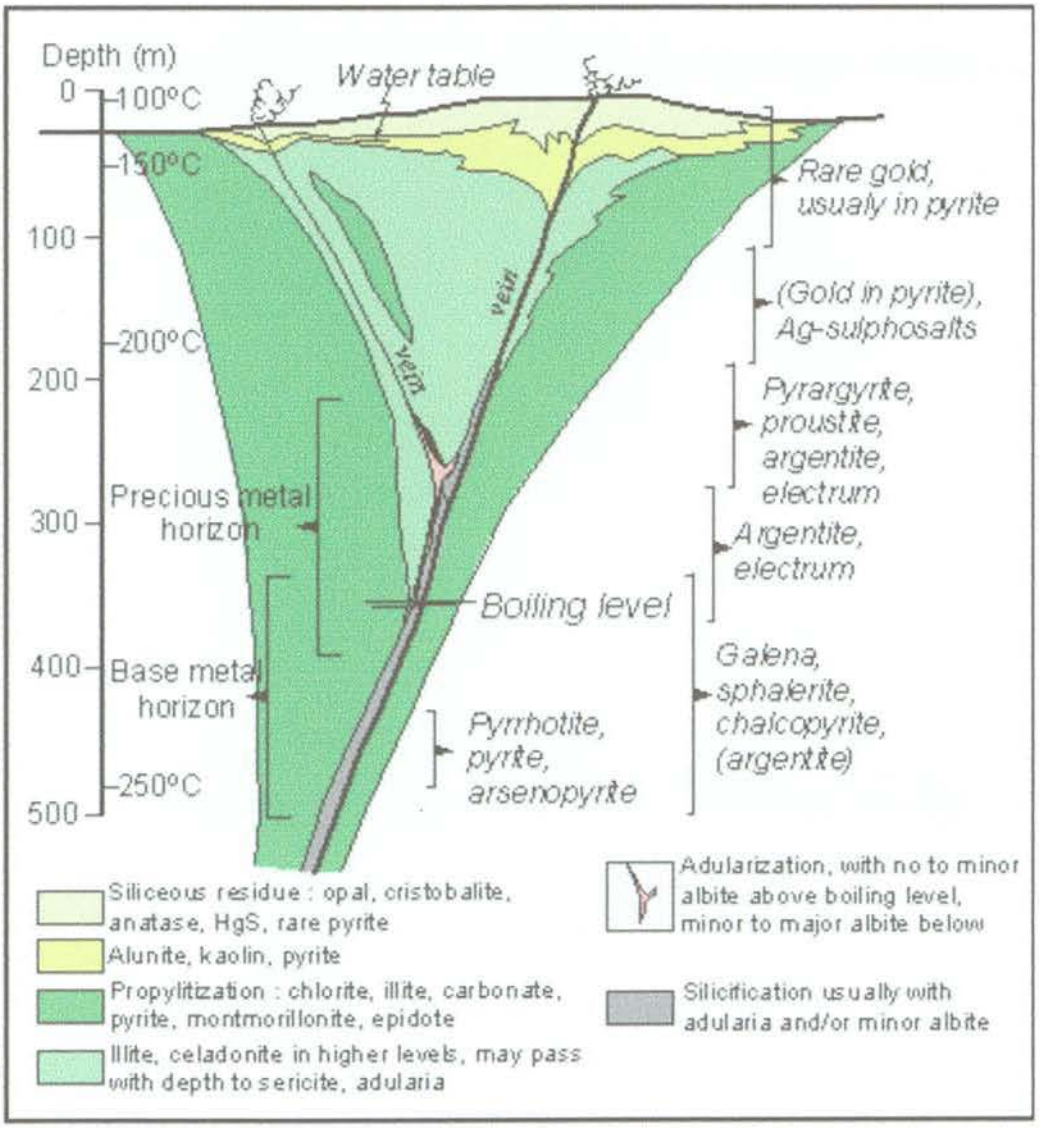

Figure 2.1 : Schematic cross-section of vein-type epithermal deposits (after Buchanan, 1981)

Conceptual models presented by Berger and Eimon (1983) include Hot-Springs and Open Vein Deposition Models. In the hot-spring model (Figure 2.2), precious-metals are deposited at very shallow depths below vents and in breccias as a result of the sudden

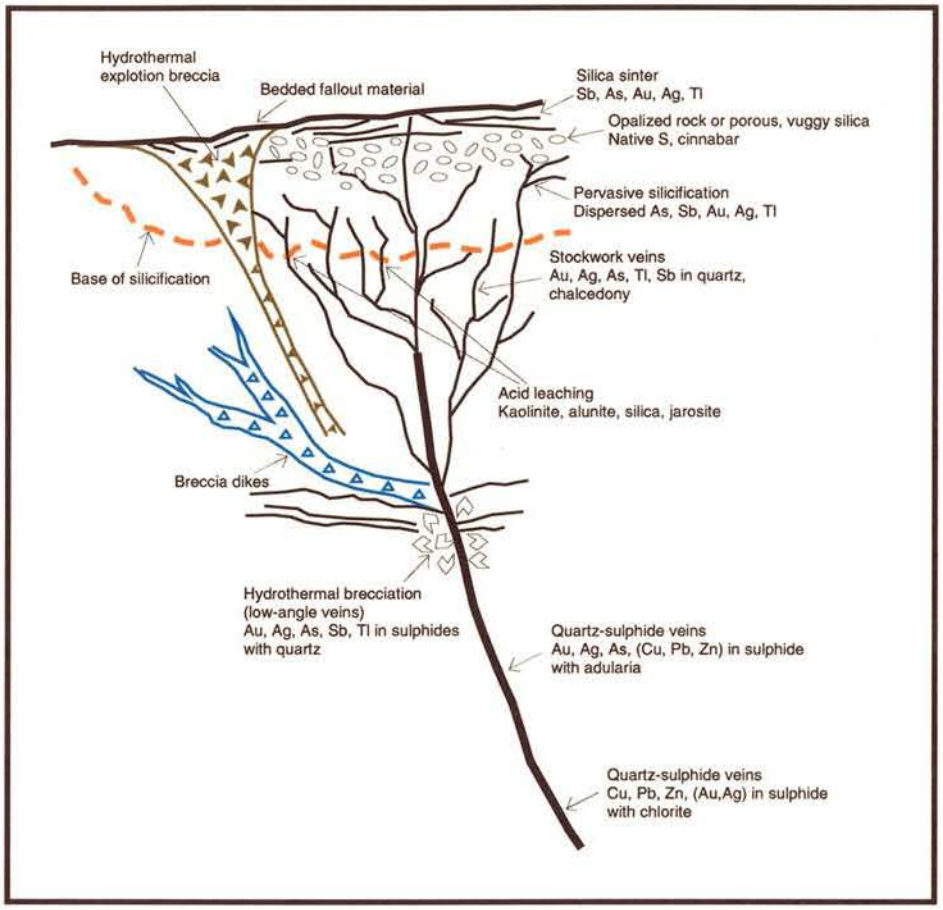

Figure 2.2 : Schematic cross-section of hot spring-type epithermal deposits (after Berger and Eimon, 1983)

release of abnormally high fluid temperatures and pressures. The ore deposits are associated with the deposition of silica sinter at the surface. High-grade precious-metals are found in closest proximity to the vents and possibly in bedded zones in the sinter resulting from multiple periods of metal transport in the hydrothermal fluids. In contrast, the open vein model (Figures 2.3a and 2.3b) shows that ore deposits form as veins at deeper levels compared to the hot spring type and contain high grade gold and base-metals. Brecciation is less developed in this system. Examples of the hot-springs- type deposits are Round Mountain in Nevada, DeLamar in Idaho and McLaughlin in California, while the open vein type deposits are represented by the Creede district (Colorado) and Guanajuato (Mexico).

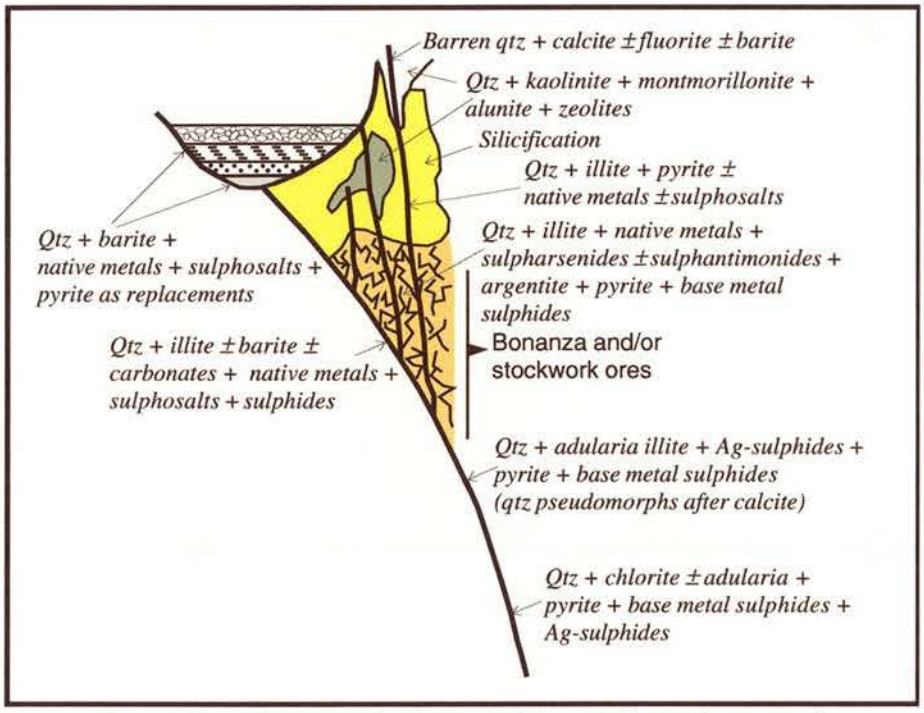

Figure 2.3a : The stacked-cell convection model including areas of stockwork fracturing and replacement-type deposits (after Berger and Eimon, 1983)

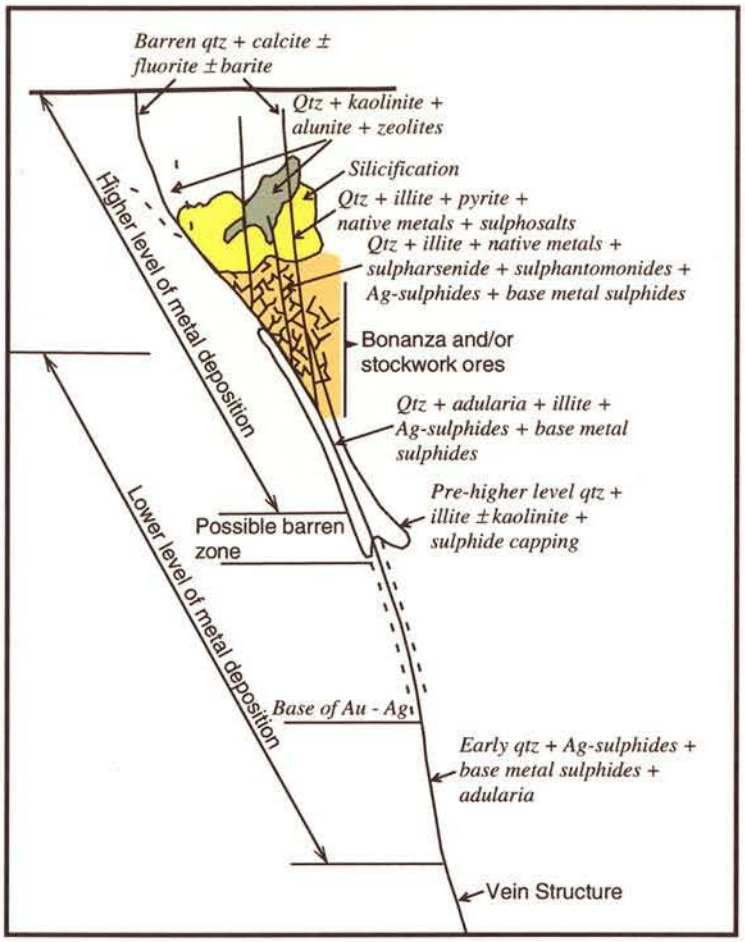

Figure 2.3b : The closed-cell convection model including two levels of mineralisation resulting in stacked orebodies, separated by a barren zone (after Berger and Eimon, 1983).

2.4 Geology of The Regional Prospects

The Kelian, Muyup and Ritan districts are located within the northwestern part of the Kutai Basin. The Basement rocks which outcrop at the western boundary of the Kutai Basin, comprise volcanic, sedimentary and metamorphic rocks of Late Jurassic to Early Cretaceous age. The Kutai basin stratigraphy (Pieters, 1999) is given in Figure 2.4.

The regional prospects cover all of the exploration areas including the sub-economic prospects of Magerang-Imang, Nakan, Sopandua and Buan, which are located immediately surrounding the Kelian Gold Mine and situated within the Contract of Work of the Kelian Equatorial Mining and Rio Tinto Indonesia. In addition, the other districts such as Han, Plata and Batu Utul are also included as parts of the regional prospects, because they are included in the early regional exploration programs and they are conveniently accessible from the Kelian Gold Mine.

The regional prospects are situated within the Central Kalimantan Continental Arc (Figures 2.4 and 2.5) which is made up of andesitic to trachyandesitic rocks of Late Oligocene - Middle Miocene age. This magmatic-volcanic arc is considered to be related to the southward dipping subduction zone in northwest Sarawak (Carlile and Mitchell, 1994) and hosts several low-sulfidation, epithermal gold deposits, including the deposits of Mirah, Gunung Mas, Mt. Muro, Masupa Ria, Kelian and Muyup. High-sulfidation epithermal alteration and mineralisation were also discovered in Masupa Ria (Central Kalimantan), Ritan and Magerang areas, spatially and possibly genetically related to the same porphyry system.

2.4.1. Magerang – Imang Prospect

Magerang-Imang is located 4 kilometres northwest of the Kelian Gold Mine. Geology, alteration and mineralisation of the Magerang-Imang area were mapped in detail during the Regional Exploration period of 1991-1994 (Setiabudi, 1994). The Magerang lithology comprises a series of fine-grained sandstone with intercalated siltstone, a Quarternary basalt flow and intrusive andesite (Figure 2.6). The sediments intruded by andesite at shallow depth show silicification, disturbed bedding and minor mineralisation.

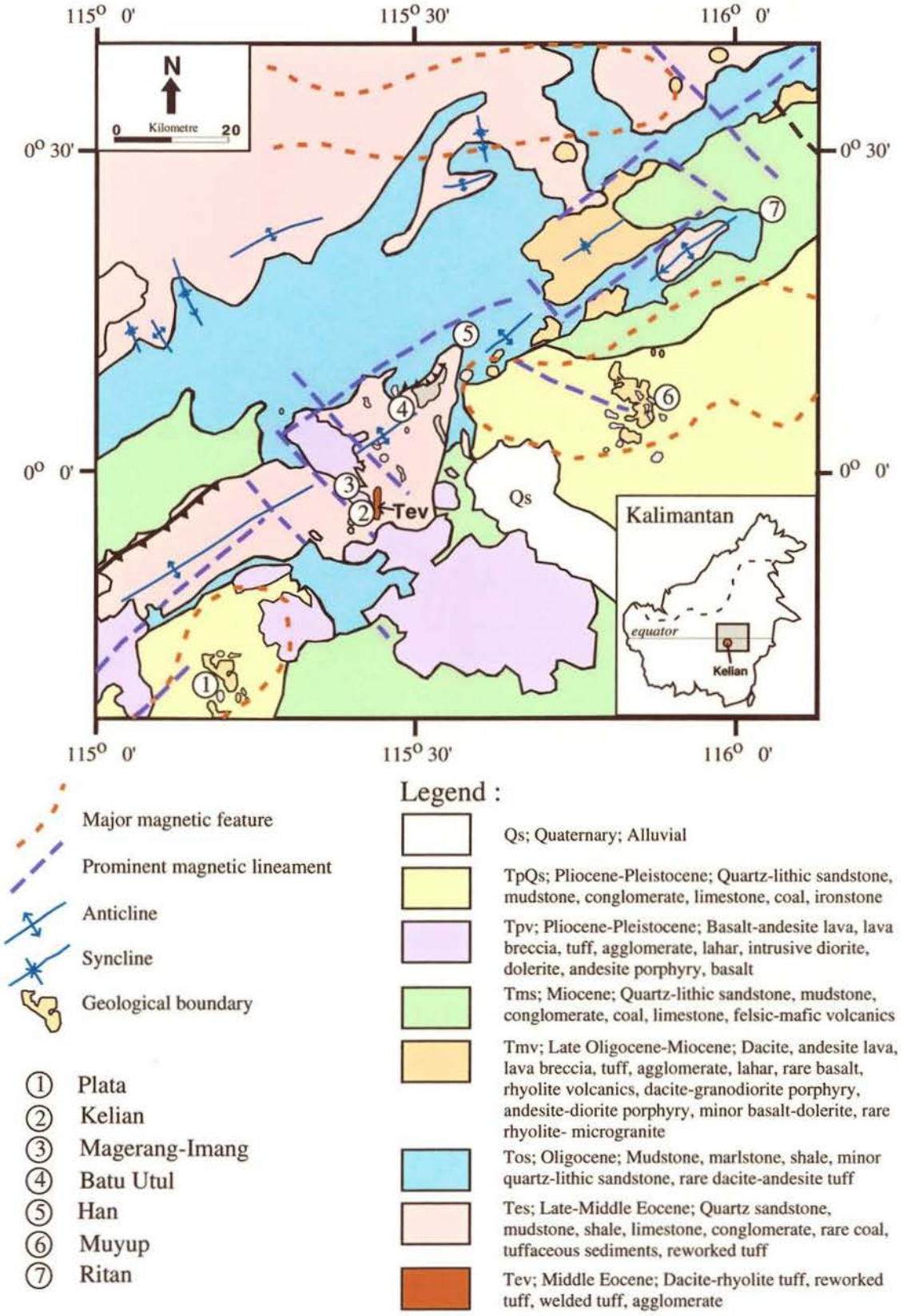

Figure 2.4 : Regional geology of the Kutai Basin (Pieters, 1999), showing stratigraphic formation, geologic and geophysical structures and location of the prospect areas.

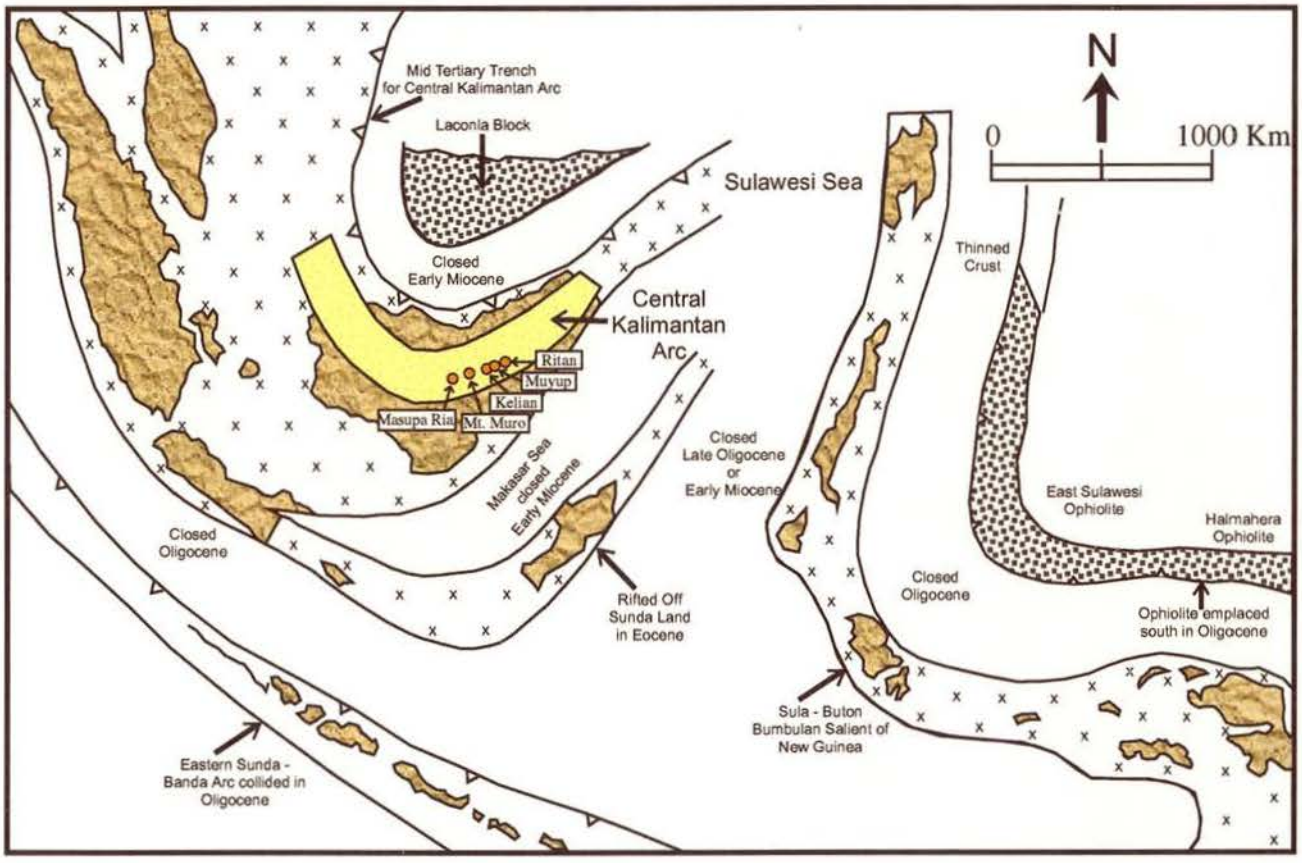

Figure 2.5 : Oligocene palaeogeography and magmatic arcs of the Indonesian region (after Carlile and Mitchell, 1994)

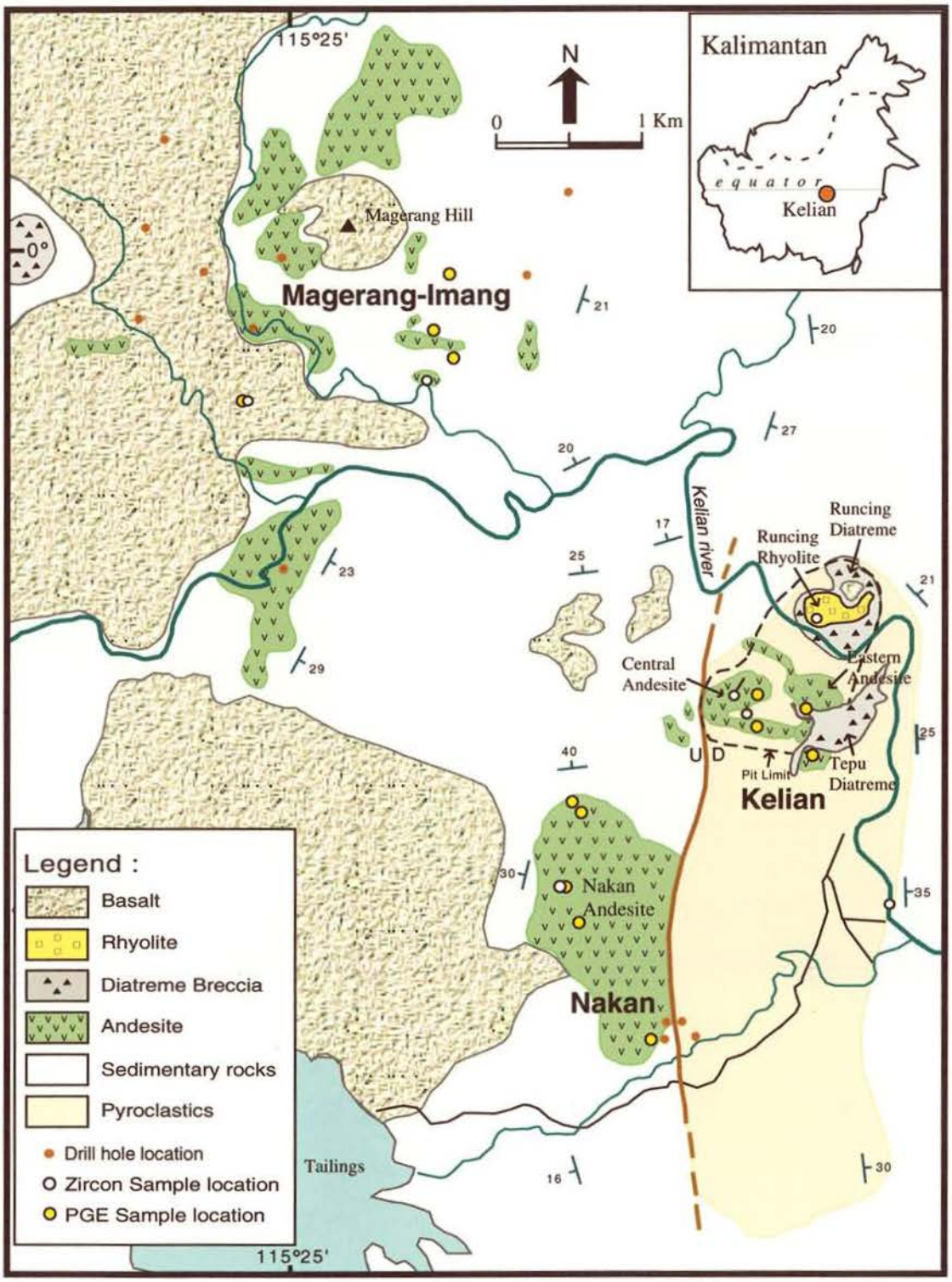

Figure 2.6 : Simplified geological map of the Kelian regional area.

In addition, a diatreme of muddy breccia is exposed in the eastern area and a Quarternary basalt plug forms the Magerang hill. The intrusive andesites that are found in the eastern part of Magerang-Imang and in drillholes under basalt in the southern area show very little evidence of alteration. The least-altered andesite of Magerang-Imang has a medium-grained, porphyritic texture, formed mainly by plagioclase and hornblende, with rare pyroxene phenocrysts set in a fine-grained, holocrystalline matrix of feldspar and mafic minerals. The phenocrysts and groundmass have undergone alteration along cracks and grain boundaries to sericite, chlorite and carbonate.

Hydrothermal alteration extends widely along 1000m E-W and 2000m N-S and ranges from propylitic (quartz-sericite-chlorite) grading to pervasive phyllic - argillic (quartz+illite+kaolinite/dickite). In some places, the remnants of highly altered vuggy silicified rock are common, showing advanced argillic alteration of quartz-alunite-diaspore-pyrophyllite. Mineralisation is confined to the southern section of Magerang and is localised by N-S trending fault along the sediment-intrusive contact. Sub-economic Cu-Mo-Au mineralisation associated with andesite intrusive bodies consists mainly of chalcopyrite and molybdenite with minor covellite, chalcocite and bornite. This alteration-mineralisation type indicates a high sulfidation system as a result of an upflow of relatively hot (>250°C), acidic (pH<3) fluids, possibly derived from a porphyry source at depth (Leach, 1991).

2.4.2 Nakan Prospect

The Nakan prospect, located a kilometre southwest of the Kelian Gold Mine is dominated by tuffaceous sandstone, fine-grained quartz sandstone and andesite porphyries. The least altered andesite shows a medium-grained, porphyritic texture, characterised by plagioclase and pyroxene phenocrysts set in fine-grained feldspar and mafic groundmass. Clinopyroxene and plagioclase phenocrysts are slightly altered to sericite, chlorite and calcite. Rare small grains of hornblende are slightly altered to chlorite. The fine-grained groundmass has been partially replaced by sericite, chlorite and carbonate.

Hydrothermal alteration at Nakan is confined to the fault contact zone of the andesite and tuffaceous sediments, which is interpreted to be the southern extention of the West Prampus Fault at Kelian. It was thought that the dextral movement of the West Prampus Fault led to the development of a NE-SW trending dilational zone similar to the

structure of the Kelian West Prampus orebody. However, the exploration drilling did not intersect any significant gold mineralisation (Hartshorn, 1995).

2.4.3 Han Prospect

The district geology lies in a northeasterly trending anticline formed predominantly by Oligocene sedimentary sequences of calcareous sandstone, mudstone, limestone, tuffaceous quartz-sandstone. High-level subvolcanic rocks occur as andesite porphyry, rhyodacite porphyry and heterolithic breccia. The least altered andesite exhibits a medium- to coarse-grained, porphyritic texture and is composed of predominantly plagioclase (labradorite) and mafic mineral phenocrysts in a fine grained quartz-feldspathic matrix. Both phenocryst and groundmass are partly altered to sericite, calcite and chlorite. Four alteration stages of a high-temperature porphyry system have been observed in the Han igneous suite (Corlett, 1999). The early potassic-type assemblage of quartz+albite+Kfeldspar+biotite±anhydrite+magnetite overprinted by propylitic-type assemblages of chlorite+calcite±sericite±epidote±quartz±rutile and phyllic-type assemblages of quartz±sericite±andalusite (a) and quartz+sericite±chlorite±calcite± tourmaline±rutile (b). The argillic-type assemblages of sericite+kaolinite+smectite also overprinted potassic alteration. The metallic mineralisation is mainly chalcopyrite and pyrite in the phyllic-altered wallrocks and magnetite associated with potassic altered andesite.

2.4.4 Plata Prospect

Lithologies of the Plata district consist of andesite lavas, coarse-grained lapilli and bedded vitric to crystal tuff, high-level intrusions of dacite porphyry, hydrothermal and phreatomagmatic breccias. The least altered andesite lava is composed mainly of plagioclase (oligoclase to andesine) with either hornblende or clinopyroxene in a fine-grained feldspar and mafic mineral groundmass. The dacite porphyry shows slightly altered phenocrysts of plagioclase, K-feldspar and hornblende in a fine-grained matrix of quartz, altered feldspar and mafic minerals. Pervasive alteration developed as concentric zones which grade vertically and laterally from vughy quartz±alunite in the centre part, through wide zones of silicification and quartz±alunite, quartz+alunite+pyrophyllite/dickite/

diaspore, quartz+dickite/pyrophyllite/diaspore and quartz+sericite, to an outer propylitic assemblage of chlorite+calcite (Leach and Corlett, 1999). High sulfidation epithermal-type mineralisation at Plata is localised as fracture and breccia filling, dominated by pyrite, enargite, chalcopyrite±tennantite and molybdnite.

2.4.5 Batu Utul Area

Sub-volcanic rocks in the Batu Utul area are composed of andesite and rhyolite porphyries. The phyllic altered-rhyolite shows quartz and altered feldspar phenocrysts in a fine grained sericitised groundmass. The andesite shows a medium-coarse texture made of weakly altered plagioclase and pyroxene phenocrysts in a fine grained feldspathic and mafic minerals. The phenocrysts and groundmass are partly altered to sericite, chlorite and iron oxide minerals.

2.5 Geology of The Kelian Gold Deposit

The stratigraphic sequence of the Kelian mine area comprises a series of intercalated Eocene felsic tuffs and volcaniclastic to epiclastic sediments in the lower section, overlain by fine- to medium-grained quartz-sandstones, shales with intercalated limestone (Figure 2.7). The pyroclastics and sedimentary rocks were uplifted and faulted during Late Oligocene to Early Miocene and intruded by Miocene stocks of andesite and rhyolite. After a period of erosion, Plio-Pleistocene basaltic volcanism took place producing lava and dykes.

The largest intrusive bodies, named Central Andesite and Eastern Andesite show vertical to inward-dipping contacts to the west and south, and hydrothermal contact breccia along the eastern margin of the Central Andesite. Although most of the Kelian Mine andesites have been variously altered, there are few samples from the southeastern area (Tepu) that show little alteration. These Tepu andesites are medium-grained, porphyritic

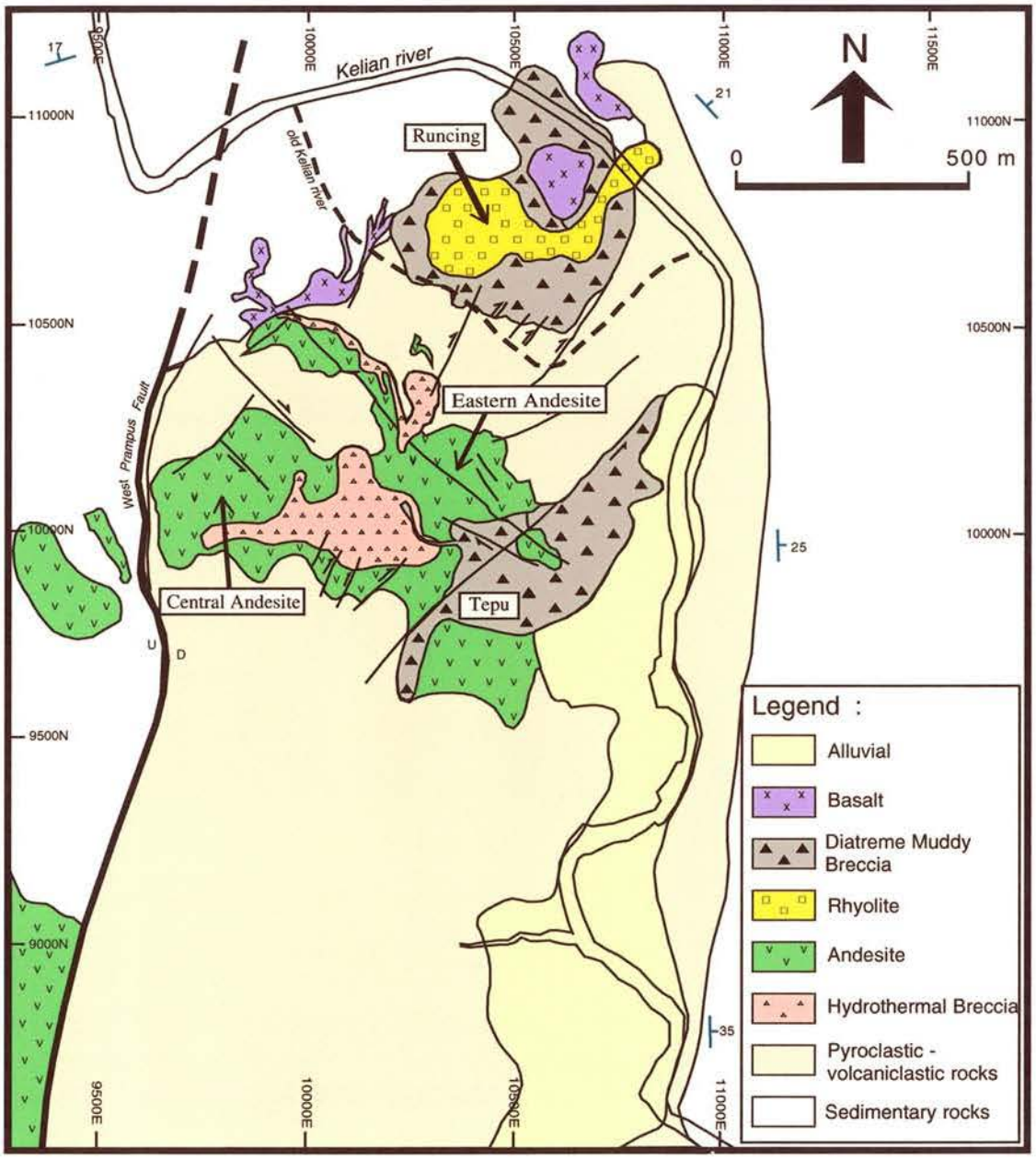

Figure 2.7 : Geology map of the Kelian mine area, based on the pit exposure map in October 1999.

and contain plagioclase, hornblende, minor K-feldspar and rare pyroxene phenocrysts within fine-grained, altered and devitrified groundmass.

Several types of breccia, including intrusion breccias, hydrothermal breccias, fault breccias and phreato-magmatic breccias, crosscut the older rock unit. The phreato-magmatic breccias are composed mainly of dark grey fragments of milled carbonaceous shale with

lesser quantities of tuff, andesite and fine-grained rhyolite within an altered clay matrix. These breccias occur as several hundred meter scale, oval-shaped bodies, locally called the Runcing and Tepu muddy breccias and are interpreted as diatreme complex (Sillitoe, 1993a). The Runcing diatreme breccia is intruded by a quartz rhyolite porphyry composed of quartz and strongly sericitised feldspar phenocrysts set in a fine-grained, highly-altered groundmass. The Runcing rhyolite porphyry can be distinguished from the fine-grained rhyolite clasts in the diatreme breccia by its distinctive grained size and phenocrist content.

The Kelian Gold Deposit, the largest disseminated gold deposit in Indonesia, has a resource potential of >97 Mt ore at an average grade of 1.85 g/t Au, including >53.5 Mt mineable ore at 1.97 g/t Au (Van Leeuwen, 1994). The deposit consists of two main orebodies, named West Prampus and East Prampus, and have a range of low-grade gold content (1-3 g/t) with Au/Ag ratios vary from 1:1 to 1:4. In addition, several high-grade mineralised zones (the 255, 339, 383, 393, and 394 Zones) contain 3-6 g/t gold. Gold mineralisation occurs in a dilational jog at the intersection of NS and NE trending fault structures (Corbett, 1993) and is localised within the margins of the andesite intrusions and a diatreme breccia. The hydrothermal alteration and mineralisation is typical of intrusive-related low sulfidation systems. The replacement and vein alteration are separated into four main assemblages based on paragenetic stages (Van Leeuwen et al., 1990). Firstly, chlorite+carbonate+ sericite+quartz±epidote assemblages (propylitic alteration - Stage 1) occur mainly as replacement alteration in the central part of the andesite intrusions. The second, phyllic alteration is characterised by sericite+quartz+adularia assemblages (Stage 2) and occurs as replacement and vein alteration in andesite, pyroclastics and muddy breccia. The third assemblage is phyllic with predominantly base-metal and carbonate minerals (Stage 3) as veins and breccias. The last, argillic alteration is a kaolinite+siderite assemblage (Stage 4) which occurs as replacement minerals, cavity fillings and veins. Kaolinite commonly overprints sericite and carbonate of earlier stages.

Sulfide minerals include pyrite with lesser sphalerite and galena, and are mainly disseminated within the matrices of the andesite and pyroclastic units, but are also found in fracture and cavity fillings in hydrothermally brecciated andesite and tuff, and in veins crosscutting the massive andesite. The high-grade gold is generally associated with phyllic alteration, particularly with carbonate and base-metal veins and breccias.

The geological model proposed by Van Leeuwen et al. (1990) demonstrates a relation between gold mineralisation and the andesite intrusion. It was thought that the hydrothermal fluid was generated by a mixing of cooling intrusive fluids with circulating meteoric water within the fractures and pyroclastic units. This relatively hot and dilute hydrothermal fluid reacted with the pyroclastics and andesite forming propylitic to phyllic alteration which resulted in deposition of sericite-adularia-pyrite and possibly gold due to boiling. The distribution of sericite-adularia is interpreted to indicate a progressive increase in gas content with time, and condensation of gases upon boiling at shallow levels (Corbett and Leach, 1995). While at a deeper level, fluid flow resulted in quartz-carbonate-sericite alteration. Stage 3 is associated with a second episode of hydrothermal activity that produced a hot, saline, CO_2-rich, magmatic-dominated fluid that carried gold and base-metals. This high-pressure fluid flow caused intensive brecciation and hydrofracturing and deposited gold and base-metals, particularly in the 255 Zone at East Prampus. Gold and base-metals were deposited together with carbonate and quartz under highly complex and variable time/space conditions involving boiling, mixing and rapid quenching.

However, gold mineralisation, particularly the high grade 394 Zone in the northeast Kelian may be related to the Runcing diatreme and concentrated in the upward-flared southern contacts of the diatreme (Sillitoe, 1993a). Gold deposition is closely associated with fault controlled base-metal veining and Mn-carbonate in tension gash veins formed between faults. Quenching in the faults may lead to isolated elevated gold grades. The 394 Zone is localised by NW trending dilation at the Runcing diatreme margin (Corbett, 1993).

The Kelian deposit shows magmatic - epithermal transitional features similar to the Porgera gold deposit, Papua New Guinea. At Porgera, the Stage I event is characterised by intense phyllic alteration associated with pyrite-sphalerite-galena-chalcopyrite (Corbett et al., 1995). Fluid inclusion data indicate fluids of magmatic origin with salinities of 7-12 eq. wt. % NaCl and temperatures of 200°-350°C (Richards, 1992). This is similar to Stage 2 at Kelian. Porgera's Stage II (quartz-roscoelite-dolomite) alteration formed by low salinity (4-8 eq. wt. % NaCl) and low temperature (~180°C) fluids is similar to Kelian's Stage 3 alteration-mineralisation, except that rhodochrosite is more developed and roscoelite is absent at Kelian. Porgera's Stage I mineralisation represents a more evolved fluid derived from a deeper magmatic source which has equilibrated with black shale during ascent (Cameron et al., 1995). Similar processes may have occured at Kelian, particularly in the 255 Zone and West Prampus orebody.

Some interpretations on structural controls seem to be oversimplified. The West Prampus fault has probably played an important role as an active structure providing pathways for fluid flow. The normal movement on the West Prampus fault may have formed a half graben rather than a narrow graben since the pyroclastics gradually changed to purely clastic sediments to the east. The formation of the Runcing diatreme may be responsible for the 394 mineralisation zone. However, an alternative possibility is to relate the 394 zone and the deeper level 393 Zone with the Burung fault as an active feeder structure and the fluid source at depth beneath the 393 Zone.

2.6 Geology of The Muyup Gold Deposit

The oldest sequence of the Muyup area comprises a series of Palaeogene sediments, termed as the Pamaluan Formation. This formation is made of quartz sandstone, conglomerate, mudstone and carbonaceous shale and siltstone. The Pamaluan Formation is overlain unconformably by Early Miocene volcanics, Muyup Volcanic Formation, made of welded and laminated rhyolite and andesitic tuffs. The Muyup Volcanic Formation is overlain by Pliocene sedimentary rocks, Kampung Baru Group, consisting of quartz sandstones, shale and coal (Wake, 1991). These volcanics are intruded by Middle to Early Miocene andesite porphyries (Figure 2.8). The youngest stratigraphic sequence in the Muyup area is the Plio-Plistocene Basalt, which occurs mainly in the northern part of the Muyup prospect.

Six isolated zones of epithermal-type mineralisation are located in the Buluh, Bengeh, Uping, Basran, Hairani and Benghok areas. The gold and minor base metal mineralisation is hosted by the andesite porphyry, rhyolitic tuff and volcaniclastic units. The mineralisation occurs at various stratigraphic levels and are exposed at a palaeodepth of 200-400m (Allen, 1988). The Muyup gold deposit has been estimated about 0.3 Mt with an average grade of 2.3 g/t Au (Wake, 1991, Van Leeuwen, 1994), mainly associated with hydrothermal breccias (with a high grade of 10-100 g/t Au) and quartz stockwork veins

(grading up to 1 g/t Au) within the andesite volcanics. The quartz veins are mainly fine grained, chalcedony with minor adularia, carbonate and minerals, overprinted by the assemblage of kaolinite, dickite and siderite. The near surface epithermal environment is evidenced by the clay alteration, low fluid inclusion temperature (230°C), the occurrence of a silica cap, as well as the enrichment in As, Sb and Hg.

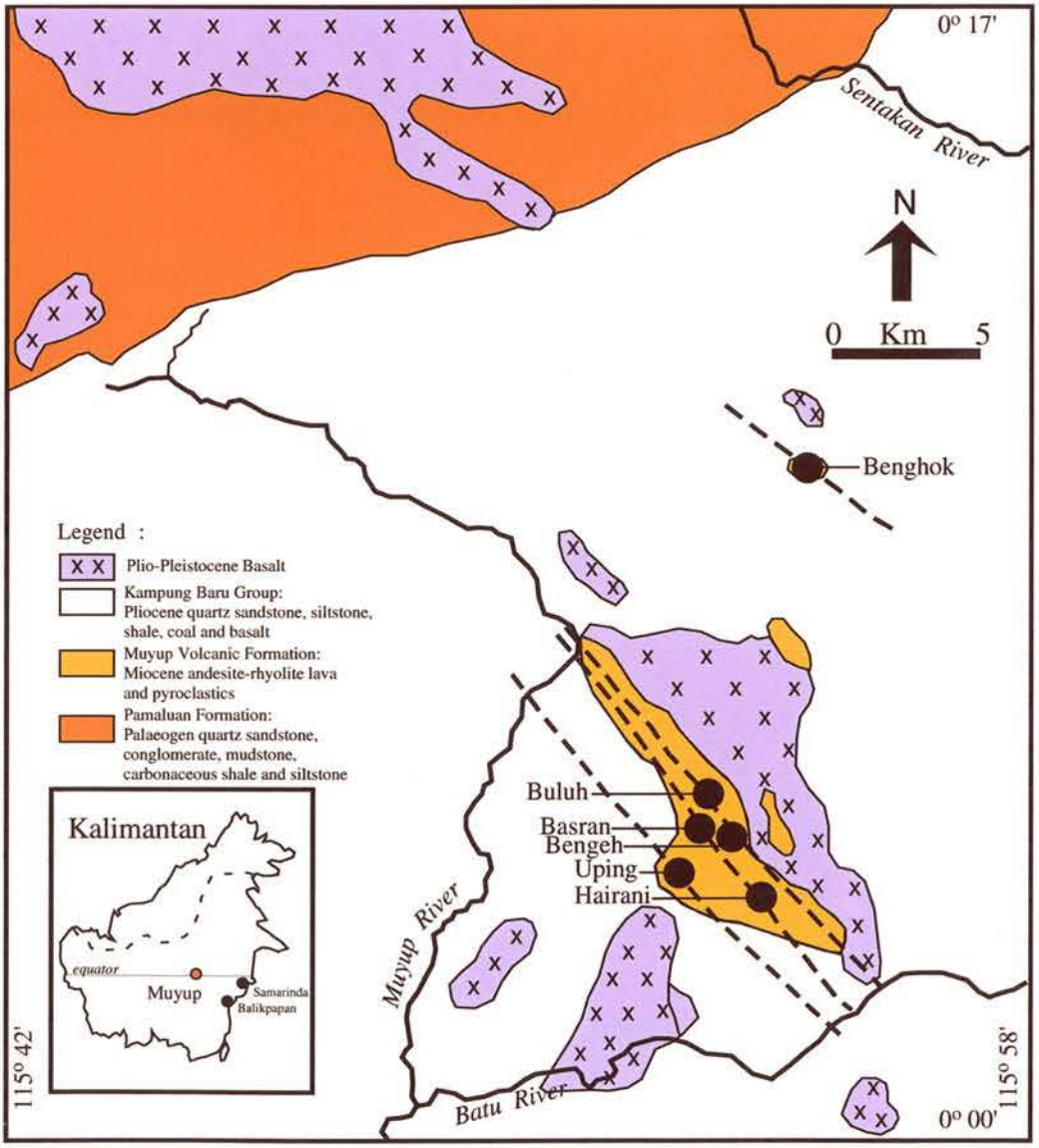

Figure 2.8 : Simplified geological map of the Muyup prospect (after Allen, 1988)

2.7 Geology of The Ritan Prospect

The Ritan prospect is located about 80 km NE of Kelian and has recently been explored in detail by Rio Tinto Indonesia, revealing a promising target of Cu-Au mineralisation within the northeast extension of the existing major ore deposits corridor. District geology comprises the Tabang Ridge volcanics of Early Miocene formed by andesite volcanic breccias, dacitic and andesitic lava flows, unconformably underlain by laminated siltstone and volcaniclastic sandstone. The Tabang volcanics are intruded by a basalt plug. Epithermal alteration is confined to the Mejuk area and comprises predominantly argillic assemblages of smectite-illite-kaolinite-pyrite and quartz-illite-kaolinite to an advanced argillic assemblage of quartz-alunite. Gold mineralisation occurs in vuggy silica rocks and a 5-7m-wide hydrothermal andesite breccia vein of the Tabang Ridge Formation, assayed about 6 ppm Au and 50 ppm Ag. In addition, elevated grades of lead and zinc were also identified from the hydrothermal breccia vein.

Chapter 3
MAJOR AND TRACE ELEMENT GEOCHEMISTRY OF THE CALC-ALKALINE IGNEOUS SUITES FROM THE KELIAN GOLD MINE AND REGIONAL PROSPECTS

3.1 Introduction

Previous petrological studies have indicated a temporal and spatial association between calc-alkaline andesite-rhyolite-dacite suites and gold-copper deposits in the Kalimantan magmatic belt (Van Leeuwen et al., 1990; Thompson et al., 1994; Abidin, 1996). Kelian, the most productive gold deposit in Indonesia, is of special interest because its association with the subduction zone magmatism has been regarded as significant in understanding the aspects of ore forming systems (Carlile and Mitchell, 1994). Geochemical studies of arc systems can therefore provide important information for assessments of mineral potential of the arc system. In particular, the regional variation in geochemistry of the sub-volcanic rocks from the East Kalimantan provides insight into the tectonic setting, origin of primary magmas and the magma source components.

This chapter deals with geochemistry of the calc-alkaline igneous suites from the East Kalimantan volcanic arc with a particular focus on the andesitic-rhyolitic intrusive rocks associated with the Kelian gold - base-metal mineralisation. Geochemical characteristics of the igneous rocks in the Kelian mine district and the other regional prospects, such as Magerang-Imang, Muyup, Ritan, Batu Utul, Han and Plata, are documented. In addition, the effect of alteration upon the chemistry of the host and country rocks is assessed. The Miocene magmatism of the Kelian region, which include the Kelian mine, Nakan and Magerang-Imang andesites and Kelian mine rhyolite (locally named as *Runcing Rhyolite*), will be referred to as the *Kelian Igneous Complex*. The Kelian mine andesites includes intrusive rock units locally named as *Central Andesite, Eastern Andesite and Tepu Andesite*.

3.2 Analytical Methods

3.2.1 Major Elements

All of the samples selected from outcrops and drill cores were crushed using a hydraulic plate crusher and pulverised in an agate ring mill for whole-rock geochemical analysis. The major element (Si, Ti, Al, Fe, Mn, Mg, Ca, Na, K, and P) concentrations in fresh and altered samples were determined by X-Ray Fluorescence spectrometry at the Department of Geology, the Australian National University, using the method of Norrish and Hutton (1969). The reported results are accurate to better than 1% for concentrations of Si, Ti, Al, Fe, Mg and Ca, and better than 2% for concentrations of Mn, Na, K and P.

In addition, major element compositions in 35 of the samples were determined from glass samples by electron microprobe (EMP) methods using a Camebax (Microbeam) system. In this quantitative EMP analysis, x-ray intensities were measured by energy-dispersive spectrometer (EDS) using lithium-drifted silicon detectors (Ware, 1991). The samples were analysed using a 15 keV accelerating voltage and a 6-7 nA beam current with the beam focused to 1 micron, with a counting time of 80 live seconds (~120 real seconds) and an output count rate of ~8000 cps. The energy resolution of the EDS is 148 eV (full-width at half maximum intensity on Mn Kα). The data reduction were carried out on-line using a software package for empirical energy dispersive spectroscopy (SPEED).

3.2.2 Trace Elements

Whole-rock trace element concentrations were determined by excimer laser ablation inductively coupled plasma mass spectrometer (ELA-ICP-MS) on fused glass samples. ELA-ICP-MS has been applied to the *in situ* determination of a wide range of trace elements in geological materials over the last few years (Loucks et al., 1995; Sylvester and Ghaderi, 1997, Sinclair et al., 1998). The UV excimer laser, as an alternative technique for sample introduction to ICP-MS, has several advantages over the Infra Red laser sampling (Perkins and Pearce, 1995). It is less dependent on the physical and chemical properties of the analysed materials, does not produce significant element fractionation and has a more predictable beam profile.

3.2.2.1 Sample Preparation: Development of a New Glass Fusion Technique for Whole-Rock Analysis by ELA-ICP-MS

Quantitative analysis of trace elements in rocks by ELA-ICP-MS requires the sample to be converted to homogenous glass prior to analyses. It has therefore been necessary to develop a new sample preparation technique for a wide range of igneous rocks to produce the homogenous glass beads required for precise and accurate analyses.

The glass method for trace element analyses by ELA-ICP-MS has several advantages over solution-nebulisation ICP-MS. Firstly, ELA-ICP-MS analysis using whole-rock glass is fast and more convenient. Secondly, refractory mineral phases, such as zircon, which are difficult to dissolve in solution, are readily dissolved in glasses. Thirdly, molecular interferences caused by oxides, as commonly encountered in solution-mode ICP-MS analysis, are negligible in ELA-ICP-MS analyses of glasses.

The new procedure involves mixing powdered whole-rock sample with lithium metaborate flux spiked with ^{169}Tm and ^{235}U. The lithium metaborate flux effectively dilutes the sample and lowers its melting temperature and the viscosity of the melt. The addition of these spikes enables correction for instrumental drift encountered during ICPMS analysis. Optimum results were achieved using a 2:1 mixture of rock powders and spiked flux, and fusing at 1200°C for 20 minutes. The high temperatures and long times of fusion may cause the loss of some volatile elements in samples.

In the final procedure for producing glass for the Kelian samples, 0.6666 g of whole-rock powder was mixed with 0.3333 g of spiked flux on a weighing paper until the powder had a uniform colour. The spiked sample was then transferred into a clean, 3 cm-wide carbon crucible and pre-heated in a Kanthal Super Rapid Furnace at 600°C for 30 minutes. Following this initial pre-heating, the carbon crucible with powder was placed in a Kanthal High Temperature Melting Furnace for pre-heating at 800°C for 5 minutes prior to fusing. After 5 minutes, the temperature was raised to 1200°C and maintained at this temperature for 20 minutes to facilitate complete fusion and homogenisation. An Ar gas flow of 2.5 litre/minute was used during both preheating (800°C) and melting (1200°C) to prevent oxidation of the samples. At the end of this sequence, the carbon crucible with molten rock was removed from the furnace and rapidly quenched into a beaker of water. The glass was dried overnight, and a 2-3 mm piece of glass shard was mounted in epoxy and polished prior to laser ICP-MS analysis. Details of the preparation procedure are given in Appendix 2. In order to test the homogeneity of glass, multiple electron microprobe (EMP) analyses of the glasses have been carried out on selected samples. The

3.2 Analytical Methods

3.2.1 Major Elements

All of the samples selected from outcrops and drill cores were crushed using a hydraulic plate crusher and pulverised in an agate ring mill for whole-rock geochemical analysis. The major element (Si, Ti, Al, Fe, Mn, Mg, Ca, Na, K, and P) concentrations in fresh and altered samples were determined by X-Ray Fluorescence spectrometry at the Department of Geology, the Australian National University, using the method of Norrish and Hutton (1969). The reported results are accurate to better than 1% for concentrations of Si, Ti, Al, Fe, Mg and Ca, and better than 2% for concentrations of Mn, Na, K and P.

In addition, major element compositions in 35 of the samples were determined from glass samples by electron microprobe (EMP) methods using a Camebax (Microbeam) system. In this quantitative EMP analysis, x-ray intensities were measured by energy-dispersive spectrometer (EDS) using lithium-drifted silicon detectors (Ware, 1991). The samples were analysed using a 15 keV accelerating voltage and a 6-7 nA beam current with the beam focused to 1 micron, with a counting time of 80 live seconds (~120 real seconds) and an output count rate of ~8000 cps. The energy resolution of the EDS is 148 eV (full-width at half maximum intensity on Mn Kα). The data reduction were carried out on-line using a software package for empirical energy dispersive spectroscopy (SPEED).

3.2.2 Trace Elements

Whole-rock trace element concentrations were determined by excimer laser ablation inductively coupled plasma mass spectrometer (ELA-ICP-MS) on fused glass samples. ELA-ICP-MS has been applied to the *in situ* determination of a wide range of trace elements in geological materials over the last few years (Loucks et al., 1995; Sylvester and Ghaderi, 1997, Sinclair et al., 1998). The UV excimer laser, as an alternative technique for sample introduction to ICP-MS, has several advantages over the Infra Red laser sampling (Perkins and Pearce, 1995). It is less dependent on the physical and chemical properties of the analysed materials, does not produce significant element fractionation and has a more predictable beam profile.

3.2.2.1 Sample Preparation: Development of a New Glass Fusion Technique for Whole-Rock Analysis by ELA-ICP-MS

Quantitative analysis of trace elements in rocks by ELA-ICP-MS requires the sample to be converted to homogenous glass prior to analyses. It has therefore been necessary to develop a new sample preparation technique for a wide range of igneous rocks to produce the homogenous glass beads required for precise and accurate analyses.

The glass method for trace element analyses by ELA-ICP-MS has several advantages over solution-nebulisation ICP-MS. Firstly, ELA-ICP-MS analysis using whole-rock glass is fast and more convenient. Secondly, refractory mineral phases, such as zircon, which are difficult to dissolve in solution, are readily dissolved in glasses. Thirdly, molecular interferences caused by oxides, as commonly encountered in solution-mode ICP-MS analysis, are negligible in ELA-ICP-MS analyses of glasses.

The new procedure involves mixing powdered whole-rock sample with lithium metaborate flux spiked with ^{169}Tm and ^{235}U. The lithium metaborate flux effectively dilutes the sample and lowers its melting temperature and the viscosity of the melt. The addition of these spikes enables correction for instrumental drift encountered during ICPMS analysis. Optimum results were achieved using a 2:1 mixture of rock powders and spiked flux, and fusing at 1200°C for 20 minutes. The high temperatures and long times of fusion may cause the loss of some volatile elements in samples.

In the final procedure for producing glass for the Kelian samples, 0.6666 g of whole-rock powder was mixed with 0.3333 g of spiked flux on a weighing paper until the powder had a uniform colour. The spiked sample was then transferred into a clean, 3 cm-wide carbon crucible and pre-heated in a Kanthal Super Rapid Furnace at 600°C for 30 minutes. Following this initial pre-heating, the carbon crucible with powder was placed in a Kanthal High Temperature Melting Furnace for pre-heating at 800°C for 5 minutes prior to fusing. After 5 minutes, the temperature was raised to 1200°C and maintained at this temperature for 20 minutes to facilitate complete fusion and homogenisation. An Ar gas flow of 2.5 litre/minute was used during both preheating (800°C) and melting (1200°C) to prevent oxidation of the samples. At the end of this sequence, the carbon crucible with molten rock was removed from the furnace and rapidly quenched into a beaker of water. The glass was dried overnight, and a 2-3 mm piece of glass shard was mounted in epoxy and polished prior to laser ICP-MS analysis. Details of the preparation procedure are given in Appendix 2. In order to test the homogeneity of glass, multiple electron microprobe (EMP) analyses of the glasses have been carried out on selected samples. The

results confirm that the glasses are homogenous within the precision of the measurements. The glasses were analysed for 37 trace elements by laser ablation ICP-MS with a precision of better than 4% for most elements. The reproducibility of ICP-MS data from multiple analyses for the least altered andesite (Nakan andesite) demonstrates the extent to which glass homogeneity has been obtained using this method (Figure 3.1).

3.2.2.2 Excimer Laser Ablation Inductively Coupled Plasma Mass Spectrometry

The Excimer Laser Ablation Inductively Coupled Plasma Mass Spectrometry (ELA-ICP-MS) system at RSES, ANU has been described by Loucks et al. (1995) and Eggins et al. (1998). A schematic diagram of the ELA-ICP-MS system is illustrated in Figure 3.2. Glass samples were ablated utilising a pulsed ArF excimer laser (Lambda Physik LPX 120I) emitting at 193nm with a nominal pulse width of 20ns and a pulse stability of $\pm$ 5%. In this study, laser sampling was carried out using a 84 micron diameter spot at a constant voltage mode of 21-23 kV with a laser output energy of 100 mJ and a repetition rate of 5 Hz. Both sample and standard discs were loaded in a translational stage in an air-tight sample cell and are viewed via a video monitor. Ablation is undertaken in Helium and both helium and argon gases are used to flush the sample cell, with a He flow rate of 300 ml/minute and Ar flow rate of 1100 ml/minute.

Data acquisition for 37 isotopes was carried out by peak hopping in pulse counting mode (3 points per peak) with a dwell time of 30 ms, obtaining data on signal intensity for each of the analysed isotopes. The glass samples were ablated for 80 seconds following a 40 second interval of background acquisition with the laser off, resulting in ~120 data scans for a penetration depth of ~40 microns (approximately 0.1 microns of material was ablated per laser pulse). The ablated materials, together with carrier gas, were transported to the ICP through a custom-made signal homogeniser. The international reference material NIST 612, a synthetic silicate glass, was used as an external calibration standard and it was analysed at the start and repeatedly measured after every a batch of 10-12 unknown samples. In addition, a second in-house standard glass, made from a Kilauea basalt (93-1487) powder spiked with 3.28 ppm ^{235}U and 109.7 ppm ^{169}Tm, was run after every 5-6 unknown samples. In order to correct intensity variations during an analytical session and temporal variations in instrument signals (instrumental drift), the ^{43}Ca peak (0.135 % of total Ca) was used as an internal standard. The Nakan andesite (Sample No.123187) was used as an additional in-house standard and was analysed in each

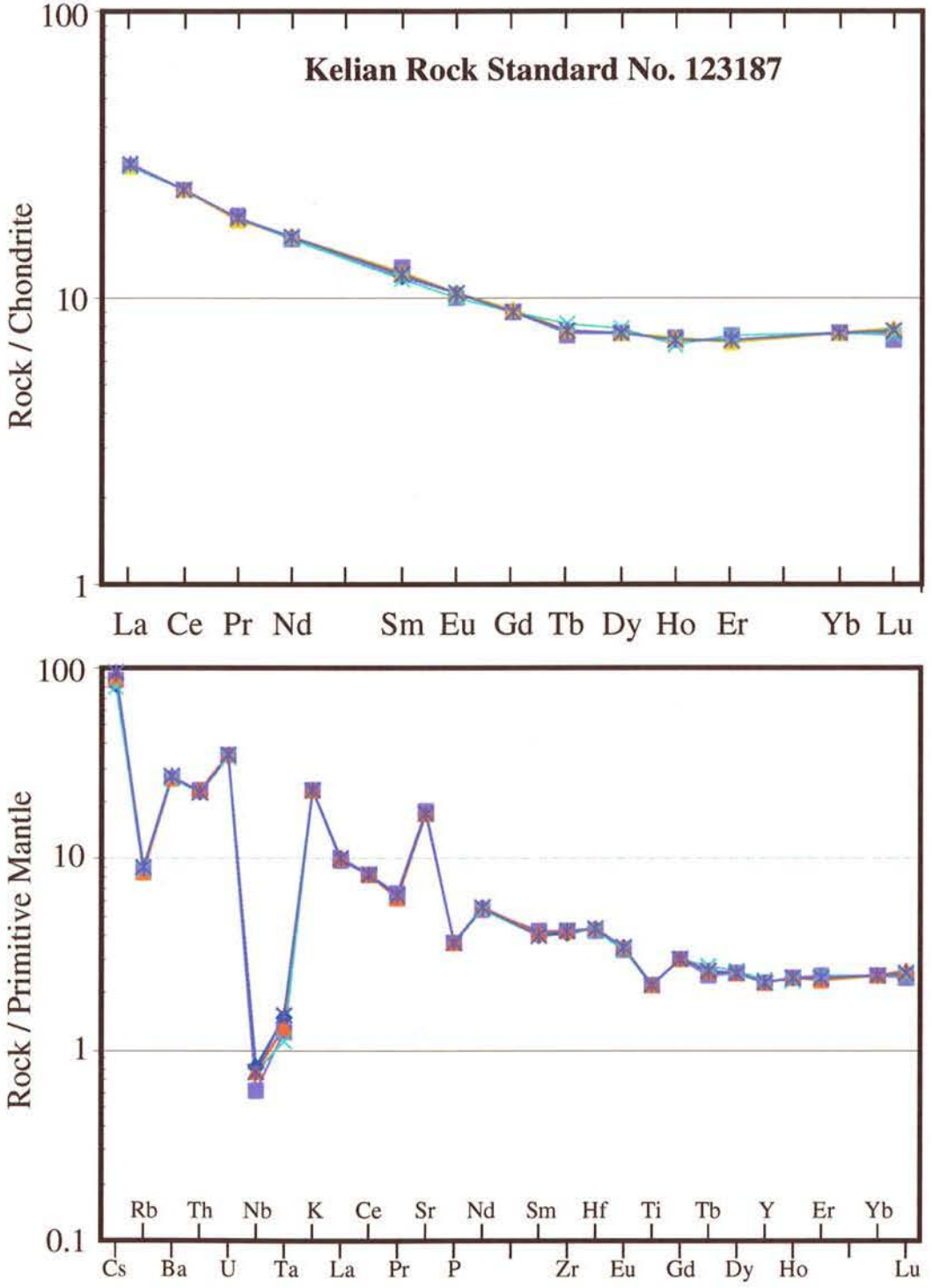

Figure 3.1 : The reproducibility of LA-ICPMS data from 5 analytical sessions using the Kelian standard sample (Nakan Andesite), showing that the glasses are homogenous to within the precision of the instrument.

analytical session, in order to monitor the quality of data. The measured isotopes and preferred values for the standards are listed in Appendix 5.

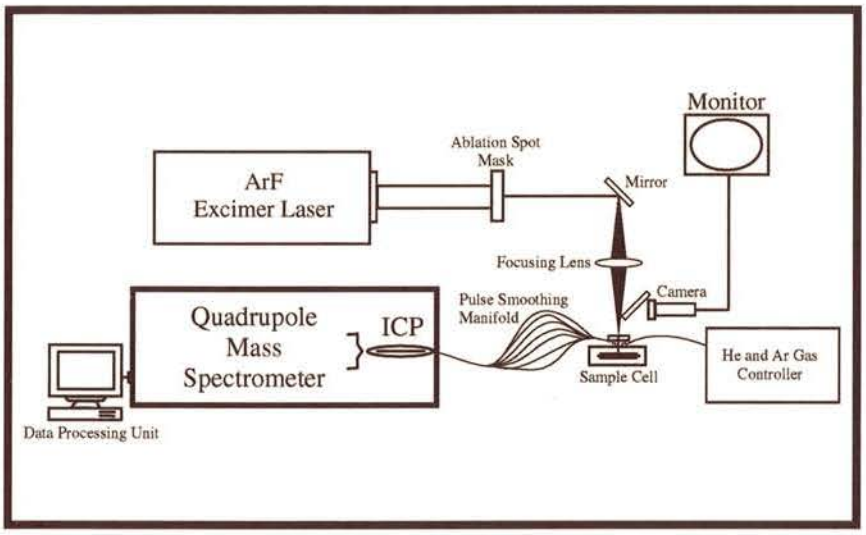

Figure 3.2: Schematic diagram of Excimer Laser Ablation Inductively Coupled-Plasma Mass Spectrometry at Research School of Earth Sciences.

3.2.2.3 Data Reduction

All data reduction was carried out off-line using a Microsoft Excel worksheet. This includes background subtraction, normalisation to Ca or Tm, correction for instrumental drift and calculation of trace element concentration. The procedure of data reduction employed in this study is modified from that described by Eggins et al. (1997, 1998).

Raw counts were recorded as counts per second (cps) data for each of ~1 second time slices by the ICP-MS computer program. Average background intensities were subtracted for the raw count rates for each isotope measured. Intensities of trace elements measured by ICP-MS were normalised to that of ^{43}Ca whose concentration has previously been determined by X-ray fluorescence methods. The element concentrations were calculated using the following formula (Sylvester and Ghaderi, 1997):

$$C_{ueu} = C_{seu} \times (I_{ueu}/I_{seu}) \times (C_{ues}/C_{ses}) / (I_{ues}/I_{ses})$$

Where : Cseu = the concentration of the internal standard element (Ca) in the unknown,

I_{ueu}/I_{seu} = the ratio in the unknown of the intensity of an isotope to be measured relative to that of an isotope of the internal standard element (^{43}Ca)

C_{ues}/C_{ses} = the ratio of concentration of element in the standard to that of the chosen internal standard element

I_{ues}/I_{ses} = the ratio in the standard of the intensity of an isotope to be measured in the unknown relative to that of the chosen isotope of the internal standard element.

A total of 137 whole-rock samples has been analysed for 37 trace elements using the ELA-ICP-MS method (Eggins, et al., 1997). The first batch of 20 samples was analysed using a HP4500 Series ICP-MS, batches 2, 3 and 4 (totally 87 samples) were analysed using a Fisons VG PlasmaQuad II+ ICP-MS, and the last batch (30 samples) was analysed using an Agilent 7500s ICP-MS.

3.3 Igneous Suites

The drill core and outcrop samples of intrusive and extrusive rocks were collected from the Kelian mine and surrounding prospects (Magerang-Imang and Nakan) as well as the Muyup, Ritan, Batu Utul, Han and Plata prospects (Plate 3.1). Petrographic and chemical analyses of the igneous suites indicate fine to medium grained textures with compositions that range from basaltic andesite, through andesite to rhyolite. Although most samples show some degree of alteration, a suite of 50 samples which show minimal disturbance to their whole-rock chemical composition has been picked as the least altered samples. In the these samples, original igneous textures are well preserved, phenocrysts of plagioclase, hornblende and pyroxene exhibit only slight alteration along rims and fractures, and plagioclase twins are clearly visible (Plate 3.2). The whole-rock chemical compositions are listed in Appendix 3.

The Kelian mine andesites (i.e. *Central Andesite, Eastern Andesite and Tepu Andesite*) have been variously altered, but there are few samples from the southeastern area (Tepu) that show little alteration (Plate 3.2). The Tepu Andesite is medium-grained, porphyritic and contains plagioclase, hornblende, minor K-feldspar and rare pyroxene phenocrysts within a fine-grained, altered and devitrified groundmass. The phenocryts are partially altered to sericite and chlorite. This mineral mode is similar to that of the Central Andesite.

The andesite porphyries that are found in the eastern part of Magerang-Imang and in drillholes under basalt in the southern area show very little alteration. The andesite has a medium-grained, porphyritic texture, formed mainly by plagioclase and hornblende,

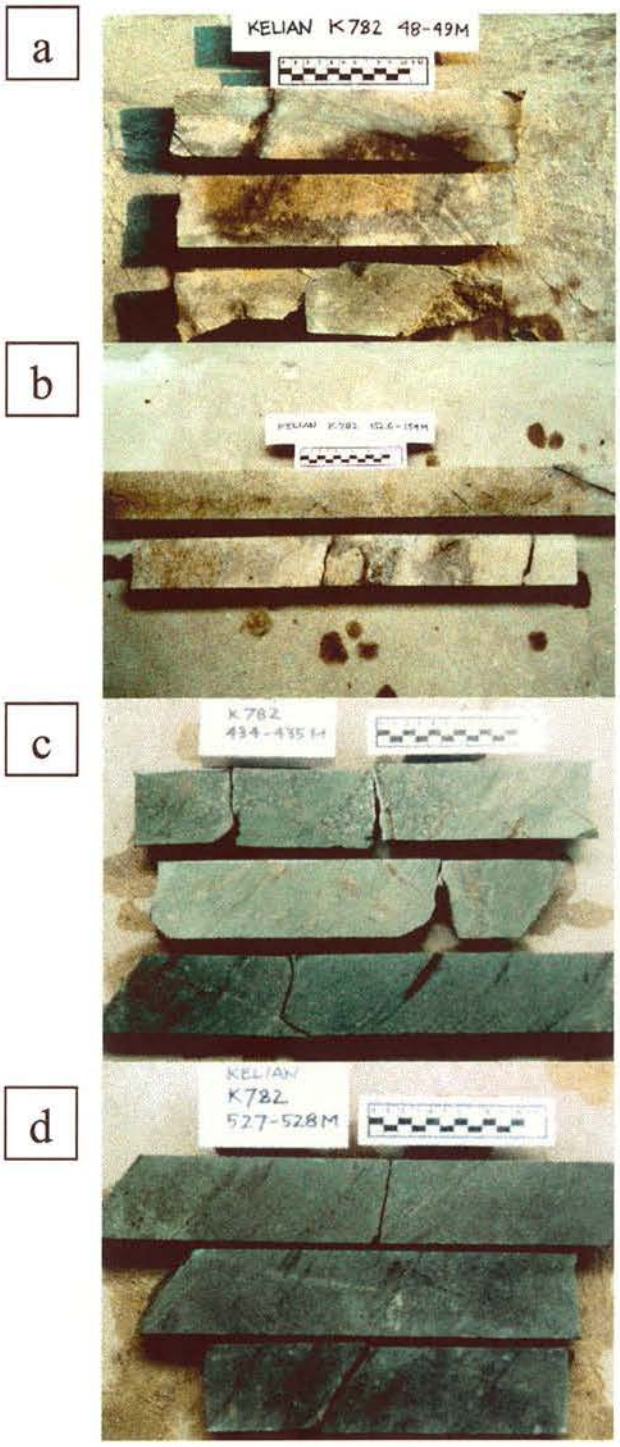

Plate 3.1: Central Andesite showing phyllic (Stage 2) alteration; quartz, sericite and calcite replacement minerals (a). Phyllic altered andesite; quartz, sericite and carbonate replacement minerals, brecciated in some places (b). Central Andesite showing propylitic (Stage 1) alteration overprinted by phyllic (Stage3) alteration. Carbonate and base-metal veinlets contains gold as indicated from the elevated gold grade (3 ppm Au) in this section (c). Central Andesite showing prophylitic alteration consisting of quartz, chlorite and minor sericite assemblage. A few calcite veinlets occur in places (d)

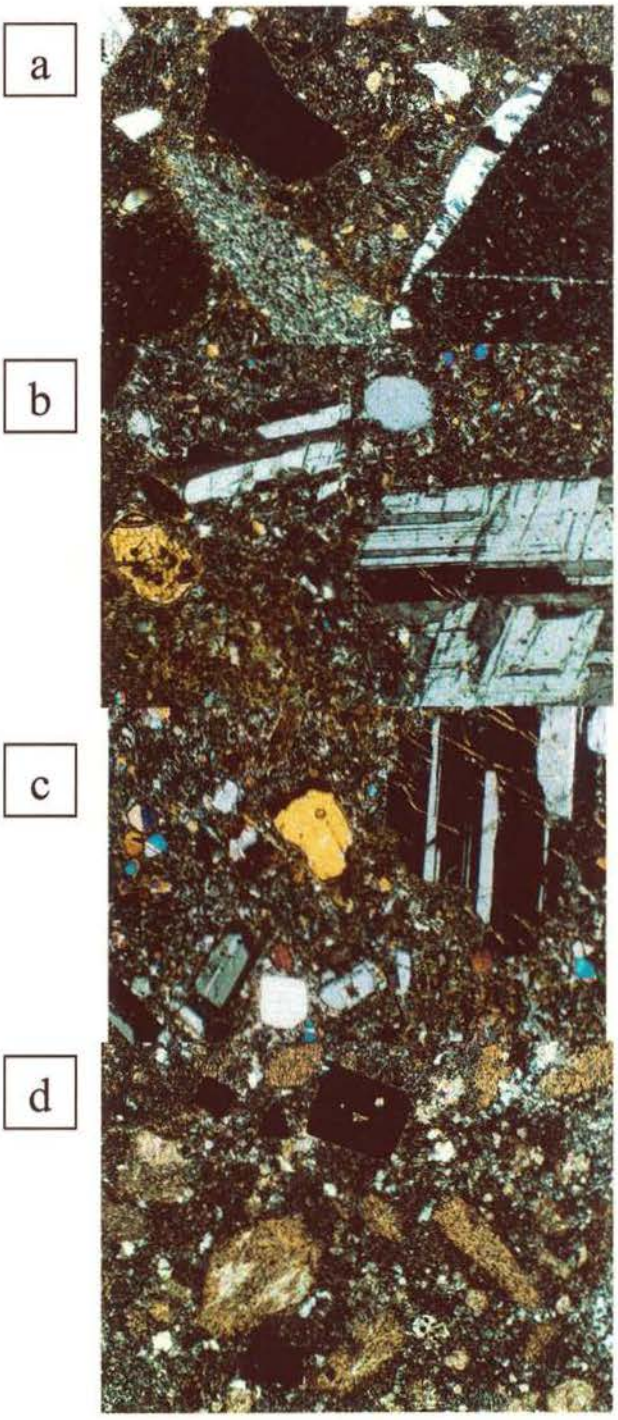

Plate 3.2: Fragment of quartz, siltstone and volcanic rocks in silty matrix of the Runcing muddy breccia. Sample 123221 G Runcing 1110RL (a). Slightly altered Magerang andesite showing phenocrysts of plagioclase, hornblende and pyroxene set in a fine grained feldspar matrix (b). Slightly altered Magerang andesite showing plagioclase, hornblende and pyroxene as phenocrysts set in a fine sericitised feldspar matrix (c). Phyllic altered andesite showing replacement alteration of sericite, carbonate and pyrite (d). Field of view 2.6 x 1.8 mm

with rare pyroxene phenocrysts set in a fine-grained, holocrystalline matrix of feldspar and mafic minerals (Plate 3.2). The phenocrysts and groundmass have undergone some replacement along cracks and grain boundaries to sericite, chlorite and carbonate.

The least altered Nakan andesite has a medium-grained, porphyritic texture and is characterised by plagioclase and pyroxene phenocrysts in fine-grained feldspar and mafic groundmass. Clinopyroxene and plagioclase phenocrysts are slightly altered to sericite, chlorite and calcite. Rare small grains of hornblende are slightly altered to chlorite. The fine-grained groundmass has been partially replaced by sericite, chlorite and carbonate.

The Han andesite (sample No.1103) is a weakly altered porphyry exposed on the Han river and is chiefly composed of plagioclase and minor pyroxene phenocrysts set in a fine grained quartz-feldspathic groundmass. The phenocryst and groundmass are slightly altered to sericite, chlorite and calcite.

The Plata dacite (sample No. 1121), collected from the drillcore of the Plata prospect (Chapter 2, Figure 2.4), shows plagioclase and hornblende phenocrysts within a fine-grained quartz, feldspar and mafic groundmass. The feldspar and mafic minerals have been slightly altered to sericite and chlorite.

3.4 Major Element Chemistry

3.4.1 Classification of rock types

Major element compositions were normalised to 100 wt% on a volatile-free basis to allow comparison of variably altered samples. Only the least altered samples were used for classifying the igneous rocks. On the basis of the FeO*/Mg - SiO_2 variation diagram (Miyashiro, 1974) all the igneous samples follow the calc-alkaline trend with the exception of the Ritan andesite (Sample 123301), which plots in the tholeiite field (Figure 3.3a). Within the calc-alkaline field, the Kelian mine andesites (Tepu Andesite) show a distinctive trend as indicated by a higher ratio of FeO*/MgO (1.9-2.1), compared to the Magerang-Imang and Nakan suites (FeO*/MgO = 0.8-1.5), over a range of 56 to 63 wt% SiO_2.

Igneous samples, which show fine to medium grained textures, have been classified using the K_2O-SiO_2 and total alkali silica (TAS) criteria (Le Maitre et al., 1989). On the TAS diagram the igneous rocks range in composition from basaltic andesite, through andesite and dacite to rhyolite. The Kelian suite plots mostly at the boundary of

low K and medium K andesite over a range in silica from 56 to 63 wt%; the volcanic suite of Muyup is medium K dacite to rhyolite, while the Ritan volcanic suite is grouped into low to medium K andesite and low K dacite to rhyolite (Figures 3.3b and 3.3c).

3.4.2 Variation of major element composition

The least-altered samples show well-defined, curvi-linear trends when major and minor elements are plotted against SiO_2 (Figures 3.4a to 3.4j), with MgO, Fe_2O_3, TiO_2 and CaO decreasing and Na_2O, K_2O and P_2O_5 increasing with increasing SiO_2. The Magerang-Imang suite has a slightly wider range of SiO_2 (56.1-64.0 wt%) than the Nakan (57.6-63.2 wt% SiO_2). Both the Magerang-Imang and Nakan andesites display increasing Al_2O_3 concentrations with increasing SiO_2. The Tepu and Ritan andesites have higher TiO_2 (0.58-0.70 wt%) and Al_2O_3 (18.1 wt%) compared to the Magerang-Imang (0.42-0.56% TiO_2 ; 15.5-17.5 wt% Al_2O_3) and Nakan (0.40-0.49 wt% TiO_2 ; 14.5-16.5 wt% Al_2O_3) andesites. In contrast, within the range of 56-62 wt% SiO_2, the Magerang-Imang and Nakan andesites have relatively high MgO (4.5-8.1 wt%) compared to the Tepu (3.1-3.5 wt%) and Ritan andesites (2.7 wt%). These differences result in two different trends for the Magerang-Imang - Nakan and the Tepu - Ritan suites, as shown in the Harker diagrams (Figures 3.4a, c and d). However, there are no distinctive variations for the other major elements between the Kelian (Tepu) igneous suites from the Kelian (Tepu) and suites from other regions.

The effects of hydrothermal alteration on major elements of the Kelian mine andesites can be assessed by comparing the chemistry of the Tepu least altered andesite with the samples from the Kelian mine that have undergone different intensities of alteration (Figures 3.5a to 3.5i). In general, samples that have undergone low-grade propylitic alteration have element concentrations that are closest to the concentrations of the Tepu least altered andesites and show less dispersion than samples that have undergone higher grade phyllic and argillic alteration. Propylitic altered samples show no evidence of Ti, Al, Fe, Ca, Mg or P oxide mobility. Data for these elements plot in a tight cluster on Harker variation diagrams, close to the Tepu least altered andesites. On the other hand, Na_2O decreased during propylitic alteration, in association with the break down of feldspar, and K_2O and MnO increased. As the intensity of alteration increases from propylitic through phyllic to argillic alteration, the mobile elements show increasing dispersion. Calcium, Na and Mg oxides show variable depletion and Fe, K and Mn oxides

show variable enrichment. Phosphor, Al and Ti oxides appear to be immobile, even in the most highly altered samples.

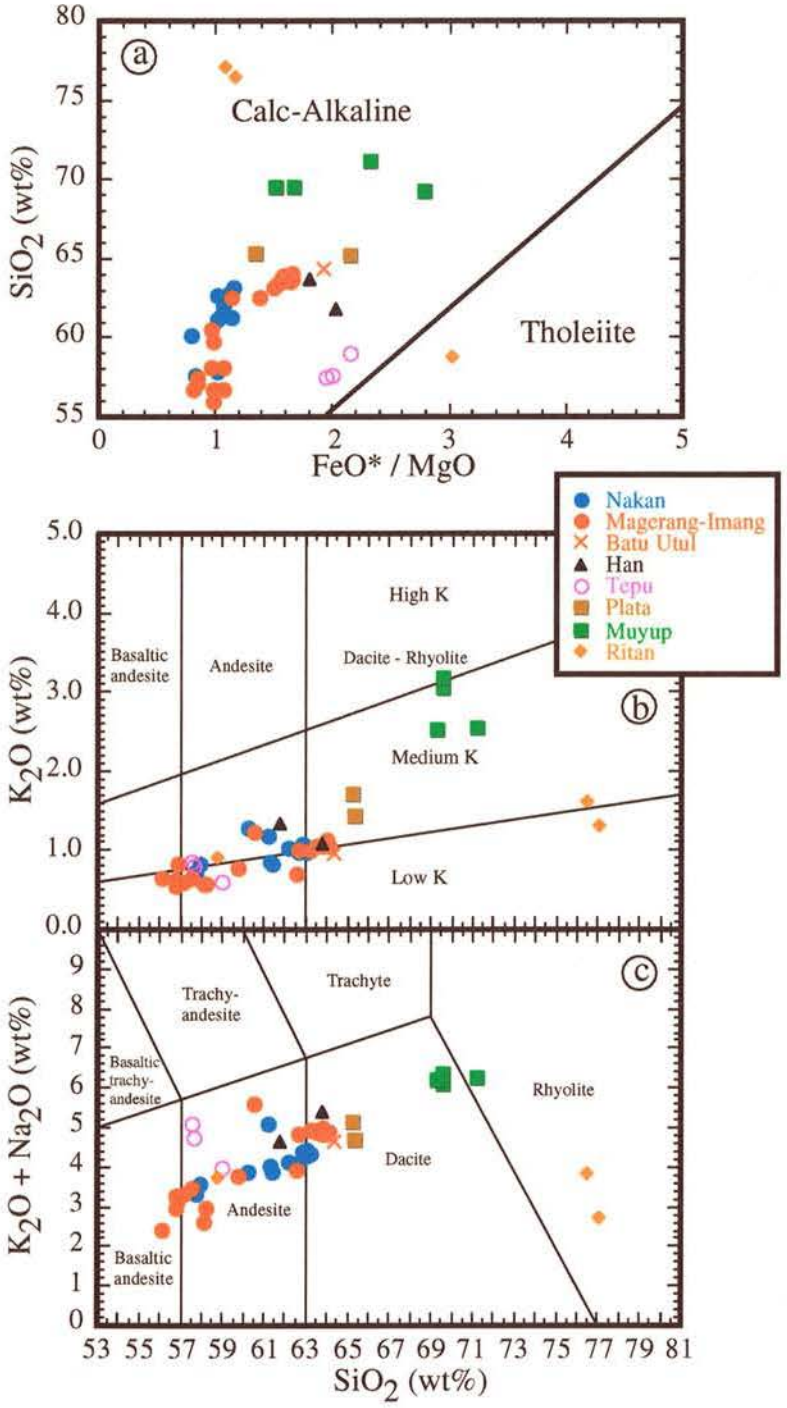

Figure 3.3: Rock classification for the Kelian Igneous Complex and regional prospects [after Miyashiro, 1974 (a) and Le Maitre et al., 1989 (b and c)].

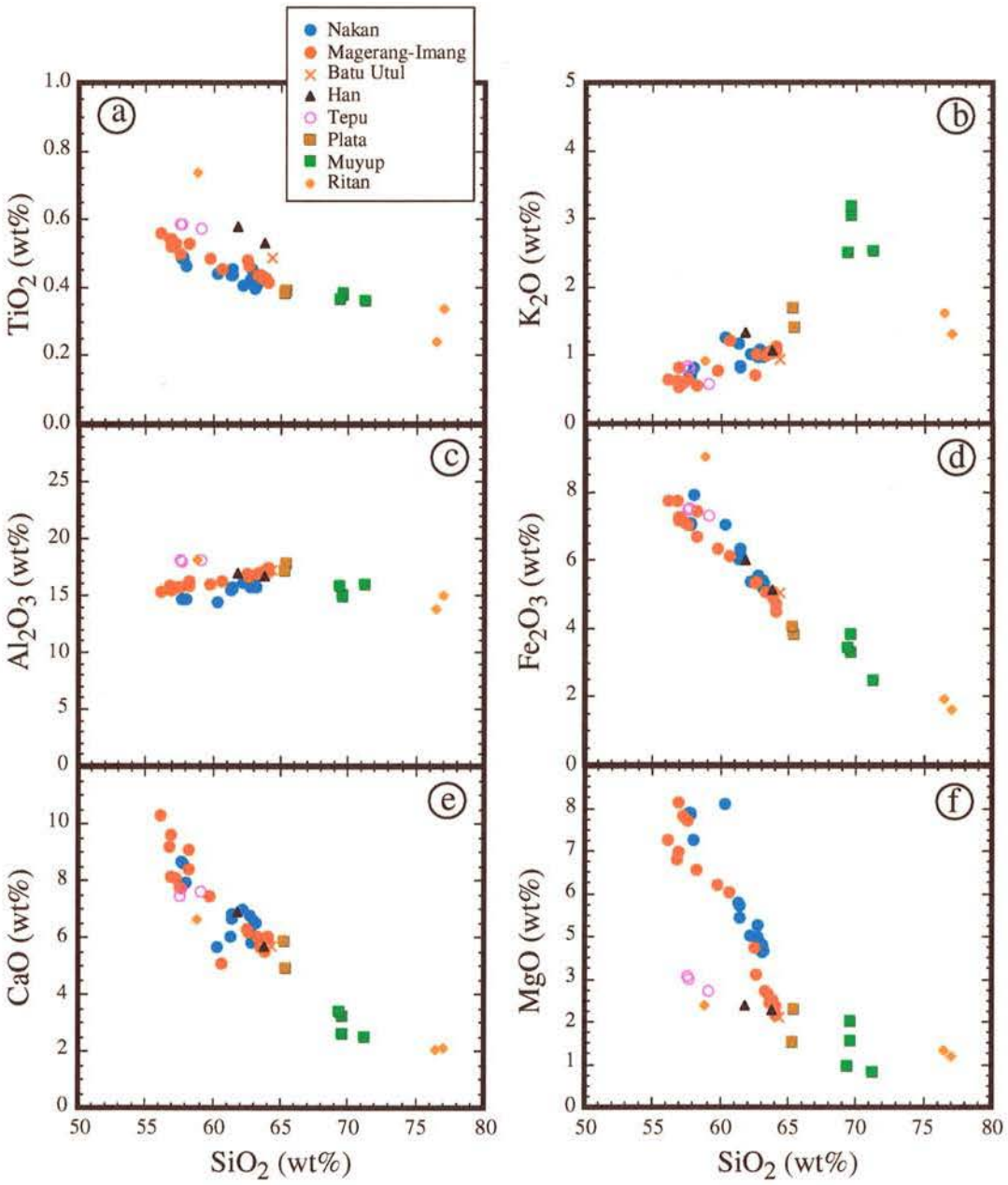

Figure 3.4 (a-f) : Harker variation diagrams for the least altered rocks from the Kelian Igneous Complex and regional prospects.

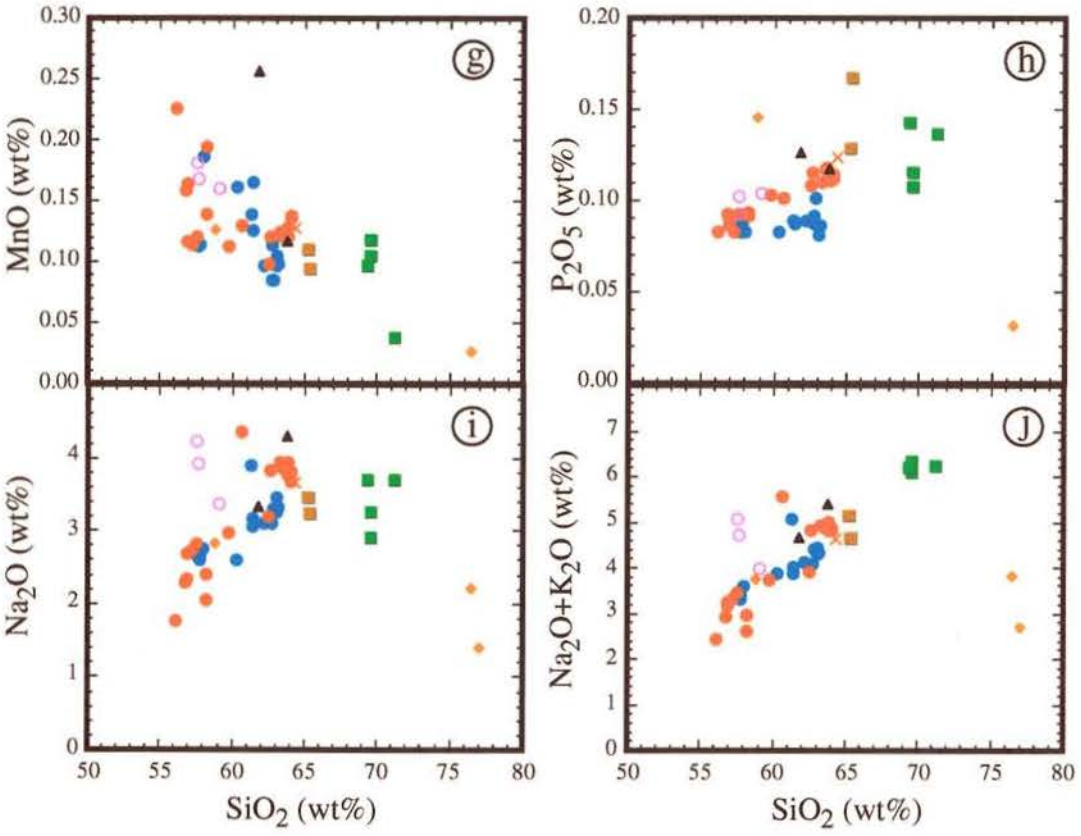

Figure 3.4 (g-j) : Harker variation diagrams for the least altered rocks from the Kelian Igneous Complex and regional prospects.

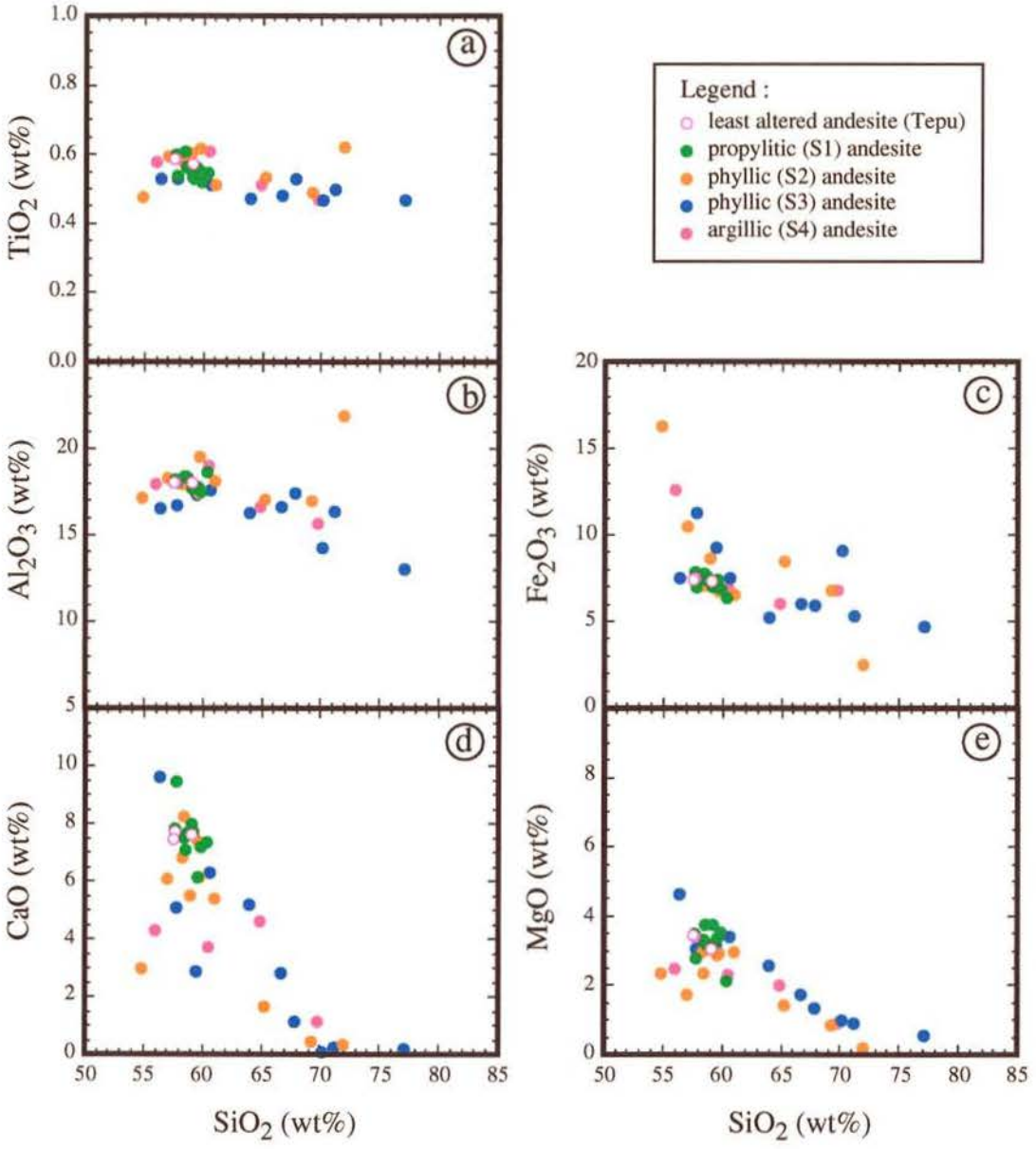

Figure 3.5 (a-e) : Harker variation diagrams for the intrusive andesites from the Kelian mine area.

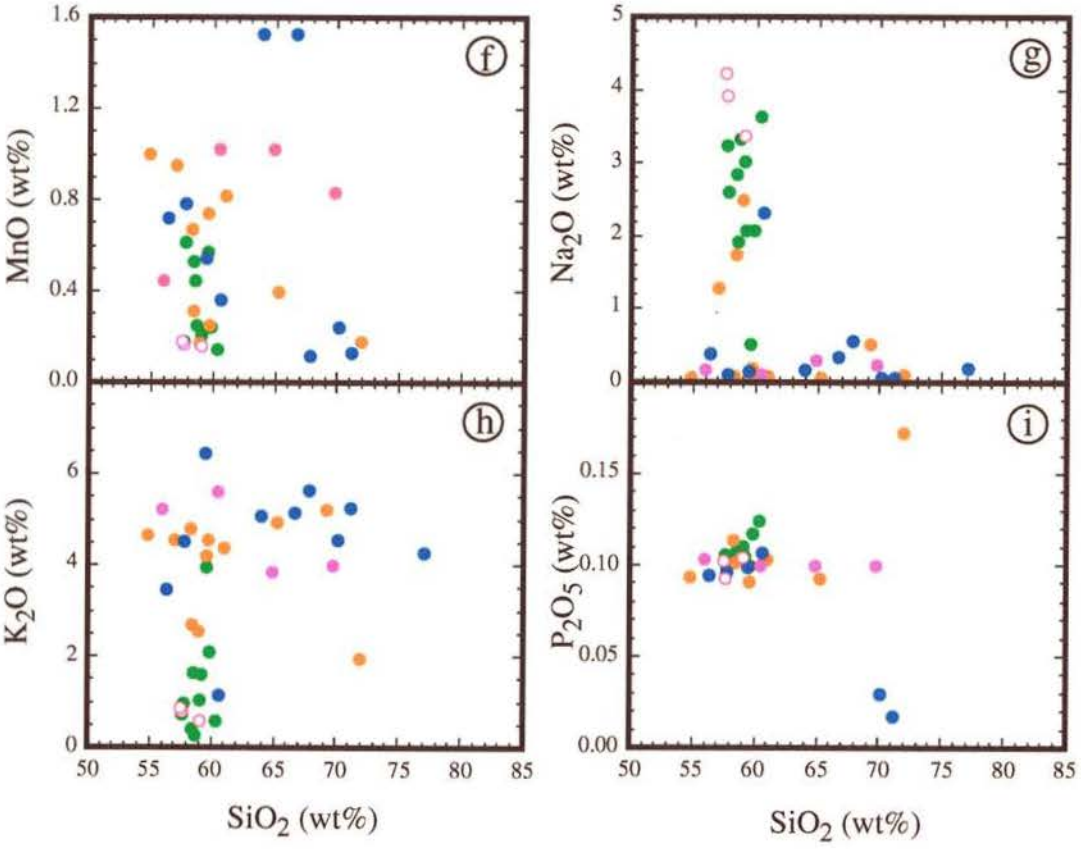

Figure 3.5 (f-i) : Harker variation diagrams for the intrusive andesites from the Kelian mine area. Symbols as in Figure 3.5 (a-e).

3.4 Trace Element Chemistry

The trace element concentrations of the least altered samples indicate that the Kelian and the other suites cluster in the field of destructive plate margin basalt on a Hf-Th-Ta diagram (Figure 3.6) and within the field of volcanic arc related magmatism on plots of Nb-Zr-Y and plots of Ba/La against La/Sm , consistent with their calc-alkaline origin (Figures 3.7 and 3.8).

The geochemistry of the least altered rocks from the Kelian Igneous Complex and regional prospects is compared using variation diagrams of trace elements versus SiO_2 (Figures 3.9a to 3.9x). In the Magerang-Imang suite, highly incompatible elements such as Th, U, Zr, Hf, Rb, Sr and Ba increase with increasing SiO_2, resulting in a distinctive, positive trend. Light rare earth elements (LREE), such as La, Ce and Pr also increase with increasing SiO_2 but weakly incompatible REE show no increase and some, such as Sm, Ho and Y actually decrease. In the Nakan suite, the REE display similar trends as those in the Magerang-Imang suite, but the trend of incompatible elements, such as U, Th, Zr, Hf does not change significantly with increasing SiO_2. Compatible elements such as V, Sc and Cr rapidly decrease with increasing SiO_2. Chromium is depleted in the Tepu, Han and Ritan andesites, but it is relatively high in the Magerang-Imang and Nakan andesites within the similar range of SiO_2, indicating different trends of magmatic differentiation. Base metal abundances including Cu, Pb, Zn, W and Mo are highly variable in the least altered samples and display scattered plots, probably due to their low concentrations in the samples.

The Kelian Igneous Complex, including the intrusive andesite and rhyolite, have a wide range of silica contents (50-80 wt% SiO_2) and have undergone variable and often intense alteration so that many major elements, including SiO_2, Na_2O and K_2O, were extensively mobilised during phyllic replacement and vein formation (stages 2 and 3). It is therefore not possible to use SiO_2 as an index of differentiation for the Kelian suite of similar age, chemistry and petrology. However, similar rock sequences occur in the Tepu, Nakan and Magerang–Imang regions and show minimal disturbance to their whole-rock chemical composition and therefore are suitable for detailed geochemical study. In the least-altered samples of Magerang-Imang, highly incompatible elements, such as U and Th correlate well with SiO_2 (Figures 3.9m and 3.9n). Because Th is much less mobile

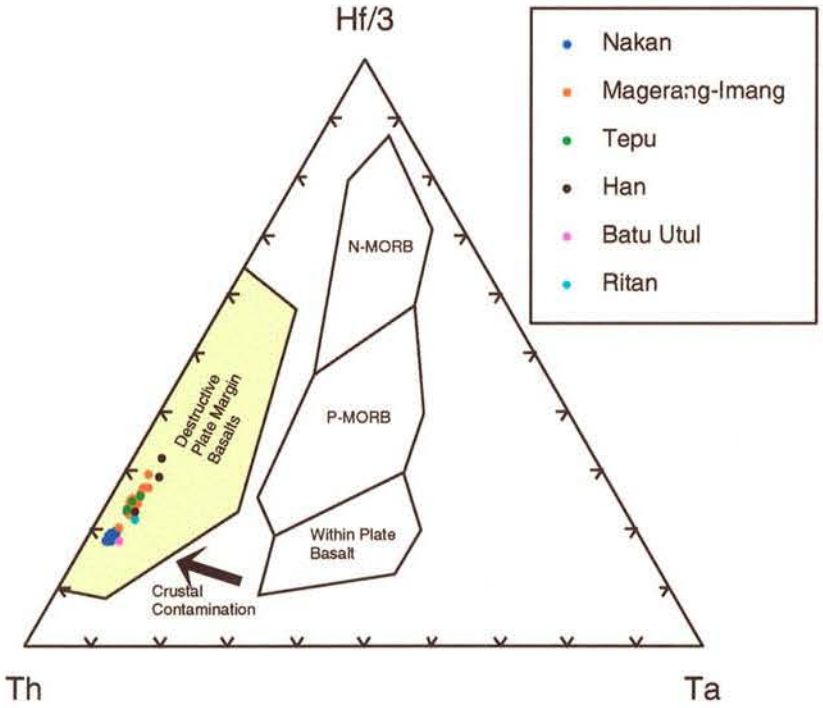

Figure 3.6 : Hf/3-Th-Ta tectonomagmatic diagram for the igneous suites of the Kelian Regional and Ritan areas (after Wood et al., 1979)

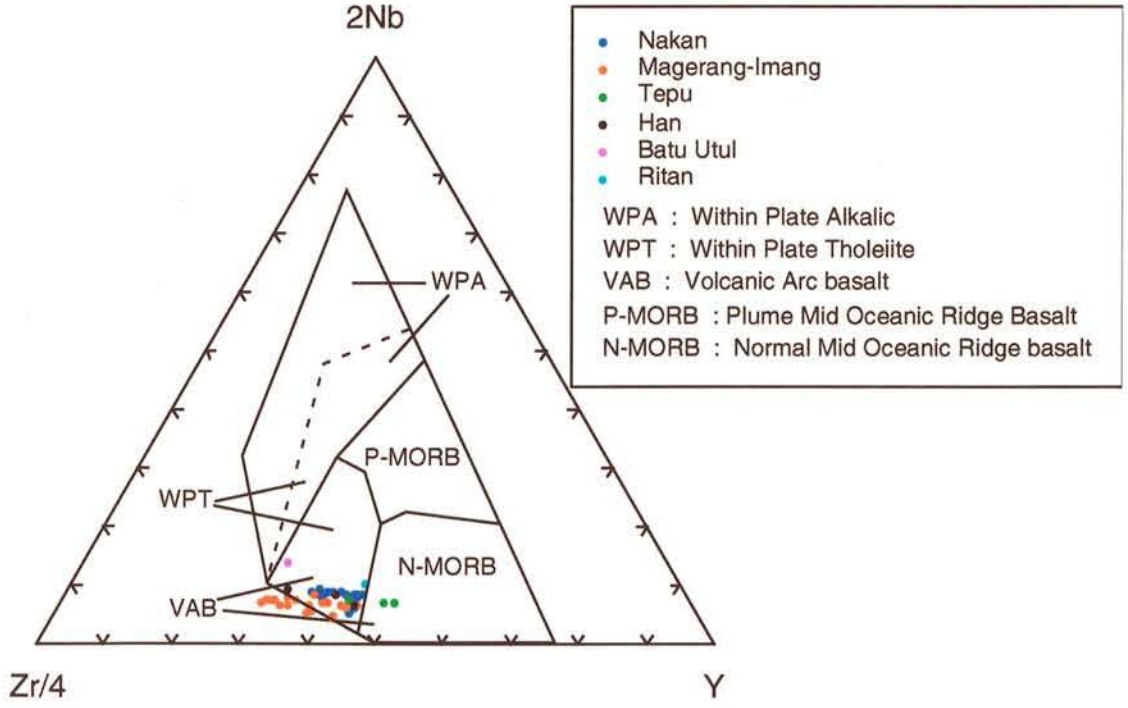

Figure 3.7 : 2Nb-Zr/4-Y tectonomagmatic diagram for the igneous suites of the Kelian Regional and Ritan areas (after Meschede, 1986).

than SiO_2 during hydrothermal alteration, it has been used as monitor of fractionation for the altered samples from the Kelian mine.

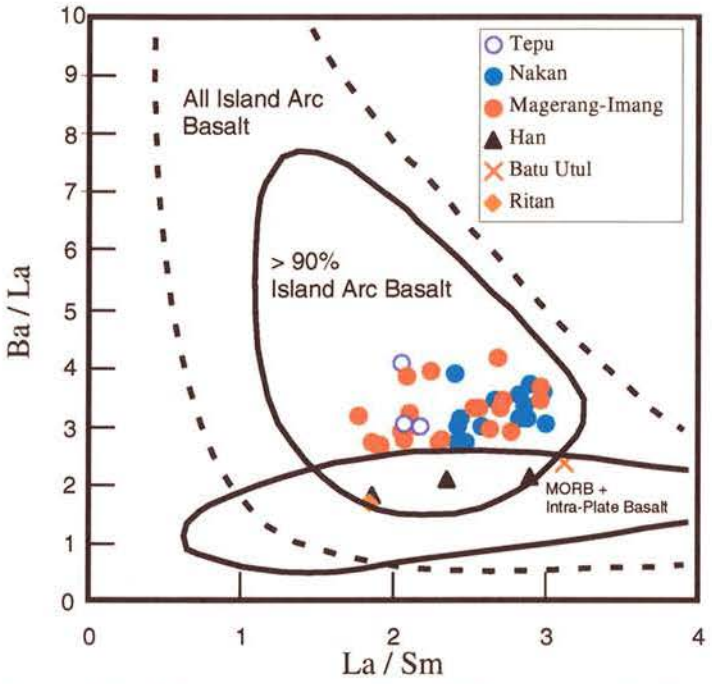

Figure 3.8: Chondrite normalised Ba/La versus La/Sm for the least altered rocks from the Kelian Igneous Complex and regional prospects (after Perfit et al., 1980; Arculus and Powell, 1986).

In the least-altered samples from Magerang-Imang, incompatible, immobile elements, such as U, Zr, Hf, Nb, Ta and light REE, increase with increasing Th concentration (Figure 3.10a to 3.10f). In the Kelian mine altered samples, these immobile elements consistently increase with increasing differentiation as shown by a positive trend, similar to that of the least altered samples. The data are more scattered in the highly altered andesite from the mine area suggesting that alteration has produced some mobility for the elements which are normally regarded as immobile (Figures 3.8a to 3.8p). Strontium and Eu have been removed during feldspar alteration, whereas Rb and Cs have been added during phyllic to argillic alteration.

In order to compare the REE patterns between rock suites and alteration types, the REE compositions were chondrite normalised using the recommended values from McDonough and Sun (1995). The chondrite normalised REE patterns in the least altered andesites of the Nakan, Magerang-Imang and Kelian mine (Tepu) regions display a concave up, light REE enriched array from La to Lu (Figures 3.11a to 3.11c).

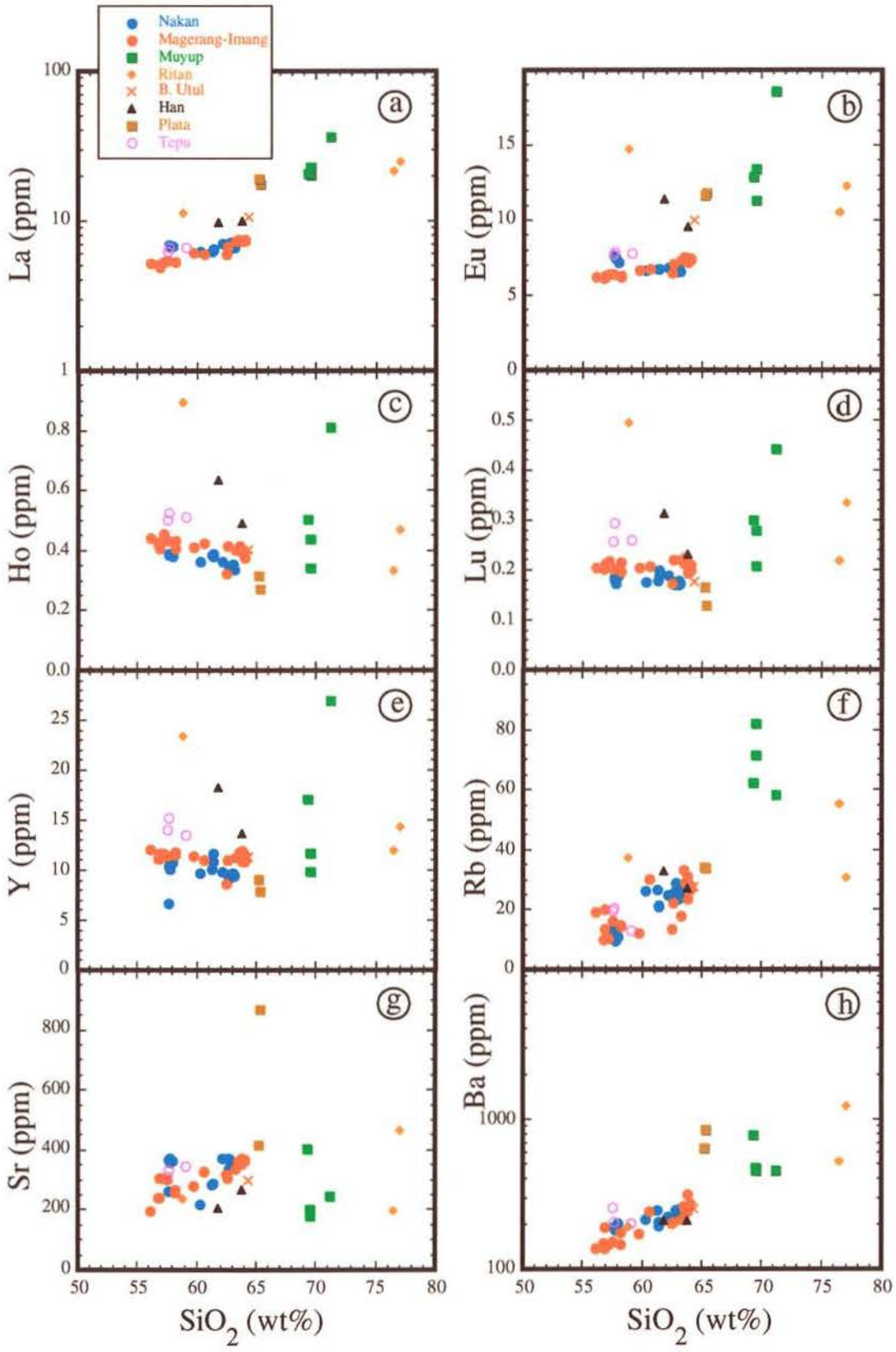

Figure 3.9 (a-h) : Variation diagrams of REE, Y, Rb, Sr and Ba vs SiO_2 for the least altered rocks from the Kelian Igneous Complex and regional prospects.

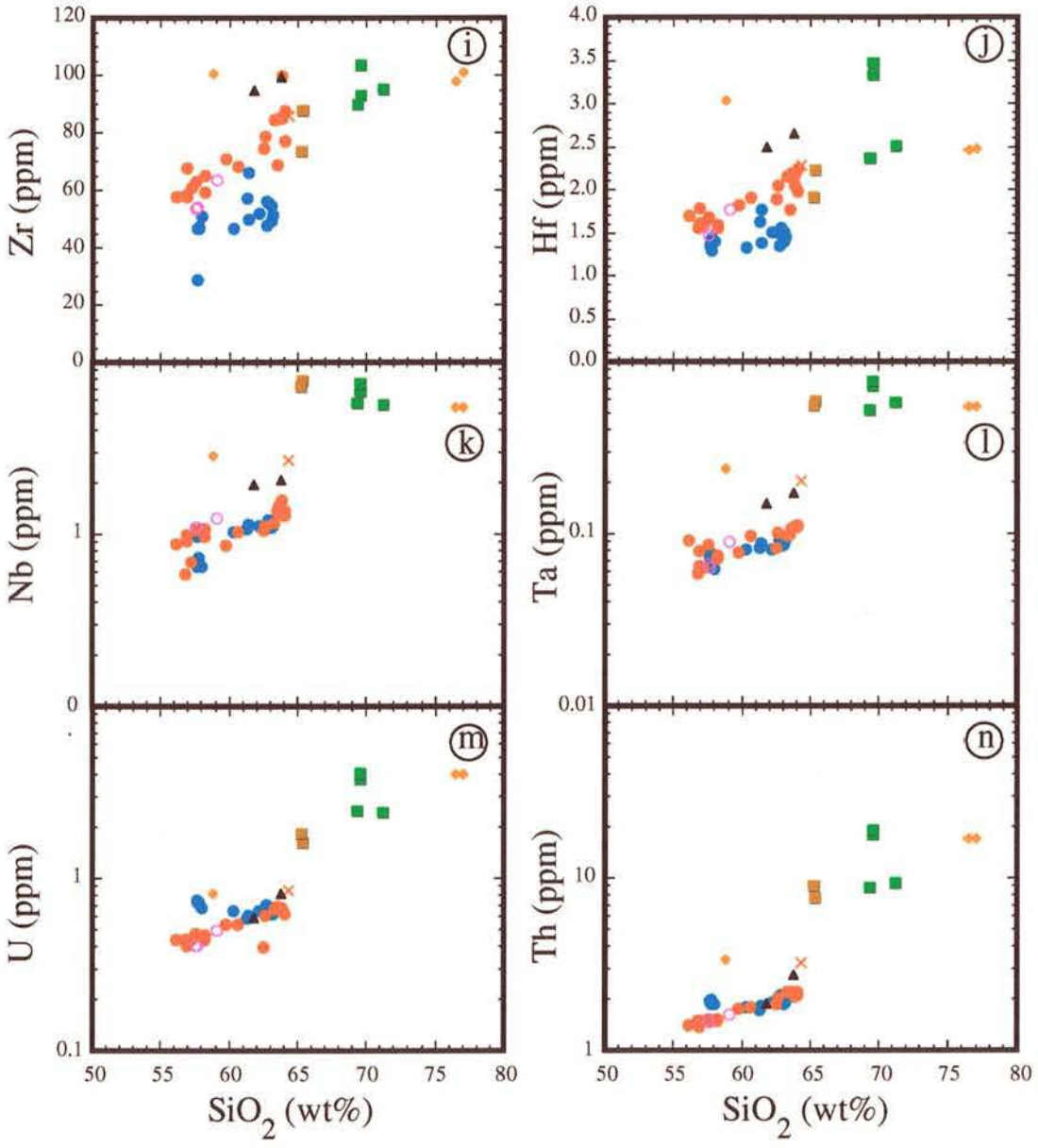

Figure 3.9 (i-n) : Variation diagrams of incompatible elements vs SiO_2 for the least altered rocks from the Kelian Igneous Complex and regional prospects. Symbols as in Figure 3.9 (a-h).

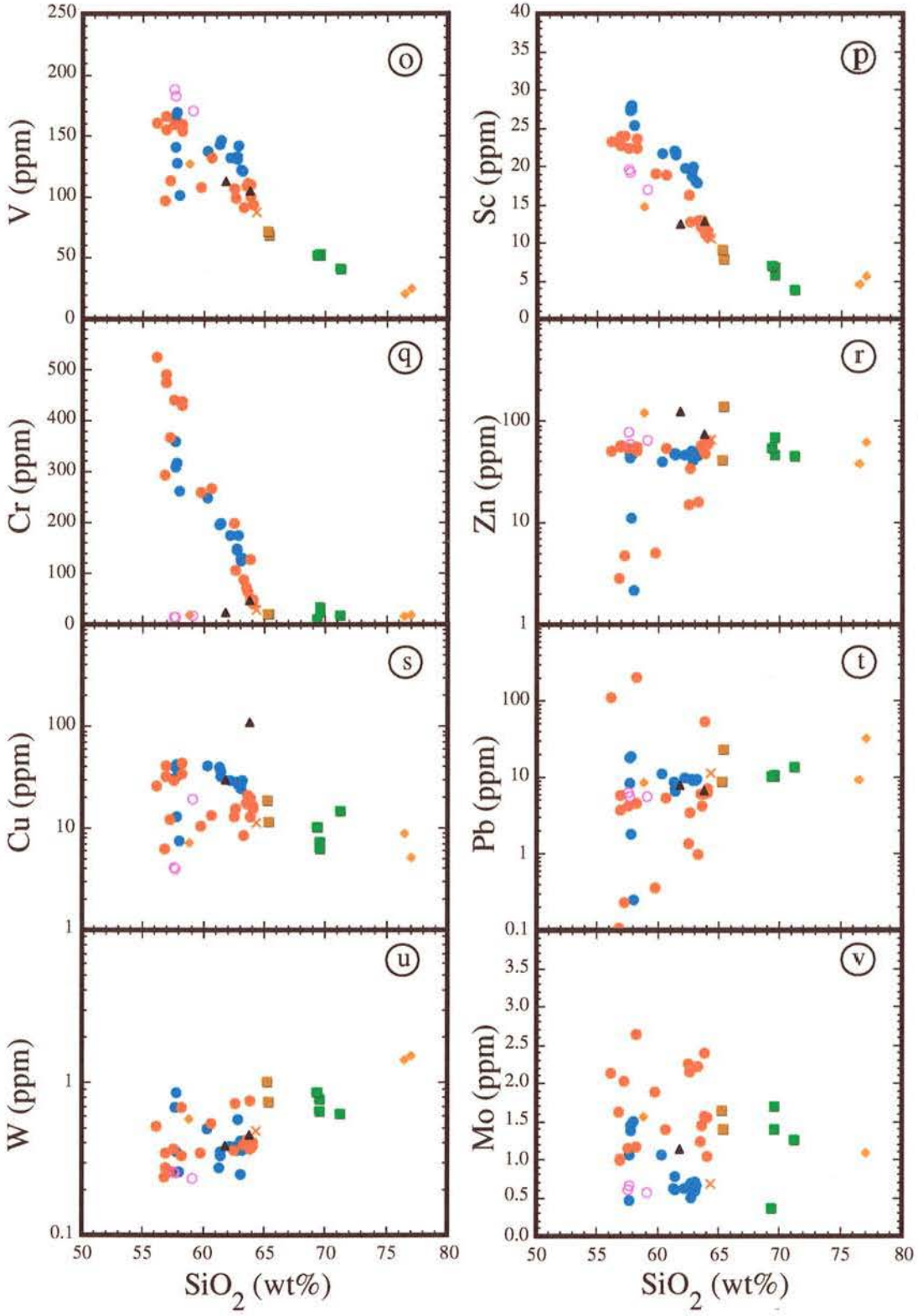

Figure 3.9 (o-v) : Variation diagrams of metals vs SiO_2 for the least altered rocks from the Kelian Igneous Complex and regional prospects. Symbols as in Figure 3.9 (a-h).

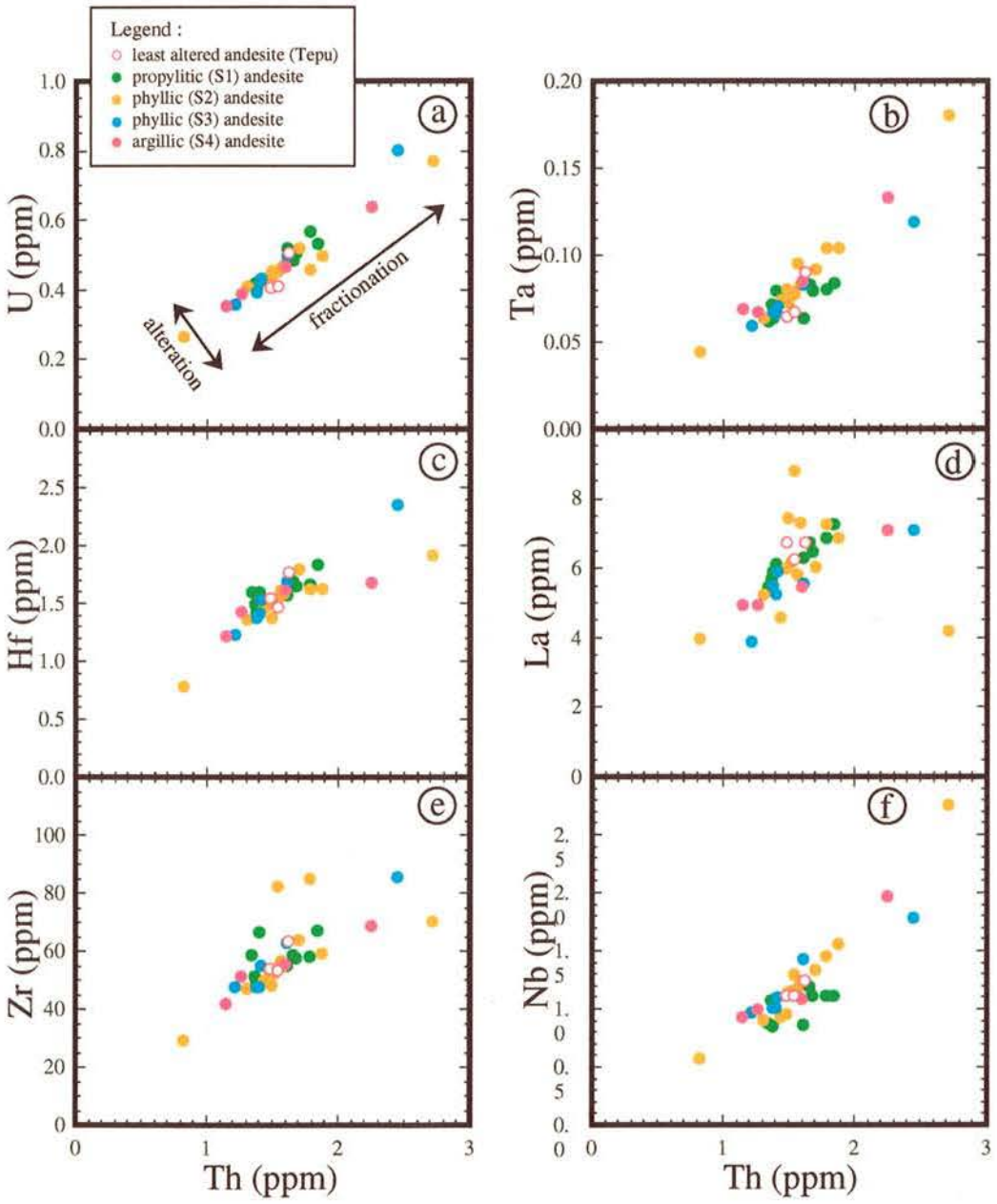

Figure 3.10 (a-f) : Variation diagrams of immobile elements versus Th for the Kelian mine altered andesites. The Tepu least altered samples are shown for comparison.

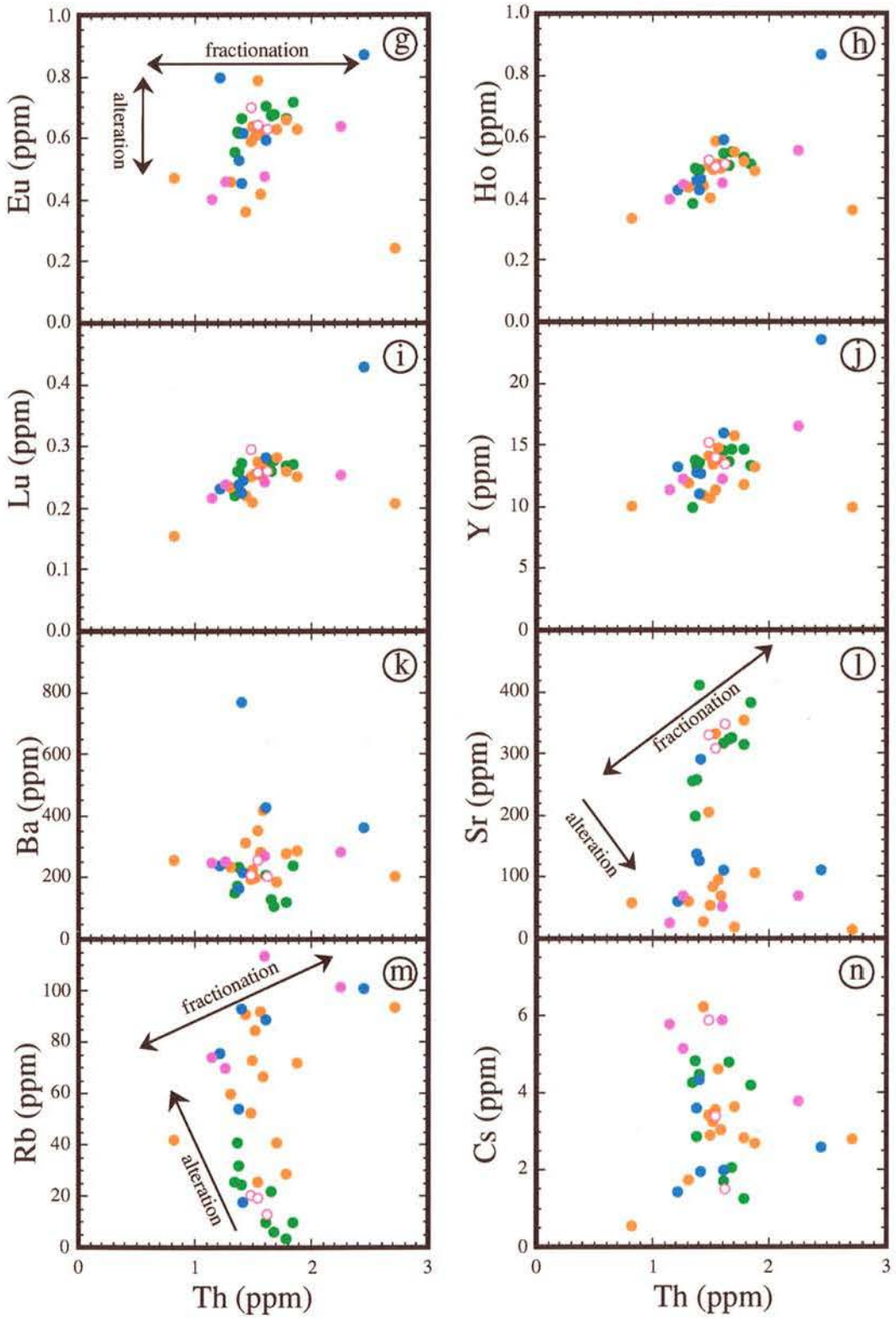

Figure 3.10 (g-n) : Variation diagrams of mobile elements versus Th for the Kelian mine altered andesites. The Tepu least altered samples are shown for comparison. Symbols as in Fig. 3.10 (a-f).

The concentrations vary consistently among these suites suggesting a genetic relation possibly through fractional crystallisation. In contrast, the REE abundance in the felsic volcanics of Batu Utul, Han, Plata, Muyup and Ritan (Figures 3.11d and 3.11f) exhibit a more curved, coherent array showing greater enrichment in light REE and depletion in heavy REE. In propylitic and phyllic altered andesite the REE, with the exception of Eu, do not appear to be affected by hydrothermal alteration and continue to form a coherent array (Figures 3.12a and 3.12b and 3.13a). Phyllic altered andesite and rhyolite show a depletion in Eu concentrations probably due to plagioclase alteration. Europium is also slightly depleted in andesite which has undergone Stage-3 phyllic (sericite-carbonate-base metal) and Stage-4 argillic (kaolinite) alteration, except for one sample from the ore zone that shows a positive Eu anomaly (Figures 3.12c and 3.12d). Strongly mineralised samples from Stage-3 phyllic andesites show an increase in light REE, relative to heavy REE suggesting that these elements may have been mobilised by the hydrothermal fluids (Figure 3.12c). Similar effects of hydrothermal alteration are also observed in the altered igneous samples from the other regional prospects (Figure 3.13).

Incompatible trace element concentrations were primitive mantle normalised (Sun and McDonough, 1989) in order to interpret the trace element characteristics and to provide a reference frame in which the concentrations in the different igneous suites can be compared. In general, primitive mantle-normalised element concentrations for the least altered andesite display patterns showing enrichment in the large ion lithophile elements (LILE), particularly Ba, K, U, Th and Sr relative to the heavy REE. In the least altered andesites, all the elements form a coherent array (Figures 3.14a to 3.14f.). The enrichment in Cs, Rb, Ba, K and Th and depletion in Nb, Ta and Ti are characteristic of calc-alkaline arc magmas (Tatsumi et al., 1986; McCulloch and Gamble, 1991; Hawkesworth et al., 1994). However, the andesites are also characterised by pronounced positive anomalies of Zr and Hf, which are less common in calc-alkaline arc magmas.

In propylitic and phyllic altered andesites, immobile elements such as Ta, Nb, Y, Ti and the REE are not affected by alteration and continue to form a coherent array. In contrast, the concentrations of elements such as Rb, Sr and K, which are regarded as mobile during hydrothermal alteration exhibit large variations depending on the type of alteration. Andesite suites that have undergone propylitic alteration are variably depleted in K and Ba and enriched in Cs and Rb (Figures 3.15a and 3.16a), whereas andesites with phyllic alteration show a significant increase in K and Rb, and depletion in Sr and possibly Ti. (Figures 3.15b-3.15f and 3.16b).

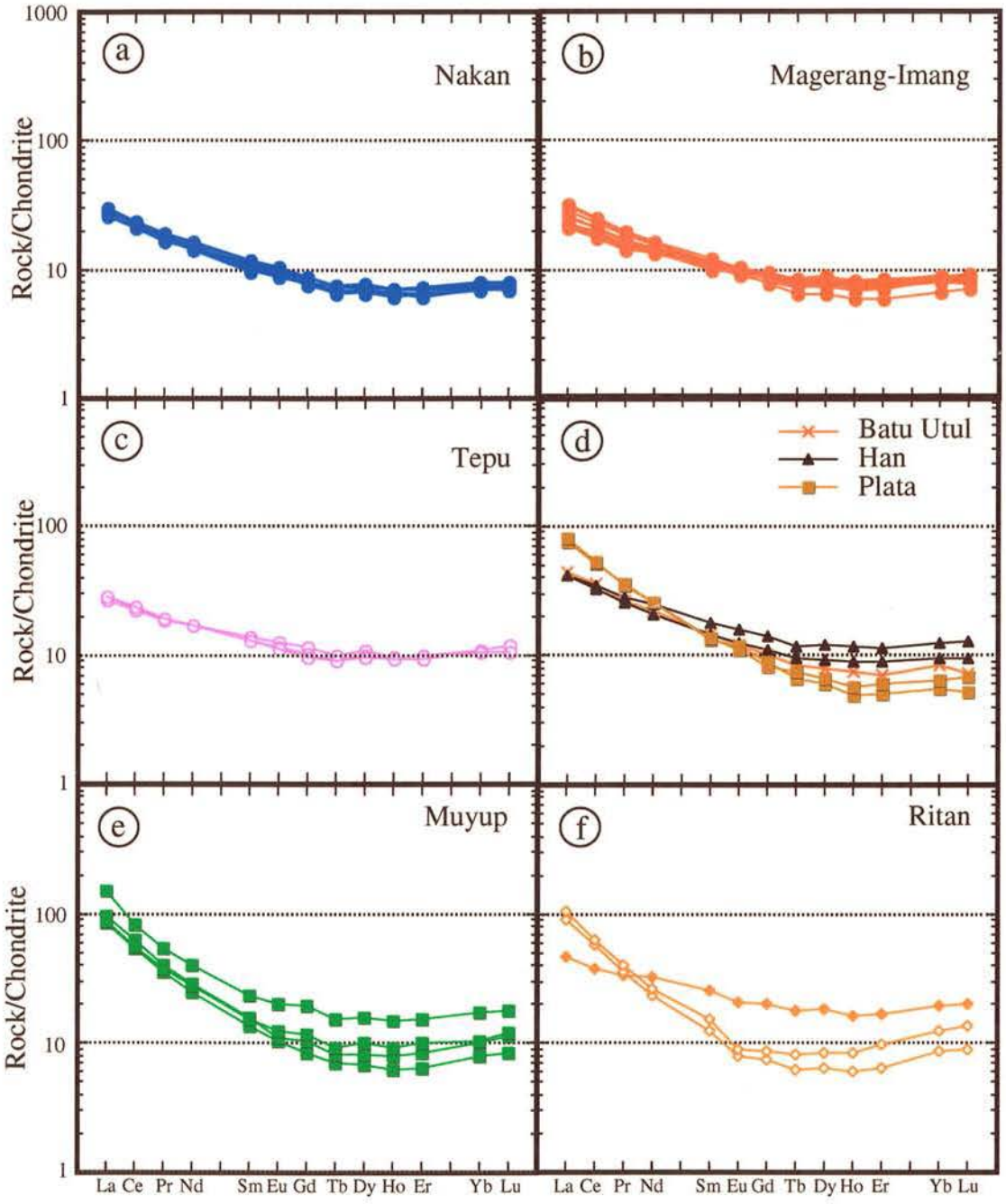

Figure 3.11: REE patterns of the least altered igneous suites.
Chondrite normalised values are taken from McDonough and Sun (1995)

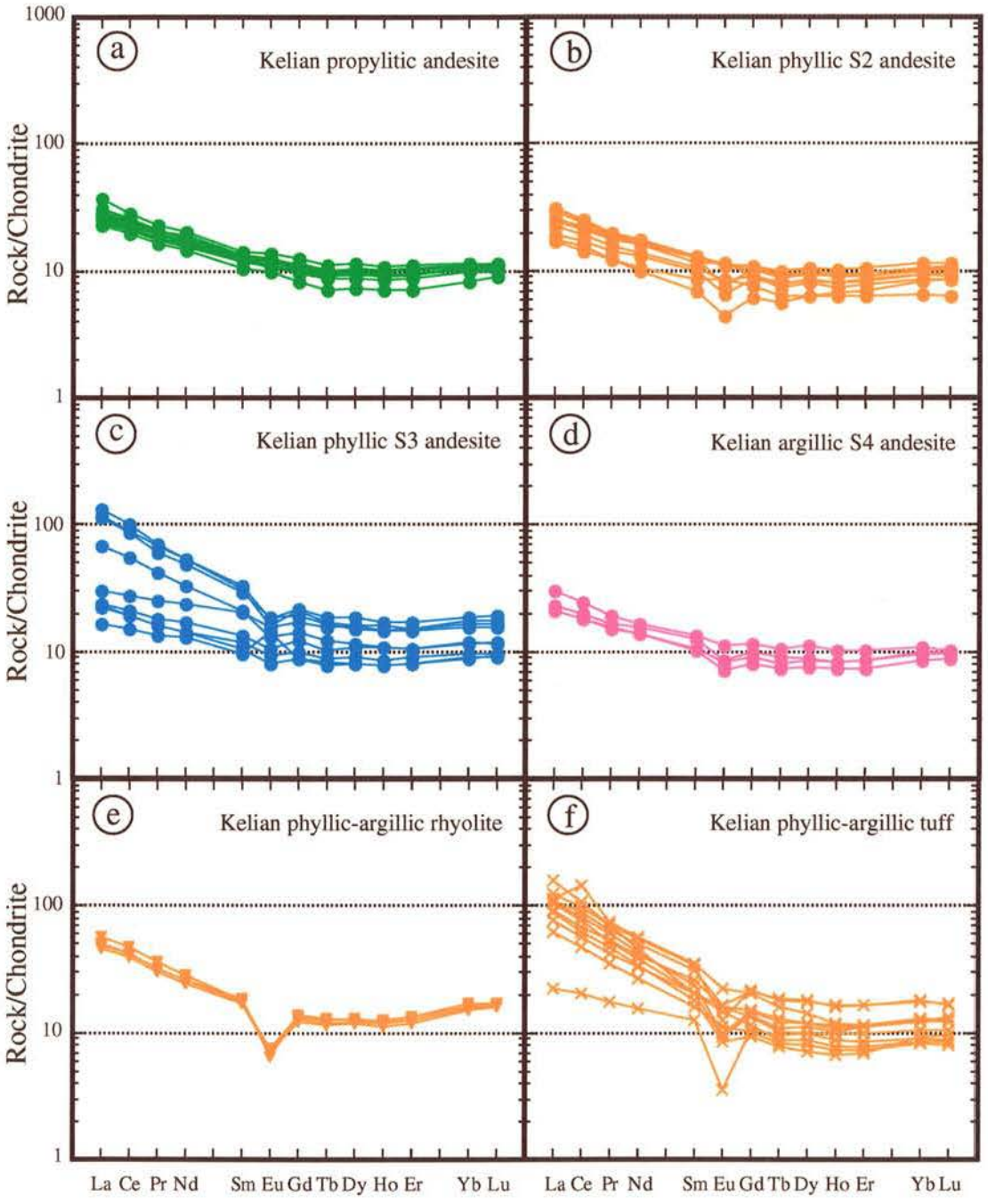

Figure 3.12: REE patterns of the Kelian altered igneous suites.
Chondrite normalised values are taken from McDonough and Sun (1995)

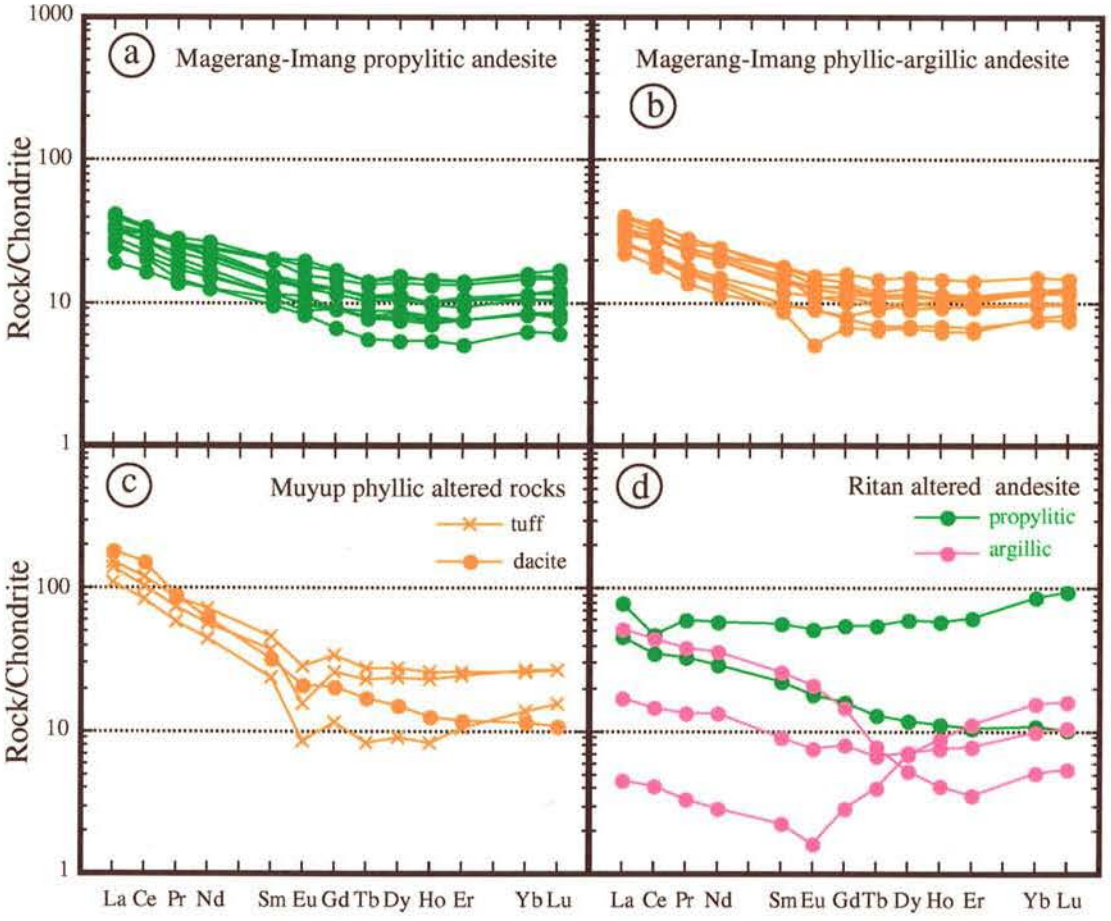

Figure 3.13: REE patterns of the altered igneous suites from the Magerang-Imang, Muyup and Ritan areas. Chondrite normalised values are taken from McDonough and Sun (1995).

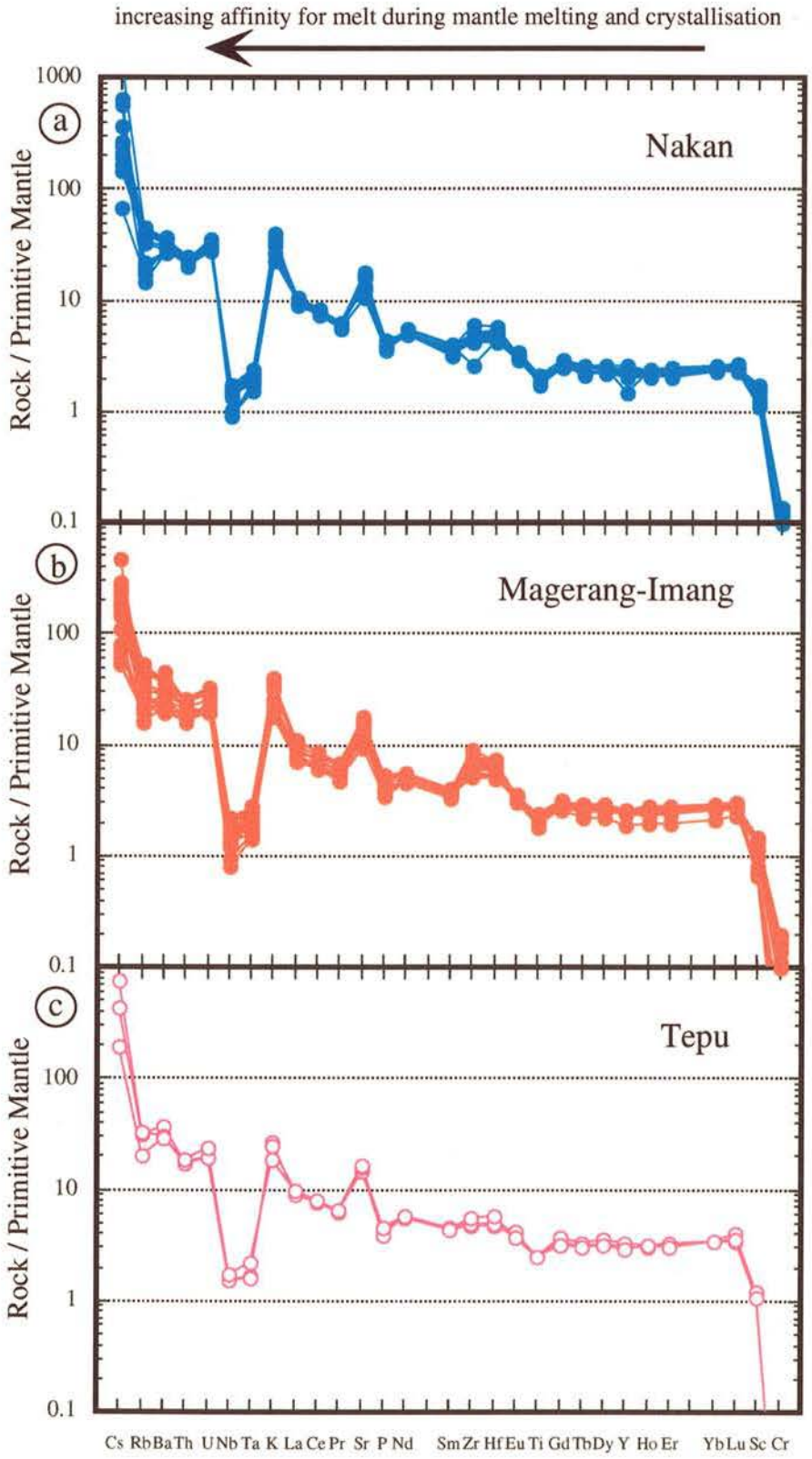

Figure 3.14 (a-c) : Primitive mantle normalised multi element patterns for the least altered andesite from the Kelian igneous complex. Primitive mantle concentrations were taken from Sun and McDonough (1989).

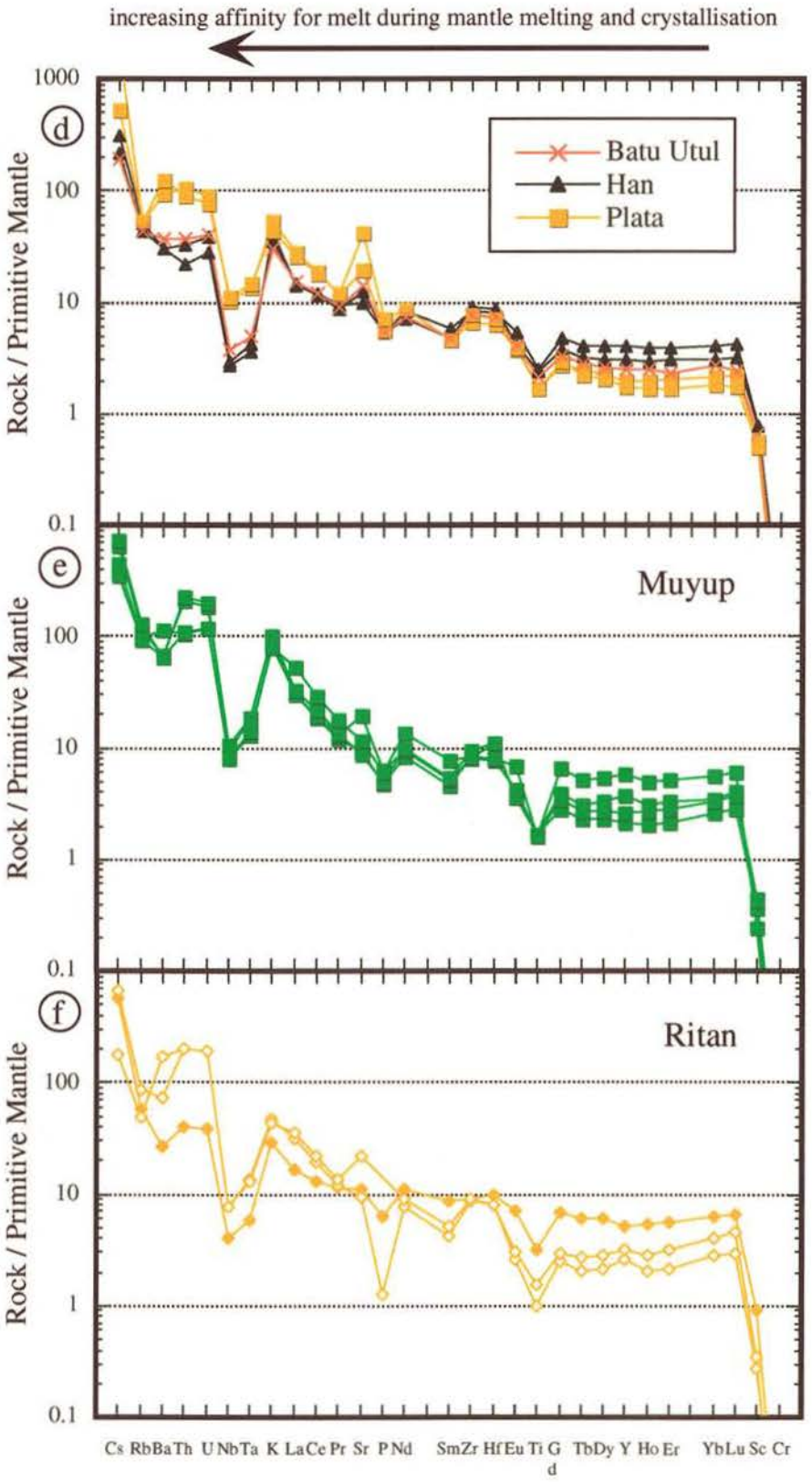

Figure 3.14 (d-f) : Primitive mantle normalised multi element patterns for the least altered andesite from the Han, Plata, Batu Utul, Muyupand Ritan prospects

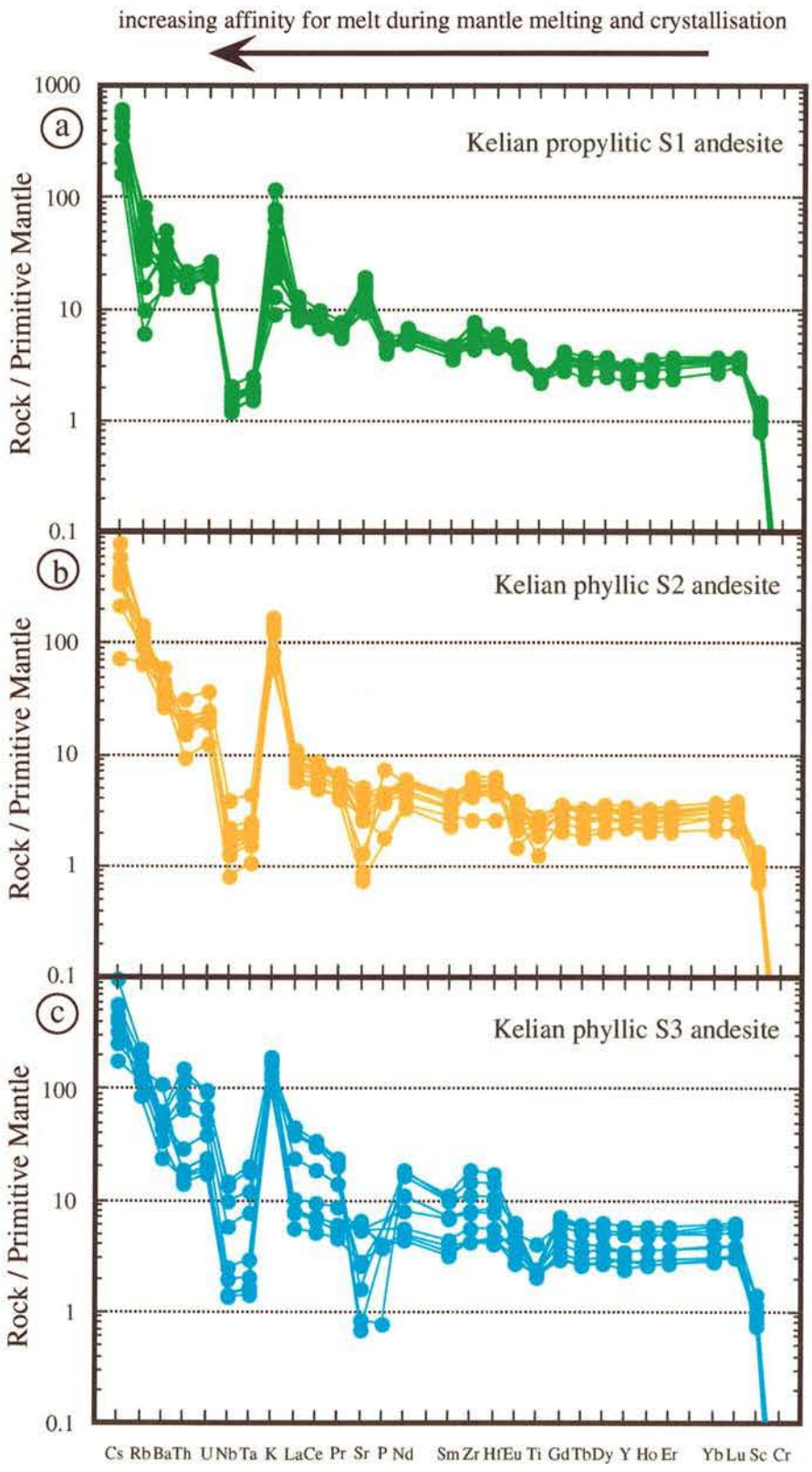

Figure 3.15 (a-c) : Primitive mantle normalised multi element patterns for the Kelian altered igneous rocks.

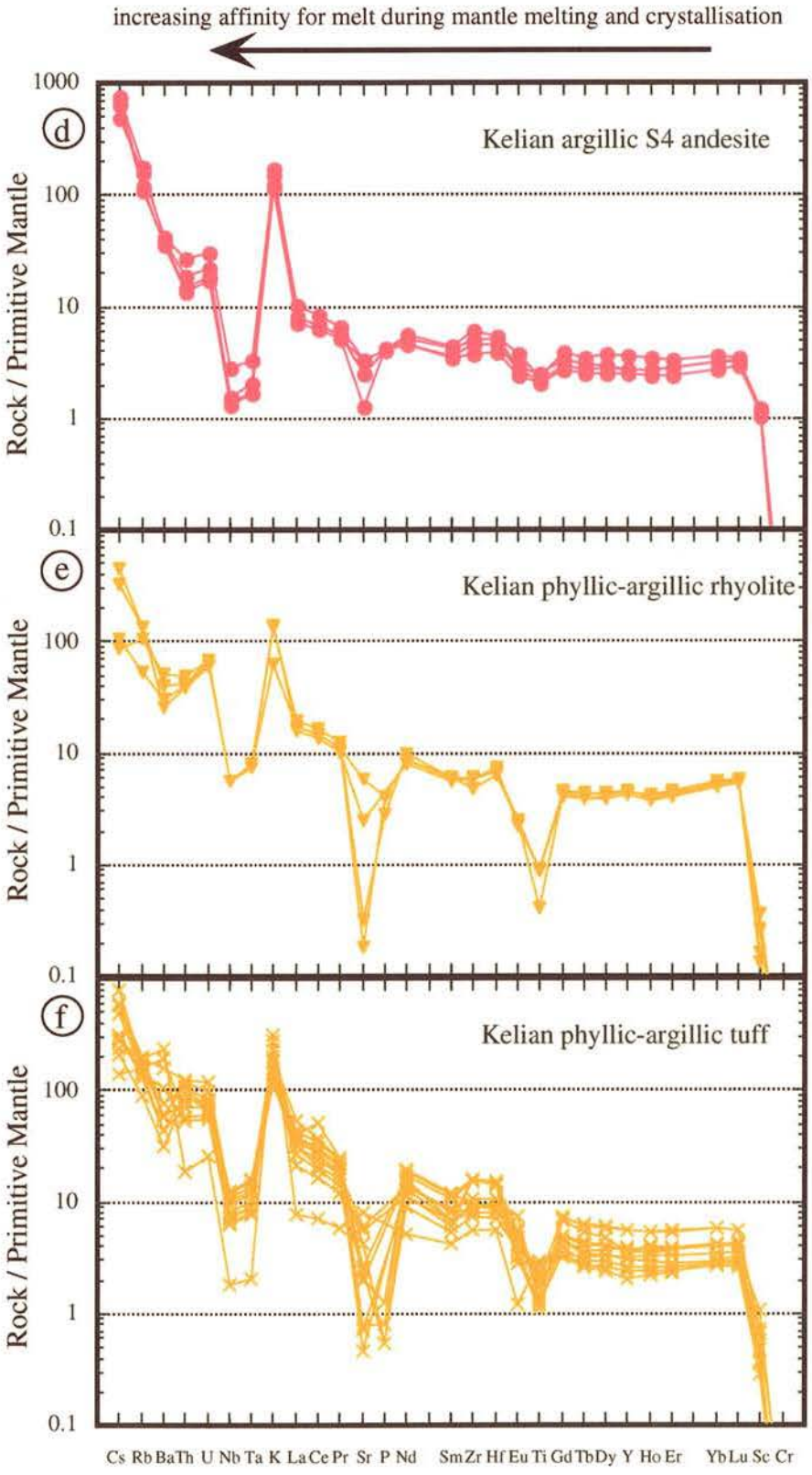

Figure 3.15 (d-f) : Primitive mantle normalised multi element patterns for the Kelian altered igneous rocks.

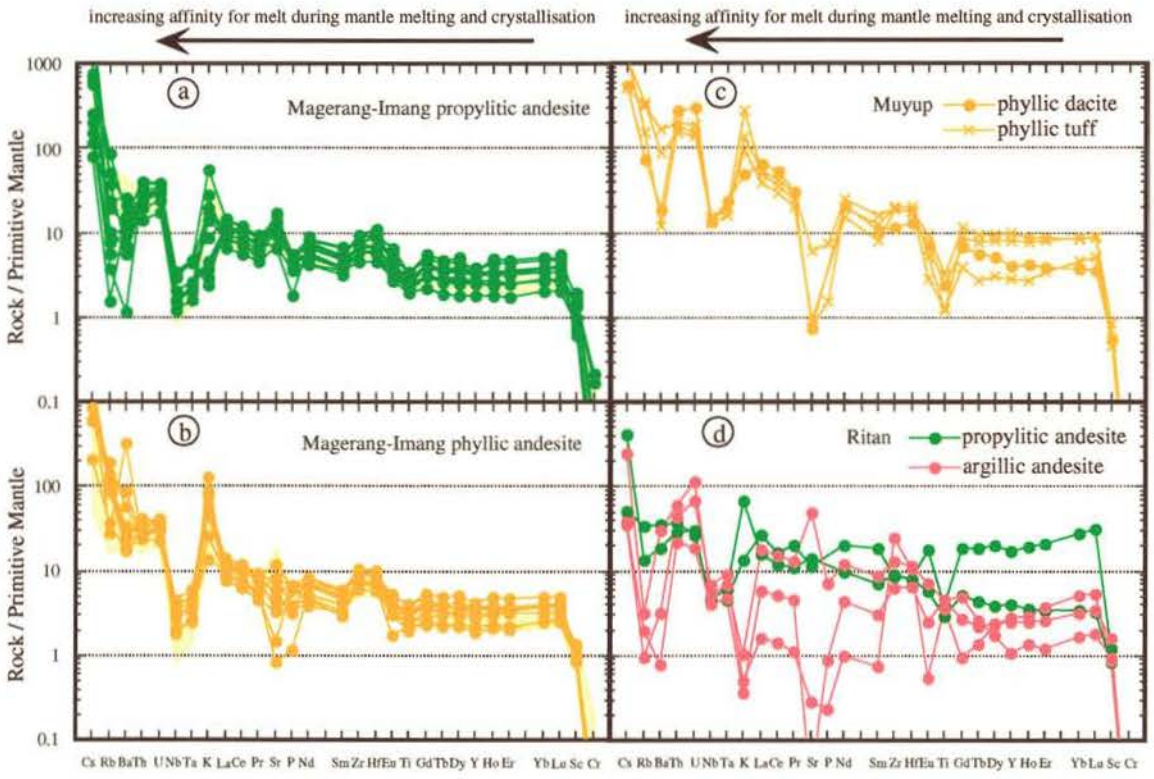

Figure 3.16: Primitive mantle normalised multi element patterns for the altered igneous suites from the Magerang-Imang, Muyup and Ritan prospects. The least altered samples of the Magerang-Imang andesite are shown as shaded patterns on the Figure 3.16a and 3.16b.

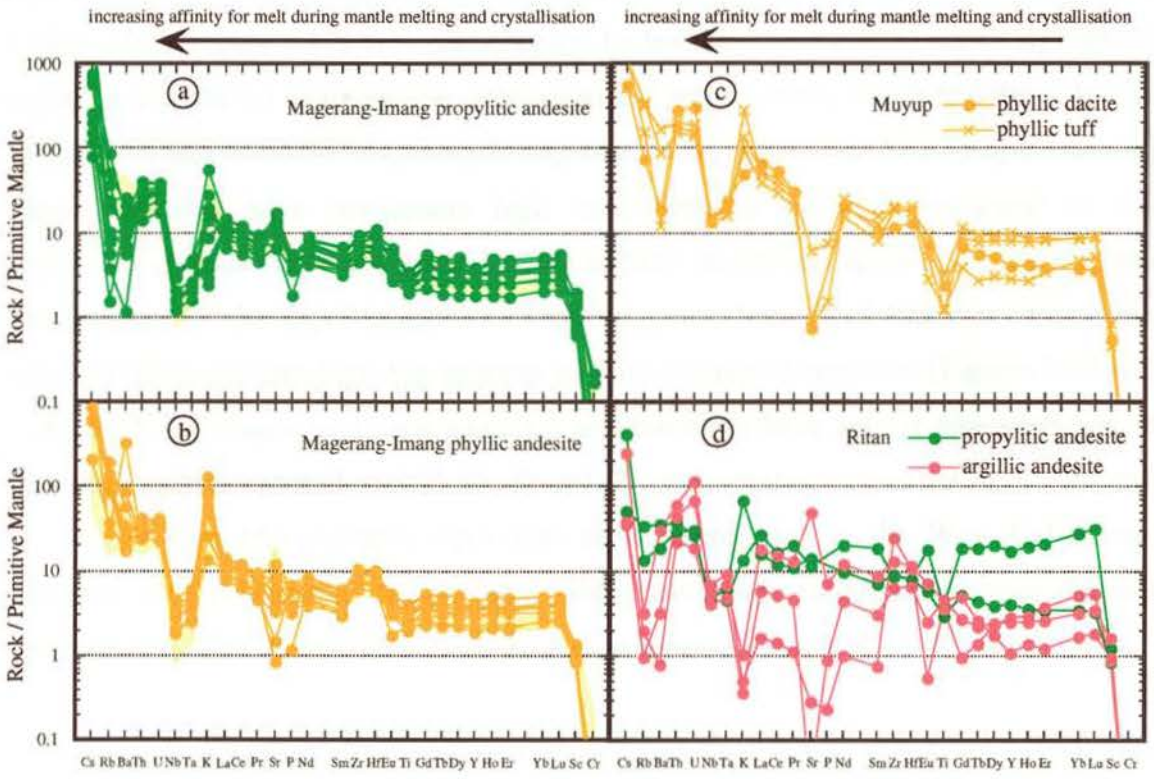

Figure 3.16: Primitive mantle normalised multi element patterns for the altered igneous suites from the Magerang-Imang, Muyup and Ritan prospects. The least altered samples of the Magerang-Imang andesite are shown as shaded patterns on the Figure 3.16a and 3.16b.

3.5 Evidence for Two Magmatic Differentiation Trends

Geochemical evolution in the Miocene calc-alkaline suites from the Kalimantan volcanic arc exhibits two distinctive trends of magmatic differentiation. The first trend is defined by a series of *productive* igneous suites from Tepu (Kelian; this study), Mount Muro (Simmons and Browne, 1990), Masuparia (Thompson, et al., 1994) and West Kalimantan (Harahap, 1993). This trend is a *typical* calc-alkaline series and is consistent with the differentiation trend for arc lavas, as shown by the Rinjani calc-alkaline trend (Foden, 1983; Figure 3.17). It is characterised by low Mg, moderate K, relatively high Ti and Al and depletion in Cr and Sc, relative to the second trend, which is defined by the chemical variations of the Magerang-Imang and Nakan suites. The Magerang-Imang and Nakan andesites have remarkably high concentrations of MgO compared to the productive igneous suites and common calc-alkaline andesites. Major and trace element geochemistry of the high Mg andesites from Magerang-Imang and Nakan is comparable with that of the Ryukyu high Mg andesite and low Ca type 2 boninites (Figures 3.17 and 3.18). Both the Magerang-Imang andesites and boninites have similar characteristics of high Mg, positive anomalies of U, Sr, Zr and Hf, and negative anomalies of Nb, Ta and Ti. Similar high Mg andesites have also been documented in the West Kalimantan (Harahap, 1993). However, the boninite suites have lower incompatible trace element concentrations than the andesites from the Kelian Igneous Complex.

3.6 Geochemical Evolution of The Kelian Igneous Complex

In the Kelian Igneous Complex, the simultaneous depletion of MgO, Fe_2O_3, TiO_2 and CaO and enrichment in Na_2O, K_2O and P_2O_5 within the suites could be controlled either by magma mixing or by fractional crystallisation. If chemical variation within the igneous suites was formed by mixing of two parental magmas, the variation of major elements should define linear lines of depletion or enrichment of oxides with increasing SiO_2 (Wilson, 1995) so long as they were not concurrently fractionating. Alternatively, if the suites were formed by fractional crystallisation, the variation in major elements should lie on a curved trend on Harker diagrams. Fractional crystallisation can also be distinguished using compatible elements which decrease rapidly with increasing silica

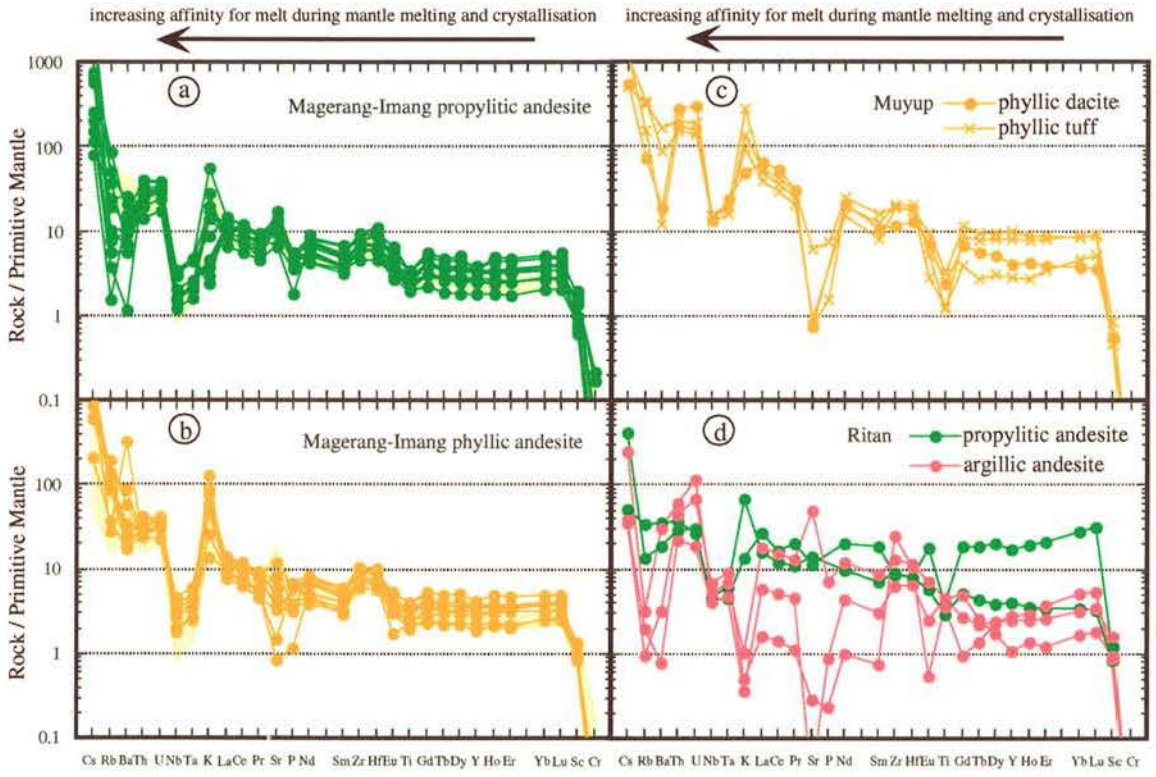

Figure 3.16: Primitive mantle normalised multi element patterns for the altered igneous suites from the Magerang-Imang, Muyup and Ritan prospects. The least altered samples of the Magerang-Imang andesite are shown as shaded patterns on the Figure 3.16a and 3.16b.

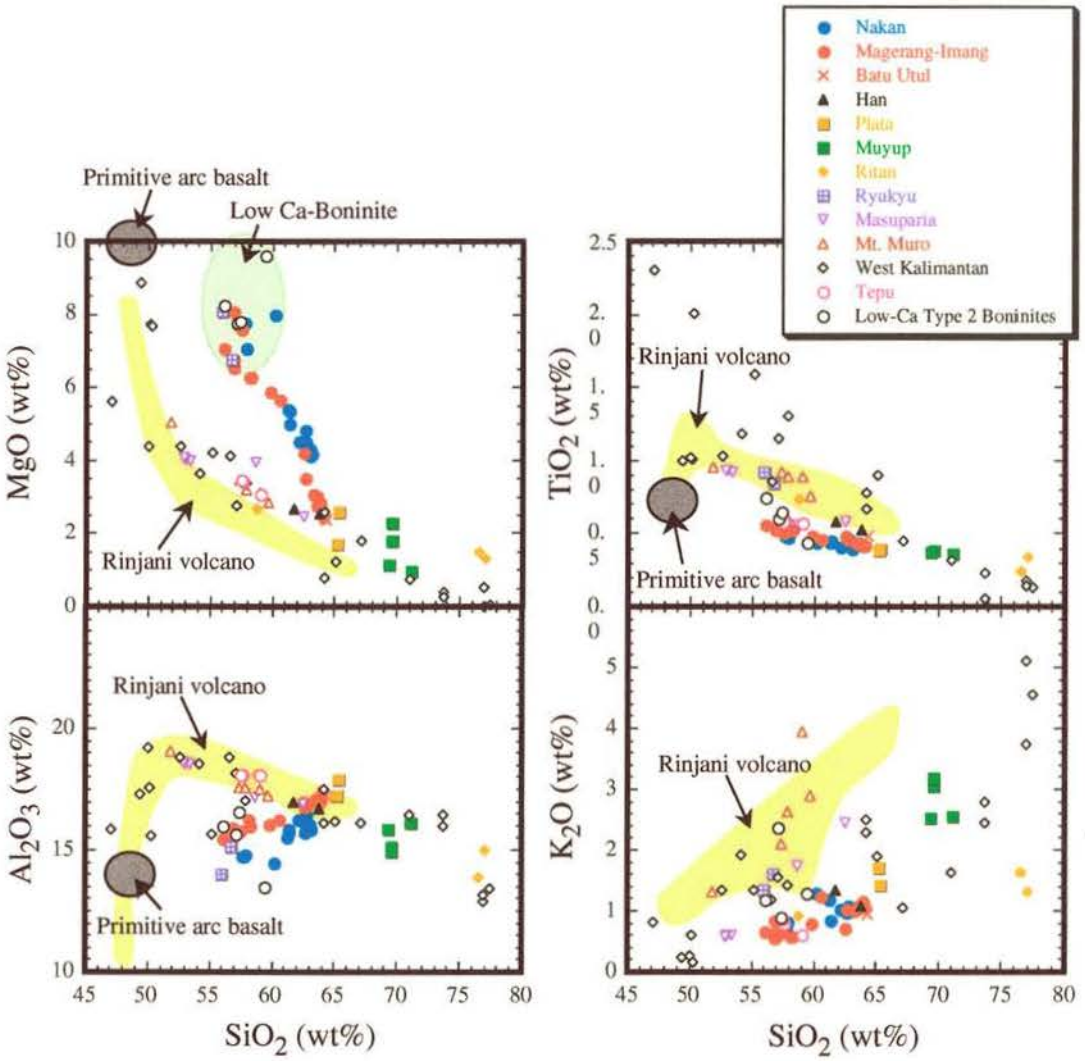

Figure 3.17 : Selected Harker variation diagrams for the Miocene calc-alkaline suites in Kalimantan. Geochemical data for the Masuparia (Thompson et.al., 1994), Mt. Muro (Simmons and Browne, 1990), West Kalimantan (Harahap, 1993), Ryukyu (Shinjo, 1999), Boninites (Crawford et al., 1989) and Rinjani (Foden, 1983) igneous suites were plotted for comparison.

early in the crystallisation history. In the Tepu, Han and Ritan suites, the declining trend in the abundance of Mg oxide and depletion in Cr and Sc with the increasing SiO_2 (Figures 3.19) follow typical trends in calc-alkaline arc suites and suggest chemical evolution by fractional crystallisation of pyroxene (Wilson, 1989) and amphibole (Foden, 1983) rather than mixing between melt and restite (Koyaguchi, 1986; Chappell, 1996; Chappell, 1997). The evidence of chemical evolution by fractional crystallisation is clearly indicated by major element trends as well as trace element trends as shown by plots of Cr, Sc, Ce/Yb and Eu/Eu* (Figure 3.19). The dominant mafic phenocryst of hornblende and the linear

horizontal trend of Eu/Eu* with the increasing La/Yb ratio indicate that amphibole fractionation dominated the evolution of the Magerang-Imang suite. On the other hand, the Nakan suite shows little variation in La/Yb ratios and contains pyroxene phenocrysts but no hornblende, and therefore, pyroxene fractionation may have played a more important role than amphibole and feldspar. This problem will be discussed further in Chapter 4.

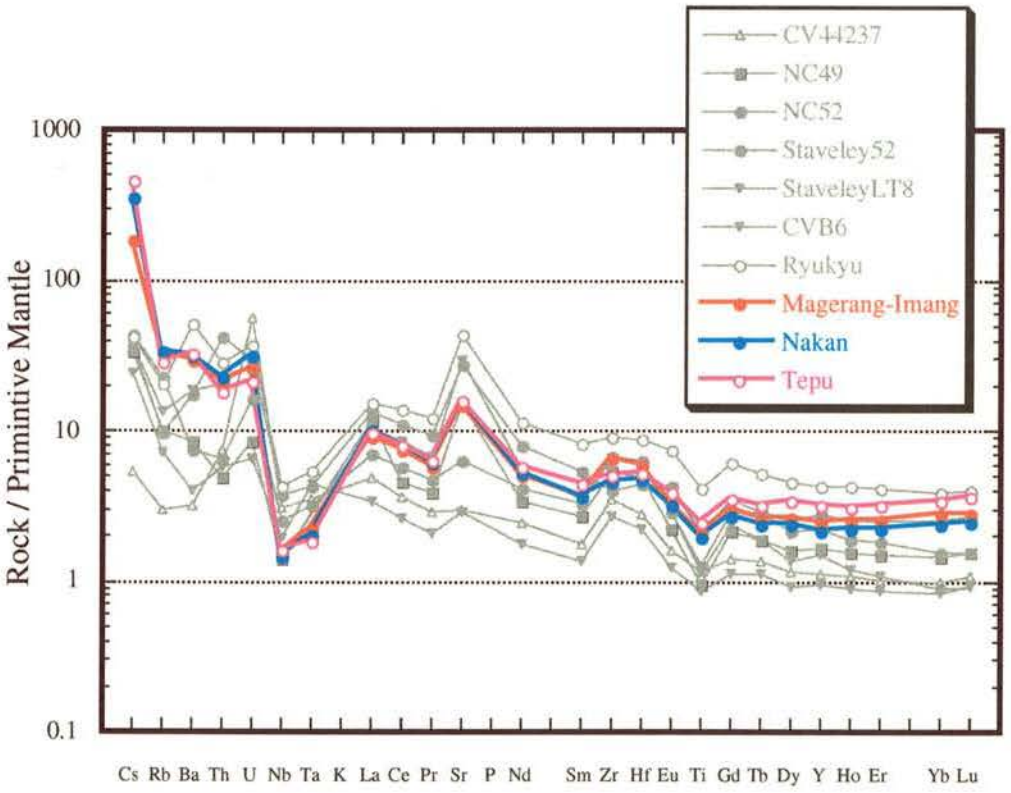

Figure 3.18 : Primitive mantle normalised multi element patterns for the Kelian Igneous Complex compared to the patterns for boninite-type rocks (Eggins, unpublished data). The high Mg andesites of the Magerang-Imang and Nakan regions closely resemble the low Ca type 2 boninites.

A striking feature of the incompatible trace element geochemistry of the Kelian Igneous Complex andesites is the presence of positive Zr and Hf anomalies in the trace element patterns (Figure 3.14) which is unusual for calc-alkaline subduction zone magmas. One possible explanation is that the parent magma had fractionated clinopyroxene prior to ascending into the upper crust. However, in the Magerang-Imang and Nakan suites, the notable curve-linear decline trend with increasing SiO_2, can not be explained either by simple liquid-crystal fractionation or by a two-magma mixing process. The chemical

diversity in the Magerang-Imang and Nakan suite, with their relatively high concentrations of Mg oxide, Sc and Cr, and concave down curvi-linear evolution trends, might have been generated by combined wallrock assimilation and fractional crystallisation (De Paolo, 1981). Zr/Sm ratios in the Magerang-Imang andesite (Figure 3.20) range from 34 to 59, higher than that in the andesite from the other regions (17-46).

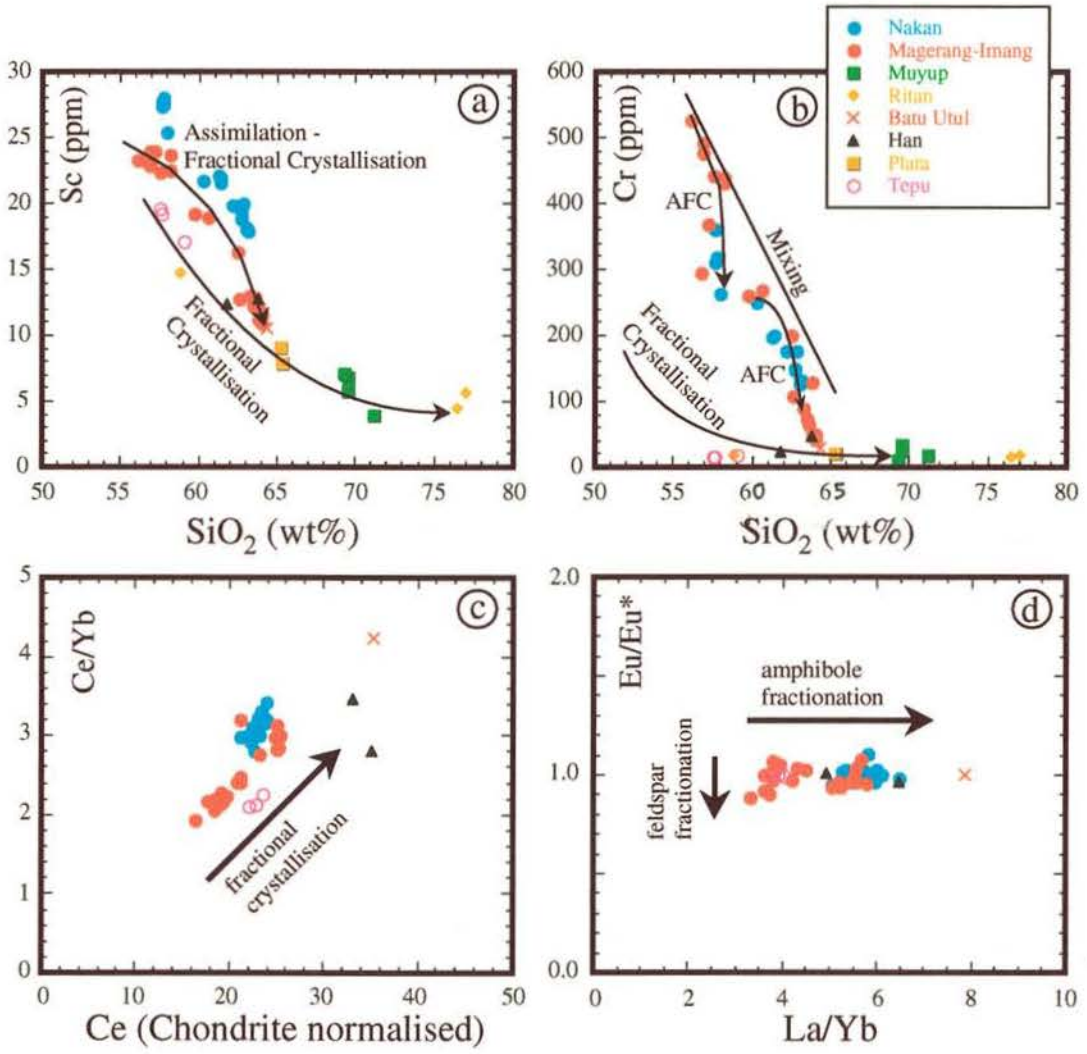

Figure 3.19 : Variation diagrams for the least altered andesites from the Kelian Igneous Complex and regional prospects. The Magerang-Imang and Nakan suites demonstrate trends of chemical evolution by combined wallrock assimilation and fractional crystallisation, whereas the other prospects demonstrate trends of chemical evolution by normal fractional crystallisation.

If the Magerang-Imang andesite is derived by a combined assimilation and fractional crystallisation, this would require a parental basaltic magma, assuming normal arc basalt, which has less than 55 wt% SiO_2, ~10 wt% MgO and a Zr/Sm ratio of 25-30 to assimilate

a Zr-rich cumulate which has more than 65 wt% SiO_2, 1-2 wt% MgO and Zr/Sm ratios of 50-55. This assimilant possibly has similar composition to the Plata and Muyup dacites but with cumulus zircon to raise its Zr/Sm ratio from the Plata and Muyup ratios of 37-46 to the required ratios of 50-55. However, the Plata and Muyup dacites have Zr/Sm ratios of 37-46 which are lower than the number expected. Alternatively, the Magerang-Imang and Nakan high Mg andesite may have been derived from a primary magma which had a high Zr/Sm ratio and a composition similar to other boninite-type rocks.

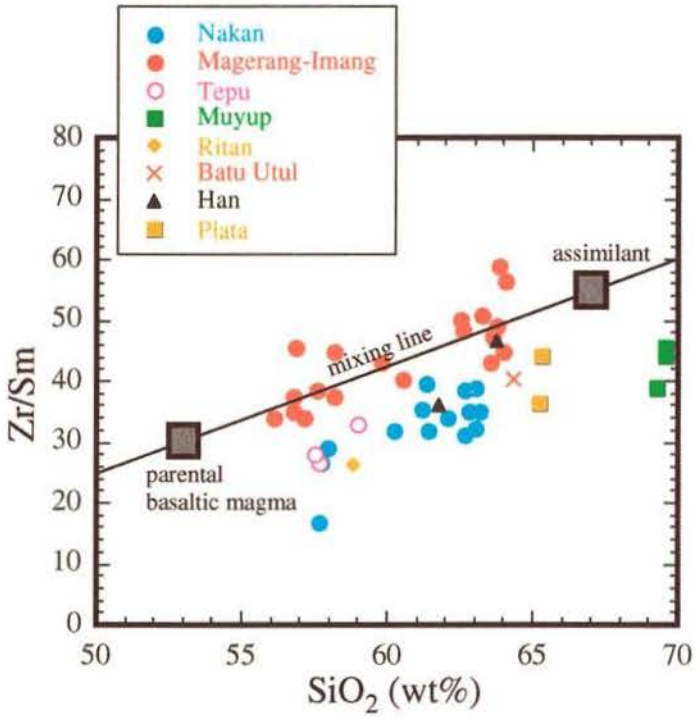

Figure 3.20: Plots Zr/Sm ratios versus SiO2 showing chemical evolution of the Magerang-Imang high Mg andesite produced by combined wallrock assimilation and fractional crystallisation.

The combined wallrock assimilation and fractional crystallisation process is consistent with the zircon geochronology of the Kelian Igneous Complex (see Chapter 6). The U-Th-Pb zircon dating indicates the presence of two large populations of inherited zircon in the Kelian mine intrusions. This requires the magma to have assimilated large amountsof slightly older zircon-bearing andesite (see Chapter 6). The Kelian mine andesites also have positive Zr and Hf anomalies. It is therefore possible that the Magerang-Imang and Nakan high Mg andesites were fed by magma chambers that formed deep in the crust, and were emplaced into pre-existing intrusions of felsic

composition that formed as part of the Kelian Igneous Complex cycle. It is suggested that the shallow level stocks at Magerang-Imang and Nakan were generated by intrusions that melted the walls and roofs of related, but pre-existing intrusions, and extracted abundant xenocrystic zircons during the assimilation process. This resulted in positive anomalies of Zr anf Hf in the Magerang-Imang and Nakan suites.

In the case of the Magerang-Imang and Nakan andesites the inherited zircons were not preserved, suggesting that the magma was not zircon saturated at the time of assimilation. This suggestion is consistent with the higher MgO content and therefore higher temperature of the Magerang-Imang and Nakan andesites compared with the Kelian mine andesites.

Trace element chemistry of the least altered samples exhibit systematic trends suggesting a single magma body. If one fractionating igneous system is represented at Kelian, then it is appropriate to further investigate the role of platinum group elements and gold in this system in order to establish the link, or lack thereof, between the igneous system and the Kelian gold deposit. The systematic trends presented in this chapter suggest that this is the case.

Chapter 4
GEOCHEMICAL MODEL OF RARE EARTH ELEMENTS IN CALC-ALKALINE IGNEOUS SUITES FROM THE KELIAN REGION

4.1 Introduction

The principal factors controlling the diversity of trace elements in calc-alkaline andesites in subduction zone environment are: (i) variations in the mantle melting processes that lead to different parental basaltic magmas, (ii) fractional crystallisation of the parental basaltic magma, and (iii) assimilation of crust or mixing with crustal melts (Best, 1969; Boettcher, 1973; Gill, 1981). The previous chapter used major and trace element data to show that fractional crystallisation and assimilation have played an important role in the genesis of the calc-alkaline suite from the Kelian region. This chapter focuses on the rare earth elements (REE) evolution of the Kelian Igneous Complex. The REE are modelled using the Rayleigh fractionation equation to constrain the nature of the cumulus phases that produced the observed trends. Detail modelling is confined to the Magerang-Imang and Nakan intrusive suites because they are the least affected by alteration and because they cover a broad range of REE concentrations. The Magerang-Imang andesites contain phenocrysts of hornblende whereas the Nakan andesites have pyroxene phenocrysts. One of the hypotheses to be tested is whether differences in the REE trends for Magerang-Imang and Nakan can be explained by hornblende being the dominant cumulus phase controlling REE geochemistry in the Magerang-Imang suite and clinopyroxene being the dominant phase in the Nakan suite. It should be emphasised that the modelling presented in this chapter is semi-quantitative. It is aimed at identifying the cumulus phases responsible for the observed REE trends, with the minimum number of assumptions, rather than producing a detailed quantitative model.

The modelling makes a number of simplifying assumptions. Firstly, it is assumed that the whole rock composition of the least altered samples represents the melt

composition from which they are crystallised. Secondly, that the most primitive sample analysed based on major and trace elements, is the parent to all other melts from the same suite. Thirdly, the role of assimilation and mixing with crustal melts has been ignored. Finally, it is assumed that the analysed phenocrysts yield D values that are appropriate for melt composition and P and T of the modelled fractionation.

4.2 Partition Coefficient

In order to model the quantity of trace elements in a closed magma chamber, it is necessary to understand the behaviour of trace elements, particularly how they are partitioned into a melt during fractional crystallisation. A trace element has a low concentration in a system so that changing its concentration will not affect the stability of any phase in the system (Hanson and Langmuir, 1978) and therefore its distribution between any two phases in the system can be estimated using a partition coefficient of mineral-melt (D) without considering the element concentration in any other phase in the system.

The partition coefficient (D) for a given element (i) between a solid phase (S) and the coexisting silicate liquid or melt (L) depends on the temperature, pressure and the composition of the mineral and melt. It is a measure of the degree of compatibility and can be expressed as follows:

$$D_{i,S/L} = \frac{C_i^S}{C_i^L}$$

where: C_i^S = weight concentration of element i in solid phase

C_i^L = weight concentration of element i in the coexisting liquid (melt)

Elements that are preferentially concentrated in the crystalline phase will have D>1 and are termed "compatible", whereas elements that are preferentially retained in the liquid phase during crystallisation will have D<1 and are termed "incompatible". However, an element may change its behaviour from incompatible to compatible during the course of magma differentiation.

Partition coefficients can be determined by two different methods: (i) synthetic crystallisation experiments (Nicholls and Harris, 1980; Green and Pearson, 1985; Nielsen et al., 1992) and (ii) partitioning between phenocrysts and a glassy matrix in volcanic rocks (Fujimaki et al., 1984; Irving and Frey, 1984; Dunn and Sen, 1994). The results of experimental studies of trace element partitioning between common igneous minerals and silicate melts have been reviewed by Irving (1978) and Green (1994). The phenocrysts and glass matrix are representatives of composition of mineral formed in equilibrium with the coexisting melt at the time of emplacement or eruption. In this study, the partition coefficients for trace elements between amphibole, clinopyroxene and plagioclase phenocrysts and groundmass in andesite were determined by ELA-ICP-MS analyses of suitable Magerang-Imang and Nakan samples. The solid/melt partition coefficients of the minerals were calculated by dividing the concentrations in minerals by those of the matrix (groundmass), assuming that the phenocrysts are in chemical equilibrium with the groundmass. These partition coefficients are preferred to experimentally determined values because their application minimises any uncertainty arising from variation in D with melt composition.

4.3 Trace Element Analyses of Selected Phenocryst-Matrix Pairs of The Magerang-Imang and Nakan Andesites

In order to determine partition coefficients between cumulate minerals and andesite melt several phenocrysts were analysed for major and trace elements using polished thin sections. These phenocrysts include amphibole, clinopyroxene and plagioclase selected from the Magerang-Imang hornblende andesite (Sample 123144) and the Nakan pyroxene andesite (Sample 123187). Major element compositions of the phenocrysts were determined by Camebax electron microprobe methods using energy-dispersive spectrometer (EDS), same as the system that was used for the whole rock analysis.

Trace element compositions of the phenocrysts were determined using polished thin sections, by excimer laser ablation inductively coupled plasma mass spectrometer (ELA-ICP-MS). The procedures for data acquisition and reduction are the same as that described

in Chapter 3. The partition coefficients resulted from this study and the other partition coefficients from published sources used in this modelling are listed in Appendix 6.

4.4 Rare Earth Element Model

The approach taken in this study is to assume that the intrusions of the Magerang-Imang and Nakan suites are each fed by magma chambers deeper in crust. Fractionation within those chambers is then modelled using the standard formula (Arth, 1976):

$$C_L = C_O F^{(D-1)}$$

Where C_O: the concentration of the element in the parental magma

F: the fraction of liquid remaining

D: the bulk distribution coefficient for the crystallising solids and the coexisting liquid.

The bulk distribution coefficient (D) is calculated from the individual mineral distribution coefficients for each element by summing the mineral distribution coefficients after multiplying each by the weight fraction of that mineral.

$$D = \sum (X_1D_1 + X_2D_2 + X_3D_3 + \ldots\ldots\ldots + X_nD_n)$$

Where X_1, X_2, X_3,..., X_n are the weight fraction of the minerals in the crystallising assemblages and D_1, D_2, D_3,...., D_n are the mineral-liquid partition coefficients of elements.

The partition coefficients of REE (D values) in andesite melt for amphibole, clinopyroxene and plagioclase measured for this study, together with the previously published partition coefficients used in the modelling, are presented in Figures 4.1.

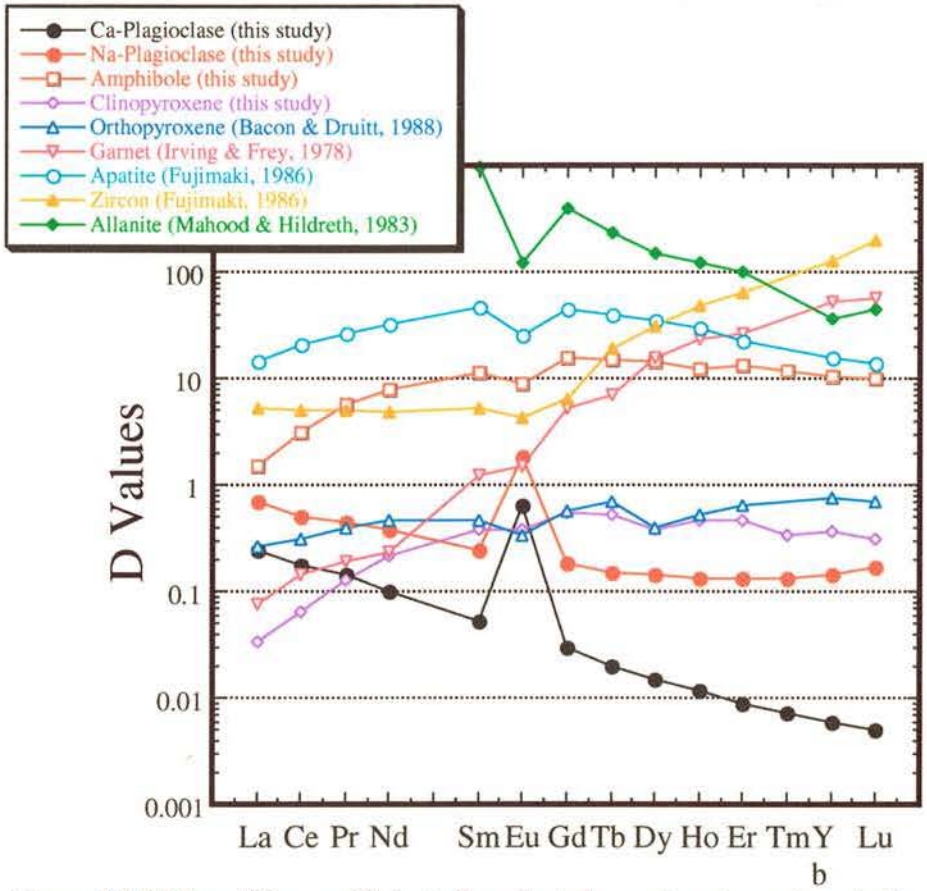

Figure 4.1 REE partition coefficients for selected cumulus phases in andesite

In order to assess the effect of fractionation of the individual cumulus phases of the REE evolution of the melt, REE patterns produced by mono mineral assemblages have been calculated. The results are shown in Figure 4.2. Plagioclase fractionation produces an increase in the concentrations of all of the REE in the melt, with the exception of Eu, which develops a negative anomaly due to the compatible behaviour of Eu in plagioclase. Clinopyroxene and orthopyroxene fractionations similarly concentrate all of the REE in the residual melt. Crystallisation of even a small amount of garnet has a profound effect on the REE concentration of the residual melt. The HREE are strongly depleted and the LREE are weakly enriched, resulting in a cross-over at Sm. For melts involving crystallisation of amphibole, the middle REE, with the exception of Eu, are more depleted than the LREE and HREE, leading to a concave upwards shape in the MREE to HREE part of the pattern. This characteristic feature of amphibole fractionation allows its presence to be readily identified in a cumulate assemblage. Apatite fractionation shows a

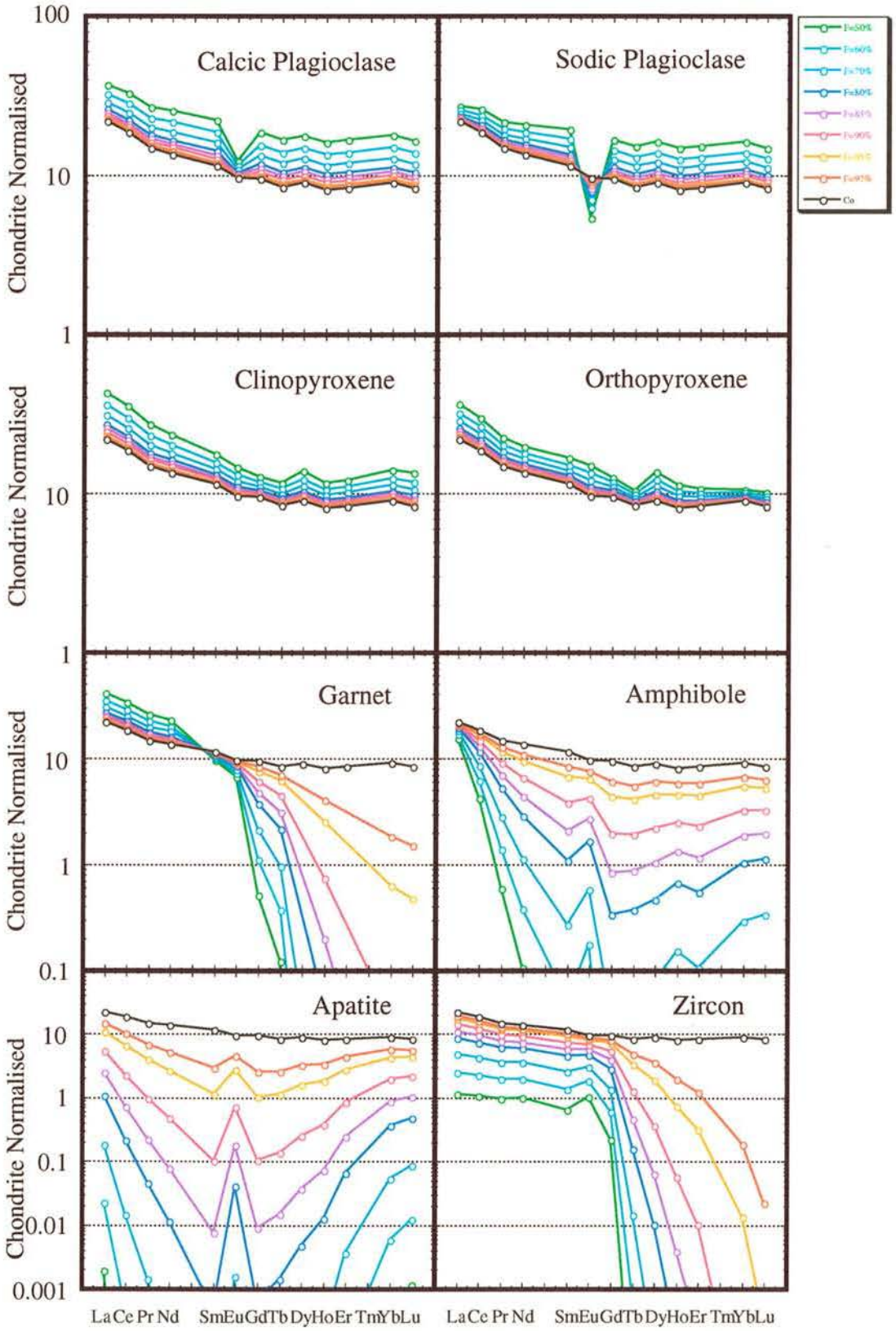

Figure 4.2 : The effects of crystal-liquid fractionation of mono-mineral in andesite magmas. Andesite sample 123108 from Magerang-Imang is used for the most primitive composition (Co).

similar concave downward pattern, but the LREE are more depleted compared to amphibole fractionation. Zircon fractionation is characterised by a flat pattern of

decreasing the LREE, but a steep pattern of the HREE depletion. This means that only a small fraction of zircon crystallisation (less than 3%) will significantly deplete the HREE concentration in the residual melt.

The chondrite normalised REE pattern for the Magerang-Imang suite is a concave upwards shape with the REE becoming more enriched with fractionation between La and Nd and more depleted between Sm and Lu (Figures 3.11a). The consistent enrichment of the LREE relative to the HREE suggests crystallisation of plagioclase, clinopyroxene and orthopyroxene, and therefore these cumulus phases were used in the initial model. As shown in Figure 4.3a, the fractionation of plagioclase, clinopyroxene and orthopyroxene caused enrichment in all of the REE. The addition of 5% amphibole into the cumulus assemblage enriched the LREE and HREE but resulted in little change in the MREE concentrations (Figure 4.3b). Enrichment of the HREE relative to the MREE is mainly controlled by fractionation of orthopyroxene. It is therefore necessary to remove orthopyroxene from the cumulus assemblage to affect depletion in the HREE. Modelling using an assemblage of plagioclase(65%)-clinopyroxene(25%)-amphibole(10%) resulted in a pattern that shows a reasonable agreement with the observed REE pattern, but the modelled MREE are slightly more depleted than the observed values(Figure 4.3c). These small differences in the observed and modelling REE patterns are probably due to the choice of the D values used and the other factors, especially assimilation, not taken into account in the modelling. The presence of garnet in the fractionating melt causes more depletion in the HREE relative to the MREE than the observed (Figure 4.3d). The crystallising assemblage is therefore constrained to contain less than 1% garnet. An interesting feature of the data is that extensive plagioclase fractionation produces no detectable negative Eu anomaly. This is because the effects of plagioclase, with its positive Eu anomaly are balanced by amphibole fractionation, which has a negative anomaly. Although the negative anomaly of amphibole is much smaller than the positive anomaly in plagioclase, the concentration of Eu in amphibole is an order of magnitude higher, allowing it to effectively balance plagioclase.

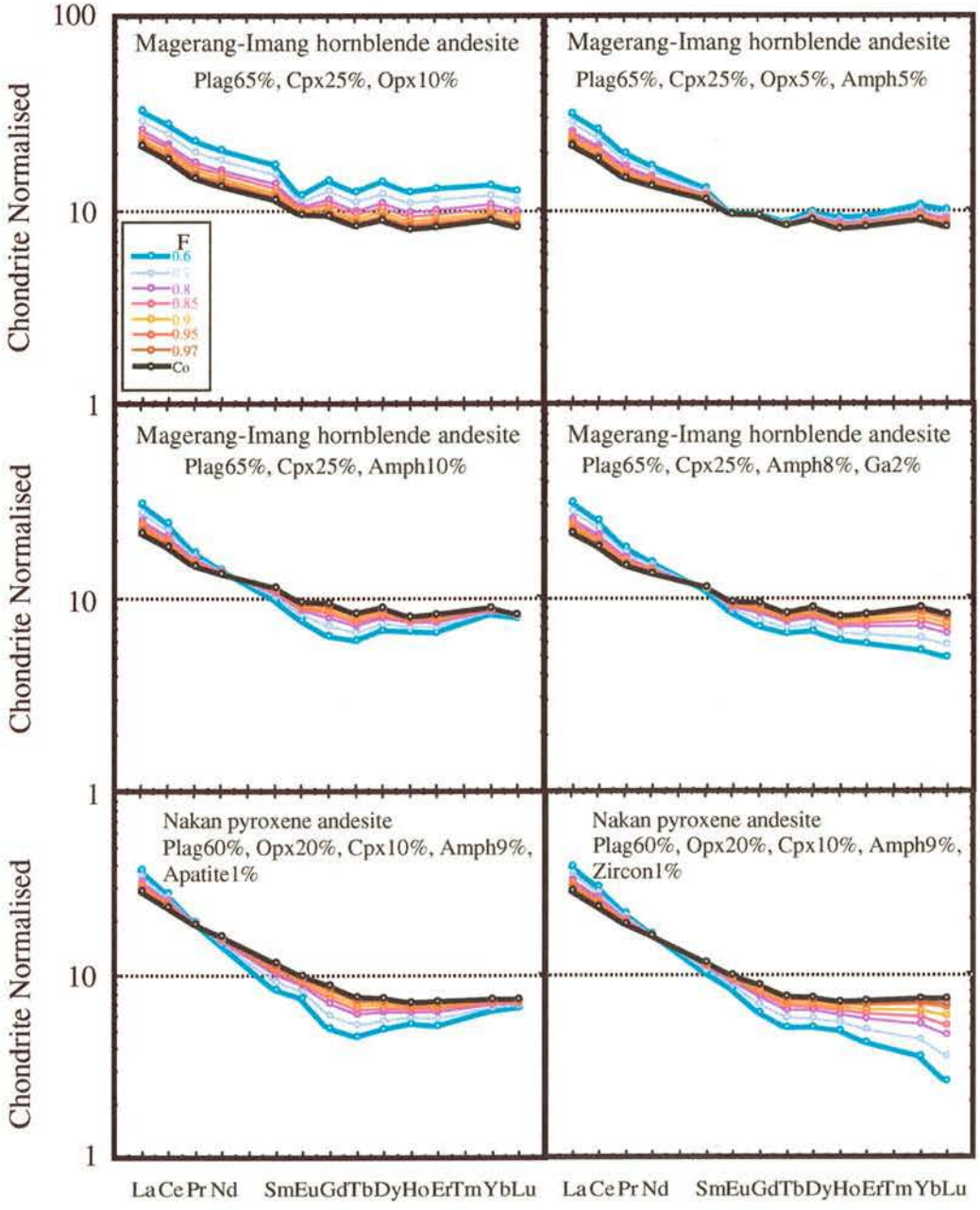

Figure 4.3 : The effects of crystal-liquid fractionation of mono-mineral in andesite magmas. Andesite sample No. 123108 from Magerang-Imang is used for the most primitive composition (Co).

The observed trend of the REE in the Nakan suite indicates decreasing concentrations of REE with increasing differentiation. Fractionation of plagioclase and pyroxene produces a REE trend that shows increasing concentrations of the REE in the residual melt, and the additional fractionation of hornblende causes depletion in the HREE and enrichment in the LREE resulting in a cross-over at a point between Nd and Sm.

Fractionation of these phases can not produce the decrease in REE with fractionation seen in the Nakan suite.

In andesitic melt compositions, the REE behave as compatible elements in accessory phases such as zircon, apatite and allanite. These phases have very high partition coefficients and may strongly influence the REE pattern, and produce REE depletion, even when they are present in small quantities (less than 0.5%). Apatitite fractionation depletes the MREE relative to the LREE and HREE (Figure 4e), zircon fractionation depletes the HREE relative to the LREE, and allanite fractionation depletes the LREE. Accessory phases appear to be required to produce the decreasing trend of REE with fractionation in the Nakan andesite. A calculation using a cumulus assemblage of plagioclase(60%) - orthopyroxene(20%) - clinopyroxene(13%) - amphibole(6%) - apatite (0.4%)-zircon(0.15%)-allanite(0.027%) produced a REE pattern which matchs the observed trend. A comparison between the modelled and observed REE trends is shown in Figures 4.4 and 4.5. The modelled REE trends demonstrate good agreement with the observed trends indicating that the fractionation of the selected cumulus assemblages can simulate the chemical evolution of the Magerang-Imang and Nakan calc-alkaline suites.

As stressed throughout this chapter, the modelling presented here ignores many of the complications likely to have affected the geochemistry of the intrusive andesite suites that make up to Kelian Igneous Complex. In particular, it ignores the effects of assimilation. The occurrence of xenocrystic zircons was used in Chapter 6 to argue that the magma chambers, which are believed to feed the Kelian andesite suites, intruded into slightly older related intrusions, which also formed during the Kelian igneous event. Because these intrusions crystallised from closely related magmas, their REE patterns are likely to be similar to those of the new pulses of intruding magma. Assimilation of this material may change the REE concentration in samples but it should not change the slope of the patterns. Changes in the LREE to HREE ratio and the decrease in REE abundances with increasing SiO2 in the Magerang-Imang and Nakan andesite suites respectively, are almost certainly due to fractional crystallisation. However, it is not clear whether the required fractionation occurs during crystallisation of the new pulse of magma or whether it was acquired from early fractionation in the assimilated andesite. What it clear is that

the change in slope of the Magerang-Imang REE patterns requires crystallisation of an assemblage that included plagioclase, clinopyroxene and about 10% amphibole. The concentration of garnet in this assemblage, if it was present at all, can not exceed 1%.

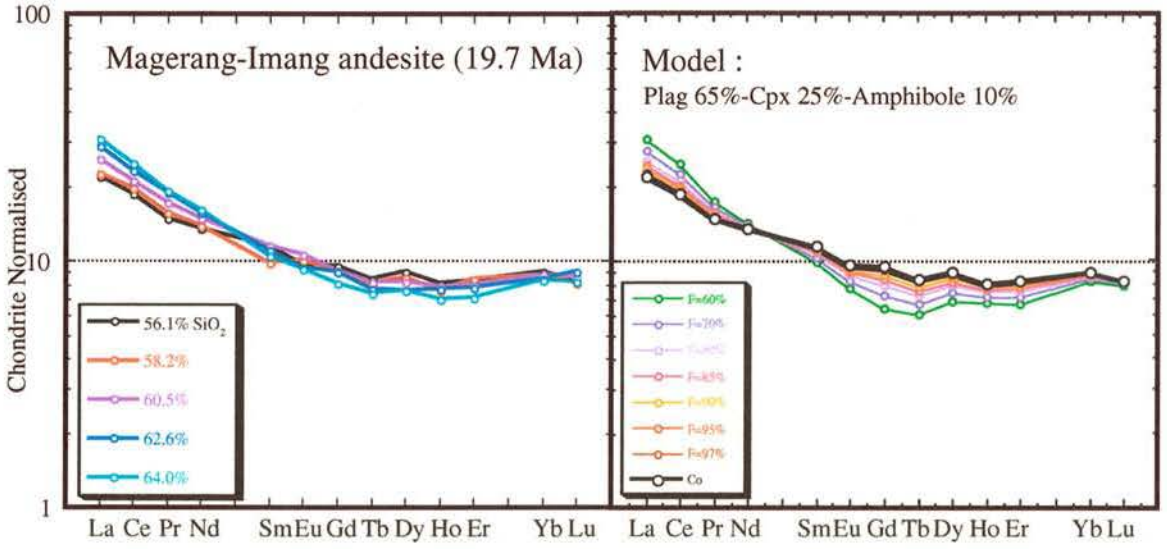

Figure 4.4 Chondrite-normalised REE pattern for the Magerang-Imang andesite compared with the modelled REE pattern produced by fractional crystallisation of cumulus phase assemblages of plagioclase, clinopyroxene and amphibole.

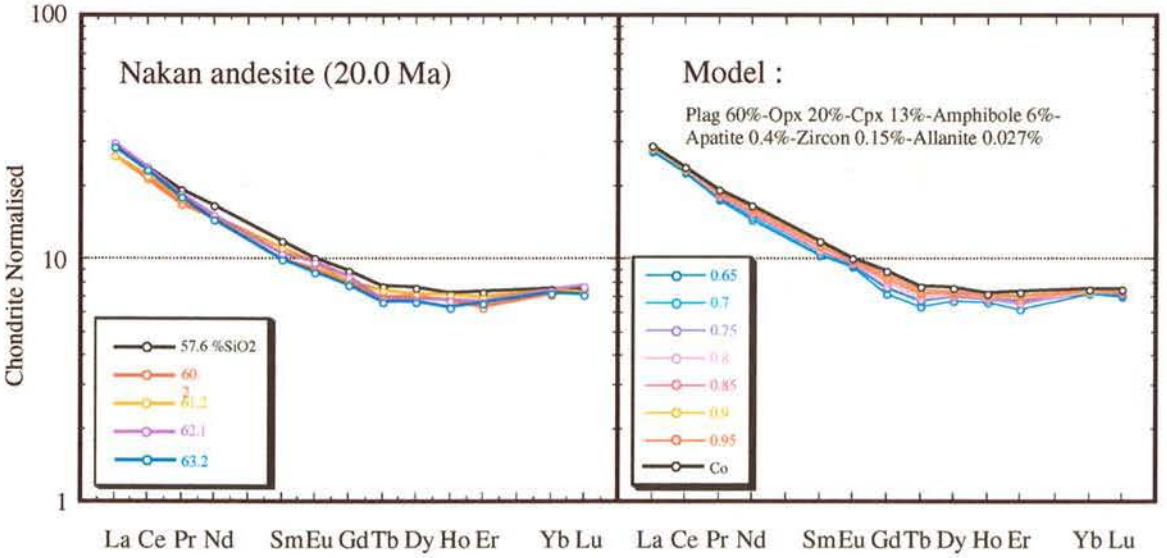

Figure 4.5 Chondrite-normalised REE pattern for the Nakan andesite compared with the modelled REE pattern produced by fractional crystallisation of cumulus phase assemblages of plagioclase, clinopyroxene, orthopyroxene, amphibole, apatite, zircon and allanite.

Similarly, the decrease in the REE concentrations in the Nakan suite appears to require the presence of small amounts of apatite, zircon and allanite. These phases may also have been present during the fractionation of the Magerang-Imang melt but if they were, their presence is obscured by the dominating influence of amphibole. The presence of inherited zircons and positive Zr and Hf anomalies in the trace element patterns, show that zircon became saturated early in the fractional crystallisation of these magmas.

Chapter 5
PLATINUM GROUP ELEMENTS, RHENIUM AND GOLD SYSTEMATICS IN THE ANDESITE PORPHYRIES OF THE KELIAN IGNEOUS COMPLEX

5.1 Introduction

The correlation between epithermal gold deposits and calc-alkaline volcanism is well known (Hayba et al, 1985; White and Hedenquist, 1990; Simon et al., 1999). What is less well understood is the cause of this relationship. Is the gold of magmatic-hydrothermal origin, with the gold deposited from hydrothermal fluids released during the final stages of fractionation of a calc-alkaline system, or do the andesitic or rhyolitic stocks that are commonly associated with the gold merely act as a heat source that drives the ore-forming hydrothermal system? If the ore is deposited from a magmatic-hydrothermal fluid, do the associated calc-alkaline rocks follow a fractionation trend that leads to the concentration of gold in the residual melt?

Igneous intrusions associated with gold deposits are commonly highly oxidised (White and Hedenquist, 1990). If this is an important geochemical factor, it might be that magmatic-hydrothermal deposits are produced by extreme fractional crystallisation of oxidised calc-alkaline magma systems. Gold is chalcophile and will partition strongly into an immiscible sulfide phase. As a consequence, if the magma becomes sulfur saturated during fractionation, gold will be rapidly depleted in the fractionating system. Sulfur saturation during fractional crystallisation is common in mafic–intermediate igneous rocks (Wendlandt, 1982, Hoatson and Keays, 1989, Keays, 1995) and Au is generally thought to complex with S and to be concentrated by this process (Seward, 1991, Hedenquist and Lowenstern, 1994). Alternatively, if the magma is highly oxidised, sulfur will reside in the magma as sulphate rather than sulfide and gold will complex with Cl instead of bisulfide and therefore behave as an incompatible element concentrated during fractionation (Loucks and Mavrogenes, 1999).

In order to test the hypothesis that gold is concentrating during the fractional crystallisation of the calc-alkaline systems associated with major gold deposits, Au, Cu

and platinum group elements (PGE) were analysed in the igneous suite associated with the Kelian gold deposit, a typical epithermal gold deposit associated with calc-alkaline intrusions.

The behaviour of PGE (Pd, Pt, Rh, Ru, Ir and Os) are the focus of this study for two reasons. Firstly, the PGE partition more strongly into sulfides than Au with partition coefficients that are very high, possibly in excess of 10^5 (Keays and Campbell, 1981, Campbell and Barnes, 1984, Bezmen et al., 1994) These elements are therefore more sensitive indicators of sulfide fractionation than Cu and Au. This factor, together with their relative immobility during alteration, make them ideal elements for testing the importance of sulfur saturation on chalcophile element geochemistry in a fractionating calc-alkaline system. If it can be shown that the PGE (and by inference Au) are concentrated by fractional crystallisation, it could provide strong support for the magmatic-hydrothermal hypothesis for epithermal gold deposits.

Secondly, the PGE are more resistant to mobilisation by hydrothermal fluids than Au or Cu, and more likely to record primary igneous values. The andesites that host the gold at Kelian are highly altered, which raises the possibility that the PGE may have been mobilised during alteration. The Kelian analyses have therefore been supplemented by PGE analyses of andesites from two adjacent prospects, Magerang-Imang and Nakan, which are of similar age and geochemistry to the Kelian andesites, but are less altered. Alteration in the samples selected from these prospects is minimal and they allow the effects of igneous processes on PGE geochemistry to be assessed free of the influence of alteration.

After first establishing that the Kelian igneous rocks are a single, continuous fractionating, it is the logical next step to monitor Au, Cu and PGE during fractionation. This study represents the first PGE data for a fractionated suite of calc-alkaline andesite. Until recently, low level trace elements were impossible to analyse in felsic igneous rocks. The development of this technique represents a breakthrough in our ability to monitor important ore elements in felsic igneous system.

5.2 Analytical Methods

Platinum-group elements (PGE) and gold were concentrated using the nickel-sulfide fire assay method which has been widely used for PGE analysis; for example

Hoffman et al. (1978), Gregoire (1988), Martin (1990) and Jackson et al. (1990). This study employed a modified version of this method with pre-fusion spiking for isotope dilution, similar to that described by Ravizza and Pyle (1997). The analysis used mixed spike solutions of PGE (^{185}Re, ^{105}Pd, ^{195}Pt, ^{99}Ru and ^{191}Ir) and ^{190}Os prior to sample fusion. The procedure involved spiking the sample-NiS borax mixture, fusion of the powdered sample, NiS bead digestion, filtration, filter-paper digestion and final solution preparation for PGE analysis by ICPMS. Concentrations of PGE and gold were determined by isotope dilution for all PGE except the mono-isotopic elements rhodium and gold. Concentrations of Rh and Au were calculated using ^{106}Pd and ^{194}Pt, respectively. The assumption being that any losses of Rh and Au during processing were similar to losses of Pd and Pt, respectively.

5.2.1 Sample Preparation

The spike was weighed accurately in 7ml clean teflon vials on a fine balance in a clean laboratory. Five grams of whole-rock powdered sample were weighed into a Coors ceramic crucible. The spike was poured into the sample and dried at 70°C for an hour. It was then tipped from the crucible onto a weighing paper and mixed by rolling the spiked sample until a homogenous mixture was obtained. The spiked sample was then replaced in the crucible and mixed thoroughly with 5 grams of lithium metaborate flux, 0.5 grams Ni (Aldrich nickel powder) and 0.25 grams S (sublimated, sulfur powder). The crucible was placed inside a second 50 ml crucible, covered with a lid and fused in a pre-heated furnace at 1050°C for 1.5 hours, except for the fusion blank which was fused for 1 hour. After heating, the crucible was removed from the furnace, cooled, opened and the NiS bead was recovered. The bead was weighed and stored in a disposable aluminium dish. Recovery was generally 85 – 95%.

Bead digestions and filtrations were carried out in a laminar flow hood on a hot plate in a clean laboratory. Clean 15 ml Teflon vials were weighed before bead digestion, and prepared for filter-paper storage after filtration. The beads were placed in 150ml 6N HCl in clean Erlenmeyer flasks, covered with a watch glass and boiled (at ~150°C) to degas the HCl. The dissolution was regularly checked to maintain acid levels, prevent vigorous boiling and to keep the bead fizzing gently. This process normally took 2 to 6 hours. When the bead was completely dissolved as indicated by the absence of H_2S gas production, the flask was removed from the hot plate and allowed to cool. In few samples fine flakes of grey insoluble materials floated on the acid surface.

The solution was filtered through millipore filter paper using an assembly of Erlenmeyer flask, stopper, clean Pyrex funnel and hand pump. Milli-Q water was used to rinse the funnel rim and wall at the end of filtration. The filter paper was transferred into a weighed 15 ml Teflon vial and the filtrate was discarded. After filtration was completed, 3ml of 6N HNO3 was added into each vial, which was sealed well and refluxed at about 100°C for 2 hours until digeston was complete. When the papers were digested and there was no visible residue, the vials were opened and dried down to approximately 120 μL. The samples were then diluted with 6 ml of Milli-Q water and refluxed at 100°C for 2 hours, allowed to cool and stored overnight before ICPMS analysis.

5.2.2 ICPMS measurement

The measurements were made using an Agilent 7500 series ICPMS with an attached autosampler. Data were acquired in peak jumping mode and the counts at each mass were calculated from the average of measured rates at the three channels across the peak top. The following 28 masses were measured: ^{59}Co, ^{62}Ni, ^{65}Cu, ^{66}Zn, ^{89}Y, ^{90}Zr, ^{99}Ru, ^{101}Ru, ^{102}Ru, ^{103}Rh, ^{105}Pd, ^{106}Pd, ^{108}Pd, ^{180}Hf, ^{181}Ta, ^{185}Re, ^{187}Re, ^{188}Os, ^{189}Os, ^{190}Os, ^{191}Ir, ^{192}Os, ^{193}Ir, ^{194}Pt, ^{195}Pt, ^{196}Pt, ^{197}Au, ^{202}Hg. Instrumental calibration was carried out using a 10 ppb tuning solution containing a range of masses from 7 to 238. Common instrument operating conditions are listed in Table 5.1. Sensitivity varied from 248000 cps (1.6 %RSD) for mass 24, 348000 cps (<2 %RSD) for mass 115, and 220000 cps (1.35 %RSD) for mass 238, all at the 10 ppb level. LaO (155) to La (139) ratio was 0.6 – 0.75%. Washing between samples was 26 minutes, consisting of 2 minutes dilute triton, 5 minutes H_2O, 5 minutes 1N HCl, 5 minutes 5%HNO_3 and 5 minutes 2%HNO_3. All washes were at the rate of ~3 ml per minute. Molecular interferences on the analyte isotopes were corrected by measuring the interference solutions consisting of Ni+Y, Cu+Zr, Zn, Ta and Co elements before analysis of unknown. Samples were introduced to the ICPMS in automatic mode at a rate of about 1 ml / minute.

5.2.3 Data Processing

Raw count data of ICP-MS were processed in a Microsoft Excell worksheet. Reported PGE concentrations are calculated after blank substraction, interference solution correction factors and mass fractionation correction factors were applied. The interference elements and correction factors are listed in Table 5.2.

5.3 Analytical Results

A total of 19 andesite samples were selected from 3 different intrusive bodies of the Magerang-Imang, Nakan and Kelian mine areas and analysed for PGE and gold (Figure 5.1). A fusion blank (FB) was prepared and analysed in every session of ICPMS measurement. Concentrations of PGE, except Os in the FB were consistently lower than those measured in samples. The Os values are high in the FB, possibly due to overspiking. Copper concentrations in the samples were measured by a glass fusion technique with the laser ablation ICPMS. The concentrations of PGE, Au and Cu in the Kelian, Magerang-Imang and Nakan andesites are presented in Table 5.3. Tables 5.1, 5.2 and 5.3 are given in Appendix 9. The primitive mantle normalised PGE, Au and Cu concentrations are presented in order of increasing melting points and degree of compatibility in Figure 5.2.

5.4 Platinum Group Elements, Rhenium and Gold Distributions in The Andesite Porphyries of The Kelian Igneous Complex

In the Magerang-Imang hornblende andesite, patterns are sub-parallel over a range of PGE concentrations that vary by a factor of 20 (Figure 5.2a). All the Magerang-Imang samples are depleted in Ru, Ir and Os relative to Re, Pd, Pt and Rh and have moderate Pd/Ir ratios of 15 to 54. Slopes of the patterns flatten between Ru and Ir so that Ru/Ir ~1 and Ir/Os <1 on the normalised plot. Iridium and Os concentrations vary more erratically than the other PGE, and this variation is probably due to the difficulty of analysing Ir and Os at concentrations close to their detection limits. The concentration of all PGE decrease with increasing SiO_2 (Figures 5.3) and with increasing Th (Figure 5.4), suggesting that they are depleted by fractional crystallisation. Gold is depleted by an order of magnitude relative to Re and Pd, the adjacent elements on the mantle-normalised PGE diagram.

The Nakan pyroxene andesite shows similar pattens to the Magerang-Imang andesite but with a more restricted range in PGE concentrations. This is consistent with a more restricted range in SiO_2 and therefore less fractional crystallisation (Figure 5.2b). Slopes of the normalised patterns between Ru and Ir do not show the turn around seen in

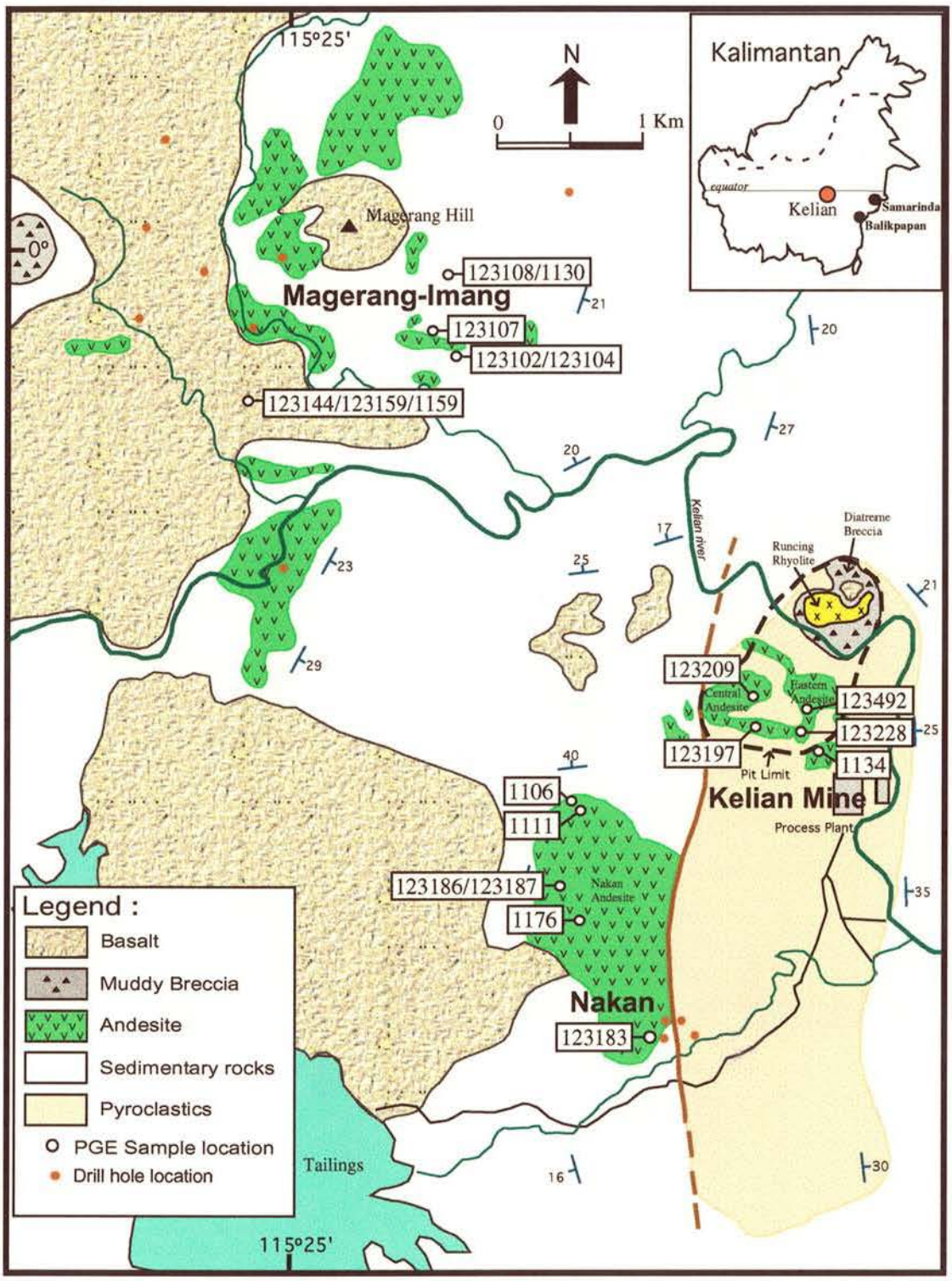

Figure 5.1: Simplified geological map of the Kelian area and location of the PGE samples

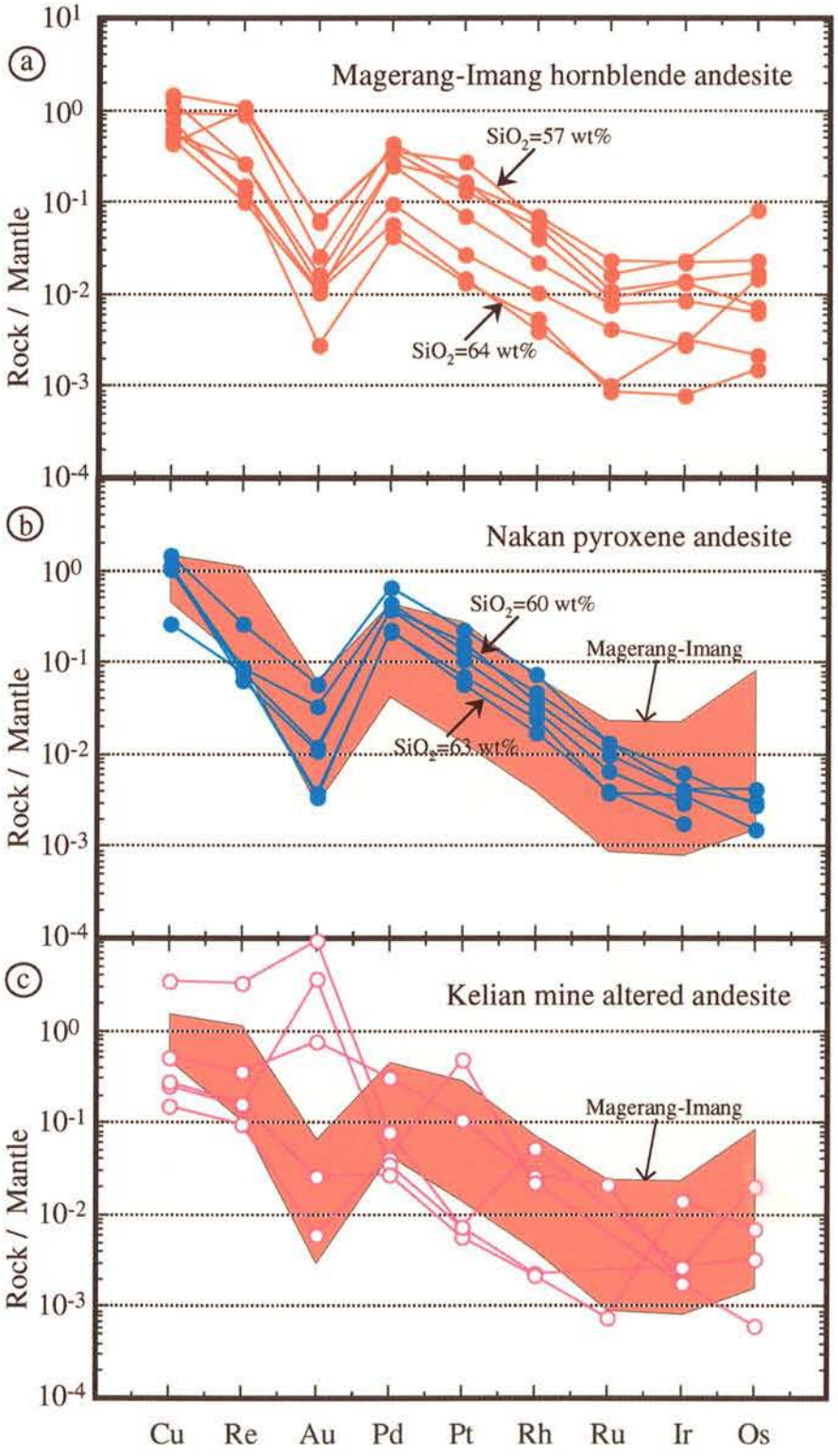

Figure 5.2 : Mantle-normalised metal abundances for the igneous suites from Magerang-Imang, Nakan and Kelian. Mantle values are taken from Barnes et al.(1988).

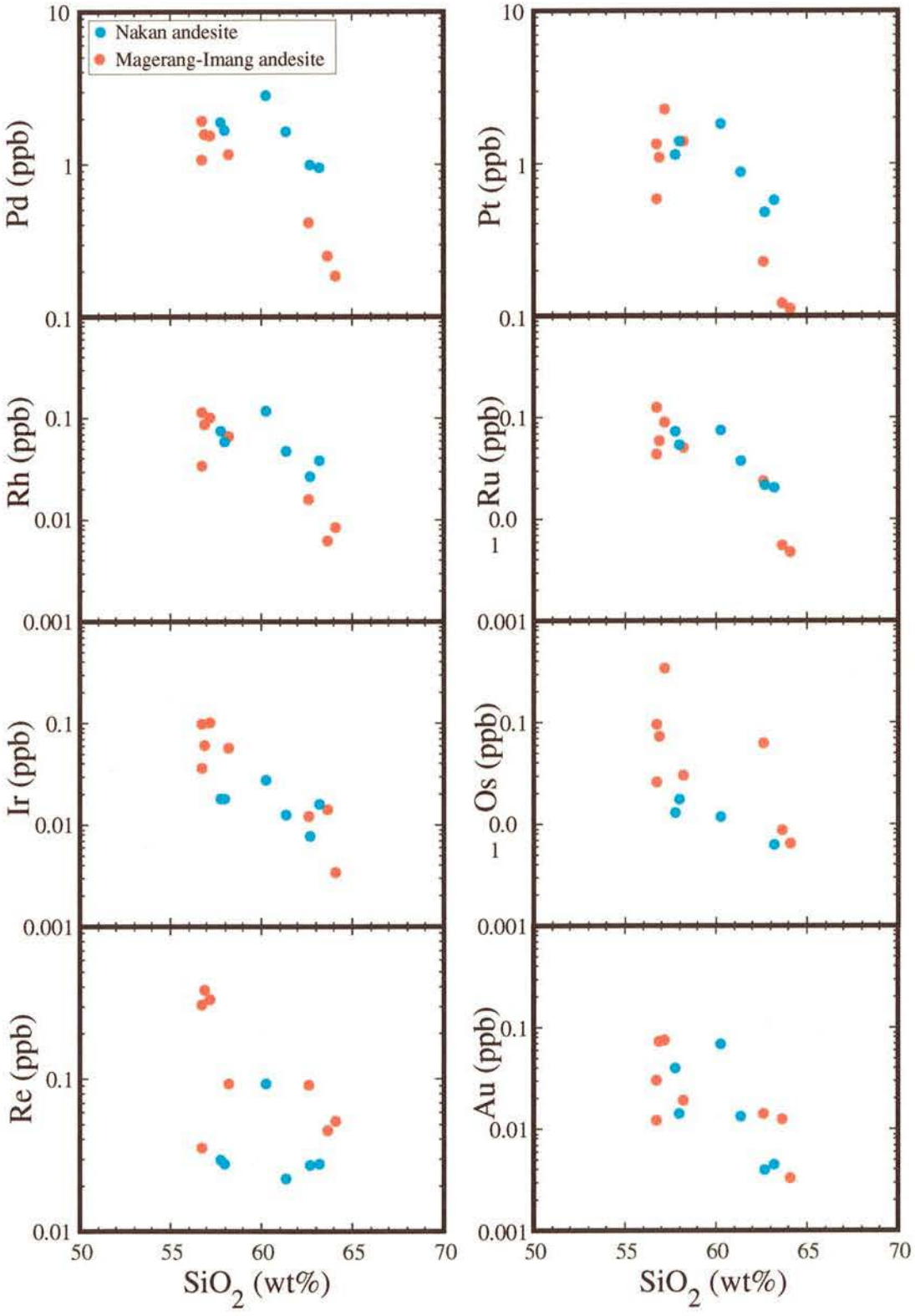

Figure 5.3 : Variation diagrams of PGE vs SiO_2 for the Magerang-Imang hornblende andesite and Nakan pyroxene andesite

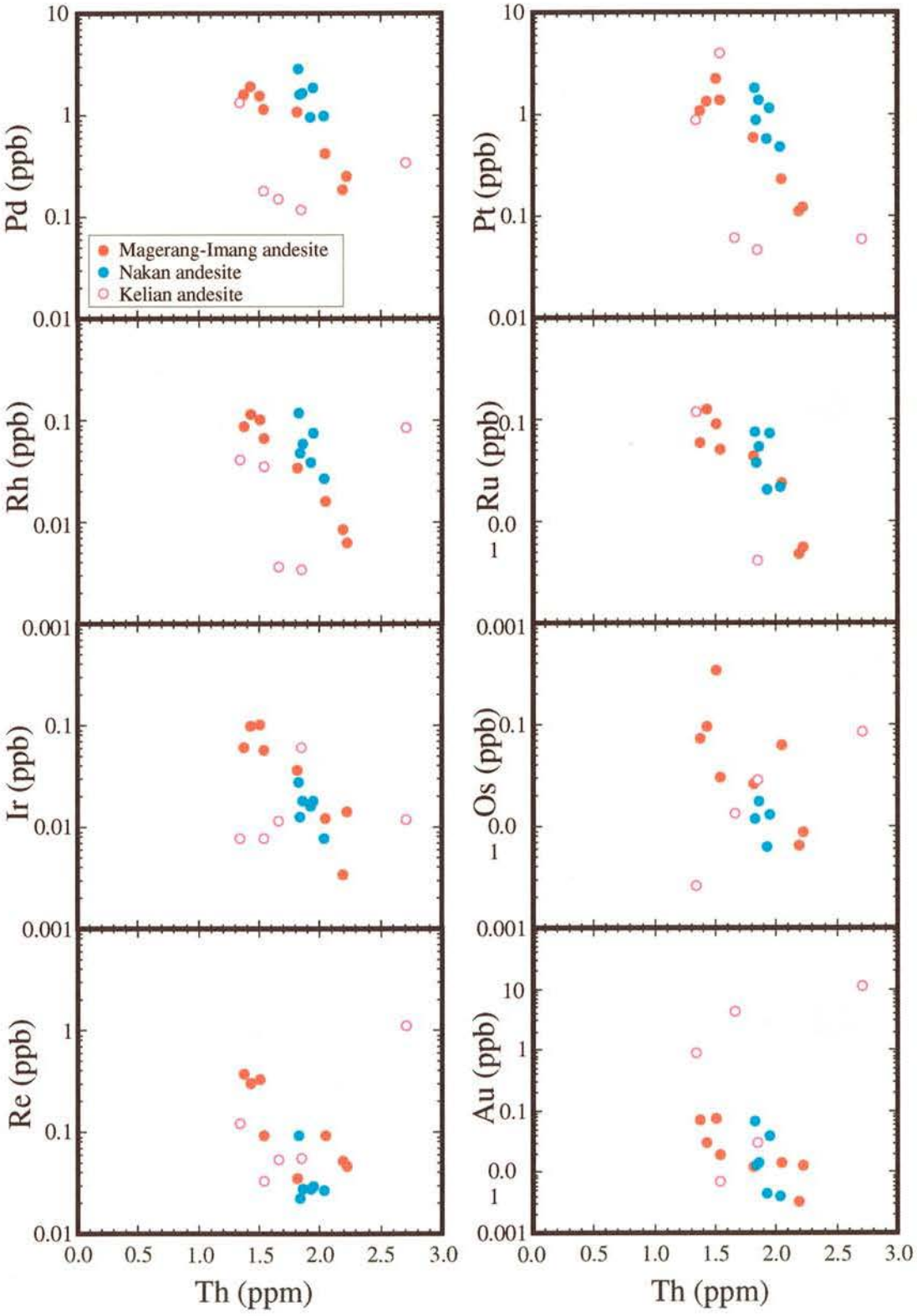

Figure 5.4 : Variation diagrams of PGE vs Th for the Magerang-Imang hornblende andesite, Nakan pyroxene andesite and Kelian altered andesite

the Magerang-Imang suites so that the order of concentration of PGE is Ru > Ir > Os. As a consequence, Pd/Ir values are 60 –129 for the Nakan suite, which is greater than those for the Magerang-Imang suite. Plots of Ir versus Pd display a strong positive correlation in the Magerang-Imang suite and indicate that the Nakan suite is depleted in Ir (Figure 5.5). The higher Pd/Ir ratio in the Nakan andesite is therefore due to Ir depletion rather than Pd enrichment relative to the Magerang andesite.

In the Kelian mine samples, the PGE values tend to be more erratic than those in the Magerang-Imang and Nakan samples (Figure 5.2c). This may be due to mobility of the PGE during the extreme alteration associated with the gold mineralisation. Plots of PGE against Th show that PGE are generally lower at a given level of fractional crystallisation for Kelian than for the Magerang-Imang and Nakan suites (Figure 5.4). A notable exception is sample 123492 which has high Re and moderate Pd, Rh and Os. It may be significant that this is the most fractionated of the analysed samples as indicated by its high Th concentration. The Pd/Ir ratio in the Kelian mine andesite varies widely. The Central Andesite, for example, has a Pd/Ir ratio of 174 due to Pd and Au enrichment, which contrasts with a Pd/Ir ratio of 2 for the Tepu propylitic andesite due to the anomalous Ir value. The slightly altered samples from the Kelian mine area show a negative anomaly of Au similar to that of the Magerang-Imang suite, whereas the highly altered andesite exhibits a positive anomaly of Au, probably because Au was introduced by the ore-forming hydrothermal fluid. Os abundance in the Kelian mine samples are very low and close to the FB value. However, Os concentrations increase with increasing degree of fractionation as indicated by the Th content in the Kelian andesites.

In a fractional crystallisation system, if olivine, chromite and clinopyroxene have crystallised, Pd and Pt are expected to behave as incompatible elements, but Pd and Pt do not correlate with the lithophile incompatible elements (Barnes and Picard, 1993). Palladium, Pt and Rh tend to remain in the silicate melt until sulfur saturated, when the sulfide melt extracts the Pd, Pt and Rh. The PGE behave more compatible relative to Au and Cu as indicated by depletion in PGE relative to Au and Cu in the andesite samples. In the Kelian andesite suite, Pd, Pt and Rh behave as compatible elements, but tend to be more mobile with increasing degrees of fractional crystallisation. Whereas Ir and Os behaviour is less consistent, but tends to be more enriched with increasing differentiation. The metal distribution pattern of the Kelian altered andesite suggests that Au and Cu have been affected by hydrothermal fluid. Although alteration is not a major factor in the PGE

fractionation (Barnes et al., 1985), Pd is probably also mobile as indicated by the low Pd/Ir ratio in the Kelian altered andesite.

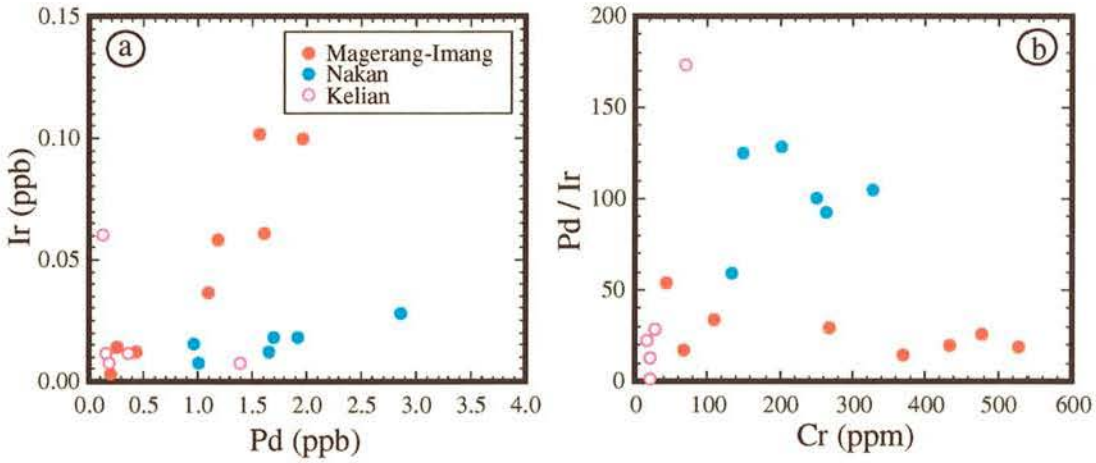

Figure 5.5 : The ratio of Pd/Ir in the Magerang-Imang, Nakan and Kelian suites indicating the low abundance of Ir in the Nakan andesite relative to the Magerang-Imang andesite (a) causing high ratios of Pd/Ir in the Nakan andesite.

5.5 Depletion of Gold, Copper and Platinum Group Elements in The Host Intrusive Andesite of The Kelian Gold Deposit: An Unexpected Result

A feature of the mantle-normalised Cu-Au-PGE patterns, for the least altered samples from the Kelian region, is that Au is depleted by about an order of magnitude relative to the adjacent elements, Re and Pd. A plausible interpretation for the Au depletion in the Nakan and Magerang-Imang samples is that the Au was stripped during the hydrothermal event that gave rise to the gold at Kelian. There are, however, two observations that are inconsistent with this hypothesis. Firstly, the Nakan and Magerang-Imang samples selected for analysis show little sign of alteration. Secondly, the magnitude of the Au depletion is similar in samples of variable SiO_2 content, including the most primitive samples. It is concluded that the gold depletion developed prior to emplacement of the andesites into the upper crust and that these values were not significantly affected by alteration.

The low concentration of gold in the igneous rocks associated with the Kelian gold deposit is unexpected. The host rocks to most metal deposits are already enriched in the metal of interest, e.g. Au in Archaean greenstone, Ni in komatiites and basalt, Fe in banded iron formation, Cr in gabbros, etc. It is therefore surprising to find a major gold deposit in host rocks that are depleted in Au.

Another unexpected feature of the data is that Au and the PGE decrease with increased fractional crystallisation. This relationship suggests that the calc-alkaline magmas in the Kelian region became sulfur saturated early in their crystallisation history. If the gold at Kelian has a magmatic-hydrothermal origin, the reverse might be expected to be true. It might be argued that the Nakan and Magerang-Imang prospects are not associated with major gold deposits and have a different sulfur saturation history to the calc-alkaline rocks directly associated with the mineralisation at Kelian. However, plots of PGE against Th show that the Kelian andesites have even lower PGE concentrations at a given level of fractionation than their Nakan and Magerang-Imang equivalents. These observations, together with the low Au content of the host rocks make it difficult to reconcile the mineralisation with a magmatic-hydrothermal hypothesis that links the gold with the Kelian andesites.

Another enigmatic feature of the data is that the Cu-Au-PGE patterns remain parallel as their concentrations decrease with increasing SiO_2. The Au and PGE ratios change little during fractionation. This is surprising because it implies either that the partition coefficients for the PGE into the sulfides are similar, which seems unlikely, or that Au and the PGE are not being depleted by simple equilibrium fractional crystallisation of sulfide. This is unlikely to be due to simple equilibrium of fractional crystallisation involving an immiscible sulfide melt. If the immiscible sulfide melt maintains equilibrium with the magma in the chamber, the Cu-Au-PGE patterns can only remain parallel if partition coefficients for Cu, Au and all of the PGE between immiscible sulfide and silicate melts are the same which is unlikely. Most of the sulfides in layered intrusions are found near the margins of the intrusions where the magma chamber is loosing heat through its wall (Keays and Campbell, 1981). A more realistic explanation for the parallel Cu-Au-PGE patterns is that the chalcophile element depletion in the Nakan, Magerang-Imang and Kelian andesites is due to a non-equilibrium process. It is possible that sulfide precipitation occurs in a narrow boundary layer of cool magma at the margins of the intrusion.

The implication is that sulfide precipitation in the parent intrusion to the Kelian andesites can not have been an equilibrium process. Sulfide precipitation in a layered intrusion is concentrated at the margins where the magma cools against the sides of the intrusion (Keays and Campbell, 1981). It is possible that sulfide precipitation in the Kelian parent magma chamber occurred rapidly, under disequilibrium conditions at the cooling margin of the intrusion.

5.6 Discussion

The fact that Au and the PGE decrease in a similar manner during the evolution of the Kelian igneous suite is difficult to explain. There are four possible explainations for gold and PGE fractionation in igneous suites. First, Au, Cu and PGE are fractionated due to sulfur saturation during fractional crystallisation. As chalcophile elements with very high partition coefficients, gold and PGE show extremely compatible behaviour in mafic magma system and would be preferentially concentrated in the sulfide fraction. Based on the magmatic theory of ore formation, a sulfide liquid segregates from silicate magma, carrying the gold and PGE with it and discrete precious metal minerals subsequently form from the products of fractional crystallisation. Evidence for this chalcophile tendencies is clearly observed in the PGE sulfide phases associated with Ni-Cu sulphide ores (Naldrett et al, 1979, Campbell et al., 1983). The sulfur saturation possibly originates in the magma source region (Wendlandt, 1982). Second, Au, Cu and PGE are fractionated due to fluid saturation. Third, in the absence of sulfide phases, PGE fractionation may be governed by their solubility and partitioning behaviour in oxide and silicate phases (Capobianco and Drake, 1994; Nell and O'Neill, 1997). It has been recognised that PGE, in particular Ru, Rh (Capobianco and Drake, 1990), Pd and Ir partition into spinel (Mitchell and Keays, 1981). Partitioning of gold in titanomagnetite during fractional crystallisation has been observed in island-arc tholeiitic rocks (Togashi and Terashima, 1997). However, in these three processes, whereby Au and PGE are physically removed, none of these processes remove Au and individual PGE to the same degree. For instance, Ru partitions readily into spinel but Ir does not (Nell and O'Neill, 1997). Thus, spinel crystallisation strongly fractionates Ru, from Ir, which is not shown in the Kelian suite. Similarly, partition coefficients between silicate and sulfide melts for Re and Ir differ by

orders of magnitude, such that sulfur saturation would quantitatively deplete the melt of Ir, but not Re. Again, the Kelian data do not support such a process. Although less well understood, exsolution of a hydrothermal fluid efficiently transports Au, Cu, Sn and W, but has not been shown to be an effective carrier of Pt or Ir. Fourth, assimilation of crustal material. This appears to be the most plausible process for the gradual depletion of Au and all of the PGE at Kelian. It is suggested that simple dilution with crustal material that contains no Au or PGE is the most likely process that will decrease the abundance of all of the PGE equally. This conclusion is consistent with the results obtained from major and trace element geochemistry (Chapter 3) and geochronology (next Chapter 6).

Chapter 6

GEOCHRONOLOGY OF THE KELIAN IGNEOUS COMPLEX AND ASSOCIATED EPITHERMAL GOLD MINERALISATION

6.1 Introduction

The Kelian disseminated gold deposit is mostly hosted by the andesite porphyries, locally named Central Andesite and Eastern Andesite, and this relation suggests that the mineralisation is genetically associated with a specific event in the evolution of the Kelian igneous complex. The presence of quartz and sulfide veins cutting the Central Andesite (Van Leeuwen et al., 1990) may indicate that the emplacement of the andesite took place shortly before the main hydrothermal event. Near-surface convective systems that produce hydrothermal ore deposits are likely to cool on a time scale of few tens of thousands of years up to 100 thousand years (Cathles et al., 1997). It is therefore possible that the gold mineralisation at Kelian is related to the emplacement of the Kelian igneous complex. However, the time constraint of the host rocks and mineralisation is not known, nor has it been established whether the gold mineralisation was formed by a hydrothermal fluid system driven by the andesitic magmatism or by processes related to the phreatomagmatic activity associated with the intrusion of a maar-diatreme complex (the Runcing diatreme) that occurs in close spatial association with the ore. Alternatively, the gold mineralisation may be post the Kelian igneous complex and related to a later thermal event at depth.

The absolute age of the various igneous rocks at Kelian has not been established. The volcaniclastic rock units have been assigned a Late Eocene age (Van Leeuwen et al., 1990), based on the biostratigraphic age of intercalated limestones. The

Central Andesite and Eastern Andesite join at depth and contain xenoliths of tuff and volcaniclastic sediments indicating that they are younger than those units. The Tepu diatreme breccia is clearly younger than the andesites as it contains fragments of andesite near its margins. The Central Andesite, Eastern Andesite and the Runcing diatreme breccia are cut by mineralised veins indicating that all three units are older than mineralisation. The absence of Au-bearing veins in the Runcing Rhyolite porphyry suggests that this unit was emplaced after the main gold mineralisation event. Thus, on the basis of geologic relations, the gold mineralisation is younger than the Central Andesite but older than the Runcing Rhyolite.

This chapter describes ELA-ICP-MS U-Pb zircon dates for andesite and rhyolite intrusions from the Kelian area and attempts to relate the ages obtained with published K-Ar age for the mineralisation at Kelian. If there is a resolvable age difference between the andesite and rhyolite porphyries, it may be possible to relate the mineralisation with either the andesite or maar-diatreme emplacement. Alternatively, if they have similar ages, both andesite and rhyolite may have been derived from a single evolving magmatic-hydrothermal system that can be related to the mineralisation. This study also tests possible temporal links between the low sulfidation Kelian gold deposit and high sulfidation mineralisation at Magerang-Imang, by dating the host rocks to both types of mineralisation. In addition, samples of andesite-dacite porphyries from the Nakan, Han and Plata prospects were dated in this study to constrain the timing of calc-alkaline magmatism in these areas. Two sets of detrital zircons from the Kelian and Mahakam rivers were also dated to constrain the overall duration of regional-scale magmatic events in the Kelian and Mahakam areas and to relate the timing of the gold mineralisation to these events.

6.2 Principles of U-Pb Zircon Geochronology

Unstable radioactive elements, such as uranium, thorium and lead, decay by the spontaneous emission of alpha and beta particles from their nuclei through chain reactions of unstable atoms ending with stable daughter isotopes. Each radioactive isotope has a decay constant (λ) and a half-life which is an interval of time for a radioactive isotope to

decay to half of the original number of parent atoms. By measuring daughter to parent atom ratios, the age of a mineral can be determined using the following equation:

$$t = \frac{1}{\lambda} \ln(1 + \frac{D^*}{N})$$

Where: t is time, λ is a decay constant, D* is the number of daughter atoms and N is the number of remaining parent atoms.

There are three radioactive isotopes of uranium: ^{238}U, ^{235}U and ^{234}U and one radioactive isotope of thorium: ^{232}Th. ^{238}U, ^{235}U and ^{232}Th decay to ^{206}Pb, ^{207}Pb and ^{208}Pb, respectively via a series of short-lived intermediate daughter products. In addition, lead has an isotope of ^{204}Pb which is weakly radioactive but not radiogenic. ^{204}Pb is commonly used as a stable reference isotope for rationing the other radiogenic U-Pb isotopes. In a system that has remained closed to uranium, thorium and lead during the history of crystallisation, the lead isotopes produced by the decay of uranium and thorium can be determined by the following equations (Faure, 1977):

$$\frac{^{206}Pb}{^{204}Pb} = \left(\frac{^{206}Pb}{^{204}Pb}\right)_o + \frac{^{238}U}{^{204}Pb}(e^{\lambda_{238}t} - 1)$$

$$\frac{^{207}Pb}{^{204}Pb} = \left(\frac{^{207}Pb}{^{204}Pb}\right)_o + \frac{^{235}U}{^{204}Pb}(e^{\lambda_{235}t} - 1)$$

$$\frac{^{208}Pb}{^{204}Pb} = \left(\frac{^{208}Pb}{^{204}Pb}\right)_o + \frac{^{232}Th}{^{204}Pb}(e^{\lambda_{232}t} - 1)$$

where $\frac{^{206}Pb}{^{204}Pb}, \frac{^{207}Pb}{^{204}Pb}, \frac{^{208}Pb}{^{204}Pb}$ = isotope ratios of lead in the mineral at the time of analysis,

$\left(\frac{^{206}Pb}{^{204}Pb}\right)_o, \left(\frac{^{206}Pb}{^{204}Pb}\right)_o, \left(\frac{^{206}Pb}{^{204}Pb}\right)_o$ = initial isotope ratios of lead incorporated into the mineral at the time of its formation,

$\frac{^{238}U}{^{204}Pb}, \frac{^{235}U}{^{204}Pb}, \frac{^{232}Th}{^{204}Pb}$ = isotope ratios in the mineral at the time of analysis,

$\lambda_{238}, \lambda_{235}, \lambda_{232}$ = decay constants,

t = time elapsed since closure of the mineral to U, Th, Pb and all intermediate daughters.

The ultimate parent-daughter pairs of uranium and thorium with their decay constants are given as follows (Jaffey et al., 1971):

Decay series	Half-life (billion years)	Decay constant λ (year^{-1})
$^{238}U \rightarrow {}^{206}Pb$	4.47	1.55125×10^{-10}
$^{235}U \rightarrow {}^{207}Pb$	0.704	9.8485×10^{-10}
$^{232}Th \rightarrow {}^{208}Pb$	14.01	0.49475×10^{-10}

By using appropriate values of initial lead isotope ratio, the date can be defined based on the decay of ^{238}U to ^{206}Pb as

$$t_{206} = \frac{1}{\lambda} \ln \left[\frac{\left(\frac{^{206}Pb}{^{204}Pb} - \left(\frac{^{206}Pb}{^{204}Pb} \right)_o \right)}{\frac{^{238}U}{^{204}Pb}} + 1 \right]$$

The other dates, based on the decay series of $^{232}Th/^{208}Pb$ and $^{235}U/^{207}Pb$, can be solved using the similar formulas. If these three independent ages are equal, they are named as "concordant", then they represent the age of mineral within a closed, undisturbed U-Pb system.

Zircon minerals ($ZrSiO_4$) in various crustal rocks contain trace amount of uranium and thorium concentrations, in order of a few hundred to a few thousand parts per million, which allow for relatively precise and accurate measurement of Pb/U and Pb/Pb ratios by a mass spectrometer. The decay of uranium to lead in zircon has become one of the most widely used geochronometer with a relatively high closure temperature of 900°C (Lee et al., 1997). Zircon minerals are resistant to hydrothermal processes and weathering as well, so they are therefore suitable to dating altered rocks and to constrain the duration of magmatism in a region.

6.3 Analytical Methods of U-Pb Zircon Dating by Excimer Laser Ablation Inductively Coupled Plasma Mass Spectrometer

Zircons were separated from whole-rock samples using standard magnetic and heavy liquid separation techniques. Sample and standard zircons were mounted in epoxy, polished and photographed in transmitted and reflected light. A scanning electron microscope was used to produce cathodoluminescence (CL) images of all mounts. Standards used in this study were the synthetic glass NIST 612 (Pearce et al., 1997) and zircon grains from the Temora gabbro which has an age of 417 Ma (Black et al., 2000). Zircon U-Th-Pb isotope dates were determined in situ using ELA-ICP-MS.

Zircons were ablated using a pulsed ArF excimer laser (Lambda Physik LPX 120I) emitting at 193nm with a nominal pulse width of 20ns and a pulse stability of about 5%. For this zircon dating, laser sampling was carried out using a 48 micron diameter spot, at a constant voltage of 21-23 kV and a repetition rate of 5 Hz. The sample discs were loaded in a translational stage in a gas-tight sample cell that can be viewed through a video monitor. The sample cell is flushed by He at a flow rate of 300 ml/minute and Ar at a flow rate of 1100 ml/minute. Targets for laser ablation were chosen as near as possible to the rims of zircons, which were clear, unfractured and free of inclusions, as can be seen on the photomicrograph and CL image (Figure 6.1 and 6.2). The zircon crystals were ablated for 50 seconds following a 20 second interval of background acquisition with the laser off, resulting in ~100 data scans for a penetration depth of ~25 microns. The ablated material, together with carrier gas, was transported to an Agilent 7500 (HP) Series-ICPMS through a custom-designed signal homogeniser.

Data were acquired for 8 isotopes (^{29}Si, ^{31}P, ^{96}Zr, ^{206}Pb, ^{207}Pb, ^{208}Pb, ^{232}Th and ^{238}U) was carried out by peak hopping in pulse counting mode. The ^{204}Pb isotope was not measured due to a high background of ^{204}Hg. Temora standard zircon and NIST 612 standard glass were measured twice after every 10 and 20 analyses of unknown samples, respectively. The unknowns were measured on a rotational order consisting of two laser ablation spots on each grain from each sample making batches of 10 unknowns per rotation. In this study, U-Pb zircon dates were based on 26 to 32 spot analyses for each

igneous rock sample and 127 and 153 spot analyses for the Kelian and Mahakam river detrital samples, respectively.

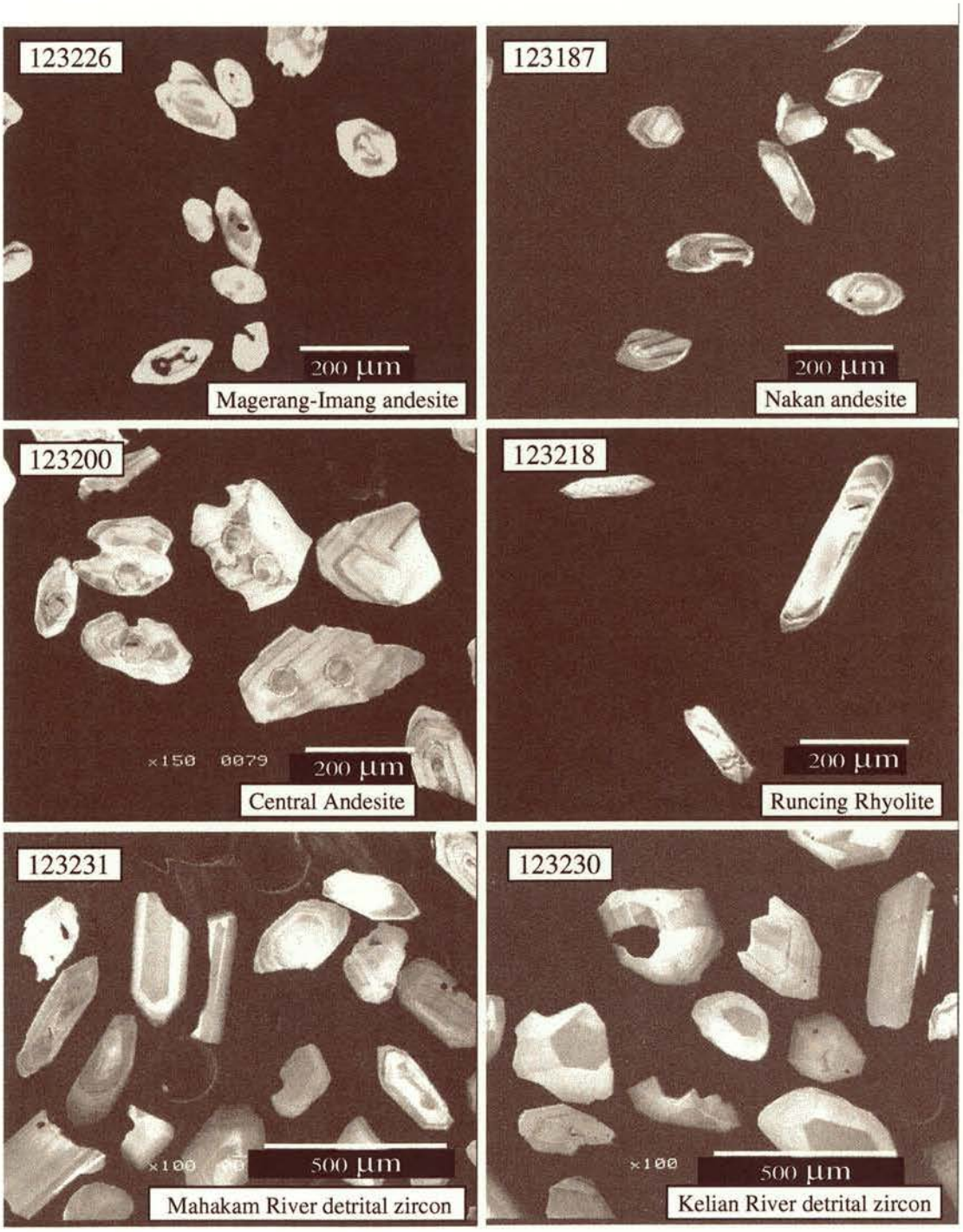

Figure 6.1: Cathodoluminescene (CL) images of zircon samples from the Kelian region

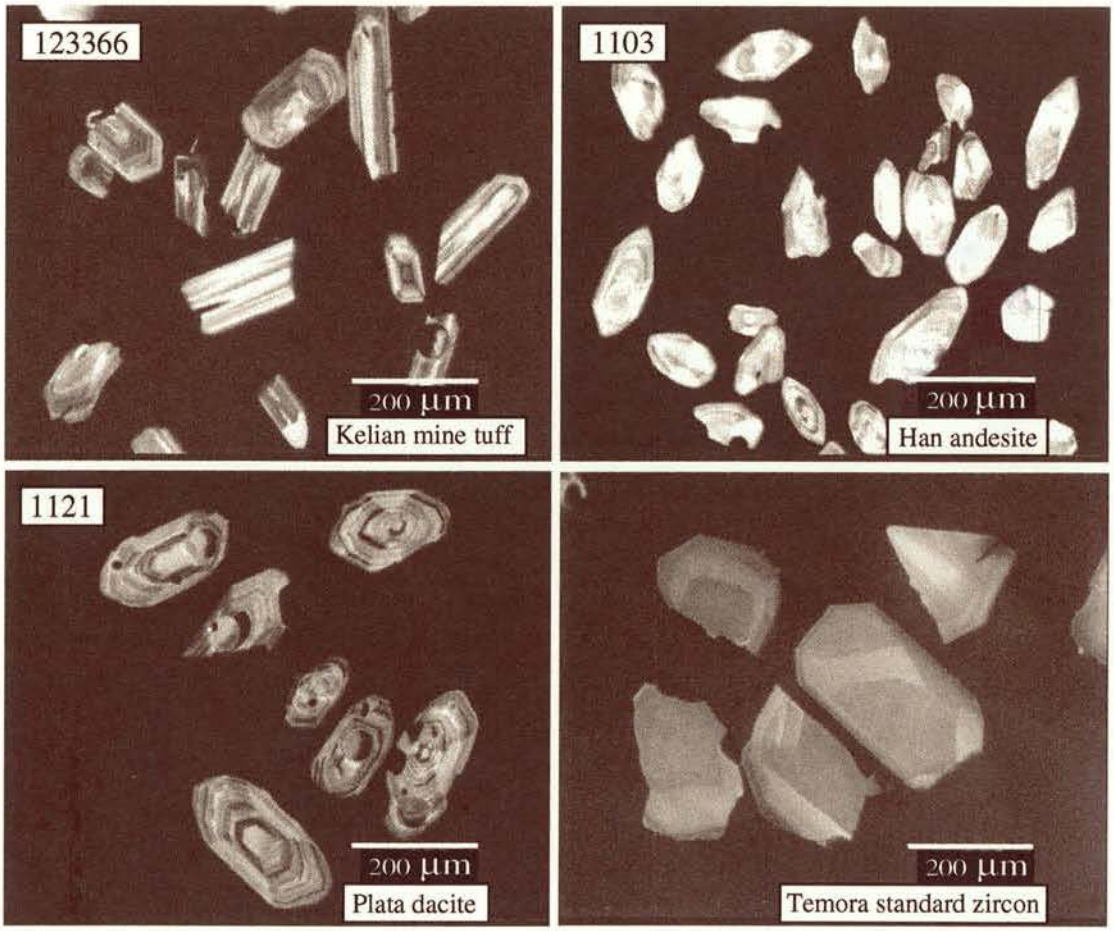

Figure 6.2: Cathodoluminescene (CL) images of zircon samples from the Kelian mine and regional prospects, and the Temora standard zircon .

6.4 Data Reduction

Data reduction was processed offline in a Microsoft Excel 98 spreadsheet, which allowed background subtraction, outlier detection, isotope ratio calculation for standard zircon (Temora) and glass (NIST 612) and U-Pb date calculation for each spot analysis (Palin et al., 1998, Ballard et al., 2001). The first 5-10 data scans obtained after switching on laser had high common Pb from surface contamination and were excluded from the calculation. U-Pb date calculation for each spot analysis involved calculation of background-subtracted and mass fractionation-corrected ratios of $^{206}Pb/^{238}U$, and calculation of common Pb corrected ratios of $^{206}Pb/^{238}U$. Depth-related elemental fractionation of U-Th-Pb (e.g. Hirata and Nesbitt, 1995; Horn et al., 2000) and instrumental mass bias were corrected using measured $^{207}Pb/^{206}Pb$, $^{206}Pb/^{238}U$ and $^{208}Pb/^{232}Th$ ratios in the Temora zircon standard (Black et al., 2000) averaged over the course of an analytical session. Drift in instrumental mass bias was calculated from correlated variations between $^{206}Pb/^{238}U$ and $^{29}Si/^{96}Zr$ in the standard zircon over the course of the analytical session. Common lead corrections were made following the method employed by Compston et al. (1984). $^{206}Pb/^{238}U$ ratios were then corrected for common Pb using $^{207}Pb/^{206}Pb$, assuming that the measured $^{206}Pb/^{238}U$ and $^{208}Pb/^{232}Th$ were concordant within analytical error.

Reported U-Pb ages for the igneous rocks are weighted averages of data selected from individual spot analyses. Uncertainties for the individual spot analyses, at the 95% confidence level, were calculated by two methods to obtain what we have called observed and expected errors. The observed error was calculated from the observed variance in the individual dates calculated for each of the ~ 80 data scans made during the analyses of individual grains, whereas the expected error was obtained from the counting statistics. All grains which had individual MSWD values larger than 2 or had ratios of observed/expected error larger than 3 are excluded from age calculation. Only data that lie within 95% of concordance at the 1 σ level were used for the age calculation.

There is evidence of multiple age populations in some samples. In order to test this possibility, the data from each sample were examined using cumulative probability diagrams. If the data represent a single age population, most points will lie on a straight

line with the possible exception of short tails at each end due to the expansion of the scale in this region. Outliers lying above this line at old ages were assumed to represent inherited zircons and outliers falling below the line at young ages were ascribed to lead loss and were rejected. Statistical calculations were done after these outliers were excluded and the population that represents the age of sample was selected. The mean square of weighted deviates (MSWD) was then calculated in order to test whether the selected grains formed a statistically acceptable single population. If the observed deviations from the sample mean are within analytical error and there is no geological error due to inhomogenity in the sample, the expected (mean) value of MSWD is about 1 (Wendt and Carl, 1991). Estimated minimum and maximum expected values of MSWD were also calculated at the 95% confidence level according to formulas in Wendt and Carl (1991). Age populations have MSWD values above the expected maximum value if the analytical errors are underestimated or if the dates for the grain give a range of ages that lie outside analytical uncertainty. If the weighted average date for a population have higher MSWD values than the upper limit of the estimated MSWD values, the MSWD of the population can be reduced by excluding the grains which contribute most to the high MSWD values. The mean and 2σ error are given in Table 6.1 for both populations. The less selective data are considered in the discussion.

The data from samples that yield multiple age populations, such as the Central Andesite, Runcing Rhyolite and Kelian Tuff, were initially processed the same way as for single population data. The data for these samples form two or more straight line-segments separated by ***S*** shaped curves on probability plots. Individual populations are separated by points of inflection between the straight lines. The mean age of each population was calculated using the ***Mix*** program written by Gallagher and Sambridge (1992) for processing multi-component data sets.

Detrital zircon raw data were reduced using the similar method of date calculation as for igneous zircon samples, but the grains were treated individually and the population MSWD criteria were not applied.

6.4 Data Reduction

Data reduction was processed offline in a Microsoft Excel 98 spreadsheet, which allowed background subtraction, outlier detection, isotope ratio calculation for standard zircon (Temora) and glass (NIST 612) and U-Pb date calculation for each spot analysis (Palin et al., 1998, Ballard et al., 2001). The first 5-10 data scans obtained after switching on laser had high common Pb from surface contamination and were excluded from the calculation. U-Pb date calculation for each spot analysis involved calculation of background-subtracted and mass fractionation-corrected ratios of $^{206}Pb/^{238}U$, and calculation of common Pb corrected ratios of $^{206}Pb/^{238}U$. Depth-related elemental fractionation of U-Th-Pb (e.g. Hirata and Nesbitt, 1995; Horn et al., 2000) and instrumental mass bias were corrected using measured $^{207}Pb/^{206}Pb$, $^{206}Pb/^{238}U$ and $^{208}Pb/^{232}Th$ ratios in the Temora zircon standard (Black et al., 2000) averaged over the course of an analytical session. Drift in instrumental mass bias was calculated from correlated variations between $^{206}Pb/^{238}U$ and $^{29}Si/^{96}Zr$ in the standard zircon over the course of the analytical session. Common lead corrections were made following the method employed by Compston et al. (1984). $^{206}Pb/^{238}U$ ratios were then corrected for common Pb using $^{207}Pb/^{206}Pb$, assuming that the measured $^{206}Pb/^{238}U$ and $^{208}Pb/^{232}Th$ were concordant within analytical error.

Reported U-Pb ages for the igneous rocks are weighted averages of data selected from individual spot analyses. Uncertainties for the individual spot analyses, at the 95% confidence level, were calculated by two methods to obtain what we have called observed and expected errors. The observed error was calculated from the observed variance in the individual dates calculated for each of the ~ 80 data scans made during the analyses of individual grains, whereas the expected error was obtained from the counting statistics. All grains which had individual MSWD values larger than 2 or had ratios of observed/expected error larger than 3 are excluded from age calculation. Only data that lie within 95% of concordance at the 1 σ level were used for the age calculation.

There is evidence of multiple age populations in some samples. In order to test this possibility, the data from each sample were examined using cumulative probability diagrams. If the data represent a single age population, most points will lie on a straight

line with the possible exception of short tails at each end due to the expansion of the scale in this region. Outliers lying above this line at old ages were assumed to represent inherited zircons and outliers falling below the line at young ages were ascribed to lead loss and were rejected. Statistical calculations were done after these outliers were excluded and the population that represents the age of sample was selected. The mean square of weighted deviates (MSWD) was then calculated in order to test whether the selected grains formed a statistically acceptable single population. If the observed deviations from the sample mean are within analytical error and there is no geological error due to inhomogenity in the sample, the expected (mean) value of MSWD is about 1 (Wendt and Carl, 1991). Estimated minimum and maximum expected values of MSWD were also calculated at the 95% confidence level according to formulas in Wendt and Carl (1991). Age populations have MSWD values above the expected maximum value if the analytical errors are underestimated or if the dates for the grain give a range of ages that lie outside analytical uncertainty. If the weighted average date for a population have higher MSWD values than the upper limit of the estimated MSWD values, the MSWD of the population can be reduced by excluding the grains which contribute most to the high MSWD values. The mean and 2σ error are given in Table 6.1 for both populations. The less selective data are considered in the discussion.

The data from samples that yield multiple age populations, such as the Central Andesite, Runcing Rhyolite and Kelian Tuff, were initially processed the same way as for single population data. The data for these samples form two or more straight line-segments separated by ***S*** shaped curves on probability plots. Individual populations are separated by points of inflection between the straight lines. The mean age of each population was calculated using the ***Mix*** program written by Gallagher and Sambridge (1992) for processing multi-component data sets.

Detrital zircon raw data were reduced using the similar method of date calculation as for igneous zircon samples, but the grains were treated individually and the population MSWD criteria were not applied.

6.5 Samples

Rock samples dated in this study were collected from the Kelian igneous complex, including Magerang-Imang and Nakan, and the Han and Plata prospects. The samples were selected based on the spatial relationship between the igneous intrusions and hydrothermal mineralisation (Figure 6.3). These included two hornblende andesite porphyries from Magerang-Imang; a pyroxene andesite porphyry from Nakan; and the Central Andesite porphyry, the Runcing Rhyolite porphyry and lithic-crystal tuff from the Kelian mine. Samples were collected from exploration drill cores, with the exception of the Central Andesite (sample 123200), Runcing Rhyolite (sample 123218) and Magerang-Imang andesite (sample 123226) which were collected from pit exposures and outcrops. The Magerang-Imang andesites (samples 123158 and 123226) have porphyritic textures, formed by medium-grained phenocrysts of mainly plagioclase, K-feldspar and hornblende set in a fine-grained, holocrystalline groundmass of feldspar and mafic minerals. Both phenocrysts and groundmass have been slightly altered to sericite, chlorite and carbonate along cracks and grain boundaries. The Nakan andesite (sample 123187) exhibits a porphyritic texture, characterised by medium-grained phenocrysts of plagioclase and pyroxene set in fine-grained groundmass of feldspar and mafic minerals. Clinopyroxene and plagioclase phenocrysts are slightly altered to sericite, chlorite and calcite and rare small grains of hornblende are slightly altered to chlorite. The fine-grained groundmass has been partially replaced by sericite, chlorite and carbonate. The Central Andesite (sample 123200) has undergone propylitic alteration as indicated by partial alteration of the phenocrysts and groundmass of feldspar and mafic minerals to sericite, chlorite and calcite. The Runcing Rhyolite (Sample 123218) has undergone phyllic- to argillic-type alteration and is composed of quartz and sericitised feldspar phenocrysts set in a fine-grained, strongly altered groundmass.

The Han andesite (sample 1103) is a weakly altered porphyry exposed on the Han River and is chiefly composed of plagioclase and minor pyroxene phenocrysts set in a fine grained quartz-feldspathic groundmass. The phenocryst and groundmass are slightly altered to sericite, chlorite and calcite. The Plata dacite (sample 1121), collected from the drillcore

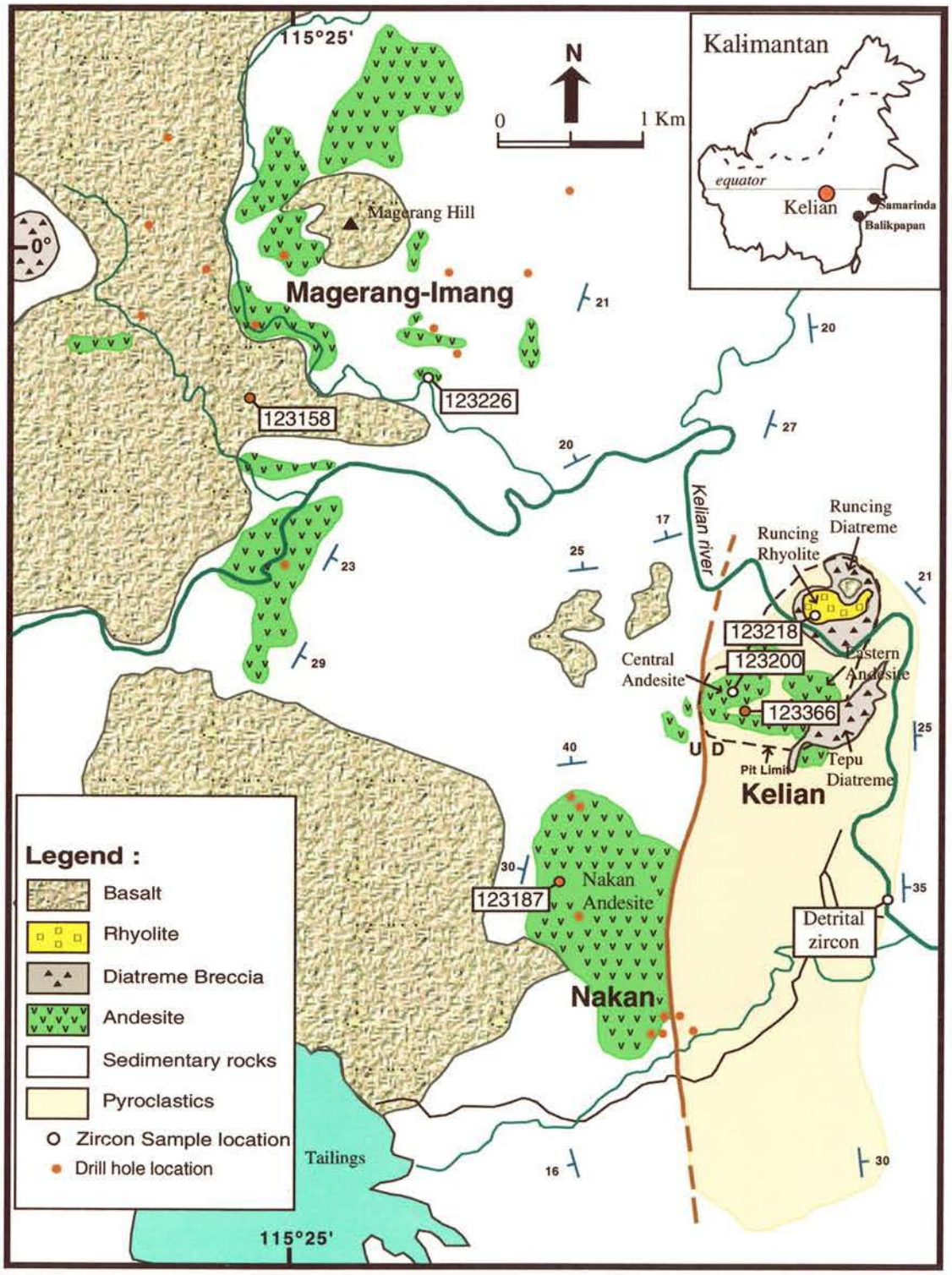

Figure 6.3 : Simplified geological map of the Kelian region and location of the zircon samples. Samples 123158, 123187 and 123366 were collected from drillcores.

of the Plata prospect, shows plagioclase and hornblende phenocrysts within a fine-grained quartz, feldspar and mafic groundmass. The feldspar and mafic minerals have been slightly altered to sericite and chlorite.

Two detrital zircon samples were collected to constrain the duration of magmatism on local and regional scales. The first set of detrital zircons (Sample 123230) was collected by panning fluvial sediment from a point bar of the Kelian River, located 1.5 km southeast down-stream of the Kelian gold mine. This sample was assumed to be representatives of zircons derived from magmatic events which occurred locally within the Kelian drainage system. The second set was panned from a point bar of the Mahakam River, the largest river in East Kalimantan, located approximately 20 km down stream from the point of entry of the Kelian River (Figure 6.4).

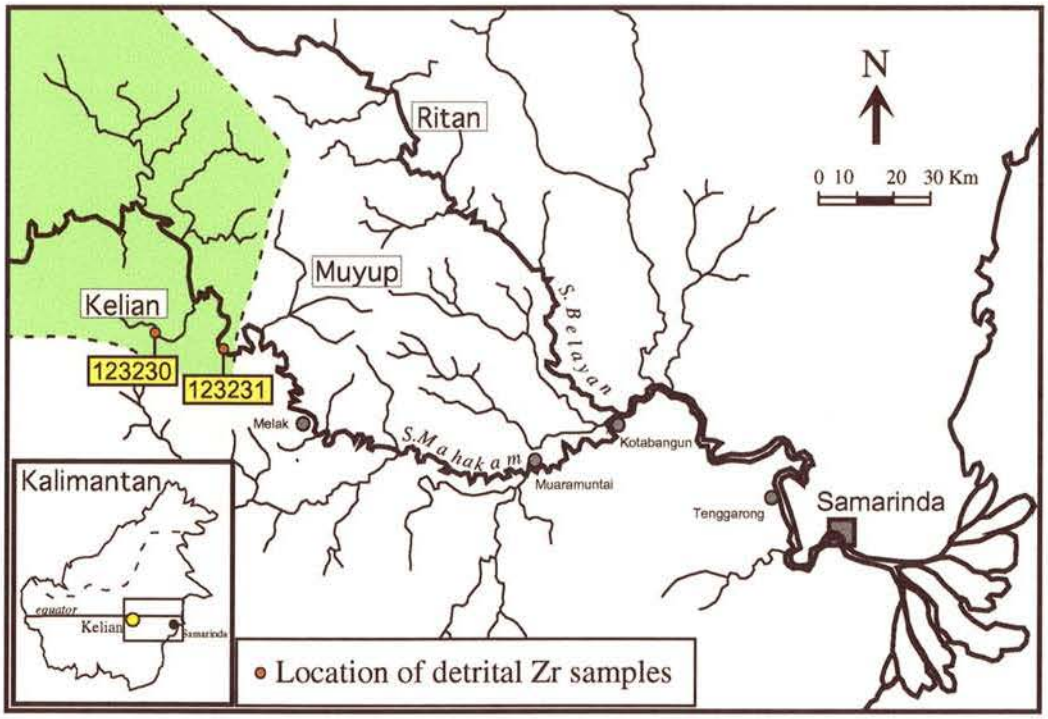

Figure 6.4 : Location of detrital zircon samples

6.6 Analytical Results

The pooled population ages with uncertainties, number of grains analysed and MSWD values for the rock samples are listed in Table 6.1. The complete data for the igneous and detrital zircons are given in the Appendix 7. Tera-Wasserburg concordia diagrams for each sample are presented in Figures 6.5 and 6.6. Zircons from the Magerang-Imang, Nakan, Han andesites and Plata dacite exhibit pooled single population ages. For each of these samples, most of the data lie on a single straight line when plotted on a probability diagram. The pooled population ages, which were calculated based on the criteria of spot MSWD and the ratio of observed/expected error, have higher MSWD values than that expected for a single normal distribution at 95% confidence level, with the exception of sample No. 1121(Table 6.1-A). Population ages with acceptable values of MSWD were obtained by excluding the grains which contribute most to the high MSWD values. This approach did not significantly change the age, but the MSWD values and uncertainties are reduced (Table 6.1-B). In this paper, the results of both calculations are presented, but we use the more complete date sets (Table 6.1-A and 6.1-C) for our age interpretations.

6.6.1 Single age populations

The first Magerang-Imang andesite (sample 123158) yielded a single age population of 19.62 Ma $\pm$ 0.21 (28 of 32 spots; MSWD = 6.59). Four of 32 spot analyses were excluded on the basis of the within-spot MSWD values being greater than 2. There are no inherited zircons in this sample. The second Magerang-Imang andesite (sample 123226) was measured in two different analytical sessions. The two sets of data were calculated separately and the results are consistent with each other, giving single age populations (Figures 6.7a, 6.7b). The first session included 32 spots and yielded an average date of 19. 29 Ma $\pm$ 0.16 (30 of 32 spots; MSWD = 2.78) with 2 spots excluded due to the within-spot MSWD values being greater than 2. The second session included 26 spots and yielded a date of 19.45 Ma $\pm$ 0.19 (23 of 26 spots; MSWD = 3.04) with 3 spots excluded on the basis of the plot of probability distribution which indicated that these grains were

Table 6.1 : U-Pb zircon ages for the Kelian Igneous Complex and regional prospects

A. Weighted average dates calculated from single date populations based on probability plots

Sample No.	Location	Rock Type	Population	Date (Ma)	±2se	N	MSWD	max MSWD
123158	Magerang	Andesite	1	19.62	0.21	28 of 32	6.59	1.54
123226	Magerang	Andesite	1	19.38	0.12	53 of 58	2.95	1.39
123187	Nakan	Andesite	1	20.01	0.15	30 of 32	5.59	1.53
1103	Han	Andesite	1	19.31	0.16	25 of 26	5.17	1.58
1121	Plata	Dacite	1	18.52	0.07	23 of 26	1.55	1.60

B. Weighted average dates after excluding the grains which give highest contribution to the MSWD values

Sample No.	Location	Rock Type	Population	Date (Ma)	±2se	N	MSWD	max MSWD
123158	Magerang	Andesite	1	19.69	0.12	19 of 32	1.45	1.67
123226	Magerang	Andesite	1	19.33	0.11	46 of 58	1.38	1.42
123187	Nakan	Andesite	1	20.06	0.09	21 of 32	1.52	1.63
1103	Han	Andesite	1	19.26	0.13	20 of 26	1.52	1.65

C. Weighted average dates calculated from multiple date populations using the "Mix" program

Sample No.	Location	Rock Type	Population	Date (Ma)	±2se	N	MSWD	
123200	Central And.	Andesite	Population1	19.7	0.12	23	0.94	(2 youngest spots excluded)
	Central And.	Andesite	Population2	20.5	0.12	23	0.45	
	Central And.	Andesite	Population3	21.2	0.32	14	1.30	
123218	Runcing	Rhyolite	Population1	19.3	0.12	10	1.34	
	Runcing	Rhyolite	Population2	20.0	0.20	7	1.33	(2 oldest spots excluded)
	Runcing	Rhyolite	Population3	20.8	0.14	8	1.82	(6 oldest spots excluded)
123366	Kelian mine	Tuff	Population1	70.0	0.34	13	5.91	
	Kelian mine	Tuff	Population2	76.5	0.40	8	6.38	(5 oldest spots excluded)

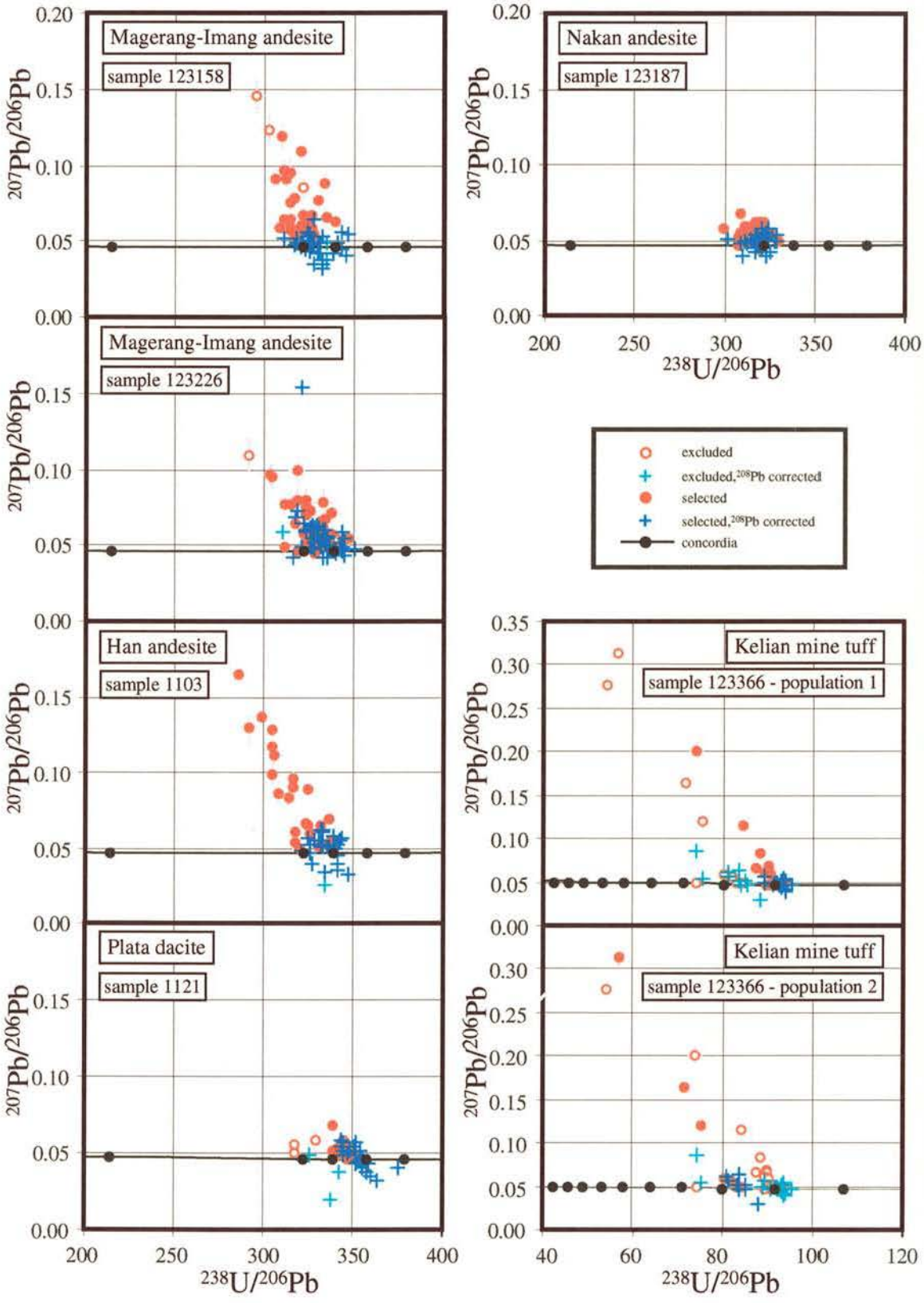

Figure 6.5 : Tera-Wasserburg concordia diagrams for the igneous zircons from the Kelian igneous complex and regional prospects

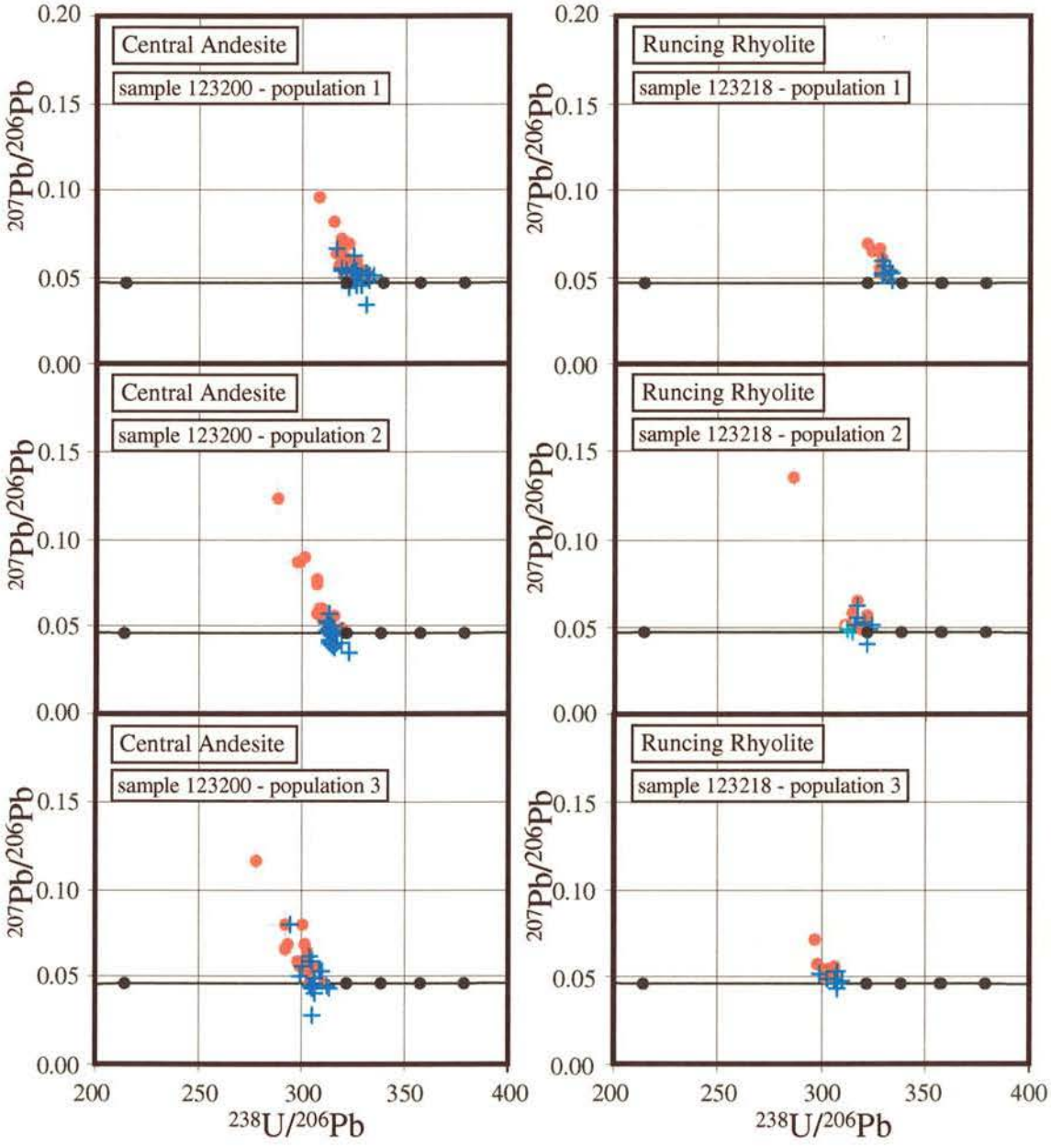

Figure 6.6 : Tera-Wasserburg concordia diagrams for the igneous zircons from the Central Andesite and Runcing Rhyolite

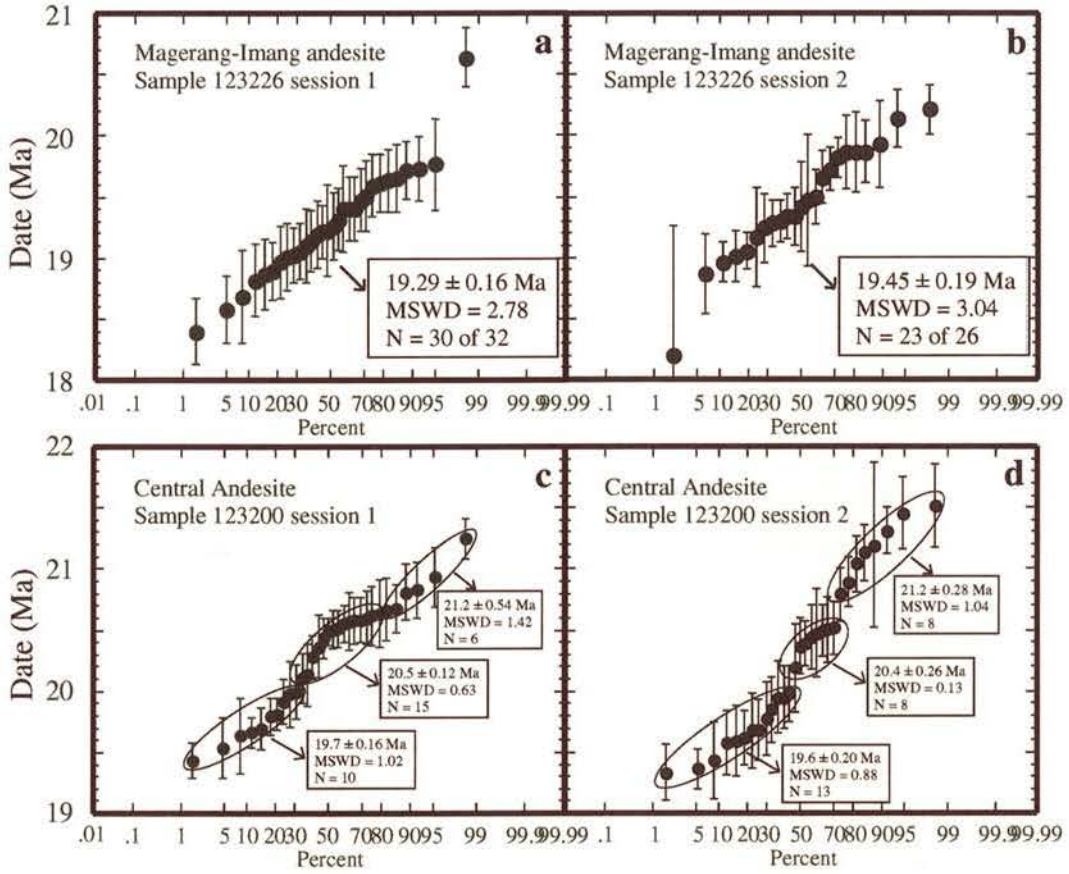

Figure 6.7 : Cumulative probability plots for the Magerang-Imang andesite sample 123226 and the Central Andesite sample 123200 dated in two different courses of analytical sessions

inherited zircons. These grains had ages of 59.4 Ma, 67.4 Ma and 103.6 Ma and were probably derived from Cretaceous volcanic and sedimentary rocks in the basement. The combined data set resulted in an age of 19.38 Ma $\pm$ 0.12 (53 of 58 spots; MSWD = 2.95) (Figure 6.8b).

The Nakan pyroxene andesite (sample 123187) yielded a single age population of 20.01 Ma $\pm$ 0.15 (30 of 32 spots; MSWD = 5.59). Two out of 32 spots were rejected based on the within-spot MSWD values being larger than 2. There were no inherited zircons recorded in this sample (Figure 6.8c).

The Han andesite (sample 1103) yielded a single age population of 19.31 Ma $\pm$ 0.16 (25 of 26 spots; MSWD = 5.17) (Figures 6.8d). One spot was excluded from the age calculation for the Han sample due to the within-spot MSWD value being larger than 2.

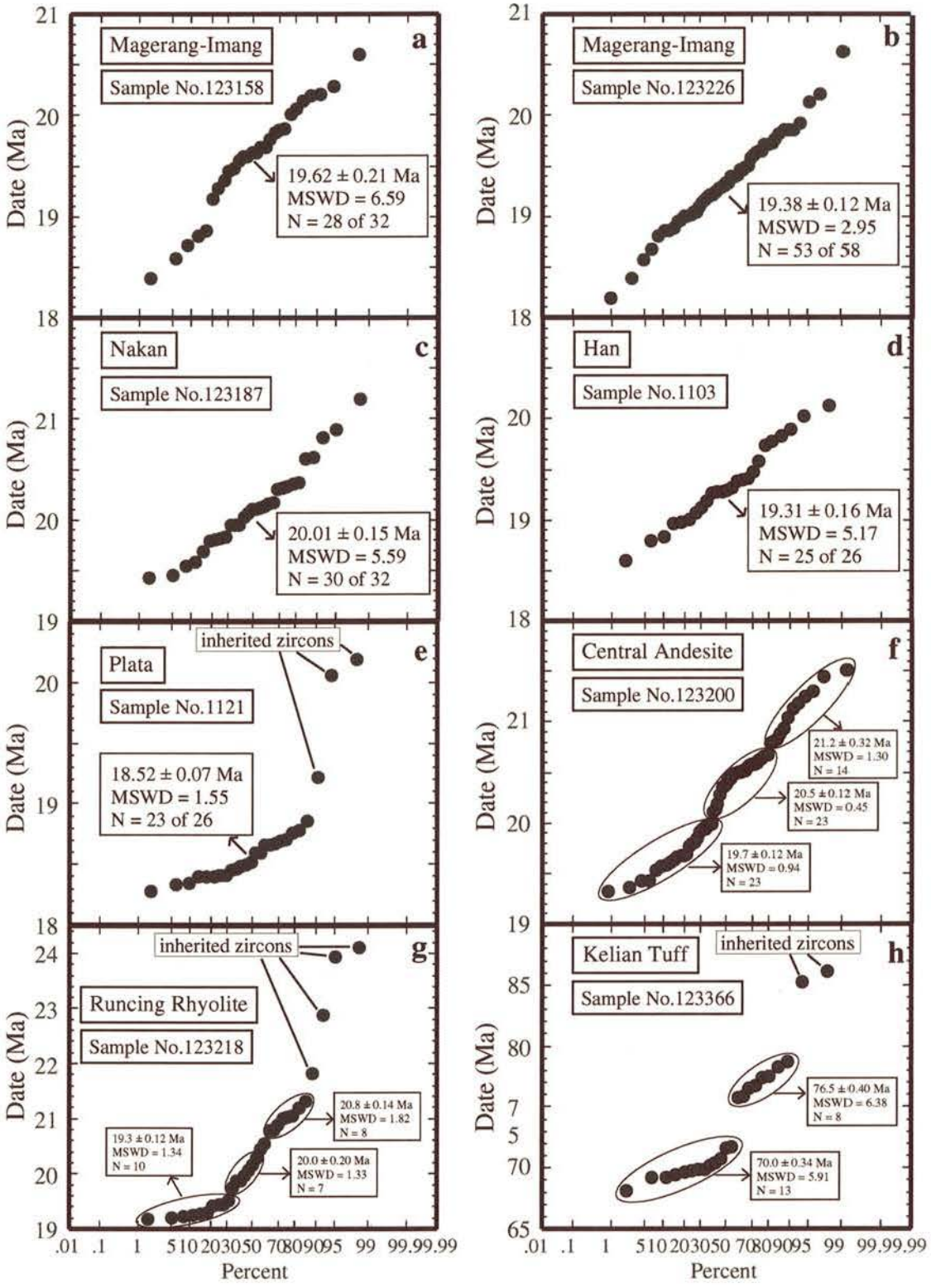

Figure 6.8 : Cumulative probability plots for the igneous zircons from the Kelian igneous complex and regional prospects

The Plata dacite (sample 1121) gave a single age population of 18.52 ± 0.07 (23 of 26 spots; MSWD = 1.55). There were 3 of 26 spots excluded from the calculation for the Plata zircon population on the basis of the plot of the probability distribution (Figure 6.8e). These grains, which yielded dates of 19.2 Ma, 20.1 Ma and 20.2 Ma, were considered to be inherited zircons.

6.6.2 Multiple age populations

The age of the Central Andesite porphyry was measured during two different analytical sessions. These 2 data sets were calculated separately and the consistency of the results again demonstrates the reproducibility of U-Pb zircon dating by ELA-ICP-MS. Data from both the first and second analytical sessions do not lie on a single straight line on a cumulative probability plot, but have 3 distinct populations separated by points of inflection (Figures 6.7c and 6.7d). Ages were calculated for each of these populations using the "Mix" program of Gallagher and Sambridge (1992).

The average ages of populations were 19.7 ± 0.16, 20.5 ± 0.12 and 21.2 ± 0.54 Ma, obtained from 32 spot analyses in the first session and 19.6 ± 0.20, 20.4 ± 0.26 and 21.2 ± 0.28 Ma obtained from 26 spot analyses in the second session. There were 4 spots excluded from the age calculation; 2 spots were rejected due to their high values of the within-spot MSWD and the other 2 spots were rejected based on the probability plot as outliers that lay below the line at the young end population, possibly due to Pb loss. The two sets of data were then combined and the final dates obtained were 19.7 ± 0.12 Ma, 20.5 ± 0.12 Ma and 21.2 ± 0.32 Ma (Figure 6.8f).

The Runcing Rhyolite sample also yielded 3 distinct age populations: 19.3 ± 0.12, 20.0 ± 0.2 and 20.8 ± 0.14 Ma (Figure 6.8g). The ages were calculated following the same method used for the Central Andesite sample. In this sample, all grains which had within-spot MSWD values greater than 4 were excluded. Two additional spots were excluded from the calculation of the second population based on the probability plot. The six oldest spots were excluded from the calculation of the third population because of inherited zircons or high common Pb.

The Kelian Tuff sample yielded 2 distinct populations of dates from 26 spot analyses: 70.0 ± 0.34 Ma and 76.5 ± 0.40 Ma (Figure 6.8h). Five grains were excluded from the calculation of the second population. These oldest grains were dated 85.3, 86.2, 429, 434 and 1680 Ma. They are interpreted to be inherited zircons derived from the basement rocks. This sample shows high MSWD values due to a wide range of dates as might be expected in a pyroclastic rock. The Cretaceous age of the tuff indicates that this unit is the basement of the Kelian rock sequences which is consistent with the previous interpretation (Van Leeuwen et al., 1990).

6.6.3 Detrital zircons

Two sets of detrital zircons from the Kelian and Mahakam rivers yielded a wide spectra of U-Pb zircon dates ranging from 1.7 Ma to 373 Ma, dominated by Pliocene, Miocene, Cretaceous, Triassic, Permian and Carboniferous populations (Figure 6.9). The Tertiary zircon populations range from 1.7 to 2.8 Ma and 15.8 to 21.7 Ma, while the Cretaceous population ranges from 67.6 to 126 Ma with a large peak at 105 Ma. The complete data are given in Appendix 7.

6.7 Time Constraints on The Emplacement of The Kelian Igneous Complex and Associated Epithermal Gold Mineralisation

The U-Pb zircon dating for the Central Andesite porphyry produced 3 distinct age populations. The oldest population (21.2 ± 0.32 Ma) is interpreted to represent the age of an inherited zircon population that formed during a previous thermal event in the melt source region. The other age populations have 2 possible interpretations. First, the intermediate age population (20.5 ± 0.12 Ma) could be assigned to the emplacement of the andesite and the youngest zircon population (19.7 ± 0.12 Ma) to a period of Pb loss due to hydrothermal activity. However, this possibility is unlikely because the hydrothermal alteration and mineralisation at Kelian occured only a short time after emplacement of the andesite and the zircons do not have excessively high concentration of uranium so the

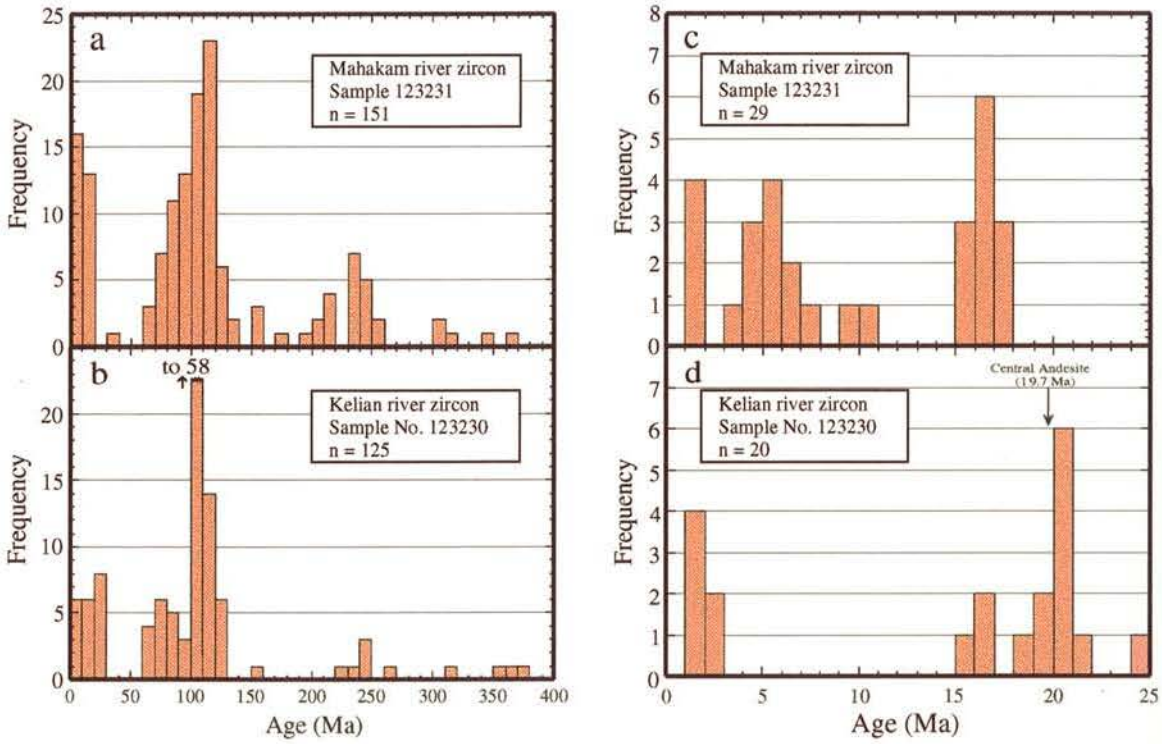

Figure 6.9 : Histograms showing U-Pb age distributions for the Mahakam (a and c) and Kelian (b and d) detrital zircons; n is the number of analytical spots

zircons could not have been metamict. Furthermore the temperature of the hydrothermal fluid (270°-330°C; Van Leeuwen et al., 1990) was close to the fission track annealing temperature and far below the closure temperature for Pb diffusion (Cherniak and Watson, 2000) of zircon making it unlikely that the U-Pb system in zircon was reset during mineralisation. The second, and more likely interpretation is that the youngest zircon age population (19.7 $\pm$ 0.12 Ma) is the emplacement age of the Central Andesite porphyry and the intermediate age population (20.5 $\pm$ 0.12 Ma) represents a second population of inherited zircons.

The Runcing Rhyolite sample also yielded 3 distinct zircon age populations. Following the same line of reasoning as above, the youngest age population (19.3 $\pm$ 0.12 Ma) is interpreted to be the emplacement age of the Runcing Rhyolite porphyry and the older two populations (20.0 $\pm$ 0.20 Ma and 20.8 $\pm$ 0.14 Ma) to represent ages of inherited zircons. The emplacement age for the Runcing Rhyolite, which is younger than that of the Central Andesite (19.7 $\pm$ 0.12 Ma), coupled with the absence of the quartz and base metal veining in the Runcing Rhyolite suggest that the Runcing Rhyolite formed after the main

stage of hydrothermal mineralisation and is, therefore, not be directly related to the formation of the Kelian gold deposit. The age of gold mineralisation must be younger than 19.7 Ma, the age of the Central Andesite, but older than 19.3 Ma, the age of the Runcing Rhyolite (Figure 6.10). Thus, although gold mineralisation took place during the Kelian igneous event, its genetic relationship to the Central Andesite remains uncertain. The K-Ar age of adularia associated with mineralisation hosted by the Central Andesite is 20.2 $\pm$ 0.3 Ma (Van Leeuwen et al., 1990), slightly older than the U-Pb age for the central Andesite but is comparable within stated error, assuming the uncertainty for K-Ar age is 1σ. These differences are probably due to the presence of excess ^{40}Ar trapped from the original magmas as encountered in the Porgera gold deposit (Richards and McDougall, 1990) or from fluid inclusion introduced with the mineralisation.

The emplacement age of the Magerang-Imang andesite implies that the high-sulfidation Cu-Au mineralisation at Magerang is the same age or younger than the host rocks to the low-sulfidation Au deposit at Kelian. The age difference between the Kelian and Magerang-Imang andesites suggests that the duration of magmatism and related epithermal mineralisation in the larger Kelian region, was between 0.5 - 1 Ma (Figure 6.10). During this period, the magmatic-hydrothermal system has produced 2 distinctive types of epithermal mineralisation: firstly, low sulfidation Au deposit at Kelian and secondly, high sulfidation Cu-Au mineralisation at Magerang-Imang.

6.8 Nested Cannibalistic Intrusions Below The Kelian Gold Deposit: Discussions

The magma sequence indicated by U-Pb zircon geochronology of the Kelian igneous complex matches with that expected for andesites. The Magerang-Imang hornblende andesite is younger than the Nakan pyroxene andesite, which is consistent with clinopyroxene preceeding hornblende in the normal crystallisation sequence for an andesitic magma (Green, 1972). Furthermore, the geochemically most evolved Magerang-Imang andesite is the youngest of the two dated samples. The Kelian andesites exhibit trace

element characteristics of hornblende crystallization and are intermediate in age between the Nakan and Magerang-Imang andesites. If all these units form part of a single fractionating system, then the life span was at least 0.7 m.y.

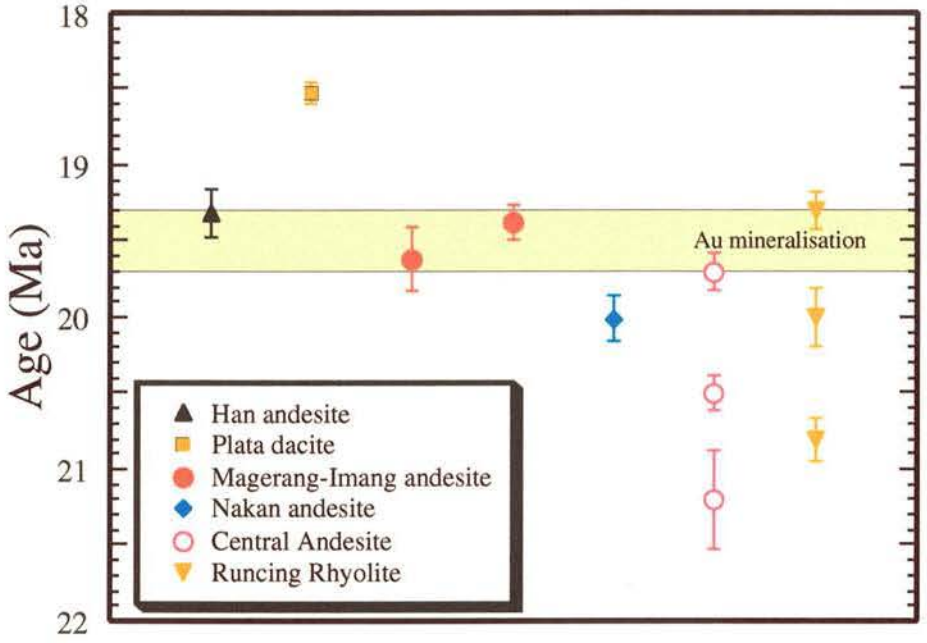

Figure 6.10 : U-Pb zircon ages showing the temporal relationships among the Kelian igneous complex and the regional prospects. Three ages of the Central Andesite and Runcing Rhyolite come from 3 different populations which the two oldest ages being inherited zircons. Two ages of the Magerang-Imang andesite come from 2 different intrusive units.

The study of detrital zircons from the Kelian River shows that the Kelian igneous complex was active for about 3.5 m.y. Gold mineralisation appears to have occurred toward the end of this activity (Figure 6.9). The Kelian igneous complex is not represented in the Mahakam detrital grains, indicating that it was not geographically widespread on a region scale. It is surprising that a major gold deposit occurs in association with a period of igneous activity that is insignificant on a region scale.

The inheritance pattern in the Kelian andesite and Runcing Rhyolite is unusual. The Kelian andesite stocks and Runcing diatreme, intrude into 70 - 76 Ma pyroclastics and

sediments. Unless there is an unrecognised thrust underlying the Kelian region, the crust below the deposit must therefore consist of rocks that are Cretaceous and older. Under these conditions the expected pattern of inheritance is one or more small populations, often consisting of a single grain, with ages of 70 Ma or older. The total number of inherited grains is usually small compared with the number of grains in the emplacement population. The occurrence of two populations of inherited grains in the Kelian andesite and Runcing Rhyolite, which are sub-equal in size to, and less than 1.6 m.y. older than the zircon population age that defines their emplacement age, is therefore unexpected.

The two large inheritance populations in both the Central Andesite and Runcing Rhyolite lie within the time range of the Kelian igneous complex as defined by the Kelian River detrital zircons. They must be derived from crustal intrusions that formed as part of the Kelian cycle. It is suggested that both the Kelian Andesite and Runcing Rhyolite were fed by 2 magma chambers that formed deep in the crust, each of which were long lived. This is not unexpected. Magmas rise in the crust until they reach their own density level (the neutral buoyancy level) where they spread out to form a magma chamber (Ryan, 1987). Provided the density structure of the crust remains the same, successive batches of magmas of similar composition should pond at the same crustal level. This is particularly true if there is a laterally extensive intrusion which will act as a density barrier that prevents these new batches of magma ascending to the upper crust (Huppert and Sparks, 1980).

It is suggested that the magma chambers that fed the Kelian Andesite and Runcing Rhyolite were emplaced into pre-existing intrusions of similar composition that formed as part of the Kelian igneous complex. The abundance of xenocrystic zircons in both units suggests that these earlier intrusions were still hot, or perhaps even partially molten, at the time of magma emplacement. That is the shallow level stocks and diatremes at Kelian were fed by nested, cannibalistic intrusions deep in the crust that melted the walls and roofs of related, but pre-existing intrusions, and inherited abundant xenocrystic zircons in the process. The ages of the inherited zircons are interpreted as the ages of these earlier intrusions. Both the Kelian Andesite and the Runcing Rhyolite have two populations of inherited zircons, which indicate that the pre-existing intrusions formed in two distinct episodes, 0.7 to 0.8 m.y. apart. The difference between the emplacement age and the age of the oldest of the inherited zircon populations shows that this cannibalistic activity took

place over 1.5 m.y. The interval of magmatic activity in these chambers corresponds to the period of peak activity in the Kelian igneous complex as defined by the detrital zircons (Figure 6.9).

Chapter 7
SUMMARY AND CONCLUSIONS

This Chapter summarises the major results of this study, particularly geochemical and geochronological aspects of the igneous suites associated with the Kelian gold deposit.

The Kelian Igneous Complex and regional prospects show a calc-alkaline trend and range in composition from basaltic andesite, through andesite and dacite to rhyolite. The Kelian suite plots mostly at the boundary of low K and medium K andesite over a range in silica from 56 to 63 wt%. In the Magerang-Imang suite, highly incompatible elements such as Th, U, Zr, Hf, Rb, Sr and Ba increase with increasing SiO_2, resulting in a distinctive, positive trend. Light rare earth elements (LREE), such as La, Ce and Pr also increase with increasing SiO_2 but weakly incompatible REE show no increase and some, such as Sm, Ho and Y actually decrease. In the Nakan suite, the REE display similar trends as those in the Magerang-Imang suite, but the trend of U, Th, Zr, Hf does not change significantly with differentiation. Compatible elements such as V, Sc and Cr rapidly decrease with increasing SiO_2. Chromium is depleted in the Tepu, Han and Ritan andesites, but it is relatively high in the Magerang-Imang and Nakan andesites within the similar range of SiO_2, indicating different trends of magmatic differentiation.

The Kelian Igneous Complex has undergone variable and often intense alteration so that many major elements were extensively mobilised during phyllic alteration. Propylitic Central Andesites have element concentrations that are closest to the concentrations of the least altered Tepu andesites and show no evidence of Ti, Al, Fe, Ca, Mg or P oxide mobility. On the other hand, Na_2O decreased during propylitic alteration, in association with the break down of feldspar, and K_2O and MnO increased. As the intensity of alteration increases from propylitic through phyllic to argillic alteration, the mobile elements show increasing dispersion. Phosphor, Al and Ti oxides appear to be immobile, even in the most highly altered samples. In propylitic and phyllic altered andesites, immobile elements such as Ta, Nb, Y, Ti and the REE are not affected by alteration. On

the contrary, the concentrations of elements such as Rb, Sr and K are mobile during hydrothermal alteration and exhibit large variations depending on the type of alteration. Andesite suites that have undergone propylitic alteration are variably depleted in K and Ba and enriched in Cs and Rb, whereas andesites with phyllic alteration show a significant increase in K and Rb, and depletion in Sr and Ti.

The primitive mantle-normalised element concentrations for the least altered andesite display patterns showing enrichment in the large ion lithophile elements (LILE), particularly Ba, K, U, Th and Sr relative to the heavy REE. In the least altered andesites, all the elements form a coherent array. The enrichment in Cs, Rb, Ba, K and Th and depletion in Nb, Ta and Ti are characteristic of calc-alkaline arc magmas. However, the andesites are also characterised by pronounced positive anomalies of Zr and Hf, which are less common in calc-alkaline arc magmas.

Geochemical evolution in the Miocence calc-alkaline suites from the Kalimantan volcanic arc exhibits two distinctive trends of magmatic differentiation The *normal* trend is a "typical" calc-alkaline series defined by the *productive* igneous suites such as Kelian, Mount Muro, Masuparia and Muyup. This suite is characterised by low Mg, moderate K, relatively high Ti and Al and depletion in Cr and Sc and is consistent with the differentiation trend for arc lavas in general. The second trend is defined by the chemical variations of the Magerang-Imang and Nakan suites showing remarkably high concentrations of MgO compared to the productive igneous suites and common calc-alkaline andesites. Major and trace element geochemistry of the high Mg andesites from Magerang-Imang and Nakan is comparable with that of the Ryukyu high Mg andesite and low Ca type 2 boninites. Both the Magerang-Imang andesites and boninites have similar characteristics of high Mg, positive anomalies of U, Sr, Zr and Hf, and negative anomalies of Nb, Ta and Ti.

The evidence of chemical evolution by fractional crystallisation is clearly indicated by major element trends as well as trace element trends as shown by plots of Cr, Sc, Ce/Yb and Eu/Eu*. The dominant mafic phenocryst of hornblende and the linear horizontal trend of Eu/Eu* with the increasing La/Yb ratio indicate that amphibole fractionation dominated the evolution of the Magerang-Imang suite. On the other hand, the Nakan suite shows little variation in La/Yb ratios and contains pyroxene phenocrysts

but no hornblende, and therefore, pyroxene fractionation may have played a more important role than amphibole and feldspar.

The incompatible trace element geochemistry of the Kelian Igneous Complex andesites is characterised by the presence of positive Zr and Hf anomalies in the trace element patterns which is unusual for calc-alkaline subduction zone magmas. The chemical diversity in the Magerang-Imang and Nakan suite, with their relatively high concentrations of Mg oxide, Sc and Cr, and concave down curvi-linear evolution trends, might have been generated by combined wallrock assimilation and fractional crystallisation. The Magerang-Imang andesite is derived by fractional crystallisation of a parental basaltic magma mixed with a Zr-rich cumulate. Alternatively, the Magerang-Imang and Nakan high Mg andesite may have been derived from a primary magma which had a high Zr/Sm ratio and a composition similar to other boninite-type rocks.

Geochemical modelling using an assemblage of plagioclase(65%)-clinopyroxene (25%)-amphibole(10%) yielded in a pattern that shows a good agreement with the observed REE pattern, but the modelled MREE are slightly more depleted than the observed values. Plagioclase fractionation produces no detectable negative Eu anomaly because the effects of plagioclase, with its positive Eu anomaly, are balanced by a negative anomaly of amphibole fractionation and the high concentration of Eu in amphibole. The observed trend of the REE in the Nakan suite indicates decreasing concentrations of REE with increasing differentiation. A calculation using a cumulus assemblage of plagioclase (60%) - orthopyroxene(20%) - clinopyroxene(13%) - amphibole(6%) - apatite(0.4%) - zircon(0.15%) - allanite(0.027%) produced a REE pattern which matchs the observed trend. The modelled REE trends demonstrate good agreement with the observed trends indicating that the fractionation of the selected cumulus assemblages can simulate the chemical evolution of the Magerang-Imang and Nakan calc-alkaline suites. Changes in the LREE to HREE ratio and the decrease in REE abundances with increasing SiO2 in the Magerang-Imang and Nakan andesite suites respectively, are due to fractional crystallisation.

The combined wallrock assimilation and fractional crystallisation process is consistent with the zircon geochronology of the Kelian Igneous Complex. The U-Th-Pb zircon dating indicates the presence of two large inherited zircon populations in the Kelian mine intrusions. This requires the magma to have assimilated large amounts of slightly

older zircon-bearing andesite. The Kelian mine andesites also have positive Zr and Hf anomalies. It is therefore possible that the Magerang-Imang and Nakan high Mg andesites were fed by magma chambers that formed deep in the crust, and were emplaced into pre-existing intrusions of felsic composition that formed as part of the Kelian Igneous Complex cycle. It is suggested that the shallow level stocks at Magerang-Imang and Nakan were generated by intrusions that melted the walls and roofs of related, but pre-existing intrusions, and extracted abundant xenocrystic zircons during the assimilation process. This resulted in positive anomalies of Zr and Hf in the Magerang-Imang and Nakan suites. Zircon U-Th-Pb isotope dates have been determined *in situ* using excimer laser ablation ICP-MS methods. The two different bodies of the Magerang hornblende andesite yielded ages of 19.3 $\pm$ 0.13 Ma and 19.7 $\pm$ 0.12 Ma, while the Nakan pyroxene andesite, gave an age of 20.1 $\pm$ 0.09 Ma. The U-Pb zircon dating for the Central Andesite porphyry produced 3 distinct age populations. The older two populations (21.2 Ma and 20.5 Ma) represent the age of inherited zircon populations that formed during a previous thermal event in the melt source region. The youngest age population (19.7 ± 0.12 Ma) is the emplacement age of the Central Andesite porphyry. The Runcing Rhyolite sample also yielded 3 distinct zircon age populations. The youngest age population (19.3 ± 0.12 Ma) is interpreted to be the emplacement age of the Runcing Rhyolite porphyry and the older two populations (20.0 Ma and 20.8 Ma) represent ages of inherited zircons. The emplacement age for the Runcing Rhyolite, which is younger than that of the Central Andesite (19.7 Ma), coupled with the absence of the quartz and base metal veining in the Runcing Rhyolite suggest that the Runcing Rhyolite formed after the main stage of hydrothermal mineralisation and is, therefore, not be directly related to the formation of the Kelian gold deposit. The age of gold mineralisation must be younger than 19.7 Ma, the age of the Central Andesite, but older than 19.3 Ma, the age of the Runcing Rhyolite. Thus, although gold mineralisation took place during the Kelian igneous event, its genetic relationship to the Central Andesite remains uncertain.

The emplacement age of the Magerang-Imang andesite implies that the high-sulphidation Cu-Au mineralisation at Magerang is younger than the low-sulphidation Au deposit at Kelian. Andesites at Kelian and Magerang exhibit a relatively short age range suggesting that the duration of magmatism and related epithermal mineralisation in the greater Kelian region was between 0.5 – 1 Ma. During this time interval, one or more

magmatic-hydrothermal systems produced 2 distinctive types of epithermal deposits: firstly, low-sulphidation Au mineralisation at Kelian and secondly high-sulphidation Cu-Au mineralisation at Magerang-Imang.

The magma sequence indicated by U-Pb zircon geochronology of the Kelian igneous complex matches with that expected for andesites. The Magerang-Imang hornblende andesite is younger than the Nakan pyroxene andesite, which is consistent with clinopyroxene preceeding hornblende in the normal crystallisation sequence for an andesitic magma.. Furthermore, the geochemically most evolved Magerang-Imang andesite is the youngest of the two dated samples. The Kelian andesites also exhibit trace element characteristics of hornblende crystallization and are intermediate in age between the Nakan and Magerang-Imang andesites. If all these units form part of a single fractionating system, then the life span was at least 0.7 m.y.

The study of detrital zircons from the Kelian River shows that the Kelian igneous complex was active for about 3.5 m.y. Gold mineralisation appears to have occurred toward the end of this activity. The Kelian igneous complex is not represented in the Mahakam detrital grains, indicating that it was not geographically widespread on a region scale.

The inheritance pattern in the Kelian andesite and Runcing Rhyolite is unusual. The Kelian andesite stocks and Runcing diatreme, intrude into 70 - 76 Ma pyroclastics and sediments. Unless there is an unrecognised thrust underlying the Kelian region, the crust below the deposit must therefore consist of rocks that are Cretaceous and older. The occurrence of two populations of inherited grains in the Kelian andesite and Runcing Rhyolite, which are sub-equal in size to, and less than 1.6 m.y. older than the zircon population age that defines their emplacement age, is therefore unexpected.

The two large inheritance populations in both the Central Andesite and Runcing Rhyolite lie within the time range of the Kelian igneous complex as defined by the Kelian River detrital zircons. They must be derived from crustal intrusions that formed as part of the Kelian cycle. It is suggested that both the Kelian Andesite and Runcing Rhyolite were fed by 2 magma chambers that formed deep in the crust, each of which were long lived. Magmas rise in the crust until they reach their own density level (the neutral buoyancy level) where they spread out to form a magma chamber.

It is concluded that the magma chambers that fed the Kelian Andesite and Runcing Rhyolite were emplaced into pre-existing intrusions of similar composition that formed as part of the Kelian igneous complex. The abundance of xenocrystic zircons in both units suggests that these earlier intrusions were still hot, or perhaps even partially molten, at the time of magma emplacement. That is the shallow level stocks and diatremes at Kelian were fed by nested, cannibalistic intrusions deep in the crust that melted the walls and roofs of related, but pre-existing intrusions, and inherited abundant xenocrystic zircons in the process. The ages of the inherited zircons are interpreted as the ages of these earlier intrusions. Both the Kelian Andesite and the Runcing Rhyolite have two populations of inherited zircons, which indicate that the pre-existing intrusions formed in two distinct episodes, 0.7 to 0.8 m.y. apart. The difference between the emplacement age and the age of the oldest of the inherited zircon populations shows that this cannibalistic activity took place over 1.5 m.y. The interval of magmatic activity in these chambers corresponds to the period of peak activity in the Kelian igneous complex as defined by the detrital zircons.

The decrease in PGEs with increased fractional crystallisation seen in the Kelian Igneous Complex suggests that the parent magmas of each of these suites became sulphide saturated early in their fractionation history. This appears to be inconsistent with a magmatic-hydrothermal hypothesis for Kelian in which the Au was concentrated in a sulphide undersaturated parent magma chamber. Another puzzling feature of the data is the depletion of Au relative to adjacent elements on the mantle-normalized metal abundance diagram for the unaltered calc-alkaline rocks from the Kelian area. Most metal deposits are found in association with rocks that are already enriched in the metal of interest, e.g. Au in greenstones, Ni in komatiites, Cr in gabbros etc. This is apparently not true for Au deposits in calc-alkaline volcanics.

It is also interesting that the Cu-Au-PGE patterns remain parallel as their concentrations decrease with increasing SiO_2. The Au and PGE ratios change little during fractionation. This is surprising because it implies either that the partition coefficients for the PGE into the sulfides are similar, which seems unlikely, or that Au and the PGE are not being depleted by simple equilibrium fractional crystallisation of sulfide. This is unlikely to be due to simple equilibrium of fractional crystallisation involving an immiscible sulfide melt. Alternative explanation for the parallel Cu-Au-PGE patterns is that the chalcophile element depletion in the Kelian Igneous Complex is due to a non-

equilibrium process. It is possible that sulfide precipitation occurred rapidly under disequilibrium conditions in a narrow boundary layer of cool magma at the margins of the intrusion. However, the most plausible process for the gradual depletion of Au and all of the PGE at Kelian is crustal assimilation. Simple dilution with crustal material that contains no Au or PGE is the only process that will decrease the abundance of all of the PGE equally.

The major conclusions of this study, which link the igneous suite with the economic mineralisation spatially and temporally, but not chemically, strongly suggest that there was no direct magmatic input of gold. Thus the intrusives acted as a *heat engine*, triggering convection of meteoric fluids which leached Au from a large volume of rock and, upon cooling, precipitated gold in a favourable structural setting. Therefore, it is inappropriate to target specific igneous rock-types (such as rhyolite or andesite) as there is no direct link between igneous intrusion and gold deposition.

As this is the first analytical study of the behaviour of Au and PGE in a fractionating felsic system, the implications are unclear and need to be confirmed by future studies.

REFERENCES

Abidin, H.Z., 1996. The tectonic history and mineral deposits of the East-Central Kalimantan Volcanic Belt, Indonesia : A comparative study of the Kelian, Muyup and Masupa Ria Gold Deposits. PhD Thesis. University of Adelaide, 286pp.

Allen, J.M., 1988. Evaluation of mineral exploration in the Muyup COW area, East Kalimantan, Indonesia, P.T. Muyup Mas Murni, Unpublished report, 21pp.

Arculus, R.J. and Powell, R., 1986. Source component mixing in the regions of arc magma generation. Journal of Geophysical Research 91, pp. 5913-5926.

Ballard, J.R., Palin, J.M., Williams, I.A., Campbell, I.H. and Faunes, A., 2001. Two ages of porphyry intrusion resolved for the super-giant Chuquicamata copper deposit of northern Chile by ELA-ICPMS and SHRIMP. Geology 29, pp. 383-386.

Barnes, S.J., Naldrett, A.J. and Gorton, M.P., 1985. The origin of the fractionation of platinum group elements in terrestrial magmas. Chemical Geology 53, pp. 303-323.

Barnes, S.J., Boyd, R., Korneliussen, A., Nilson, L.P., Often, M., Pedersen, R.B. and Robins, B., 1988. The use of mantle normalization and metal ratios in discriminating between the effect of partial melting, crystal fractination and sulfide segregation on platinum group elements, gold, nickel and copper : Example from Norway. In H.M. Prichards, P.J. Potts, J.F.W. Bowles and S.J. Cribb (Editors), Geo-Platinum '87. Elsevier, London, pp. 113-143.

Barnes, S.J. and Picard, C.P., 1993. The behaviour of platinum group elements during partial melting, crystal fractionation and sulfide segregation : An example from the Cape Smith Fold Belt, northern Quebec. Geochimica et Cosmochimica Acta 57, pp. 79-87.

Berger, B.R. and Eimon, P.I., 1983. Conceptual models of epithermal precious metal deposits. In: W.C. Shanks (Editor), Cameron Volume on Unconventional Mineral Deposits. Society of Mining Engineers of AIME, pp. 191-205.

Berger, B.R. and Henley, R.W., 1989. Advances in the understanding of epithermal gold-silver deposits, with special reference to the western United States. In: R.R. Keays, W.R.H. Ramsay and D.I. Groves (Editors), The Geology of Gold Deposits: The Perspective in 1988. Economic Geology Monograph 6, pp405-423.

Best, M.G., 1969. Differentiation of calc-alkaline magmas. In: A.R. McBirney (Editor), Proceedings of the andesite conference. Department of Geology and Mineral Industries Oregon, Bulletin 65, pp. 65-75.

Bezmen, N.I., Asif, M., Brugmann, G.E., Romanenko, I.M. and Naldrett, A.J., 1994. Distribution of Pd, Rh, Ru, Ir, Os and Au between sulfide and silicate metals. Geochimica et Cosmochimica Acta 58, pp. 1251-1260.

Boettcher, A. L., 1973. Volcanism and orogenic belts – The origin of andesites. Tectonophysics 17, pp.223-240.

Buchanan, L.J., 1981. Precious metal deposits associated with volcanic environments in the southwest. In: W.R. Dickinson and W.D. Payne (Editors), Relations of Tectonics to Ore Deposits in the Southern Cordillera. Arizona Geological Society Digest 14, pp. 237-262.

Black, L.P., Kamo, S.L., Williams, I.S., Foudoulis, C., Claoue-Long, J.C., Korsch, R.J. and Davis, D.W., 2000. The quest for a high-quality zircon standard for microbeam Pb-U-Th Geochronology. Geological Society of Australia, Abstracts No. 59, pp. 43.

Cameron, G.H., Wall, V.J., Walshe, J.L. and Heinrich, C.A., 1995. Gold mineralisation at the Porgera gold mine, Papua New Guinea, in response to fluid mixing. In: J.L. Mauk and J.D. St. George (Editors), Pacrim Congress 1995: Exploring the Rim. Proceedings, Australasian Institute of Mining and Metallurgy, pp. 99-100.

Campbell, I.H. and Barnes, S.J., 1984. A model for the geochemistry of the platinum-group elements in magmatic sulfide deposits. Canadian Mineralogist 22, pp. 151-160.

Campbell, I.H., Naldrett, A.J. and Barnes, S-J., 1983. A model for the origin of platinum-rich horizons in the Bushveld and Stillwater complexes. Journal of Petrology 24, pp. 133-165.

Capobianco, C.J. and Drake, M.J., 1990. Partitioning of ruthenium, rhodium, and palladium between spinel and silicate melt and implications for platinum group elements fractionation trends. Geochimica et Cosmochimica Acta 54, pp. 869-874.

Capobianco, C.J. and Drake, M.J., 1994. Partitioning and solubility of PGEs in oxides and silicates. Mineralogical Magazine 58A, pp. 144-145.

Carlile, J.C. and Mitchell, A.H.G.,1994. Magmatic Arcs and associated gold and copper mineralisation in Indonesia. In: T.M. van Leeuwen, J.W. Hedenquist, L.P. James andJ.A.S. Dow (Editors), Indonesian Mineral Deposits - Discoveries of the Past 25 Years. Journal of Geochemical Exploration 50, pp. 91-142.

Cathles, L.M., Erendi, A.H.J. and Barrie, T., 1997. How long can a hydrothermal system be sustained by a single intrusive event ? Economic Geology 92, pp. 766-771.

Chappell, B.W., 1996. Magma mixing and the production of compositional variation within granite suites: Evidence from the granites of Southeastern Australia. Journal of Petrology 37, pp. 449-470.

Chappell, B. W., 1997. Compositional variation within granite suites of the Lachlan Fold Belt : its causes and implications for the physical state of granite magma. Transactions of the Royal Society of Edinburgh : Earth Sciences 88, pp. 159-170.

Cherniak, D.J. and Watson, E.B., 2000. Pb diffusion in zircon. Chemical Geology 172, pp. 5-24.

Compston, W., Williams, I.S. and Meyer, C., 1984. U-Pb geochronology of zircons from lunar breccia 73217 using a sensitive high mass-resolution ion microprobe. Journal of Geophysical Research 89 Supplement, pp. B525-B542.

Corbett, G.J., 1993. A Review of the structural controls to gold mineralisation at the Kelian mine and environs, Indonesia. P.T. Kelian Equatorial Mining, Unpublished report, 23 pp.

Corbett, G.J. and Leach, T.M., 1995. SW Pacific Rim Au/Cu System : Structure, Alteration and Mineralisation. Workshop presented at University of British Columbia, 141pp.

Corbett, G.J., Leach, T.M., Stewart, R. and Fulton, B., 1995. The Porgera Gold Deposit : Structure, Alteration and Mineralisation. In: J.L. Mauk and J.D. St. George (Editors), Pacrim Congress 1995: Exploring the Rim. Proceedings, Australasian Institute of Mining and Metallurgy, pp. 151-156.

Corlett, G., 1999. The petrology of ten core samples from drillholes DD99HN01, DD99HN02 and DD99HN03, Sg. Han prospect, Kalimantan. PT. Rio Tinto Indonesia, Unpublished Report, 15pp.

Crawford, A.J., Falloon, T.J. and Green, D.H., 1989. Classification, petrogenesis and tectonic setting of boninites. In: A.J. Crawford (Editor), Boninites. Unwin Hyman, London, 465pp.

DePaolo, D.J., 1981. Trace element and isotopic effects of combined wallrock assimilation and fractional crystallisation. Earth and Planetary Science Letters 53, pp. 189-202.

Eggins, S.M., Rudnick, R.L. and W.F. McDonough, 1998. The Composition of peridotites and their minerals : a laser-ablation ICP-MS study. Earth and Planetary Science Letters 154, pp. 53-71.

Eggins, S.M., Woodhead, J.D., Kinsley, L.P.J., Mortimer, G.E., Sylvester, P., McCulloch, M.T., Hergt, J.M. and Handler, M.R., 1997. A simple method for the precise determination of ≥ 40 trace elements in geological samples by ICP-MS using enriched isotope internal standardisation. Chemical Geology 134, 311-326.

Dunn, T. and Sen, C., 1994. Mineral/matrix partition coefficients for orthopyroxene, plagioclase, and olivine in basaltic to andesitic systems: A combined analytical and experimental study. Geochimica et Cosmochimica Acta 58, pp. 717-733.

Faure, G., 1977. Principles of isotope geology. New York, John Wiley and Sons, 464pp.

Foden, J.D., 1983. The petrology of the calc-alkaline lavas of Rinjani Volcano, East Sunda Arc: A model for island arc petrogenesis. Journal of Petrology 24, pp.98-130.

Fujimaki, H, Tatsumoto, M. and Aoki, K., 1984. Partition coefficients of Hf, Zr and REE between phenocrysts and groundmasses. Journal of Geophysical Research 89, pp. B662-B672.

Gallagher, K. and Sambridge, M., 1992. The resolution of past heat flow in sedimentary basins from non-linear inversion of geochemical data: the smoothest model approach with synthetic examples. Geophysical Journal International 109, pp. 78-95.

Gill, J.B., 1978. Role of trace element partition coefficients in models of andesite genesis. Geochimica et Cosmochimica Acta 42, pp. 709-724.

Gill, J.B., 1981. Orogenic andesites and plate tectonics. Springer-Verlag, Berlin, 390pp.

Green, T.H., 1972. Crystallisation of calc-alkaline andesite under controlled high-pressure hydrous conditions. Contributions to Mineralogy and Petrology 34, pp. 150-166.

Green, T.H., 1994. Experimental studies of trace element partitioning applicable to igneous petrogenesis – Sedona 16 years later. Chemical Geology 117, pp.1-36.

Green, T.H. and Pearson, N.J., 1985. Experimental determination of REE partition coefficients between amphibole and basaltic to andesitic liquids at high pressure. Geochimica et Cosmochimica Acta 49, pp. 1465-1468.

Gregoire, D.C., 1988. Determination of platinum, palladium, ruthenium and iridium in geological materials by inductively coupled plasma mass spectrometry with sample introduction by electrothermal vaporisation. Journal of Analytical Atomic Spectrometry 3, pp. 309-314.

Hanson, G.N. and Langmuir, C.H., 1978. Modelling of major and trace elements in mantle-melt systems using trace element approaches. Geochimica et Cosmochimica Acta 42, pp.725-741.

Harahap, B.H., 1993. Geochemical investigation of Tertiary magmatic rocks from Central West Kalimantan, Indonesia. Proceedings of the 22nd Annual Convention of the Indonesian Association of Geologists, pp. 304-326.

Hartshorn, G., 1995. Kelian Brownfield Exploration. Half Yearly Report January-July 1995. Rio Tinto Indonesia, Unpublished report, 29pp.

Hayba, D.O., Bethke, P.M., Heald, P. And Foley, N.K., 1985. Geologic, mineralogic, and geochemical characteristics of volcanic-hosted epithermal precious-metal deposits. In: B.R. Berger and P.M. Bethke (Editors), Geology and Geochemistry of Epithermal Systems. Society of Economic Geologists, Reviews in Economic Geology 2, pp129-167.

Hawkesworth, C.J., Gallagher, K., Hergt, J.M. and McDermott, F., 1994. Destructive plate margin magmatism: Geochemistry and melt generation. Lithos 33, pp. 169-188.

Heald, P., Foley, N.K. and Hayba, D.O., 1987. Comparative anatomy of volcanic-hosted epithermal deposits: acid-sulfate and adularia-sericite types. Economic Geology 82, pp. 1-26.

Hedenquist, J.W., 1987. Mineralization associated with volcanic-related hydrothermal systems in the Circum Pacific Basin. In : M.K. Horn (Editor), Transactions of the Fourth Circum-Pacific Energy and Mineral Resources Conference, Singapure. American Association of Petroleum Geologists, pp. 513-524.

Hedenquist, J.W. and Lowenstern, J.B., 1994. The role of magmas in the formation of hydrothermal ore deposits. Nature 370, pp. 519-527.

Henley. R.W., 1991. Epithermal gold deposits in volcanic terranes. In: R.P. Foster (Editor), Gold Metallogeny and Exploration. Blackie, Glasgow, pp. 133-164.

Hirata, T. and Nesbitt, R.W., 1995. U-Pb isotope geochronology of zircon: Evaluation of the laser probe inductively coupled plasma mass spectrometry technique. Geochimica et Cosmochimica Acta 59, pp. 2491-2500.

Hoatson, D.M. and Keays, R.R., 1989. Formation of platiniferous sulfide horizons by crystal fractionation and magma mixing in the Munni Munni Layered Intrusion, West Pilbara Block, Western Australia.

Hoffman, E.L., Naldrett, A.J., Van Loon, J.C., Hancock, R.G.V. and Mason, A., 1978. The determination of all the platinum group elements and gold in rocks and ore by neutron activation analysis after preconcentration by a nickel sulfide fire-assay technique of large samples. Analytica Chimica Acta 102, pp. 157-166.

Horn, I., Rudnick, R.L. and McDonough, W.F., 2000. Precise elemental and isotope ratio determination by simultaneous solution nebulization and laser ablation ICPMS: Application to U-Pb geochronology. Chemical Geology 164, pp. 281-301.

Huppert, H.E and Sparks, R.S.J., 1980. The fluid dynamics of a basaltic magma chamber replenished by influx of hot, dense ultrabasic magma. Contributions to Mineralogy and Petrology 75, pp. 279-289.

Irving, A.J., 1978. A review of experimental studies of crystal/liquid trace element partitioning. Geochimica et Cosmochimica Acta 42, pp. 743-770.

Irving, A.J. and Frey, F.A., 1984. Trace element abundances in megacrysts and their host basalts: Constraints on partition coefficients and megacrysts genesis. Geochimica et Cosmochimica Acta 48, pp. 1201-1221.

Jackson, S.E., Fryer, B.J., Gosse, W., Healey, D.C., Longerich, H.P. and Strong, D.F., 1990. Determination of the precious metals in geological materials by inductively coupled plasma mass spectrometry (ICP-MS) with nickel sulfide collection and tellurium coprecipitation. Chemical Geology 83, pp. 119-132.

Jaffey, A.H., Flynn, K.F., Glendenin, L.E., Bentley, W.C. and Essling, A.M., 1971. Precision measurement of the half lives and specific activities of ^{235}U and ^{238}U. Physics Reviews C4, pp. 1889-1907

Keays, R.R., 1995. The role of komatiitic and picritic magmatism and S-saturation in the formation of ore deposits. Lithos 34, pp. 1-18.

Keays, R.R. and Campbell, I.H., 1981. Precious metals in the Jimberlana Intrusion, Western Australia: Implications for the genesis of platiniferous ores in layered intrusions. Economic Geology 76, pp. 1118-1141.

Koyaguchi, T., 1986. Textural and compositional evidence for magma mixing and its mechanism, Abu volcano group, Southwestern Japan. Contributions to Mineralogy and Petrology 93, pp. 33-45.

Leach, T.M., 1991. Distribution of Hydrothermal Alteration at S. Magerang and Kelian Cahai, P.T. Kelian Equatorial Mining, Unpublished report, 13pp.

Leach, T.M and Corlett, G., 1999. Petrological evaluation of core samples from the Plata prospect, East Kalimantan. PT. Danum Bukit Minerals, Unpublished report, 38pp.

Le Maitre, R.W., et al., (Editors), 1989. A Classification of Igneous Rocks and Glossary of Terms. Blackwell Scientific Publications, Oxford, 193 pp.

Lee, J.K.W., Williams, I.S. and Ellis, D.J., 1997. Pb, U and Th diffusion in natural zircon. Nature 390, pp. 159-161.

Lindgren, W., 1922. A suggestion for the terminology of certain mineral deposits. Economic Geology 17, pp.202-204.

Lindgren, W., 1933. Mineral Deposits. Mc.Graw Hill, New York, 930pp.

Loucks, R.R., Eggins, S.M., Shelley, L.M.G., Kinsley, L.P.J. and Ware, N.G., 1995. Development of the inductively-coupled-plasma mass-spectrometry ultraviolet laser trace-element micro-analizer (ICPMS-ULTEMA). Research School of Earth Sciences, Annual Report 1995, pp.138-140.

Loucks, R.R., Eggins, S.M., Shelley, L.M.G., Kinsley, L.P.J., Ware, N.G., 1995. Development of the inductively-coupled-plasma mass-spectrometry ultraviolet laser trace-element micro-analizer (ICPMS-ULTEMA). Research School of Earth Sciences, Annual Report 1995, pp.138-140.

Loucks, R.R. and Mavrogenes, J.A., 1999. Gold solubility in supercritical hydrothermal brines measured in synthetic fluid inclusions. Science 284, pp. 2159-2163.

Martin, C. E., 1990. Rhenium-osmium isotope geochemistry of the mantle. PhD. thesis, Yale University.

McCulloch, M.T and Gamble, J.A., 1991. Geochemical and geodynamical constrains on subduction zone magmatism. Earth and Planetary Science Letters 102, pp. 358-374.

McDonough, W.F and Sun, S.-s., 1995. The composition of the earth. Chemical Geology 120, pp. 223-253.

Meschede, M., 1986. A method of discriminating between different types of mid-ocean ridge basalts and continental tholeiites with the Nb-Zr-Y diagram. Chemical Geology 56, pp. 207-218.

Mitchell, R.H. and Keays, R.R., 1981. Abundance and distributions of gold, palladium and iridium in some spinel and garnet lherzolites: implications for the nature and origin of precious metal-rich intergranular components in the upper mantle. Geochimica et Cosmochimica Acta 45, pp. 2425-2442.

Miyashiro, A., 1974. Volcanic rock series in island arcs and active continental margins. American Journal of Science 274, pp. 321-355.

Naldrett, A.J., Hoffman, E.L., Green, A.H., Chou, C.L. and Naldrett, S.L., 1979. The composistion of Ni-sulfide ores with particular reference to their content of PGE and Au. Canadian Mineralogist 17, pp. 403-415.

Nell, J and O'Neill, H.St.C., 1997. The Gibbs free energy of formation and heat capacity of Rh_2O_3 and $MgRh_2O_4$, the MgO-Rh-O phase diagram, and constraints on the stability of $Mg_2Rh^{4+}O_4$. Geochimica et Cosmochimica Acta 61, pp. 4159-4171.

Nicholls, I.A and Harris, K.L., 1980. Experimental rare earth element partition coefficients for garnet, clinopyroxene and amphibole coexisting with andesitic and basaltic liquids. Geochimica et Cosmochimica Acta 44, pp. 287-308.

Nielsen, R.L., Gallahan, W.E. and Newberger, F., 1992. Experimentally determined mineral-melt partition coefficients for Sc, Y and REE for olivine, orthopyroxene, pigeonite, magnetite and ilmenite. Contributions to Mineralogy and Petrology 110, pp. 488-499.

Norrish, K. and Hutton, J.T., 1969. An accurate X-ray spectrographic method for the analysis of a wide range of geological samples. Geochimica et Cosmochimica Acta 33, pp. 431-453.

Palin, J.M., Campbell, I.H. and Smith, K., 1998. Pb-U dating of zircon by Excimer Laser Ablation ICP-MS. Research School of Earth Sciences, Annual Report 1998, pp. 10.

Panteleyev, A., 1986. A Canadian Cordilleran Model for Epithermal Gold-Silver Deposits, Geoscience Canada 13, pp. 101-111.

Pearce, N.J.G., Perkins, W.T., Westgate, J.A., Gorton, M.P., Jackson, S.E., Neal, C.R. and Chenery, S.P., 1997. A compilation of new and published major and trace element data for NIST SRM 610 and NIST SRM 612 glass reference materials, Geostandards Newsletter 21, pp. 115-144.

Perfit, M.R., Gust, D.A., Beace, A.E., Arculus, R.J. and Taylor, S.R., 1980. Chemical characteristics of island-arc basalts: implications for mantle sources. Chemical geology 30, pp. 227-256.

Perkins, W.T and Pearce, N.J.G., 1995. Mineral microanalysis by laser probe inductively coupled plasma mass spectrometry. In P.J. Pott, J.F.W. Bowles, S.J.B. Reed and M.R. Cave (Eds), Microprobe Techniques in the Earth Sciences. Chapman and Hall, London, pp. 291-325.

Pieters, P.E., 1999, Notes on regional geology of the tenement areas held by PT. Riotinto exploration in Central Kalimantan. PT. Rekasindo Guriang Tandang, Unpublished report, 10 pp.

Ravizza, G. and Pyle, D., 1997. PGE and Os isotopic analyses of single sample aliquots with NiS fire assay preconcentration. Chemical Geology 141, pp.251-268.

Richards, J.P., 1992. Magmatic-epithermal transitions in alkalic systems: Porgera gold deposit, Papua New Guinea. Geology 20, pp. 547-550.

Richards, J.P. and McDougall, I., 1990. Geochronology of the Porgera gold deposit, Papua New Guinea : Resolving the effects of excess argon on K-Ar and 40Ar/39Ar age estimates for magmatism and mineralization. Geochimica et Cosmochimica Acta 54, pp. 1397-1415.

Ryan, M., 1987. Neutral buoyancy and the mechanical evolution of magmatic systems. In: B.O. Mysen (Ed), Magmatic Processes: Physicochemical Principles. Geochemical Society Special Publication 1, pp. 259-287.

Schmith, H., 1950. Origin of the "epithermal" mineral deposits. Economic Geology 45, pp. 191-200.

Setiabudi, B.T., 1994. Regional Exploration of The Sopandua - Kelian Cahai - Magerang areas, P.T. Kelian Equatorial Mining, Unpublished report, 27pp.

Seward, T.M., 1991. The hydrothermal geochemistry of gold. In : R.P. Foster (Ed), Gold Metallogeny and Exploration. Blackie and Sons Ltd., pp. 37-62.

Sinclair, D.J., Kinsley, L.P.J. and McCulloch, M.T., 1998. High resolution analysis of trace elements in corals by laser ablation ICP-MS. Geochimica et Cosmochimica Acta 62, pp. 1889-1901.

Shinjo, R., 1999. Geochemistry of high Mg andesites and the tectonic evolution of the Okinawa Trough-Ryukyu arc system. Chemical Geology 157, pp. 69-88.

Sillitoe, R.H., 1993a. Comments on geological models and exploration at Magerang and Kelian, East Kalimantan, Indonesia. Unpublished report, 7 pp.

Sillitoe, R.H., 1993b. Epithermal Models: Genetic Types, Geometrical Controls and Shallow Features. In: R.V. Kirkham, W.D. Sinclair, R.I. Thorpe and J.M. Duke (Editors), Mineral Deposit Modelling. Geological Association of Canada Special Paper 40, pp. 403-417.

Silvester, P.J., and Ghaderi, M., 1997. Trace element analysis of scheelite by excimer laser ablation—inductively coupled plasma—mass spectometry (ELA—ICP—MS) using a synthetic silicate glass standard. Chemical Geology 141, pp. 49-65

Simmons, S.F. and Browne, P.R.L., 1990. Minearlogic, alteration and fluid inclusion studies of epithermal gold-bearing veins at Mt. Muro prospect, Central Kalimantan (Borneo), Indonesia. In: J.W. Hedenquist, N.C. White and G. Siddeley (Editors), Epithermal Gold Mineralisation of the Circum-Pacific: Geology, Geochemistry, Origin and Exploration, I. Journal of Geochemical Exploration 35, pp. 63-103.

Simon, G., Kesler, S.E., Russell, N., Hall, C.M., Bell, D. and Pinero, E., 1999. Epithermal Gold Mineralisation in an Old Volcanic Arc: The Jacinto Deposit, Camaguey District, Cuba. Economic Geology 94, pp. 487-506.Seward, T.M., 1991. The hydrothermal geochemistry of gold. In : R.P. Foster (Ed), Gold Metallogeny and Exploration. Blackie and Sons Ltd., pp. 37-62.

Sun, S.-s. and McDonough, W.F., 1989. Chemical and isotopic systematics of oceanic basalts : implication for mantle composition and processes. In: A.D. Saunders and M.J. Norry (Editors), Magmatism in the Ocean Basins, Geological Society Special Publication 42, pp. 313-345.

Tatsumi, Y., Hamilton, D.L. and Nesbitt, R.W., 1986. Chemical characteristics of fluid phase released from a subducted lithosphere and origin of arc magmas: Evidence from high-pressure experiments and natural rocks. Journal of Volcanology and Geothermal Research 29, pp. 293-309.

Thompson, J.F.H., Abidin, H.Z, Both, R.A., Martosuroyo, S., Rafferty, W.J. and Thompson, A.J.B., 1994. Alteration and epithermal mineralisation in the Masupa Ria volcanic center, Central Kalimantan, Indonesia. In: T.M. van Leeuwen, J.W. Hedenquist, L.P. James andJ.A.S. Dow (Editors), Indonesian Mineral Deposits - Discoveries of the Past 25 Years. Journal of Geochemical Exploration 50, pp. 429-456.

Togashi, S. and Terashima, S., 1997. The behaviour of gold in unaltered island arc tholeiitic rocks from Izu-Oshima, Fuji, and Osoreyama volcanic areas, Japan. Geochimica et Cosmochimica Acta 61, pp. 543-554.

Van Leeuwen, T.M., 1994. 25 Years of mineral exploration and discovery in Indonesia. In: T.M. van Leeuwen, J.W. Hedenquist, L.P. James andJ.A.S. Dow (Editors), Indonesian Mineral Deposits - Discoveries of the Past 25 Years. Journal of Geochemical Explorartion 50, pp.13-90.

Van Leeuwen, T.M., Leach, T., Hawke, A.A. and Hawke, M.M., 1990. The Kelian disseminated gold deposit, East Kalimantan, Indonesia. In: J.W. Hedenquist, N.C. White and G. Siddeley (Editors), Epithermal Gold Mineralisation of the Circum-Pacific: Geology, Geochemistry, Origin and Exploration, I. Journal of Geochemical Exploration 35, pp. 1-61.

Wake, A.W., 1991. Gold mineralization at the Muyup Prospect, East Kalimantan, Indonesia. In : Proceedings of World Gold 91, pp.271-278.

Ware, N.G., 1991. Combined energy-dispersive-wavelength-dispersive quantitative electron microprobe analysis. X-Ray Spectrometry 20, pp. 73-79.

Wendt, I. And Carl C., 1991, The statistical distribution of the mean squared weighted deviation: Chemical Geology (Isotope Geoscience Section), v. 86, p. 275-285.

Wendlandt, R.F., 1982. Sulfide saturation of basalt and andesite melts at high pressures and temperatures. American Mineralogist 67, pp. 877-885.

Wilson, M., 1989. Igneous Petrogenesis. A global tectonic approach. Chapman and Hall, London UK, 466pp.

Wilson, M., 1995. Magmatic differentiation. In: M.J. Le Bas (Ed), Milestones in Geology, Geological Survey, London, Memoir No. 16, pp. 205-218.

Wood, D.A., Joron, J.L. and Treuil, M., 1979. A re-appraisal of the use of trace elements to classify and discriminate between magma series erupted in different tectonic settings. Earth and Planetary Science Letters 45, pp. 326-336

White, D.H., Muffler, L.J.P. and Truesdell, A.H., 1971. Vapour-dominated hydrothermal systems compared with hot-water systems. Economic Geology 66, pp. 75-97.

White, N.C. and Hedenquist, J.W., 1990. Epithermal environments and styles of mineralisation: variations and their causes, and guidelines for exploration. In: J.W. Hedenquist, N.C. White and G. Siddeley (Editors), Epithermal Gold Mineralisation of the Circum-Pacific: Geology, Geochemistry, Origin and Exploration, I. Journal of Geochemical Exploration 35, pp 445-474.

White, N.C., Leake, M.J., McCaughey, S.N. and Parris, B.W., 1995. Epithermal gold deposits of the southwest Pacific. Journal of Geochemical Exploration 54, pp. 87-136.

White, N.C. and Poizat, V., 1995. Epithermal Deposits : diverse styles, diverse origin ? In: J.L. Mauk and J.D. St. George (Editors), Pacrim Congress 1995: Exploring the Rim. Proceedings, Australasian Institute of Mining and Metallurgy, pp. 623-628.

APPENDIX 1-1

List of samples for whole-rock geochemistry

ANU No.	Sample No.	Kelian	Drillhole No.	Location	Kelian Mine Grid		R.L. (m)	Rock Type	Alteration
		Drill Section			Northing	Easting			
99069	1132	50N	KFD1-415m	Tepu	9540	10149	1171	andesite porphyry	least altered
99070	1134	50N	KFD1-452m	Tepu	9540	10149	1171	andesite porphyry	least altered
98020	123188	250N	K782-48m	East Pramp Pit	9951	9990	1060	andesite porphyry	phyllic S2
98022	123191	250N	K782-153m	East Pramp Pit	9951	9990	1060	andesite porphyry	phyllic S2
99034	123193	250N	K782-182m	East Pramp Pit	9951	9990	1060	hydrothermal breccia	phyllic S3
99024	123197	250N	K782-357m	East Pramp Pit	9951	9990	1060	andesite porphyry	propylitic S1
98026	123362	250N	K782-434m	East Pramp Pit	9951	9990	1060	andesite porphyry	propylitic S1
98027	123365	250N	K782-527m	East Pramp Pit	9951	9990	1060	andesite porphyry	propylitic S1
99035	123367	250N	K782-610m	East Pramp Pit	9951	9990	1060	lithic tuff	phyllic-S2
99071	1143	390N	K418-27.5m	Tepu	9624	10527	1124	andesite porphyry	least altered
99047	123524	390N	K622-174m	East Pramp Pit	9790	10361	1136	andesite porphyry	phyllic S2
98075	123532	390N	K625-240m	East Pramp Pit	9883	10262	1119	andesite porphyry	propylitic S1
98039	123418	590N	K621-155m	East Pramp Pit	10121	10313	1119	andesite porphyry	phyllic S2
98038	123419	590N	K621-178m	East Pramp Pit	10121	10313	1119	andesite porphyry	phyllic S2
98041	123427	590N	K626-302m	East Pramp Pit	10078	10357	1120	andesite porphyry	propylitic S1
98042	123432	590N	K629-199m	East Pramp Pit	10078	10357	1120	andesite porphyry	phyllic S3
99036	123433	590N	K629-319m	East Pramp Pit	10078	10357	1120	hydrothermal breccia	phyllic S3
99037	123434	590N	K629-337m	East Pramp Pit	10078	10357	1120	hydrothermal breccia	phyllic S3
98043	123436	590N	K629-397m	East Pramp Pit	10078	10357	1120	andesite porphyry	phyllic S3
99038	123437	590N	K708-360m	East Pramp Pit	10111	10318	1100	andesite porphyry	phyllic S3
98048	123473	710N	K609-228m	And 393 Zone	10333	10275	1129	andesite porphyry	phyllic S3
98050	123476	710N	K610-155m	East Pramp Pit	10160	10446	1129	andesite porphyry	propylitic S1
98049	123475	710N	K610-329m	East Pramp Pit	10160	10446	1129	hydroth. bx tuff	phyllic-S2
99040	123479	710N	K610-352m	East Pramp Pit	10160	10446	1129	hydroth. bx tuff	argillic-S4
99041	123480	710N	K610-373m	East Pramp Pit	10160	10446	1129	hydroth. bx tuff	phyllic-S3
98051	123485	710N	K637-148m	East Pramp Pit	10116	10487	1120	andesite porphyry	phyllic S2
98052	123486	710N	K637-275m	East Pramp Pit	10116	10487	1120	andesite porphyry	phyllic S3
99048	123578	710N	K681-15m	East Pramp Pit	10122	10483	1120	hydrothermal breccia	phyllic S3
99042	123487	710N	K681-239m	East Pramp Pit	10122	10483	1120	andesite porphyry	phyllic S3
99043	123489	710N	K681-308m	East Pramp Pit	10122	10483	1120	vitric tuff	phyllic S3
99044	123490	710N	K681-365m	East Pramp Pit	10122	10483	1120	vitric tuff	phyllic-S2
99045	123492	710N	K686-74m	East Pramp Pit	10081	10523	1120	andesite porphyry	phyllic S2
99049	123583	710N	K686-151m	G. Runcing	10081	10523	1120	muddy breccia	phyllic S2
98053	123493	710N	K691-134m	S. Jiu	10576	10046	1120	rhyolite porphyry	phyllic-S2
98054	123501	750N	K633-277m	East Pramp Pit	10289	10372	1119	andesite porphyry	phyllic S2
99046	123502	750N	K634-80m	East Pramp Pit	10327	10334	1118	lithic tuff	phyllic-S2
98056	123505	750N	K634-181m	East Pramp Pit	10327	10334	1118	lithic tuff	phyllic-S3
98058	123509	750N	K636-131m	East Pramp Pit	10216	10443	1119	andesite porphyry	propylitic S1
98059	123511	750N	K643-211m	East Pramp Pit	10177	10477	1120	andesite porphyry	argillic S4
98011	123218	950N	pit exposure	G. Runcing	10600	10380	1110	rhyolite porphyry	phyllic-S2
98072	123219	1030N	pit exposure	G. Runcing	10640	10425	1110	rhyolite porphyry	phyllic-S2
98012	123220	1110N	pit exposure	G. Runcing	10650	10510	1120	rhyolite porphyry	phyllic-S2
99030	123203	870N	pit exposure	East Pramp Pit	10475	10355	1090	tuff lapilli	argillic-S4
99031	123204	870N	pit exposure	East Pramp Pit	10465	10370	1090	hydroth. bx tuff	argillic-S4
99032	123215	360N	pit exposure	East Pramp Pit	10000	10105	1110	lithic tuff	argillic-S4
99033	123236	950N	pit exposure	G. Runcing	10460	10485	1090	mudstone/diatreme bx	phyllic S2
98001	123200	250N	pit exposure	West Pramp Pit	10130	9825	1170	andesite porphyry	propylitic S1
98002	123201	610N	pit exposure	East Pramp Pit	10260	10200	1020	andesite porphyry	propylitic S1
98007	123209	210N	pit exposure	West Pramp Pit	10100	9800	1170	andesite porphyry	propylitic S1
98073	123210	40N	pit exposure	West Pramp Pit	9960	9695	1170	andesite porphyry	propylitic S1
98008	123212	90N	pit exposure	West Pramp Pit	10070	9655	1170	andesite porphyry	propylitic S1
98014	123228	660N	pit exposure	East Pramp Pit	9980	10575	1090	andesite porphyry	propylitic S1
98004	123206	50N	pit exposure	West Pramp Pit	9975	9695	1170	andesite porphyry	phyllic S2
98005	123207	50N	pit exposure	West Pramp Pit	9985	9685	1170	andesite porphyry	phyllic S2
98003	123205	580N	pit exposure	East Pramp Pit	10055	10360	1020	andesite porphyry	argillic S4
98009	123213	140N	pit exposure	West Pramp Pit	10130	9675	1170	andesite porphyry	argillic S4
98074	123214	120N	pit exposure	West Pramp Pit	10100	9665	1170	andesite porphyry	argillic S4

APPENDIX 1-2

List of samples for whole-rock geochemistry

ANU No.	Sample No	Reg. Exploration	Prospect	Kelian Mine Grid				
		Drillhole No.		Northing	Easting	R.L.(m)	Rock Type	Alteration
99054	123122	DDM1-28m	Magerang	12300	6420	1249	andesite	phyllic
98080	123124	DDM1-75m	Magerang	12300	6420	1249	andesite	propylitic
99050	123131	DDM2-33m	Magerang	13040	6620	1249	andesite	adv.argillic
99051	123132	DDM2-49m	Magerang	13040	6620	1249	andesite	phyllic
99052	123137	DDM3-86m	Magerang	12300	6420	1249	andesite	phyllic
99053	123138	DDM3-117m	Magerang	12300	6420	1249	andesite	phyllic
98062	123140	DDM3-172m	Magerang	12300	6420	1249	andesite	phyllic
99055	123164	DDM3-236m	Magerang	12300	6420	1249	andesite	phyllic
98088	123167	DDM3-300m	Magerang	12300	6420	1249	andesite	phyllic
99056	123170	DDM3-389m	Magerang	12300	6420	1249	andesite	phyllic
98063	123147	DDM5-312m	Magerang	13000	6020		andesite	propylitic
98082	123148	DDM5-339m	Magerang	13000	6020		andesite	phyllic
99078	1158	DDM6-129m	Magerang	12094	6516	1270	andesite	least altered
98081	123144	DDM6-140m	Magerang	12094	6516	1270	andesite	least altered
99079	1159	DDM6-151m	Magerang	12094	6516	1270	andesite	least altered
98064	123158	DDM6-177m	Magerang	12094	6516	1270	andesite	least altered
98086	123159	DDM6-192m	Magerang	12094	6516	1270	andesite	least altered
99080	1160	DDM6-206m	Magerang	12094	6516	1270	andesite	least altered
98087	123160	DDM6-221m	Magerang	12094	6516	1270	andesite	least altered
99081	1161	DDM6-233m	Magerang	12094	6516	1270	andesite	least altered
98083	123151	DDM7-67m	Magerang	12631	5692	1282	andesite	propylitic
98084	123152	DDM7-82m	Magerang	12631	5692	1282	andesite	propylitic
98065	123153	DDM7-115m	Magerang	12631	5692	1282	andesite	propylitic
98085	123154	DDM7-138m	Magerang	12631	5692	1282	andesite	propylitic
98076	123101	EdI2-36m	Imang	12400	7850	1185	andesite	propylitic
99076	1130	EdI2-41m	Imang	12400	7850	1185	andesite	least altered
99072	1126	EdI2-46m	Imang	12400	7850	1185	andesite	propylitic
98077	123102	EdI2-56m	Imang	12400	7850	1185	andesite	least altered
99073	1127	EdI2-66.5m	Imang	12400	7850	1185	andesite	least altered
99074	1128	EdI2-92.5m	Imang	12400	7850	1185	andesite	least altered
98060	123104	EdI2-96m	Imang	12400	7850	1185	andesite	least altered
98078	123107	EdI3-65m	Imang	12600	7850		andesite	least altered
98079	123108	EdI4-15m	Imang	13000	7900		andesite	least altered
99075	1129	EdI4-26m	Imang	13000	7900		andesite	propylitic
98061	123109	EdI4-36m	Imang	13000	7900		andesite	least altered
99077	1155	EdI4-47m	Imang	13000	7900		andesite	least altered
98066	123171	DSD1-51m	Magerang	11038	6705	1177	andesite	phyllic
98089	123172	DSD1-78m	Magerang	11038	6705	1177	andesite	propylitic
98067	123176	DSD1-206m	Magerang	11038	6705	1177	andesite	propylitic
98090	123178	DSD1-245m	Magerang	11038	6705	1177	andesite	propylitic
98070	123226	S. Magerang	Magerang	12240	7560		andesite	least altered
98071	123227	S. Taliyuda	Magerang	12520	7380		andesite	least altered

APPENDIX 1-3

List of samples for whole-rock geochemistry

ANU No.	Sample No.	Drillhole No.	Prospect	Kelian Mine Grid		R.L.(m)	Rock Type	Alteration
				Northing	Easting			
98068	123183	EdN5-63m	Nakan	7797	9277	1211	andesite	least altered
99057	123184	EdN6-29m	Nakan	7784	9619	1118	Volc. Sandstone	least altered
99082	1106	NWD4-6.5m	Nakan	9405	8790	1170	andesite	least altered
99083	1107	NWD4-12.5m	Nakan	9405	8790	1170	andesite	least altered
99086	1110	NWD4-20m	Nakan	9405	8790	1170	andesite	least altered
99084	1108	NWD4-22m	Nakan	9405	8790	1170	andesite	least altered
99085	1109	NWD5-8.5m	Nakan	9350	8825	1210	andesite	least altered
99087	1111	NWD5-30m	Nakan	9350	8825	1210	andesite	least altered
99088	1174	NWD6-24m	Nakan	9286	8840	1225	andesite	least altered
99089	1175	NWD9-12m	Nakan				andesite	least altered
99090	1176	NWD10-24.5m	Nakan				andesite	least altered
99091	1177	NWD11-29.5m	Nakan				andesite	least altered
98091	123186	NWD13-23m	Nakan	8784	8633	1216	andesite	least altered
98069	123187-1	NWD13-29m	Nakan	8784	8633	1216	andesite	least altered
98069	123187-2	NWD13-29m	Nakan	8784	8633	1216	andesite	least altered
98069	123187-3	NWD13-29m	Nakan	8784	8633	1216	andesite	least altered
98069	123187-4	NWD13-29m	Nakan	8784	8633	1216	andesite	least altered
ANU No.	Sample No.	Location	Prospect	RTI Reg. Exploration Grid		R.L.(m)	Rock Type	Alteration
				Northing	Easting			
98092	123301	G. Tinggi, Tabang	Ritan	50750 mN	398500 mE		andesite	least altered
99058	123305	G. Botak	Ritan	67750 mN	410500 mE		andesite	propylitic
98093	123307	S. Batuliten	Ritan	42850 mN	394250 mE		rhyolite	least altered
99059	123308	S. Belayan	Ritan	44800 mN	393500 mE		rhyolite	least altered
99060	123313	timber road, Mejuk	Ritan	63775 mN	400075 mE		andesite	adv. argillic
99061	123317	vein zone, Mejuk	Ritan	63850 mN	400125 mE		andesite	argillic
99062	123320	discovery o/c, Mejuk	Ritan	64350 mN	401050 mE		andesite	argillic
99063	123325	timber road, Mejuk	Ritan	63275 mN	398750 mE		andesite	propylitic
ANU No.	Sample No.	Location	Prospect	Northing	Easting	R.L.(m)	Rock Type	Alteration
99064	123337	Bengeh	Muyup				tuff	phyllic
99065	123342	S. Tresia	Muyup				tuff	phyllic
99066	123343	S. Tresia	Muyup				tuff	phyllic
98094	123348	S. Buluh Hulu	Muyup				dacite	least altered
98095	123349	S. Buluh Hulu	Muyup				dacite	least altered
99067	123351	S. Buluh Hulu	Muyup				tuff	phyllic
98096	123353	S. RTM	Muyup				dacite	least altered
98097	123354	S. RTM	Muyup				dacite	least altered
99068	123357	G. Manuk	Muyup				andesite	adv. argillic
ANU No.	Sample No.	Location	Prospect	Northing	Easting	R.L.(m)	Rock Type	Alteration
99092	1101	B.Utul-1	Batu Utul				rhyolite	phyllic
99093	1102	B.Utul-2	Batu Utul				andesite	least altered
99094	1103	S. Han-1	Han	16210	342990		andesite	least altered
99095	1105	SYKBHan-3	Han	16720	342400		andesite	propylitic
99096	1115	99HN1-59m	Han	16455	342250		andesite	least altered
99097	1119	98PT5-97m	Plata				andesite	least altered
99098	1121	98PT5-169m	Plata				andesite	least altered

APPENDIX 2

Sample Preparation Techniques

1. Whole-rock sample preparation

Selected samples from outcrops and drillcores, weighing about 200 grams are crushed using a hydraulic plate crusher and a manually operated splitter. Chips of an approximately 0.25 inch are then collected and split into 2 portions. One hundred grams of the sample is stored and the other 100 grams are split. Thirty grams of samples are first pulverised for 5 minutes to decontaminate the agate mill, then 50 grams of samples are pulverised for 10 minutes. The sample powders are put into a sterilised plastic container. The mill bowl is then cleaned with alcohol and the agate puck is cleaned with Milli-Q water in an ultrasonic bath.

2. Spiked flux preparation

The Lithium Metaborate ($LiBO_2$) flux is dried at 500°C for 5 hours, then after cooling is stored in a dessicator prior to mixing with the spike solution. The Pt crucible is cleaned and decontaminated using $LiBO_2$ flux. The Pt crucible filled with flux is heated at 500°C for 15 minutes and then at 1000°C for 15 minutes to melt the flux. The molten flux is poured into the water in a glass beaker; the remaining flux is scraped off and the Pt crucible is washed with warm Milli-Q water using a sterilised spatula. The spike solution, 109.7 ppm ^{169}Tm and 3.28 ppm ^{235}U, is poured into a 15ml teflon vial and is accurately measured. In a clean Pt crucible, the $LiBO_2$ flux is weighed out to make a flux to spike ratio of 2:1. The spike solution is poured into the Pt crucible and the total weight of the spiked flux and Pt crucible is recorded. The mixed spike solution and flux is then dried in the oven over a 4 day period with the following sequence. The spiked flux is dried at 90°C in the oven overnight (approx. 18 hours), cooled down. The weight of flux and the loss of water are measured. The temperature is raised to 140°C and dried overnight. After cooling down the weight of flux is noted. Using the same procedure, the flux is dried at 160°C overnight, then at 200°C nextnight. Subsequently, the Pt crucible is placed in a high temperature furnace to heat at 250°C (60 minutes) and afterwards raised to 300°C (60 minutes), cooled down and the weight of flux is monitored. When the spiked flux is completely dried out, the flux is heated at 500°C for 15 minutes, then the temperature is raised to 1000°C to allow melting for 30 minutes. Once complete, the Pt crucible is quenched in the 3 litre glass beaker. The extracted glass is pulverised using an agate mill for 2 minutes. In order to produce homogenous flux powder, the glass powder was remelted in the furnace at 1000°C for 1 hour, following pre-

heating at 500°C for 15 minutes. After being quenching, the flux glass is remilled and stored in a sterilised container.

3. Glass Sample Fusion

To make the sample/flux ratio of 2:1, 0.6666 grams of whole-rock powder is mixed with 0.3333 grams of spike flux on a piece of weighing paper by folding the paper by thumb and forefinger, rolling the sample and flux powder over each other until a homogenous mixture is made. Then the sample powder is poured into a clean, 3 cm-wide carbon crucible, and pre-heated in the Kanthal Super Rapid Furnace at 600°C for 30 minutes. The carbon crucible is transfered into the Kanthal EPD High Temperature Melting Furnace for pre-heating the sample at 800°C for 5 minutes prior to fusing. After 5 minutes, the temperature is raised to 1200°C and the sample is melted for 20 minutes. Argon gas flow of 2.5 litre/minute is used during the preheating (800°C) and melting (1200°C). At the end of sequence, the carbon crucible is taken out and quickly dropped into cold water in a 3 litre beaker to allow quenching. The temperature is then lowered to 800°C, to allow the sample stage cool down for a few minutes before putting the next sample on the stage. Finally, the glass is washed, placed in a vial with a label on it, and dried overnight at 60°C in the oven.

4. Glass mount and polish

The dry glass in the vial is shaken to break up, then a selected 2-3 mm-wide glass shard is placed on double-sticky tape on a glass plate. Note that the selected glass should be dry, shiny, vitreous, and having least concavo-convex surface. The glass should be mounted with the internal face down in contact with the tape, representing those parts for laser ablation. The samples are arranged within a diameter of mounting disc in a unique configuration and the sample position is mapped for identification. It is useful to select 2 pieces of glass shards from each sample and position them in three rows on a disc so that a disc can accommodate 10 different samples. Several pieces of glass shards of the rock standard (Kilauea Basalt - ANU No.93-1489) are mounted on a separate disc. The sample is mounted in a mixture of epoxy (5g compound and 0.7 g hardener) using a plastic cylinder tube and left to dry overnight. The mount disc should be cut to 5 mm in thickness and polished for 30 minutes using 3mm polishing chemicals. Prior to analysing the samples, it is useful to take photographs or to scan the glass disc, to enable positioning the glass during laser ablation ICP-MS analysis.

	APPENDIX 3-1								
	Major and trace element compositions of whole-rock samples								
	Nakan Prospect								
	1	2	3	4	5	6	7	8	9
Location	Nakan	Nakan	Nakan	Nakan	Nakan	Nakan	Nakan	Nakan	Nakan
	EdN5-63m	NWD13-23m	NWD13-29m	NWD13-29m	NWD13-29m	NWD13-29m	NWD4-6.5m	NWD4-12.5m	NWD4-22m
Rock Type	andesite	andesite	andesite	andesite	andesite	andesite	andesite	andesite	andesite
Alteration	least altered	least altered	least altered	least altered	least altered	least altered	least altered	least altered	least altered
Sample No.	123183	123186	123187-1	123187-2	123187-3	123187-4	1106	1107	1108
Major elements	(normalised 100 wt%) analysed by XRF								
SiO2	57.92	60.21	57.71	57.66	57.68	57.65	62.67	62.10	62.79
TiO2	0.47	0.44	0.49	0.49	0.49	0.49	0.43	0.41	0.46
Al2O3	14.79	14.48	14.76	14.74	14.75	14.77	16.12	16.24	16.47
Fe2O3	7.92	7.06	7.12	7.08	7.07	7.12	5.42	5.41	5.47
MnO	0.19	0.16	0.11	0.11	0.11	0.11	0.09	0.10	0.09
MgO	7.06	8.00	7.75	7.78	7.77	7.75	4.84	4.53	4.38
CaO	7.96	5.67	8.65	8.69	8.63	8.68	6.25	6.98	5.83
Na2O	2.77	2.61	2.60	2.65	2.69	2.65	3.11	3.12	3.31
K2O	0.83	1.28	0.72	0.72	0.72	0.71	1.00	1.03	1.09
P2O5	0.08	0.08	0.08	0.09	0.09	0.08	0.09	0.09	0.10
Na2O + K2O	3.60	3.90	3.32	3.37	3.40	3.37	11.08	11.51	10.22
Trace elements	(in ppm) analysed by Laser Ablation ICPMS								
Cs	0.54	2.85	2.12	5.02	4.44	5.16	2.06	2.00	1.95
Rb	11.14	26.32	9.47	13.75	13.06	11.70	25.72	25.05	29.16
Ba	204.01	216.68	185.48	190.43	184.78	190.45	216.79	224.81	246.14
Th	1.85	1.82	1.88	1.96	1.98	1.95	2.03	1.92	2.09
U	0.69	0.65	0.72	0.76	0.74	0.74	0.71	0.65	0.67
Nb	0.66	1.04	0.74	0.98	1.07	0.65	1.16	1.14	1.23
Ta	0.06	0.08	0.06	0.08	0.07	0.07	0.09	0.08	0.10
La	6.76	6.24	6.86	6.90	6.80	6.90	7.02	7.08	7.27
Ce	14.17	13.00	14.49	14.66	14.33	14.61	14.41	14.51	14.64
Pr	1.70	1.54	1.74	1.76	1.76	1.77	1.66	1.70	1.72
Sr	363.66	221.67	361.78	369.54	371.10	265.34	372.99	375.09	347.91
Nd	7.16	6.70	7.46	7.64	7.45	7.52	6.91	6.84	6.89
Sm	1.74	1.46	1.75	1.78	1.74	1.74	1.46	1.54	1.59
Zr	50.84	46.97	46.80	47.10	47.65	29.07	56.15	52.29	55.84
Hf	1.41	1.33	1.30	1.36	1.45	1.35	1.50	1.50	1.56
Eu	0.55	0.50	0.57	0.58	0.59	0.56	0.49	0.54	0.51
Gd	1.73	1.56	1.73	1.76	1.76	1.77	1.52	1.66	1.54
Tb	0.27	0.25	0.27	0.27	0.27	0.27	0.25	0.24	0.24
Dy	1.85	1.68	1.81	1.85	1.87	1.84	1.62	1.67	1.65
Y	10.76	9.74	10.19	10.42	10.65	6.71	9.17	9.93	9.63
Ho	0.38	0.36	0.38	0.39	0.39	0.39	0.34	0.36	0.34
Er	1.14	1.01	1.11	1.15	1.18	1.16	1.03	1.06	1.01
Yb	1.24	1.14	1.20	1.21	1.18	1.20	1.17	1.18	1.12
Lu	0.19	0.18	0.17	0.19	0.18	0.18	0.17	0.19	0.18
Sc	25.36	21.73	28.06	27.38	27.48	27.77	19.29	19.83	20.00
Cr	263.04	249.25	317.59	359.72	317.42	311.10	148.93	175.55	176.72
Tl	0.00	0.03	0.00	0.01	0.01	0.01	0.09	0.07	0.09
Pb	0.25	11.21	1.82	18.34	19.18	8.58	9.73	9.93	9.35
Bi	0.00	0.10	0.00	0.06	0.07	0.03	0.17	0.26	0.09
V	101.62	138.54	128.23	166.72	170.27	141.15	133.28	132.83	142.98
Cu	7.58	41.87	13.08	40.14	43.21	32.09	29.34	29.42	27.57
Zn	2.18	40.69	11.25	49.11	47.48	44.59	51.27	46.62	41.80
Ga	9.81	12.94	11.66	13.69	12.73	9.71	22.02	21.88	23.17
As	0.21	3.61	0.94	12.58	19.14	11.88	0.74	0.91	0.44
Mo	1.51	1.08	1.39	1.08	1.46	0.47	0.71	0.64	0.61
W	0.26	0.50	0.35	0.70	0.87	0.26	0.37	0.39	0.58

	APPENDIX 3-1							
	Major and trace element compositions of whole-rock samples							
	Nakan Prospect							
	10	11	12	13	14	15	16	17
Location	Nakan	Nakan	Nakan	Nakan	Nakan	Nakan	Nakan	Nakan
	NWD5-8.5m	NWD4-20m	NWD5-30m	NWD6-24m	NWD9-12m	NWD10-24.5m	NWD11-29.5m	EdN6-29m
Rock Type	andesite	andesite	andesite	andesite	andesite	andesite	andesite	Volcaniclastics
Alteration	least altered	least altered	least altered	least altered	least altered	least altered	least altered	least altered
Sample No.	1109	1110	1111	1174	1175	1176	1177	123184
Major elements								
SiO2	62.65	63.00	63.16	62.99	61.40	61.33	61.20	72.90
TiO2	0.42	0.41	0.41	0.40	0.44	0.45	0.44	0.35
Al2O3	15.75	15.84	15.84	16.06	15.83	15.72	15.51	14.41
Fe2O3	5.59	5.43	5.35	5.22	6.18	6.35	6.04	3.35
MnO	0.11	0.10	0.10	0.11	0.13	0.17	0.14	0.09
MgO	4.52	4.30	4.16	4.12	5.33	5.00	5.39	0.41
CaO	6.78	6.53	6.55	6.56	6.69	6.86	6.08	4.11
Na2O	3.11	3.27	3.33	3.48	3.07	3.17	3.91	3.54
K2O	0.98	1.04	1.02	0.99	0.84	0.86	1.19	0.82
P2O5	0.09	0.09	0.09	0.08	0.09	0.09	0.09	0.03
Na2O + K2O	11.30	10.83	10.70	10.68	12.02	11.86	11.47	4.35
Trace elements								
Cs	1.31	1.50	1.64	1.14	1.31	1.65	9.23	1.35
Rb	25.95	26.88	24.95	23.58	21.16	21.63	26.76	23.52
Ba	220.57	248.76	254.17	244.23	196.79	208.60	246.26	374.12
Th	1.94	1.90	1.92	1.86	1.81	1.83	1.73	6.69
U	0.63	0.65	0.63	0.63	0.60	0.62	0.59	1.12
Nb	1.10	1.13	1.13	1.12	1.14	1.16	1.08	4.27
Ta	0.08	0.09	0.09	0.09	0.09	0.09	0.08	0.33
La	6.95	6.95	6.74	6.70	6.48	6.56	6.26	29.58
Ce	14.15	14.31	14.10	13.72	13.64	13.88	13.41	50.65
Pr	1.68	1.65	1.66	1.60	1.64	1.62	1.61	5.20
Sr	336.47	343.72	349.84	341.18	290.75	290.24	284.42	313.01
Nd	6.88	6.76	6.58	6.60	6.78	6.80	6.76	17.95
Sm	1.54	1.53	1.46	1.41	1.57	1.68	1.63	2.80
Zr	47.96	49.33	51.37	54.68	49.89	66.57	57.60	64.30
Hf	1.35	1.40	1.45	1.51	1.39	1.77	1.63	1.92
Eu	0.50	0.51	0.49	0.53	0.54	0.54	0.54	1.25
Gd	1.63	1.57	1.54	1.51	1.64	1.77	1.58	2.21
Tb	0.23	0.23	0.24	0.24	0.27	0.28	0.27	0.30
Dy	1.76	1.70	1.63	1.67	1.81	1.93	1.74	1.85
Y	9.59	9.80	9.43	9.53	10.94	11.76	10.20	8.82
Ho	0.34	0.36	0.34	0.35	0.39	0.38	0.39	0.36
Er	1.03	0.99	1.04	1.01	1.15	1.19	1.10	1.05
Yb	1.17	1.13	1.15	1.16	1.23	1.30	1.18	1.18
Lu	0.17	0.18	0.17	0.17	0.19	0.20	0.18	0.16
Sc	18.76	18.10	17.87	18.04	21.62	21.92	22.12	6.40
Cr	147.37	127.67	132.17	131.34	201.36	199.89	197.97	28.62
Tl	0.10	0.06	0.05	0.06	0.02	0.05	0.02	0.05
Pb	9.58	9.13	9.62	9.06	7.46	6.74	8.79	55.74
Bi	0.10	0.08	0.04	0.01	0.02	0.02	0.02	0.08
V	131.13	122.72	121.63	122.91	147.12	146.73	143.48	90.28
Cu	28.77	24.95	30.06	26.45	36.64	32.52	40.68	5.07
Zn	46.86	47.32	45.61	45.07	48.64	47.22	48.71	34.58
Ga	21.30	21.41	21.77	21.18	20.32	20.84	20.37	13.24
As	0.75	1.58	0.43	0.85	1.40	0.91	1.62	0.00
Mo	0.52	0.59	0.67	0.72	0.79	0.62	0.63	0.93
W	0.38	0.42	0.37	0.25	0.33	0.36	0.28	0.69

	APPENDIX 3-2								
	Major and trace element compositions of whole-rock samples								
	Magerang-Imang Prospect								
	1	2	3	4	5	6	7	8	9
Location	Magerang	Magerang	Magerang	Magerang	Magerang	Magerang	Magerang	Magerang	Magerang
	DDM6-129m	DDM6-151m	DDM6-206m	DDM6-233m	DDM6-140m	DDM6-177m	DDM6-192m	DDM6-221m	S. Magerang
Rock Type	andesite	andesite	andesite	andesite	andesite	andesite	andesite	andesite	andesite
Alteration	least altered	least altered	least altered	least altered	least altered	least altered	least altered	least altered	least altered
Sample No.	1158	1159	1160	1161	123144	123158	123159	123160	123226
Major elements	(normalised 100 wt%) analysed by XRF, except (*) analysed by Electron Microprobe (EDS)								
SiO2	63.75	64.05	63.50	63.96	63.59	63.22	62.59	63.79	62.52
TiO2	0.43	0.42	0.44	0.42	0.43	0.44	0.47	0.43	0.48
Al2O3	17.19	17.46	17.13	17.07	17.11	16.95	16.77	17.00	16.98
Fe2O3	5.08	4.51	5.11	4.72	5.07	5.08	5.38	4.93	5.34
MnO	0.13	0.14	0.12	0.14	0.12	0.12	0.12	0.12	0.10
MgO	2.78	2.46	3.01	2.67	2.78	3.07	3.50	2.84	4.21
CaO	5.52	5.97	5.66	6.07	5.81	6.05	6.20	5.94	6.34
Na2O	3.95	3.81	3.87	3.68	3.89	3.95	3.83	3.78	3.21
K2O	1.06	1.07	1.05	1.15	1.07	1.00	1.02	1.06	0.72
P2O5	0.12	0.11	0.12	0.11	0.12	0.11	0.12	0.11	0.11
Na2O + K2O	5.01	4.88	4.92	4.83	4.96	4.95	4.85	4.83	3.93
Trace elements	(in ppm) analysed by Laser Ablation ICPMS								
Cs	2.18	1.95	2.22	1.36	1.82	0.48	1.19	1.37	0.43
Rb	23.79	26.58	33.14	27.90	29.06	18.09	22.26	31.06	13.53
Ba	315.23	274.08	263.63	264.04	247.32	217.54	205.52	245.43	201.37
Th	2.09	2.18	2.18	2.12	2.22	2.22	2.04	2.21	1.86
U	0.68	0.63	0.70	0.63	0.67	0.67	0.62	0.68	0.41
Nb	1.34	1.38	1.37	1.30	1.47	1.17	1.14	1.59	1.05
Ta	0.11	0.11	0.10	0.11	0.11	0.10	0.10	0.11	0.08
La	7.41	7.38	7.58	7.51	7.36	7.44	6.83	7.34	6.02
Ce	15.36	15.18	15.60	15.43	15.29	15.43	14.22	15.31	12.97
Pr	1.78	1.77	1.85	1.82	1.83	1.81	1.75	1.76	1.54
Sr	372.26	364.05	363.59	366.82	355.94	338.83	305.20	357.57	320.23
Nd	7.35	7.33	7.59	7.45	7.53	7.40	7.09	7.18	6.48
Sm	1.73	1.55	1.60	1.73	1.80	1.67	1.63	1.70	1.48
Zr	85.03	87.86	68.75	77.57	85.33	85.02	78.82	100.17	74.59
Hf	2.05	2.25	1.76	1.98	2.20	2.16	2.06	2.18	1.89
Eu	0.55	0.52	0.57	0.56	0.57	0.53	0.53	0.56	0.54
Gd	1.75	1.60	1.76	1.78	1.78	1.77	1.78	1.83	1.53
Tb	0.27	0.27	0.27	0.28	0.29	0.28	0.28	0.28	0.24
Dy	1.82	1.84	1.89	1.90	2.01	1.99	1.85	1.91	1.62
Y	10.93	10.87	11.43	11.54	11.84	11.34	11.12	11.92	8.69
Ho	0.39	0.38	0.40	0.40	0.42	0.41	0.42	0.40	0.32
Er	1.16	1.14	1.22	1.23	1.20	1.24	1.24	1.18	0.95
Yb	1.29	1.34	1.36	1.35	1.42	1.42	1.35	1.36	1.07
Lu	0.19	0.20	0.21	0.21	0.23	0.22	0.22	0.22	0.17
Sc	11.23	10.93	12.19	11.55	12.93	13.07	12.74	12.20	16.31
Cr	49.29	40.95	74.43	49.15	65.53	89.90	108.14	129.99	200.72
Tl	0.03	0.05	0.10	0.02	0.12	0.00	0.02	0.06	0.00
Pb	6.10	6.36	6.08	7.14	4.28	0.99	3.57	53.67	1.37
Bi	0.01	0.03	0.04	-0.01	0.03	0.19	0.01	0.03	0.00
V	101.44	94.06	110.19	94.47	111.92	92.63	100.16	110.37	107.85
Cu	20.14	16.86	17.69	15.89	21.54	8.53	15.85	13.27	12.99
Zn	61.30	60.00	57.86	65.84	53.96	16.14	35.08	48.92	15.17
Ga	22.81	22.22	22.98	21.25	16.08	15.88	14.03	17.09	14.17
As	3.02	2.94	2.84	3.85	5.02	0.46	3.99	0.00	1.10
Mo	1.58	1.56	1.25	1.05	1.46	2.23	2.17	2.40	2.27
W	0.37	0.39	0.40	0.41	0.43	0.40	0.75	0.77	0.37

	APPENDIX 3-2								
	Major and trace element compositions of whole-rock samples								
	Magerang-Imang Prospect								
	10	11	12	13	14	15	16	17	18
Location	Magerang	Imang	Imang	Imang	Imang	Imang	Imang	Imang	Imang
	S. Taliyuda	EdI2-66.5m	EdI2-92.5m	EdI2-41m	EdI4-47m	EdI2-56m	EdI2-96m	EdI3-65m	EdI4-15m
Rock Type	andesite	andesite	andesite	andesite	andesite	andesite	andesite	andesite	andesite
Alteration	least altered	least altered	least altered	least altered	least altered	least altered	least altered	least altered	least altered
Sample No.	123227	1127	1128	1130	1155	123102	123104	123107	123108
Major elements									
SiO2	59.76	57.55	56.80	56.83	58.13	60.55	57.15	58.20	56.07
TiO2	0.49	0.50	0.54	0.52	0.53	0.46	0.53	0.53	0.56
Al2O3	16.03	15.79	15.76	15.54	16.28	16.28	15.83	15.96	15.46
Fe2O3	6.37	7.07	7.22	7.29	7.46	6.12	7.16	6.73	7.75
MnO	0.11	0.12	0.12	0.16	0.19	0.13	0.11	0.14	0.23
MgO	5.88	7.59	8.07	6.75	6.28	5.68	7.71	6.28	7.07
CaO	7.49	7.81	8.14	9.62	8.40	5.09	8.08	9.08	10.33
Na2O	2.98	2.82	2.70	2.36	2.06	4.36	2.73	2.42	1.79
K2O	0.79	0.66	0.56	0.84	0.58	1.23	0.61	0.58	0.66
P2O5	0.10	0.09	0.09	0.09	0.09	0.10	0.08	0.09	0.08
Na2O + K2O	3.77	15.40	16.21	16.36	14.68	5.59	3.34	2.99	2.45
Trace elements									
Cs	0.42	0.56	1.14	2.26	2.05	1.44	0.62	1.61	3.65
Rb	12.37	16.16	13.70	20.04	14.77	30.34	10.68	14.50	19.12
Ba	171.45	151.99	138.42	192.68	174.90	243.71	147.36	146.14	139.54
Th	1.78	1.51	1.43	1.37	1.51	1.81	1.50	1.53	1.42
U	0.55	0.48	0.42	0.42	0.44	0.54	0.45	0.47	0.45
Nb	0.87	1.07	0.99	0.92	0.98	1.05	0.69	1.09	0.89
Ta	0.08	0.09	0.08	0.07	0.07	0.10	0.06	0.07	0.09
La	6.12	5.41	5.06	4.96	5.33	6.07	5.31	5.33	5.19
Ce	12.93	11.88	11.26	10.81	11.75	12.94	11.61	12.01	11.32
Pr	1.58	1.46	1.42	1.33	1.41	1.59	1.44	1.44	1.37
Sr	282.68	304.83	306.32	241.22	267.25	329.20	308.84	259.44	196.52
Nd	6.69	6.42	6.31	6.23	6.27	6.77	6.41	6.32	6.19
Sm	1.65	1.63	1.65	1.48	1.58	1.69	1.78	1.45	1.69
Zr	71.28	63.12	58.18	67.82	59.35	68.29	61.01	65.43	57.89
Hf	1.82	1.69	1.61	1.80	1.56	1.91	1.62	1.60	1.70
Eu	0.57	0.56	0.58	0.54	0.56	0.60	0.54	0.56	0.54
Gd	1.74	1.86	1.90	1.76	1.67	1.81	1.84	1.79	1.88
Tb	0.28	0.29	0.30	0.29	0.28	0.29	0.31	0.29	0.30
Dy	1.97	2.02	2.05	1.97	1.97	2.02	2.18	2.09	2.20
Y	11.40	11.49	11.75	11.24	11.82	11.11	11.75	11.60	12.07
Ho	0.41	0.43	0.43	0.41	0.43	0.43	0.46	0.41	0.44
Er	1.25	1.27	1.33	1.21	1.29	1.27	1.36	1.34	1.34
Yb	1.37	1.43	1.40	1.31	1.35	1.41	1.44	1.41	1.45
Lu	0.21	0.20	0.21	0.21	0.21	0.21	0.22	0.20	0.20
Sc	19.19	22.38	24.00	22.84	22.48	19.00	24.02	23.72	23.29
Cr	259.94	441.21	493.39	476.78	438.74	267.74	369.45	432.38	526.63
Tl	0.00	0.04	0.03	0.05	0.03	0.08	0.00	0.02	0.03
Pb	0.36	4.33	3.73	6.01	4.56	5.50	0.23	207.78	111.83
Bi	0.31	-0.01	-0.01	0.04	0.01	0.03	0.00	0.05	0.02
V	108.28	160.55	166.33	155.92	160.56	133.06	114.59	155.07	161.70
Cu	10.50	29.42	33.10	41.25	44.26	13.47	12.21	34.56	26.76
Zn	5.15	53.91	57.33	56.71	51.18	54.20	4.89	55.94	51.93
Ga	12.69	18.77	17.50	18.31	18.66	14.67	9.47	12.72	13.63
As	0.26	0.83	1.64	1.06	0.84	8.50	0.14	9.39	0.00
Mo	1.90	1.16	1.00	1.02	1.18	1.40	2.03	2.66	2.14
W	0.35	0.37	0.28	0.35	0.34	0.55	0.27	0.70	0.52

	APPENDIX 3-2								
	Major and trace element compositions of whole-rock samples								
	Magerang-Imang Prospect								
	19	20	21	22	23	24	25	26	27
Location	Imang	Magerang	Magerang	Magerang	Magerang	Magerang	Magerang	Magerang	Magerang
	EdI4-36m	DDM1-75m	DDM5-312m	DDM7-67m	DDM7-82m	DDM7-138m	DDM7-138m	DSD1-78m	DSD1-206m
Rock Type	andesite	andesite	andesite	andesite	andesite	andesite	andesite	andesite	andesite
Alteration	least altered	propylitic	propylitic	propylitic	propylitic	propylitic	propylitic	propylitic	propylitic
Sample No.	123109	123124	123147	123151	123152	123153	123154	123172	123176
Major elements									
SiO2	56.78	75.38	63.08	58.89	57.60	64.19	59.43	66.09	59.63
TiO2	0.55	0.67	0.49	0.78	0.80	0.53	0.80	0.47	0.63
Al2O3	15.94	19.73	17.23	18.40	18.39	17.73	18.71	17.61	17.01
Fe2O3	7.77	3.86	5.99	7.35	8.18	5.26	7.24	5.11	6.84
MnO	0.16	0.00	0.18	0.17	0.20	0.13	0.21	0.12	0.09
MgO	6.55	0.03	3.51	5.51	5.67	3.06	5.84	3.11	4.77
CaO	9.20	0.07	6.31	6.13	6.65	5.32	5.34	4.32	7.71
Na2O	2.31	0.14	2.96	2.55	2.29	3.37	1.71	2.63	3.08
K2O	0.64	0.08	0.14	0.10	0.09	0.28	0.58	0.46	0.12
P2O5	0.09	0.04	0.12	0.12	0.12	0.13	0.13	0.10	0.12
Na2O + K2O	2.96	0.22	3.10	2.65	2.39	3.65	2.29	3.09	3.20
Trace elements									
Cs	0.86	1.20	5.54	15.65	15.40	4.82	15.80	2.04	0.62
Rb	10.26	2.34	4.87	5.82	5.39	6.59	23.21	12.48	0.99
Ba	151.36	8.23	65.64	49.94	38.71	75.29	47.94	88.20	106.02
Th	1.49	3.30	2.13	2.55	2.57	2.83	2.60	2.02	2.24
U	0.45	0.77	0.64	0.62	0.64	0.70	0.63	0.62	0.64
Nb	0.59	2.19	1.06	2.20	2.30	2.39	2.10	1.09	1.43
Ta	0.06	0.18	0.09	0.18	0.19	0.19	0.19	0.08	0.11
La	5.10	9.99	6.82	7.61	8.35	9.65	7.95	6.08	7.58
Ce	11.25	20.63	14.29	18.39	19.31	20.93	18.79	12.44	16.69
Pr	1.39	2.34	1.72	2.45	2.62	2.50	2.45	1.38	2.07
Sr	242.86	139.90	362.50	300.03	274.43	294.14	196.31	247.84	345.81
Nd	6.16	9.54	7.21	10.96	12.09	10.49	11.33	5.75	9.06
Sm	1.56	2.24	1.71	2.91	3.07	2.34	3.04	1.42	2.12
Zr	58.50	107.44	84.08	83.08	84.73	107.57	82.43	70.06	76.95
Hf	1.56	2.84	2.13	2.77	2.83	2.71	2.95	1.71	2.01
Eu	0.55	0.74	0.64	0.88	1.01	0.78	1.10	0.46	0.70
Gd	1.78	2.54	1.80	2.95	3.27	2.49	3.38	1.33	2.29
Tb	0.29	0.40	0.28	0.48	0.51	0.39	0.52	0.20	0.37
Dy	1.99	2.87	1.98	3.43	3.78	2.67	3.61	1.32	2.57
Y	11.25	15.44	11.19	16.13	17.53	15.82	15.85	8.32	14.24
Ho	0.42	0.54	0.40	0.72	0.77	0.56	0.81	0.30	0.53
Er	1.24	1.67	1.22	2.14	2.31	1.63	2.28	0.83	1.50
Yb	1.35	1.71	1.36	2.39	2.57	1.87	2.51	1.00	1.68
Lu	0.20	0.26	0.21	0.36	0.41	0.29	0.37	0.15	0.25
Sc	23.09	10.12	15.38	27.34	31.32	10.98	26.03	12.92	22.32
Cr	294.40	54.40	62.99	161.16	169.03	40.71	179.11	72.62	128.43
Tl	0.00	0.01	0.00	0.00	0.00	0.00	0.04	0.07	0.00
Pb	0.11	159.84	6.30	80.36	228.75	5.98	98.19	131.23	4.66
Bi	0.00	0.44	0.01	0.12	0.05	0.15	0.66	0.05	0.02
V	97.31	120.88	101.25	178.24	179.23	84.58	169.38	119.74	154.25
Cu	6.42	14.06	5.88	5.28	167.71	9.74	7.94	6.78	16.13
Zn	2.87	9.39	30.11	75.79	198.67	54.55	133.38	49.30	30.45
Ga	9.00	14.38	12.93	18.48	17.76	16.55	17.86	15.16	16.03
As	0.22	14.71	0.39	3.83	18.83	1.84	14.81	2.67	0.47
Mo	1.63	43.90	2.20	0.72	1.49	2.31	2.02	1.24	2.55
W	0.24	3.23	0.27	0.58	0.80	0.36	0.42	0.81	0.40

	APPENDIX 3-2								
	Major and trace element compositions of whole-rock samples								
	Magerang-Imang Prospect								
	28	29	30	31	32	33	34	35	36
Location	Magerang	Imang	Imang	Imang	Magerang	Magerang	Magerang	Magerang	Magerang
	DSD1-245m	EdI2-46m	EdI4-26m	EdI2-36m	DDM1-28m	DDM2-49m	DDM3-86m	DDM3-117m	DDM3-172m
Rock Type	andesite	andesite	andesite	andesite	andesite	andesite	andesite	andesite	andesite
Alteration	propylitic	propylitic	propylitic	propylitic	phyllic S2	phyllic S2	phyllic S2	phyllic S2	phyllic S2
Sample No.	123178	1126	1129	123101	123122	123132(*)	123137	123138(*)	123140
Major elements									
SiO2	64.10	57.55	55.76	63.44	73.41	69.49	68.79	72.76	67.76
TiO2	0.47	0.58	0.59	0.56	0.65	0.54	0.76	0.73	0.90
Al2O3	16.90	16.04	15.50	16.83	17.26	19.89	19.55	20.01	21.19
Fe2O3	5.92	7.23	8.42	5.33	3.63	5.42	5.64	2.19	5.27
MnO	0.11	0.16	0.20	0.13	0.07		0.10		0.05
MgO	3.18	7.37	9.98	2.78	2.06	1.07	1.51	0.99	1.20
CaO	5.68	6.38	6.84	6.49	0.24	0.19	0.61	0.36	0.71
Na2O	3.39	3.98	1.69	2.54	0.90	0.20	0.94	0.75	1.28
K2O	0.15	0.62	0.93	1.79	1.70	3.85	1.95	2.46	1.47
P2O5	0.10	0.10	0.09	0.11	0.07		0.16		0.16
Na2O + K2O	3.53	13.75	16.82	4.33	2.60	4.05	2.90	3.21	2.76
Trace elements									
Cs	1.60	0.89	4.43	6.07	8.14	4.75	10.80	13.06	10.00
Rb	3.56	15.32	32.30	54.40	63.02	123.18	63.73	73.87	55.68
Ba	39.31	177.41	145.39	111.30	164.04	402.37	201.61	235.71	135.87
Th	2.15	1.68	1.20	3.43	3.61	2.22	2.43	2.73	2.47
U	0.67	0.49	0.36	0.80	0.82	0.71	0.69	0.78	0.89
Nb	1.46	1.13	0.88	2.44	3.21	1.29	2.42	2.64	2.18
Ta	0.11	0.09	0.07	0.20	0.25	0.11	0.17	0.20	0.16
La	8.10	5.83	4.54	9.53	9.68	5.36	7.71	7.86	8.56
Ce	16.60	12.74	10.08	20.20	21.50	11.20	17.12	17.85	19.04
Pr	1.92	1.58	1.28	2.44	2.63	1.28	2.15	2.11	2.43
Sr	286.10	278.88	146.73	203.89	103.65	70.41	122.61	79.99	164.33
Nd	7.78	6.91	5.82	10.05	11.18	5.33	9.07	9.13	11.10
Sm	1.74	1.68	1.60	2.26	2.52	1.43	2.06	2.16	2.66
Zr	68.60	66.92	51.78	107.77	121.50	84.52	108.37	113.89	97.22
Hf	1.89	1.75	1.42	3.39	3.15	2.09	2.74	2.86	2.76
Eu	0.55	0.56	0.49	0.71	0.74	0.50	0.72	0.74	0.89
Gd	1.81	1.83	1.81	2.55	2.48	1.60	2.32	2.61	3.22
Tb	0.28	0.31	0.29	0.40	0.39	0.33	0.41	0.40	0.53
Dy	1.84	2.18	2.07	2.71	2.70	2.39	2.80	2.80	3.75
Y	11.23	12.28	11.47	15.13	15.58	17.05	16.71	16.33	19.54
Ho	0.39	0.44	0.41	0.56	0.59	0.58	0.58	0.57	0.80
Er	1.22	1.22	1.22	1.73	1.74	1.69	1.77	1.60	2.29
Yb	1.33	1.39	1.37	1.88	1.86	1.85	1.88	1.95	2.46
Lu	0.20	0.21	0.19	0.30	0.28	0.29	0.30	0.31	0.37
Sc	16.27	22.50	25.26	11.80	13.57	15.43	15.52	15.66	16.83
Cr	39.93	435.39	565.25	32.14	47.57	78.82	37.13	36.22	41.79
Tl	0.01	0.03	0.13	0.09	0.37	0.82	0.37	0.58	0.39
Pb	7.53	6.60	5.14	7.98	61.62	65.50	33.06	17.16	10.12
Bi	0.08	0.08	0.02	0.01	0.15	1.86	0.05	0.09	0.65
V	137.83	160.65	172.45	96.34	97.34	145.72	124.67	120.29	137.41
Cu	75.06	43.30	32.86	18.16	438.94	258.45	227.27	102.98	727.14
Zn	53.50	59.86	61.97	62.45	102.09	41.34	122.54	59.78	78.93
Ga	14.97	19.30	16.78	14.09	15.53	19.00	19.52	10.60	20.51
As	5.03	2.48	0.54	5.17	0.16	5.42	9.45	6.88	0.00
Mo	1.30	1.25	0.83	0.75	56.31	1.37	39.10	6.89	9.35
W	0.65	0.35	0.25	0.67	5.04	0.63	3.59	17.65	2.26

	APPENDIX 3-2					
	Major and trace element compositions of whole-rock samples					
	Magerang-Imang Prospect					
	37	38	39	40	41	42
Location	Magerang	Magerang	Magerang	Magerang	Magerang	Magerang
	DDM5-339m	DDM3-236m	DDM3-300m	DSD1-51m	DDM3-389m	DDM2-33m
Rock Type	andesite	andesite	andesite	andesite	andesite	andesite
Alteration	phyllic S2	phyllic S2	phyllic S2	phyllic S2	phyllic S2	adv.argillic
Sample No.	123148	123164(*)	123167	123171	123170	123131
Major elements						
SiO2	65.59	71.76	57.78	65.59	64.91	70.83
TiO2	0.52	0.65	0.94	0.46	0.56	0.52
Al2O3	18.10	17.65	19.74	16.06	15.67	20.77
Fe2O3	5.74	6.31	10.05	4.64	7.31	4.90
MnO	0.19		0.11	0.24	0.02	0.02
MgO	6.11	0.86	5.34	3.72	2.08	1.10
CaO	0.43	0.67	3.12	4.94	6.80	0.08
Na2O	0.26	0.45	2.32	3.40	1.14	0.10
K2O	2.91	2.32	0.45	0.85	1.44	1.65
P2O5	0.14		0.15	0.09	0.08	0.03
Na2O + K2O	3.17	2.77	2.77	4.25	2.58	1.75
Trace elements						
Cs	6.69	10.89	8.32	1.62		4.87
Rb	80.31	88.60	17.89	23.33		70.77
Ba	594.08	172.00	2307.83	121.95		166.43
Th	2.17	3.08	2.00	2.11		2.24
U	0.69	0.84	0.48	0.63		0.70
Nb	1.47	2.99	1.96	1.35		1.31
Ta	0.10	0.18	0.14	0.11		0.11
La	6.12	9.38	7.08	6.44		6.24
Ce	12.86	20.39	16.83	13.38		13.65
Pr	1.49	2.27	2.18	1.56		1.63
Sr	31.65	74.10	253.70	176.59		17.81
Nd	6.10	9.57	9.87	6.57		6.95
Sm	1.32	2.33	2.56	1.49		1.77
Zr	81.20	103.01	84.71	66.63		82.09
Hf	2.06	2.66	2.27	1.79		2.12
Eu	0.29	0.62	0.86	0.51		0.63
Gd	1.35	2.21	2.78	1.56		2.04
Tb	0.24	0.35	0.42	0.25		0.35
Dy	1.66	2.21	3.11	1.71		2.49
Y	8.75	12.87	16.76	9.94		14.13
Ho	0.34	0.50	0.63	0.37		0.51
Er	1.00	1.52	1.80	1.08		1.56
Yb	1.26	1.57	1.99	1.21		1.59
Lu	0.20	0.24	0.30	0.18		0.24
Sc	15.62	17.05	20.08	14.59		21.91
Cr	78.62	122.47	41.49	67.95		63.54
Tl	0.87	0.50	0.09	0.12		0.82
Pb	114.06	59.19	142.52	14.73		58.74
Bi	0.32	0.41	0.46	0.44		3.93
V	126.77	118.99	155.16	116.51		62.87
Cu	6.50	1259.58	99.21	414.43		642.05
Zn	165.60	40.79	82.13	131.45		31.77
Ga	18.06	14.93	18.35	13.17		16.31
As	7.91	0.37	5.57	11.00		11.28
Mo	1.41	30.46	1.00	5.35		1.02
W	1.13	2.58	0.82	0.67		0.45

	APPENDIX 3-3								
	Major and trace element compositions of whole-rock samples								
	Kelian mine								
	1	2	3	4	5	6	7	8	9
Location	Tepu	Tepu	Tepu	East Pramp Pit	West Pramp Pi	East Pramp Pit	West Pramp Pi	West Pramp Pi	West Pramp Pit
	KFD1-415m	KFD1-452m	K418-27.5m	K782-357m	Central And.	East And.	Central And	Central And	Central And
Rock Type	andesite	andesite	andesite	andesite	andesite	andesite	andesite	andesite	andesite
Alteration	least altered	least altered	least altered	propylitic	propylitic	propylitic	propylitic	propylitic	propylitic
Sample No.	1132	1134	1143	123197	123200	123201	123209	123210	123212
Major elements	(normalised 100 wt%) analysed by XRF, except (*) analysed by Electron Microprobe (EDS)								
SiO2	57.62	57.48	59.00	57.78	59.73	57.66	59.12	59.03	58.51
TiO2	0.59	0.59	0.57	0.54	0.52	0.60	0.53	0.54	0.56
Al2O3	18.08	18.10	18.10	18.08	17.51	18.29	17.77	17.75	18.41
Fe2O3	7.56	7.50	7.34	7.01	6.92	7.87	7.01	7.07	7.50
MnO	0.17	0.18	0.16	0.62	0.25	0.18	0.23	0.21	0.45
MgO	3.41	3.47	3.08	2.80	3.57	3.49	3.78	3.19	3.78
CaO	7.75	7.48	7.66	9.46	7.19	7.82	7.75	8.01	7.10
Na2O	3.94	4.23	3.39	2.62	2.09	3.25	2.08	3.03	1.92
K2O	0.80	0.87	0.60	1.00	2.10	0.73	1.63	1.06	1.66
P2O5	0.09	0.10	0.10	0.10	0.12	0.11	0.11	0.11	0.11
Na2O + K2O	4.74	5.10	3.99	3.62	4.20	3.98	3.71	4.09	3.58
Trace elements	(in ppm) analysed by Laser Ablation ICPMS								
Cs	5.89	3.41	1.52	4.79	2.89	1.71	4.27	4.48	4.86
Rb	20.78	19.69	13.11	21.98	31.90	9.98	25.82	24.91	40.92
Ba	209.05	259.72	204.92	132.27	236.30	208.59	152.44	164.10	177.28
Th	1.48	1.54	1.62	1.65	1.37	1.61	1.34	1.40	1.36
U	0.41	0.41	0.51	0.49	0.41	0.52	0.41	0.43	0.42
Nb	1.12	1.11	1.26	1.19	0.85	0.87	0.88	1.10	1.09
Ta	0.06	0.07	0.09	0.08	0.06	0.06	0.06	0.08	0.07
La	6.75	6.29	6.75	6.77	5.90	6.31	5.48	6.13	5.72
Ce	13.99	13.55	14.38	14.55	13.05	13.63	12.21	13.22	12.82
Pr	1.75	1.73	1.79	1.79	1.62	1.71	1.52	1.69	1.62
Sr	331.85	309.64	348.43	325.05	259.96	318.64	256.72	411.60	200.16
Nd	7.89	7.72	7.84	7.84	7.26	7.59	6.62	7.57	7.30
Sm	2.03	1.91	1.94	1.90	1.82	1.90	1.57	1.96	1.89
Zr	54.45	53.88	63.73	59.19	49.43	55.33	58.81	66.65	51.67
Hf	1.55	1.48	1.78	1.70	1.44	1.58	1.60	1.60	1.50
Eu	0.70	0.64	0.63	0.67	0.62	0.71	0.56	0.67	0.62
Gd	2.26	2.05	1.92	2.11	2.00	2.20	1.67	2.12	2.02
Tb	0.36	0.33	0.33	0.34	0.33	0.36	0.26	0.35	0.32
Dy	2.63	2.45	2.35	2.43	2.33	2.54	1.82	2.42	2.40
Y	15.30	14.07	13.54	13.70	13.37	14.56	10.03	13.63	13.84
Ho	0.53	0.50	0.51	0.51	0.49	0.55	0.38	0.50	0.50
Er	1.60	1.50	1.49	1.55	1.51	1.62	1.16	1.53	1.54
Yb	1.73	1.69	1.67	1.70	1.70	1.77	1.34	1.71	1.71
Lu	0.30	0.26	0.26	0.26	0.26	0.27	0.22	0.28	0.26
Sc	19.26	19.61	17.09	16.17	20.58	20.29	21.54	21.83	23.68
Cr	16.81	15.92	17.23	19.92	54.89	20.93	67.98	54.88	51.49
Tl	0.05	0.02	0.02	0.03	0.01	0.00	0.01	0.07	0.08
Pb	5.65	6.40	5.80	21.55	0.24	0.33	1.11	12.57	6.62
Bi	0.01	0.00	-0.02	0.08	0.00	0.00	0.00	0.02	0.09
V	183.23	188.22	170.82	150.77	128.60	144.05	138.60	178.64	186.23
Cu	4.05	4.20	19.22	6.96	8.77	7.40	14.05	34.40	60.72
Zn	59.91	79.02	65.24	50.46	7.01	8.65	20.13	51.09	80.55
Ga	20.63	21.79	20.85	14.89	15.28	15.32	14.31	26.80	15.62
As	0.71	0.28	0.75	8.57	0.13	0.13	0.68	1.87	2.23
Mo	0.66	0.62	0.59	0.78	1.18	1.58	2.14	0.67	0.90
W	0.26	0.27	0.24	0.76	0.28	0.28	0.59	0.45	0.89

	APPENDIX 3-3							
	Major and trace element compositions of whole-rock samples							
	Kelian mine							
	10	11	12	13	14	15	16	17
Location	East Pramp Pit	East Pramp Pit	East Pramp Pit	East Pramp Pit	East Pramp Pit	East Pramp Pit	East Pramp Pit	East Pramp Pit
	Tepu And.	K782-434m	K782-527m	K626-302m	K610-155m	K636-131m	K625-240m	K782-48m
Rock Type	andesite	andesite	andesite	andesite	andesite	andesite	andesite	andesite
Alteration	propylitic	propylitic	propylitic	propylitic	propylitic	propylitic	propylitic	phyllic S2
Sample No.	123228	123362	123365	123427	123476	123509	123532	123188
Major elements								
SiO2	60.36	60.56	58.64	59.48	58.36	58.86	58.43	59.51
TiO2	0.55	0.51	0.56	0.56	0.61	0.61	0.57	0.55
Al2O3	18.65	17.66	18.34	17.83	18.44	17.86	18.38	17.49
Fe2O3	6.41	7.55	7.60	7.43	7.79	8.69	7.08	7.00
MnO	0.14	0.36	0.25	0.58	0.53	0.18	0.31	0.74
MgO	2.15	3.43	3.22	3.36	3.35	3.08	2.38	2.87
CaO	7.37	6.32	7.68	6.14	7.53	5.54	8.26	7.42
Na2O	3.64	2.33	3.34	0.53	2.85	2.51	1.76	0.09
K2O	0.60	1.18	0.28	3.98	0.42	2.56	2.72	4.23
P2O5	0.12	0.11	0.10	0.10	0.11	0.10	0.10	0.09
Na2O + K2O	4.24	3.51	3.62	4.51	3.27	5.07	4.48	4.32
Trace elements								
Cs	4.22	1.98	1.27	3.58	2.07	2.85	3.43	2.72
Rb	9.93	17.66	3.83	25.80	6.32	29.06	52.75	72.07
Ba	240.79	218.56	124.17	356.76	108.97	282.34	198.19	289.13
Th	1.84	1.41	1.78	1.54	1.68	1.78	1.48	1.87
U	0.54	0.43	0.57	0.46	0.51	0.46	0.43	0.50
Nb	1.12	1.10	1.12	1.30	1.12	1.47	0.96	1.57
Ta	0.08	0.07	0.08	0.08	0.08	0.10	0.08	0.10
La	7.29	5.91	6.91	8.83	6.49	7.30	6.00	6.87
Ce	15.74	13.04	14.89	17.54	14.18	15.65	12.92	14.75
Pr	1.93	1.62	1.83	2.13	1.77	1.93	1.63	1.80
Sr	384.53	290.67	316.46	332.70	326.60	355.94	205.34	107.87
Nd	8.21	7.21	8.08	9.32	7.80	8.73	7.45	7.81
Sm	2.01	1.73	1.97	2.11	1.99	1.99	1.86	1.90
Zr	67.25	55.43	58.53	82.75	58.17	85.33	53.15	59.70
Hf	1.84	1.54	1.67	1.56	1.66	1.63	1.49	1.63
Eu	0.72	0.62	0.67	0.79	0.68	0.66	0.59	0.63
Gd	2.15	1.90	2.18	2.54	2.22	2.27	2.01	2.02
Tb	0.34	0.31	0.36	0.41	0.36	0.37	0.33	0.32
Dy	2.39	2.15	2.54	2.80	2.61	2.40	2.31	2.29
Y	13.39	12.78	14.69	11.43	14.68	11.84	14.14	13.31
Ho	0.51	0.46	0.54	0.59	0.55	0.52	0.51	0.49
Er	1.51	1.41	1.61	1.78	1.68	1.51	1.54	1.46
Yb	1.76	1.59	1.77	1.84	1.81	1.74	1.65	1.60
Lu	0.27	0.25	0.27	0.28	0.28	0.26	0.25	0.25
Sc	16.05	19.74	18.48	14.20	20.52	12.93	17.94	15.82
Cr	19.73	53.40	24.48	91.71	25.28	65.53	32.07	20.45
Tl	0.00	0.05	0.00	0.06	0.00	0.12	0.05	0.09
Pb	0.32	180.37	3.83	3.73	5.04	4.28	72.62	27.07
Bi	0.00	0.37	0.00	0.02	0.00	0.03	0.01	0.01
V	122.69	156.08	157.55	108.30	174.75	111.92	167.29	148.32
Cu	7.89	68.83	13.85	16.15	13.63	21.54	8.10	10.12
Zn	8.95	1619.70	29.56	42.15	56.42	53.96	47.80	126.34
Ga	15.25	15.55	16.91	14.91	16.46	16.08	15.11	14.27
As	0.15	9.84	0.57	3.88	1.73	5.02	1.57	16.68
Mo	1.58	1.09	2.27	2.04	1.74	1.46	2.16	0.82
W	0.25	0.67	0.52	0.58	0.97	0.43	0.43	1.02

	APPENDIX 3-3							
	Major and trace element compositions of whole-rock samples							
	Kelian mine							
	18	19	20	21	22	23	24	25
Location	East Pramp Pit	West Pramp Pit	West Pramp Pit	East Pramp Pit	East Pramp Pit	East Pramp Pit	East Pramp Pit	East Pramp Pit
	K782-153m	Central And.	Central And	K621-155m	K621-178m	K637-148m	K686-74m	K633-277m
Rock Type	andesite	andesite	andesite	andesite	andesite	andesite	andesite	andesite
Alteration	phyllic S2	phyllic S2	phyllic S2	phyllic S2	phyllic S2	phyllic S2	phyllic S2	phyllic S2
Sample No.	123191	123206	123207	123418(*)	123419	123485	123492(*)	123501
Major elements								
SiO2	58.19	71.84	60.90	56.93	54.80	65.20	69.17	48.21
TiO2	0.58	0.63	0.51	0.60	0.48	0.53	0.49	0.34
Al2O3	18.02	21.96	18.18	18.34	17.21	17.12	17.03	10.40
Fe2O3	7.68	2.52	6.62	10.53	16.34	8.47	6.87	24.56
MnO	0.67	0.18	0.82	0.96	1.01	0.40		0.18
MgO	3.00	0.24	2.96	1.74	2.35	1.46	0.88	0.63
CaO	6.84	0.38	5.43	6.10	3.00	1.70	0.50	12.38
Na2O	0.09	0.11	0.09	1.29	0.06	0.06	0.53	0.12
K2O	4.80	1.97	4.39	4.58	4.65	4.96	5.24	3.12
P2O5	0.11	0.17	0.10		0.09	0.09		0.05
Na2O + K2O	4.90	2.08	4.47	5.87	4.71	5.02	5.77	3.24
Trace elements								
Cs	3.27	3.65	1.75	3.05	2.92	6.26	2.81	0.57
Rb	84.53	41.14	60.20	66.94	72.92	91.25	93.67	42.29
Ba	202.07	188.82	238.12	420.98	227.57	317.15	207.55	256.94
Th	1.51	1.70	1.30	1.58	1.49	1.44	2.71	0.82
U	0.45	0.52	0.41	0.48	0.46	0.44	0.77	0.27
Nb	1.15	1.34	0.90	1.24	1.14	0.94	2.76	0.58
Ta	0.08	0.09	0.06	0.08	0.07	0.07	0.18	0.04
La	6.17	6.07	5.27	7.34	7.46	4.62	4.20	3.99
Ce	13.39	13.69	11.63	15.36	15.02	10.55	9.59	8.68
Pr	1.66	1.71	1.44	1.87	1.77	1.33	1.12	1.15
Sr	84.62	18.80	60.66	70.23	54.62	27.82	15.83	59.79
Nd	7.32	7.56	6.40	8.05	7.30	5.86	4.58	4.81
Sm	1.84	1.85	1.56	1.93	1.72	1.45	1.03	1.27
Zr	52.79	64.06	47.29	55.48	48.54	49.92	70.70	29.38
Hf	1.50	1.81	1.37	1.59	1.38	1.47	1.92	0.79
Eu	0.61	0.63	0.46	0.63	0.64	0.36	0.24	0.48
Gd	2.06	2.15	1.78	2.00	1.81	1.69	1.22	1.51
Tb	0.32	0.36	0.29	0.34	0.26	0.28	0.20	0.23
Dy	2.32	2.62	2.04	2.34	1.97	2.12	1.53	1.57
Y	13.52	15.84	11.93	13.78	10.73	10.92	9.93	10.07
Ho	0.50	0.55	0.44	0.50	0.40	0.44	0.36	0.34
Er	1.44	1.68	1.32	1.52	1.23	1.36	1.09	1.00
Yb	1.65	1.87	1.52	1.68	1.36	1.51	1.35	1.05
Lu	0.26	0.28	0.24	0.27	0.21	0.22	0.21	0.16
Sc	16.51	19.36	21.06	15.26	12.76	18.55	17.04	11.77
Cr	22.09	66.95	56.66	25.63	23.08	16.92	26.27	45.68
Tl	0.10	0.08	0.01	0.15	0.09	0.28	0.12	0.05
Pb	12.40	4.74	2.31	1350.29	3603.24	4767.63	12091.37	18.19
Bi	0.01	0.02	0.00	3.38	0.22	0.38	2.01	0.20
V	164.04	210.23	151.35	150.40	117.53	162.95	136.24	110.22
Cu	1.66	26.62	15.85	44.07	128.83	18.79	95.90	37.31
Zn	32.34	32.38	25.97	10667.24	3911.32	2678.72	7219.99	70.52
Ga	14.59	21.69	16.39	17.69	14.14	15.03	16.83	9.12
As	34.07	3.67	3.16	62.63	112.08	32.13	24.45	435.34
Mo	0.78	1.64	1.91	1.35	1.54	1.47	1.21	3.07
W	1.26	2.73	1.10	1.20	1.50	2.25	3.33	1.56

	APPENDIX 3-3							
	Major and trace element compositions of whole-rock samples							
	Kelian mine							
	26	27	28	29	30	31	32	33
Location	East Pramp Pit	East Pramp Pit	East Pramp Pit	East Pramp Pit	East Pramp Pit	East Pramp Pit	East Pramp Pit	And 393 Zone
	K622-174m	K782-182m	K629-199m	K629-319m	K629-337m	K629-397m	K708-360m	K609-228m
Rock Type	andesite	Hydroth. Breccia	andesite	Hydroth. Breccia	Hydroth. Breccia	andesite	andesite	andesite
Alteration	phyllic S2	phyllic S3	phyllic S3	phyllic S3	phyllic S3	phyllic S3	phyllic S3	phyllic S3
Sample No.	123524(*)	123193(*)	123432	123433	123434(*)	123436	123437(*)	123473
Major elements								
SiO2	59.69	76.98	59.45	71.09	67.79	57.71	40.35	27.68
TiO2	0.62	0.47	0.56	0.50	0.53	0.53	0.87	0.52
Al2O3	19.55	13.10	17.39	16.38	17.45	16.78	24.35	17.79
Fe2O3	6.76	4.76	9.30	5.34	5.99	11.30	11.66	39.90
MnO	0.25		0.55	0.13	0.12	0.78	1.50	1.34
MgO	2.95	0.58	3.14	0.94	1.36	3.06	5.66	3.99
CaO	6.19	0.22	2.91	0.27	1.17	5.11	10.26	3.87
Na2O	0.19	0.20	0.15	0.07	0.58	0.11	1.06	0.07
K2O	4.58	4.27	6.45	5.26	5.66	4.51	5.48	4.73
P2O5			0.10	0.02		0.10		0.11
Na2O + K2O	4.77	4.47	6.61	5.33	6.24	4.62	6.53	4.80
Trace elements								
Cs	4.63	3.25	4.34	7.53	4.49	1.42	2.60	
Rb	92.27	101.38	93.05	146.05	129.62	75.95	101.25	
Ba	284.69	312.77	773.93	422.41	385.25	240.79	362.83	
Th	1.55	7.43	1.40	12.68	10.17	1.21	2.45	
U	0.47	1.40	0.43	1.94	2.07	0.36	0.80	
Nb	1.18	6.95	1.01	10.64	9.64	0.98	1.79	
Ta	0.10	0.50	0.07	0.82	0.74	0.06	0.12	
La	5.81	26.92	5.28	31.04	27.99	3.89	7.11	
Ce	12.76	53.45	11.67	61.50	55.56	9.18	16.81	
Pr	1.64	5.69	1.48	6.59	6.25	1.25	2.37	
Sr	95.98	14.80	127.17	17.98	34.03	60.64	112.47	
Nd	7.26	22.30	6.48	24.82	24.48	5.90	10.93	
Sm	1.86	4.40	1.56	4.58	4.91	1.44	3.03	
Zr	56.87	123.66	47.95	165.15	211.89	47.83	85.71	
Hf	1.62	3.32	1.42	4.32	5.43	1.24	2.36	
Eu	0.42	1.06	0.46	0.90	1.02	0.80	0.87	
Gd	2.04	3.84	1.75	4.19	4.30	1.76	3.43	
Tb	0.36	0.59	0.28	0.61	0.67	0.29	0.57	
Dy	2.49	3.72	1.99	3.94	4.60	1.98	4.00	
Y	14.76	22.44	11.13	23.61	26.79	13.25	23.55	
Ho	0.51	0.80	0.43	0.81	0.94	0.43	0.87	
Er	1.56	2.35	1.29	2.39	2.74	1.29	2.44	
Yb	1.70	2.48	1.46	2.63	3.00	1.41	2.83	
Lu	0.26	0.38	0.23	0.41	0.47	0.23	0.43	
Sc	22.44	12.87	18.66	12.27	14.31	14.02	23.47	
Cr	27.65	58.38	12.21	39.21	54.98	11.35	29.81	
Tl	0.20	0.24	0.15	0.22	0.15	0.08	0.05	
Pb	20.10	102.48	498.45	136.35	656.44	8299.58	9357.26	
Bi	0.05	0.18	0.20	1.23	1.18	0.11	0.09	
V	195.64	58.44	151.00	74.41	72.50	149.32	217.19	
Cu	51.45	2.08	58.73	22.45	73.46	136.08	116.64	
Zn	82.58	16.43	3525.02	6059.70	4507.41	14459.25	11447.38	
Ga	15.99	12.78	15.76	24.39	22.36	16.19	26.38	
As	22.77	435.50	32.65	0.00	49.45	166.34	43.33	
Mo	1.08	1.18	3.41	1.40	1.16	5.25	1.79	
W	1.46	3.43	5.97	2.93	2.53	1.76	2.84	

	APPENDIX 3-3							
	Major and trace element compositions of whole-rock samples							
	Kelian mine							
	34	35	36	37	38	39	40	41
Location	East Pramp Pit	East Pramp Pit	East Pramp Pit	East Pramp Pit	East Pramp Pit	West Pramp Pit	West Pramp Pit	East Pramp Pit
	K637-275m	K681-239m	K681-308m	K681-15m	255 Zone	Central And.	Central And	K643-211m
Rock Type	andesite	andesite	tuff	Hydroth. Breccia	andesite	andesite	andesite	andesite
Alteration	phyllic S3	phyllic S3	phyllic S3	phyllic S3	argillic S4	argillic S4	argillic S4	argillic S4
Sample No.	123486	123487(*)	123489	123578(*)	123205	123213	123214	123511
Major elements								
SiO2	56.36	66.56	70.06	63.96	60.47	64.80	69.67	55.96
TiO2	0.53	0.48	0.47	0.48	0.61	0.51	0.47	0.58
Al2O3	16.61	16.66	14.32	16.29	19.07	16.68	15.69	18.02
Fe2O3	7.53	6.05	9.13	5.24	6.96	6.07	6.88	12.65
MnO	0.73	1.53	0.25	1.53	1.02	1.03	0.84	0.45
MgO	4.64	1.74	1.00	2.61	2.31	2.01	0.94	2.50
CaO	9.65	2.87	0.13	5.24	3.72	4.62	1.17	4.34
Na2O	0.39	0.35	0.07	0.17	0.10	0.31	0.25	0.18
K2O	3.47	5.17	4.55	5.11	5.63	3.87	3.99	5.22
P2O5	0.10		0.03		0.10	0.10	0.10	0.10
Na2O + K2O	3.85		4.62	5.28	5.73	4.18	4.24	5.39
Trace elements								
Cs	3.60	2.00	4.49	3.16	5.90	5.17	5.80	3.79
Rb	54.30	89.03	102.88	88.99	113.73	69.84	74.37	101.80
Ba	167.03	430.77	412.14	300.26	273.47	255.36	251.76	287.01
Th	1.38	1.61	9.49	5.44	1.60	1.26	1.14	2.25
U	0.40	0.50	1.67	1.07	0.47	0.39	0.36	0.64
Nb	1.02	1.43	8.99	4.18	1.09	1.01	0.93	1.97
Ta	0.07	0.08	0.65	0.32	0.08	0.07	0.07	0.13
La	5.54	5.59	29.30	16.33	5.47	4.96	4.94	7.10
Ce	11.75	12.81	59.56	33.81	12.21	11.12	11.01	15.01
Pr	1.50	1.70	6.59	3.88	1.55	1.43	1.40	1.79
Sr	138.03	111.82	42.45	55.47	52.66	71.15	26.22	69.19
Nd	6.60	7.68	25.52	15.28	7.08	6.30	6.25	7.61
Sm	1.74	1.97	5.06	3.15	1.87	1.57	1.52	1.96
Zr	47.82	63.43	178.74	90.43	55.82	51.41	42.33	68.82
Hf	1.38	1.70	4.78	2.54	1.62	1.44	1.22	1.69
Eu	0.53	0.60	0.71	0.74	0.48	0.46	0.41	0.64
Gd	1.96	2.43	4.37	2.86	1.98	1.78	1.59	2.33
Tb	0.32	0.37	0.65	0.44	0.32	0.29	0.27	0.38
Dy	2.22	2.64	4.37	2.83	2.14	2.12	1.86	2.79
Y	12.82	16.02	25.15	15.99	12.31	12.31	11.37	16.57
Ho	0.46	0.59	0.89	0.59	0.45	0.45	0.40	0.56
Er	1.43	1.71	2.63	1.71	1.35	1.37	1.17	1.61
Yb	1.53	1.92	2.86	1.88	1.59	1.54	1.36	1.75
Lu	0.24	0.28	0.42	0.29	0.24	0.24	0.22	0.25
Sc	16.19	22.98	11.42	12.19	19.56	19.52	18.04	16.54
Cr	29.32	18.45	42.60	36.37	13.39	42.64	49.28	22.68
Tl	0.04	0.10	0.16	0.14	0.23	0.12	0.19	0.14
Pb	17.23	104.92	145.70	76.78	11.51	207.37	94.01	178.37
Bi	0.09	0.30	3.65	0.09	0.10	0.01	0.03	0.83
V	141.50	228.19	48.27	97.84	174.90	149.76	142.10	178.27
Cu	1.91	68.86	179.36	2.99	5.73	4.75	0.63	4.29
Zn	69.80	6478.93	7861.10	26.79	53.46	136.17	27.34	2079.66
Ga	11.95	23.01	20.47	12.84	15.58	13.90	14.16	19.02
As	7.22	78.20	6.91	15.51	26.72	21.65	108.92	14.77
Mo	1.35	3.44	1.26	0.75	0.51	0.91	1.49	3.01
W	0.94	1.33	2.74	1.52	2.25	1.60	2.99	1.52

	APPENDIX 3-3							
	Major and trace element compositions of whole-rock samples							
	Kelian mine							
	42	43	44	45	46	47	48	49
Location	East Pramp Pit	East Pramp Pit	East Pramp Pit	East Pramp Pit	G. Runcing	G. Runcing	G. Runcing	S. Jiu
	K782-610m	K610-329m	K681-365mm	K634-80m	1110RL	1110RL	1120RL	K691-134m
Rock Type	tuff	tuff	tuff	tuff	rhyolite	rhyolite	rhyolite	rhyolite
Alteration	phyllic-S2	phyllic-S2	phyllic-S2	phyllic-S2	phyllic-S2	phyllic-S2	phyllic-S2	phyllic-S2
Sample No.	123367(*)	123475(*)	123490(*)	123502(*)	123218	123219(*)	123220	123493
Major elements								
SiO2	72.62	71.61	71.88	74.88	76.41	75.01	78.86	80.36
TiO2	0.31	0.45	0.38	0.53	0.20	0.20	0.20	0.09
Al2O3	12.75	16.60	13.05	15.48	13.49	13.00	13.22	13.92
Fe2O3	3.79	5.38	6.12	2.52	1.72	2.17	2.26	0.72
MnO	0.16				0.26	0.62	0.41	0.10
MgO	1.71	0.66	0.19	0.54	0.53	0.82	0.55	0.35
CaO	5.33	0.12	0.22	0.12	2.01	4.13	0.18	0.08
Na2O	0.29	0.37	0.63	0.25	3.33	0.19	0.06	0.12
K2O	3.43	5.36	8.17	5.96	1.96	4.18	4.16	4.20
P2O5					0.09		0.09	0.06
Na2O + K2O	3.72	5.73	8.80	6.20	5.29	4.37	4.23	4.32
Trace elements								
Cs	1.64	4.61	1.10	2.32	0.82	2.53	3.59	0.69
Rb	56.28	126.53	99.94	118.32	34.16	86.10	83.56	66.41
Ba	217.72	409.22	1361.56	530.21	215.30	177.33	283.48	364.19
Th	7.18	10.05	4.92	8.96	3.44	3.28	3.61	4.15
U	1.59	2.05	1.26	1.43	1.36	1.28	1.43	1.45
Nb	6.70	8.64	4.60	5.38	3.94	4.03	3.92	3.99
Ta	0.49	0.63	0.33	0.37	0.30	0.30	0.31	0.33
La	21.72	26.32	18.21	37.19	11.76	11.08	11.94	13.53
Ce	42.47	54.21	34.88	65.74	25.76	24.01	25.98	29.18
Pr	4.92	6.04	3.95	6.48	3.03	2.79	3.02	3.39
Sr	129.62	55.53	119.96	41.47	123.85	53.35	3.81	6.76
Nd	18.69	23.15	14.94	21.19	11.94	11.06	11.82	13.05
Sm	3.83	4.64	3.04	3.03	2.63	2.51	2.74	2.71
Zr	121.51	169.31	100.88	90.68	67.90	65.25	64.98	54.15
Hf	3.31	4.62	2.67	2.51	2.15	2.09	2.26	1.96
Eu	0.92	0.94	0.89	0.81	0.42	0.40	0.37	0.41
Gd	3.01	4.22	2.66	2.29	2.70	2.46	2.74	2.60
Tb	0.47	0.67	0.37	0.32	0.45	0.42	0.47	0.43
Dy	2.93	4.49	2.40	2.13	3.21	2.90	3.09	3.03
Y	17.20	25.49	14.01	11.75	21.13	19.51	20.37	20.95
Ho	0.64	0.87	0.48	0.42	0.67	0.61	0.70	0.65
Er	1.81	2.65	1.36	1.25	2.13	1.91	2.16	2.04
Yb	2.01	2.90	1.44	1.36	2.60	2.40	2.72	2.53
Lu	0.30	0.41	0.21	0.21	0.41	0.40	0.42	0.40
Sc	5.99	10.57	6.22	11.65	4.22	5.82	2.66	2.19
Cr	37.55	43.50	28.56	45.24	22.49	26.71	23.67	21.80
Tl	0.12	0.17	0.19	0.23	0.01	0.17	0.19	0.08
Pb	188.04	470.47	120.06	153.57	3.00	22.25	63.69	158.93
Bi	1.13	2.04	0.77	0.41	0.00	0.02	0.02	0.00
V	43.24	40.66	25.02	98.25	24.32	23.93	25.67	4.37
Cu	45.64	105.30	210.82	21.48	5.12	3.09	7.26	3.69
Zn	10.41	3590.61	5279.34	1833.49	27.38	50.91	105.08	180.09
Ga	14.49	19.23	11.17	15.29	15.39	12.23	13.00	17.65
As	59.59	38.54	0.00	0.00	4.42	136.56	723.55	5.53
Mo	1.61	0.54	0.86	1.32	1.40	0.23	2.57	1.53
W	1.63	2.69	1.50	4.84	0.41	0.62	0.80	0.74

	APPENDIX 3-3							
	Major and trace element compositions of whole-rock samples							
	Kelian mine							
	50	51	52	53	54	55	56	57
Location	East Pramp Pit	East Pramp Pit	East Pramp Pit	East Pramp Pit	East Pramp Pit	East Pramp Pit	G. Runcing	G. Runcing
	K610-373m	K634-181m	EP1090 RL	EP1090 RL	255 Zone	K610-352m	1090RL	K686-151m
Rock Type	tuff	tuff	tuff lapilli	tuff/ HB	tuff	tuff	mudstone/MB	muddy breccia
Alteration	phyllic-S3	phyllic-S3	argillic-S4	argillic-S4	argillic-S4	argillic-S4	phyllic-S2	phyllic-S2
Sample No.	123480(*)	123505	123203	123204(*)	123215(*)	123479	123236(*)	123583
Major elements								
SiO2	69.70	75.20	80.19	77.60	64.77	71.90	70.59	66.05
TiO2	0.49	0.28	0.30	0.59	0.64	0.25	0.80	0.60
Al2O3	17.02	12.15	12.30	14.25	18.94	16.64	16.42	15.23
Fe2O3	5.69	6.20	2.69	2.39	4.61	3.22	4.78	5.45
MnO		0.05	0.04	0.38	0.59	0.08		0.47
MgO	1.01	0.31	0.50	0.42	1.01	0.52	1.96	2.43
CaO	0.64	0.06	0.05	0.10	0.42	0.06	1.32	5.48
Na2O	0.48	0.13	0.05	0.22		0.15	0.83	0.08
K2O	5.51	5.61	3.86	4.31	9.50	7.17	3.79	4.12
P2O5		0.01	0.02			0.01		0.09
Na2O + K2O	5.99	5.74		4.53	9.50	7.32	4.62	4.20
Trace elements								
Cs	2.48	2.42	3.80	6.25	1.85	2.18	7.39	4.37
Rb	82.77	89.89	93.01	109.56	121.31	123.84	132.87	87.62
Ba	303.63	725.96	299.29	406.04	1630.60	1103.41	260.51	234.63
Th	8.04	4.53	6.07	6.62	1.61	10.45	12.51	5.86
U	1.35	1.15	1.48	1.71	0.54	2.49	2.68	1.35
Nb	5.75	4.46	5.10	7.50	1.27	7.84	12.08	5.22
Ta	0.42	0.31	0.37	0.50	0.09	0.57	0.97	0.42
La	25.56	14.59	27.42	21.39	5.23	24.39	30.92	16.02
Ce	50.79	28.83	90.21	37.89	12.39	47.35	65.68	33.84
Pr	5.56	3.27	6.86	4.48	1.63	4.90	7.07	3.73
Sr	9.62	50.68	16.76	15.28	168.70	88.06	61.01	101.59
Nd	19.86	12.14	25.86	15.73	7.05	17.75	26.38	14.64
Sm	3.57	2.40	5.24	2.65	1.87	3.05	5.20	3.07
Zr	97.17	84.28	103.86	176.23	62.03	180.78	191.74	104.50
Hf	2.88	2.16	2.97	4.33	1.70	4.59	5.17	2.96
Eu	0.56	0.63	1.25	0.48	0.20	0.53	0.96	0.84
Gd	2.93	2.03	4.06	1.86	2.06	2.76	4.26	2.81
Tb	0.44	0.30	0.58	0.28	0.34	0.39	0.65	0.43
Dy	2.94	1.94	3.52	1.75	2.45	2.72	4.17	2.87
Y	16.31	10.77	16.63	9.29	14.64	17.93	23.05	16.38
Ho	0.60	0.40	0.65	0.37	0.53	0.57	0.86	0.62
Er	1.78	1.16	1.87	1.11	1.59	1.80	2.53	1.79
Yb	1.97	1.33	2.09	1.51	1.69	1.97	2.74	1.96
Lu	0.33	0.20	0.31	0.24	0.26	0.31	0.39	0.29
Sc	7.69	4.64	5.81	5.93	17.72	4.68	17.60	12.43
Cr	31.29	23.05	27.67	29.86	26.76	21.11	95.82	47.64
Tl	0.16	0.16	0.23	0.24	0.28	0.26	0.31	0.13
Pb	404.98	1668.19	451.64	571.30	72.02	45.33	22.71	103.81
Bi	0.61	0.32	0.09	0.07	0.13	0.26	0.23	0.16
V	13.18	23.43	43.23	50.94	150.33	15.33	118.98	111.96
Cu	97.61	89.41	9.96	56.06	4.48	172.81	20.98	6.46
Zn	941.49	2087.24	77.26	1156.23	70.11	153.00	45.16	135.00
Ga	13.49	12.64	12.57	13.45	16.83	16.07	18.19	13.86
As	90.80	0.00	109.78	0.00	28.36	0.00	10.67	25.67
Mo	1.70	1.23	0.99	0.83	1.06	0.74	2.86	1.16
W	1.85	3.15	4.48	8.89	4.46	1.40	2.90	1.46

APPENDIX 3-4

Major and trace element compositions of whole-rock samples

Batu Utul, Han and Plata prospects

	1	2	3	4	5	6	7
Location	Batu Utul	Batu Utul	Han	Han	Han	Plata	Plata
	BUtul-2	BUtul-1	SHan-1	99HN1-59m	SYKBHan-3	98PT5-97m	98PT5-169m
Rock Type	andesite	rhyolite	andesite	andesite	andesite	dacite	dacite
Alteration	least altered	phyllic	least altered	least altered	propylitic	least altered	least altered
Sample No.	1102	1101	1103	1115	1105	1119	1121
Major elements	(normalised 100 wt%) analysed by XRF						
SiO2	64.33	74.74	61.79	63.77	64.59	65.31	65.22
TiO2	0.49	0.15	0.58	0.53	0.58	0.40	0.38
Al2O3	17.21	14.73	16.98	16.70	15.65	17.91	17.26
Fe2O3	5.04	1.52	6.01	5.14	7.36	3.88	4.10
MnO	0.13	0.11	0.26	0.12	0.10	0.09	0.11
MgO	2.36	0.36	2.67	2.56	2.23	2.59	1.72
CaO	5.69	2.79	6.92	5.67	4.05	4.97	5.90
Na2O	3.67	3.42	3.33	4.31	4.07	3.25	3.46
K2O	0.95	2.09	1.33	1.08	1.22	1.43	1.71
P2O5	0.12	0.09	0.13	0.12	0.16	0.17	0.13
Na2O + K2O	4.63	5.51	4.66	5.39	5.29	4.68	5.16
Trace elements	(in ppm) analysed by Laser Ablation ICPMS						
Cs	6.50	1.54	2.43	1.72	6.62	4.15	11.89
Rb	56.07	27.84	33.08	27.17	29.40	33.83	34.39
Ba	168.58	255.29	209.76	213.16	168.61	851.09	645.44
Th	3.82	3.20	1.87	2.76	1.84	7.67	9.05
U	1.08	0.84	0.59	0.82	0.61	1.64	1.85
Nb	3.40	2.71	1.94	2.07	1.84	7.82	7.22
Ta	0.26	0.20	0.15	0.17	0.12	0.59	0.55
La	12.48	10.60	9.88	9.94	9.08	17.71	18.95
Ce	26.10	21.69	21.49	20.29	20.80	31.70	32.74
Pr	2.87	2.49	2.59	2.35	2.75	3.26	3.23
Sr	204.08	297.89	206.88	268.97	207.33	870.22	417.51
Nd	10.58	10.03	11.37	9.54	12.63	11.88	11.69
Sm	1.91	2.12	2.62	2.14	3.04	1.99	2.01
Zr	72.83	85.68	94.98	99.61	106.96	87.96	73.50
Hf	2.09	2.28	2.49	2.65	2.78	2.24	1.92
Eu	0.51	0.68	0.90	0.69	0.97	0.67	0.63
Gd	1.57	1.99	2.79	2.21	3.37	1.78	1.65
Tb	0.24	0.31	0.43	0.34	0.55	0.24	0.27
Dy	1.50	1.95	3.02	2.26	3.84	1.51	1.64
Y	9.63	11.39	18.23	13.64	23.50	7.85	9.11
Ho	0.31	0.41	0.63	0.49	0.83	0.27	0.32
Er	0.90	1.12	1.84	1.45	2.30	0.82	0.97
Yb	1.12	1.35	2.01	1.54	2.56	0.89	1.04
Lu	0.18	0.18	0.31	0.23	0.40	0.13	0.17
Sc	2.75	10.59	12.42	12.80	11.39	7.96	9.15
Cr	10.60	30.04	24.35	46.57	23.69	20.20	21.59
Tl	0.16	0.03	0.07	0.06	0.01	0.17	0.14
Pb	22.27	11.14	7.84	6.71	9.51	23.70	9.04
Bi	0.08	0.06	0.01	0.03	0.12	0.02	0.06
V	11.29	87.23	112.67	104.94	108.23	69.57	72.61
Cu	8.86	11.30	29.80	109.83	955.41	11.78	19.09
Zn	37.36	64.96	124.62	73.62	81.12	141.64	42.07
Ga	16.82	22.10	20.45	21.18	20.37	35.82	29.99
As	22.28	0.96	2.21	0.59	1.14	14.06	7.27
Mo	0.61	0.69	1.13	11.58	14.24	1.41	1.64
W	1.60	0.48	0.38	0.46	0.71	0.75	1.03

APPENDIX 3-5

Major and trace element compositions of whole-rock samples

Muyup Prospect

	1	2	3	4	5	6	7	8	9
Location	S. Buluh Hulu	S. Buluh Hulu	S. RTM	S. RTM	Bengeh	S. Tresia	S. Tresia	S. Buluh Hulu	G. Manuk
Rock Type	dacite	dacite	dacite	dacite	tuff	tuff	tuff	tuff	andesite
Alteration	least altered	least altered	least altered	least altered	phyllic	phyllic	phyllic	phyllic	adv. argillic
Sample No.	123348	123349	123353	123354	123337	123342(*)	123343	123351(*)	123357
Major Elements (normalised 100 wt%) analysed by XRF, except (*) analysed by Electron Microprobe (EDS)									
SiO2	69.57	69.55	69.29	71.16	71.00	83.71	75.57	74.54	97.84
TiO2	0.38	0.39	0.37	0.36	0.71	0.27	0.27	0.56	0.45
Al2O3	15.13	14.94	15.87	16.10	15.60	12.06	13.07	21.07	0.36
Fe2O3	3.32	3.84	3.47	2.48	3.82	0.96	1.57	2.03	1.34
MnO	0.11	0.12	0.10	0.04	0.15		0.06		0.00
MgO	1.79	2.29	1.12	0.97	1.03	0.16	0.84	0.64	0.00
CaO	3.25	2.64	3.41	2.50	0.65	0.14	0.07	0.21	0.00
Na2O	3.28	2.92	3.70	3.70	2.71		0.18	0.22	
K2O	3.07	3.19	2.52	2.55	4.17	2.84	8.34	0.95	0.01
P2O5	0.11	0.12	0.14	0.14	0.17		0.03		0.01
Na2O + K2O	6.34	6.11	6.22	6.25	6.88	2.84	8.52	1.16	0.01
Trace elements (in ppm) analysed by Laser Ablation ICPMS									
Cs	5.12	5.82	3.51	2.77	8.42	8.83	4.01	4.27	
Rb	71.39	81.86	62.47	58.38	216.07	97.54	197.31	46.54	
Ba	472.28	452.34	786.61	452.38	607.55	84.05	1127.94	131.16	
Th	18.02	19.30	8.90	9.38	12.72	15.15	17.29	23.97	
U	3.81	4.15	2.50	2.46	2.99	3.24	3.88	6.23	
Nb	6.85	7.55	5.80	5.70	9.44	10.35	11.09	9.80	
Ta	0.72	0.77	0.53	0.58	0.66	0.77	0.81	0.99	
La	20.48	22.94	20.55	36.15	36.24	26.47	33.33	43.80	
Ce	33.63	38.88	34.64	51.37	74.73	51.07	64.30	95.44	
Pr	3.33	3.76	3.53	5.05	8.15	5.48	6.97	8.22	
Sr	200.47	180.99	404.71	243.79	126.77	18.96	16.61	15.60	
Nd	11.31	13.38	12.91	18.56	33.01	20.30	26.38	28.82	
Sm	2.04	2.35	2.30	3.42	6.93	3.55	5.49	4.79	
Zr	93.22	103.77	90.02	95.31	217.15	211.47	226.43	131.43	
Hf	3.33	3.47	2.37	2.52	5.27	5.61	6.22	3.98	
Eu	0.59	0.61	0.71	1.13	1.59	0.48	0.87	1.20	
Gd	1.69	2.05	2.35	3.88	6.76	2.32	5.22	4.13	
Tb	0.25	0.30	0.33	0.55	1.01	0.30	0.84	0.61	
Dy	1.68	2.03	2.46	3.91	6.86	2.21	5.83	3.76	
Y	9.84	11.69	17.10	27.00	44.45	13.09	35.87	18.58	
Ho	0.34	0.44	0.51	0.81	1.44	0.45	1.27	0.68	
Er	1.02	1.36	1.62	2.50	4.19	1.67	3.87	1.89	
Yb	1.27	1.64	1.70	2.79	4.14	2.25	4.31	1.87	
Lu	0.21	0.28	0.30	0.44	0.66	0.38	0.66	0.27	
Sc	5.85	6.90	7.09	3.91	13.81	9.02	7.56	8.84	
Cr	33.43	26.44	11.47	18.78	18.38	29.79	20.95	41.82	
Tl	0.10	0.15	0.16	0.13	0.97	0.56	0.58	0.15	
Pb	10.63	10.95	10.53	13.67	33.85	44.46	163.53	69.00	
Bi	0.01	0.01	0.03	0.04	0.15	2.07	0.05	0.04	
V	53.57	52.57	52.20	41.35	37.27	23.87	5.84	87.30	
Cu	7.31	6.35	10.32	14.78	0.71	3.29	2.46	13.80	
Zn	46.80	68.80	55.09	45.83	74.74	5.09	53.15	23.02	
Ga	11.84	12.05	13.81	13.93	17.45	13.47	10.82	16.85	
As	2.29	0.00	0.00	4.30	16.51	8.21	0.00	0.00	
Mo	1.40	1.70	0.37	1.26	2.39	1.18	1.23	1.09	
W	0.65	0.78	0.87	0.63	1.68	2.84	1.20	0.76	

APPENDIX 3-6

Major and trace element compositions of whole-rock samples

Ritan Prospect

	1	2	3	4	5	6	7	8
Location	Tabang Ridge G. Tinggi	S. Batuliten	S. Belayan	Mejuk timber road	G. Botak	Mejuk vein zone	Mejuk discovery o/c	Mejuk timber road
Rock Type	andesite	rhyolite	rhyolite	andesite	andesite	andesite	andesite	andesite
Alteration	least altered	least altered	least altered	propylitic	propylitic	argillic	argillic	adv. arg
Sample No.	123301	123307	123308(*)	123325(*)	123305(*)	123317	123320	123313
Major elements (normalised 100 wt%) analysed by XRF, except (*) analysed by Electron Microprobe (EDS)								
SiO2	58.80	76.51	77.04	55.69	64.24	69.19	56.74	98.58
TiO2	0.74	0.24	0.34	0.91	0.70	1.16	1.30	0.78
Al2O3	18.11	13.88	15.01	21.01	19.91	13.20	31.03	0.45
Fe2O3	9.03	1.92	1.61	8.28	4.87	16.11	9.41	0.15
MnO	0.13	0.03				0.01	0.02	
MgO	2.68	1.49	1.34	3.79	0.07	0.02	1.43	0.01
CaO	6.62	2.06	2.12	7.90	5.84	0.05	0.02	0.01
Na2O	2.83	2.22	1.40	3.00	3.63	0.03	0.00	0.01
K2O	0.92	1.62	1.32	0.27	1.32	0.04	0.01	0.02
P2O5	0.15	0.03				0.18	0.02	0.01
Na2O + K2O	3.75	3.84	2.72	3.27	4.94	0.07	0.02	0.03
Trace elements (in ppm) analysed by Laser Ablation ICPMS								
Cs	4.53	5.27	1.40	3.20	0.40	1.92	0.31	0.28
Rb	37.23	55.25	30.59	8.60	21.88	2.03	1.24	0.62
Ba	190.92	522.88	1214.89	130.97	250.69	213.67	5.53	22.62
Th	3.35	17.03	16.86	2.45	3.09	5.17	1.86	3.71
U	0.82	4.05	4.04	0.64	0.57	2.43	0.39	1.40
Nb	2.87	5.45	5.45	2.95	3.40	3.62	2.87	4.81
Ta	0.24	0.55	0.54	0.19	0.25	0.28	0.19	0.37
La	11.25	21.55	24.72	18.57	10.87	12.30	3.99	1.08
Ce	23.29	35.06	38.25	29.45	21.44	27.67	9.13	2.56
Pr	3.14	3.31	3.74	5.58	3.08	3.61	1.25	0.31
Sr	235.00	195.98	463.55	241.04	296.30	1042.79	0.94	6.10
Nd	14.77	10.57	12.27	27.00	13.26	16.54	6.04	1.32
Sm	3.79	1.84	2.27	8.41	3.19	3.90	1.34	0.33
Zr	100.54	97.71	100.87	99.20	102.41	143.86	71.80	281.31
Hf	3.04	2.47	2.47	2.45	2.53	3.60	2.04	3.33
Eu	1.18	0.44	0.50	2.97	0.99	1.20	0.42	0.09
Gd	4.07	1.48	1.74	11.08	3.12	2.92	1.58	0.57
Tb	0.64	0.23	0.30	2.00	0.47	0.28	0.24	0.15
Dy	4.49	1.57	2.07	14.94	2.87	1.31	1.77	1.70
Y	23.49	12.02	14.40	79.95	18.20	4.89	11.19	12.81
Ho	0.90	0.33	0.47	3.24	0.59	0.22	0.41	0.48
Er	2.66	1.02	1.56	9.97	1.66	0.57	1.25	1.81
Yb	3.11	1.42	2.02	13.88	1.68	0.82	1.59	2.53
Lu	0.49	0.22	0.34	2.34	0.24	0.13	0.26	0.40
Sc	14.73	4.51	5.67	19.74	13.56	15.23	26.01	13.99
Cr	19.76	14.77	18.12	28.84	22.77	27.99	27.64	27.11
Tl	0.20	0.09	0.23	0.11	0.01	7.89	0.03	0.01
Pb	8.52	9.07	32.83	13.79	45.06	9107.70	87.08	74.01
Bi	0.02	0.05	0.20	0.05	0.06	0.55	0.31	111.11
V	127.39	20.63	25.41	166.14	102.65	269.70	257.64	33.20
Cu	7.11	8.89	5.14	33.11	14.72	42.66	56.05	7.78
Zn	119.96	38.26	60.91	92.05	32.69	1140.88	154.43	2.25
Ga	17.51	10.68	12.48	17.57	19.94	125.85	21.74	0.78
As	5.31	8.45	0.84	11.08	0.36	364.42	0.00	9.27
Mo	1.56	4.08	1.09	0.00	1.22	14.37	1.98	1.33
W	0.58	1.40	1.51	0.37	0.43	5.73	0.45	2.00

Appendix 4-1

Major and trace element compositions of selected minerals

Rock Sample No 123144

Hornblende phenocrysts

Major elements (in wt%) analysed by Electron Microprobe (EDS)

	144h1-1	144h1-2	144h1-3	144h2-1	144h2-2	144h3-1	144h3-2	144h3-3	144h4-1	144h4-2	144h5-1	144h5-2
SiO2	46.95	48.54	48.31	48.24	45.80	48.13	47.90	48.09	48.72	47.87	48.76	48.83
TiO2	1.53	1.27	1.27	1.53	2.03	1.53	1.45	1.47	1.13	1.51	1.38	1.43
Al2O3	7.71	6.48	7.08	6.72	8.49	6.86	6.97	6.95	6.41	6.95	6.58	6.09
Cr2O3	<0.08	<0.08	<0.08	<0.08	<0.08	<0.08	<0.08	<0.08	<0.08	<0.08	<0.08	<0.08
FeO	12.57	12.31	12.64	12.46	13.42	12.69	12.96	12.68	12.20	12.72	12.38	12.28
MnO	0.27	0.21	0.28	0.22	0.13	0.25	0.28	0.29	0.20	0.33	0.34	0.28
MgO	15.05	15.85	15.68	15.68	14.43	15.50	15.47	15.62	15.75	15.45	15.82	16.04
CaO	11.09	11.01	11.22	11.21	11.33	11.58	11.22	11.23	11.17	11.45	11.31	11.41
Na2O	1.75	1.22	1.16	1.19	1.65	1.35	1.30	1.32	1.20	1.48	1.15	1.20
K2O	0.22	0.14	0.19	0.19	0.26	0.23	0.20	0.16	0.09	0.20	0.20	0.15
Total	97.14	97.04	97.83	97.45	97.54	98.12	97.75	97.80	96.87	97.97	97.92	97.71

Trace elements (in ppm) analysed by Excimer Laser Ablation ICP-MS

Ba	19.84	21.58	19.90	23.86	23.18	24.56	22.64	25.68	24.73	23.67	20.76	31.40
Th	0.08	0.07	0.15	0.09	0.06	0.06	0.08	0.05	0.05	0.05	0.08	0.14
U	0.02	0.02	0.05	0.02	0.02	0.01	0.02	0.02	0.01	0.01	0.02	0.06
La	5.57	5.30	7.81	7.48	6.41	6.11	6.24	5.88	6.04	5.78	6.41	5.79
Ce	26.19	23.75	28.39	30.31	27.90	26.88	27.70	26.87	27.74	26.09	29.10	26.91
Pr	5.03	4.47	4.84	5.56	5.25	5.00	5.38	5.45	5.33	4.97	5.45	4.99
Sr	29.70	36.39	38.30	33.05	30.98	31.61	32.59	34.11	32.69	31.06	29.27	32.44
Nd	28.30	24.91	25.74	30.68	28.96	28.90	31.14	33.05	31.32	29.52	29.89	28.69
Sm	9.58	8.27	7.44	9.79	9.59	8.92	10.88	12.52	10.54	10.43	9.46	8.87
Zr	47.10	52.16	49.57	56.94	52.08	55.81	52.28	52.35	51.95	53.90	52.12	51.18
Hf	2.22	2.14	2.18	2.59	2.45	2.66	2.37	2.30	2.44	2.33	2.45	2.38
Eu	2.06	1.89	1.91	2.08	2.06	1.97	2.38	2.56	2.23	2.08	1.98	2.02
Gd	11.02	9.29	8.46	12.05	11.30	10.75	14.13	16.15	13.65	13.29	11.27	10.63
Tb	1.82	1.56	1.41	1.96	1.84	1.78	2.30	2.70	2.34	2.23	1.83	1.78
Dy	13.07	10.66	10.11	13.44	12.89	12.46	16.32	19.40	16.47	15.69	13.06	12.54
Y	70.49	61.07	56.56	77.09	74.36	69.05	88.44	100.15	88.31	83.08	71.21	69.92
Ho	2.67	2.30	2.05	2.83	2.72	2.60	3.36	4.01	3.31	3.29	2.63	2.55
Er	8.06	6.54	6.21	8.16	7.82	7.58	9.61	10.96	9.34	9.14	7.65	7.57
Tm	1.19	0.95	0.87	1.22	1.15	1.16	1.42	1.55	1.41	1.27	1.16	1.14
Yb	8.34	6.60	6.34	8.16	7.95	7.63	9.65	9.94	8.80	8.70	8.16	8.09
Lu	1.21	0.94	0.94	1.21	1.16	1.12	1.34	1.37	1.29	1.28	1.24	1.19
Sc	94.07	98.09	85.96	105.41	102.68	90.93	139.47	143.50	126.61	132.97	92.76	89.44

Appendix 4-2									
Major and trace element compositions of selected minerals									
Rock Sample No 123144									
Plagioclase phenocrysts									
Major elements (in wt%) analysed by Electron Microprobe (EDS)									
Wt%	144pl1-1	144pl1-2	144pl1-3	144pl2-1	144pl2-2	144pl2-3	144pl3-1	144pl3-2	144pl3-3
SiO2	56.16	55.73	55.57	55.16	56.18	55.97	54.00	56.51	56.56
TiO2	<0.07	<0.07	<0.07	<0.07	<0.07	<0.07	<0.07	<0.07	<0.07
Al2O3	28.38	28.37	28.28	28.61	27.90	28.02	29.38	27.29	28.04
Cr2O3	<0.08	<0.08	<0.08	<0.08	<0.08	<0.08	<0.08	<0.08	<0.08
FeO	0.27	0.32	0.41	0.24	0.36	0.39	0.45	0.35	0.34
MnO	<0.08	<0.08	<0.08	<0.08	<0.08	<0.08	<0.08	<0.08	<0.08
MgO	<0.08	<0.08	<0.08	<0.08	<0.08	<0.08	<0.08	<0.08	<0.08
CaO	10.39	10.37	10.64	10.87	9.98	10.43	12.04	9.90	9.91
Na2O	5.99	5.74	5.68	5.60	6.09	5.94	4.83	6.01	6.00
K2O	0.18	0.10	0.13	0.16	0.18	0.14	0.05	0.11	0.14
Total	101.37	100.63	100.70	100.64	100.71	100.90	100.77	100.17	100.98
Trace elements (in ppm) analysed by Excimer Laser Ablation ICP-MS									
Ba	111.10	321.58	319.27	84.75	110.22	315.83	93.65	98.59	92.55
Th	0.00	0.73	0.69	0.00	0.00	0.69	n.a.	0.00	n.a.
U	0.00	0.45	0.43	0.00	0.00	0.41	n.a.	n.a.	n.a.
La	3.53	2.68	2.67	2.61	3.21	2.58	2.96	2.97	2.95
Ce	5.25	4.53	4.66	3.75	4.79	4.49	4.50	4.28	4.42
Pr	0.41	0.51	0.52	0.32	0.40	0.50	0.35	0.37	0.37
Sr	755.28	50.94	49.04	618.78	702.76	48.97	649.63	674.41	627.99
Nd	1.36	1.89	2.05	1.17	1.15	2.13	1.04	0.87	1.27
Sm	0.12	0.32	0.35	0.18	0.16	0.35	0.03	0.07	0.20
Zr	0.19	128.17	127.16	n.a.	n.a.	129.30	n.a.	0.01	0.05
Hf	n.a.	3.15	3.21	n.a.	0.00	3.10	0.01	n.a.	0.01
Eu	0.60	0.22	0.22	0.54	0.62	0.22	0.53	0.50	0.49
Gd	0.04	0.28	0.30	0.05	0.06	0.27	0.03	0.08	0.07
Tb	n.a.	0.06	0.05	0.00	0.00	0.04	0.00	0.01	0.01
Dy	0.02	0.33	0.30	0.04	0.06	0.35	0.04	0.02	0.09
Y	0.12	2.43	2.18	0.16	0.22	2.10	0.09	0.16	0.12
Ho	0.02	0.09	0.08	0.01	0.00	0.07	0.00	0.01	0.01
Er	n.a.	0.27	0.26	0.01	0.00	0.23	0.02	0.04	0.02
Tm	0.00	0.04	0.05	n.a.	0.00	0.03	n.a.	n.a.	n.a.
Yb	0.01	0.33	0.30	0.02	0.00	0.28	0.00	0.00	0.03
Lu	0.00	0.06	0.05	0.00	n.a.	0.05	n.a.	0.00	0.00
Sc	2.17	3.04	3.21	2.29	1.31	2.45	1.30	1.39	3.71
n.a. : not available									

Appendix 4-3						
Major and trace element compositions of selected minerals						
Rock Sample No 123144						
Groundmass						
Major elements (in wt%) analysed by Electron Microprobe (EDS)						
Wt%	144m1-1	144m1-2	144m2-1	144m2-2	144m3-1	144m3-2
SiO2	78.97		74.22		78.11	
TiO2	0.09		0.36		0.10	
Al2O3	10.45		12.14		10.52	
Cr2O3	<0.08		<0.08		<0.08	
FeO	0.80		1.88		1.74	
MnO	<0.08		<0.08		<0.08	
MgO	0.53		1.59		1.71	
CaO	1.11		1.35		1.28	
Na2O	3.10		3.88		3.49	
K2O	2.80		2.53		1.41	
Total	97.85		97.95		98.36	
Trace elements (in ppm) analysed by Excimer Laser Ablation ICP-MS						
Ba	516.33	578.70	396.96	407.91	40.00	37.55
Th	0.72	5.71	6.77	5.28	0.09	0.08
U	0.23	1.03	2.74	1.08	0.06	0.05
La	4.17	3.50	4.91	4.01	0.35	0.31
Ce	7.48	6.10	13.44	7.85	0.59	0.56
Pr	0.66	0.54	1.73	0.74	0.06	0.06
Sr	175.02	162.05	139.17	167.44	6.64	5.87
Nd	2.53	1.63	7.75	2.80	0.22	0.25
Sm	0.42	0.25	2.11	0.60	0.03	0.03
Zr	15.37	74.87	96.22	73.64	14.99	15.10
Hf	0.75	1.91	2.68	2.00	0.39	0.38
Eu	0.22	0.22	0.28	0.23	0.03	0.03
Gd	0.34	0.43	1.71	0.52	0.04	0.04
Tb	0.05	0.08	0.29	0.10	0.01	0.01
Dy	0.24	0.64	2.09	0.93	0.04	0.04
Y	1.38	6.02	11.21	5.26	0.26	0.25
Ho	0.05	0.22	0.46	0.21	0.01	0.01
Er	0.11	0.68	1.11	0.59	0.03	0.03
Tm	0.02	0.12	0.18	0.09	0.00	0.00
Yb	0.14	0.93	1.35	0.68	0.04	0.04
Lu	0.02	0.16	0.20	0.10	0.01	0.01
Sc	3.00	3.09	2.68	2.89	0.30	0.40

Appendix 4-4								
Major and trace element compositions of selected minerals								
Rock Sample No 123187								
Clinopyroxene phenocrysts								
Major elements (in wt%) analysed by Electron Microprobe (EDS)								
	187px1-1	187px1-2	187px2-1	187px2-2	187px3-1	187px3-2	187px4-1	187px4-2
SiO2	52.67	52.09	50.65	51.11	51.97	51.71	52.76	52.61
TiO2	0.17	0.18	0.30	0.25	0.14	0.31	0.16	0.16
Al2O3	1.23	2.14	3.44	2.78	2.20	2.46	1.31	1.46
Cr2O3	0.32	0.66	0.13	0.20	0.72	0.62	0.22	0.61
FeO	4.37	4.74	6.80	6.46	4.64	5.26	4.28	4.32
MnO	<0.08	<0.08	<0.08	<0.08	<0.08	<0.08	<0.08	<0.08
MgO	17.30	16.82	15.40	16.14	16.52	16.48	16.92	17.38
CaO	22.11	22.43	21.93	21.84	22.54	22.66	23.18	22.42
Na2O	<0.12	0.12	<0.12	<0.12	<0.12	0.13	<0.12	<0.12
K2O	<0.04	<0.04	<0.04	<0.04	<0.04	0.05	<0.04	<0.04
Total	98.17	99.19	98.66	98.79	98.74	99.67	98.83	98.96
Trace elements (in ppm) analysed by Excimer Laser Ablation ICP-MS								
Ba	0.02	0.03	0.02	0.42	0.03	0.03	0.24	0.71
Th	0.01	0.00	0.01	0.01	0.01	0.01	0.02	0.02
U	0.00	0.00	0.00	0.01	0.00	0.00	0.00	0.00
La	0.39	0.29	0.55	0.62	0.30	0.29	0.49	0.47
Ce	1.59	1.27	1.99	2.64	1.09	1.24	2.14	1.64
Pr	0.33	0.27	0.45	0.53	0.19	0.26	0.44	0.28
Sr	39.77	36.33	34.28	33.11	39.60	40.50	32.18	40.26
Nd	2.01	1.60	2.91	3.38	1.35	1.64	2.96	2.09
Sm	0.82	0.60	0.99	1.31	0.46	0.59	1.03	0.69
Zr	2.95	1.85	5.64	7.97	1.43	1.82	5.54	2.26
Hf	0.17	0.05	0.34	0.44	0.10	0.10	0.27	0.10
Eu	0.26	0.21	0.36	0.45	0.19	0.20	0.39	0.24
Gd	1.02	0.91	1.42	1.75	0.64	0.68	1.42	0.97
Tb	0.16	0.12	0.22	0.27	0.10	0.10	0.26	0.13
Dy	1.04	0.87	1.60	1.95	0.60	0.77	1.82	0.91
Y	5.17	4.11	7.10	8.98	3.13	3.39	8.13	4.51
Ho	0.21	0.17	0.30	0.41	0.14	0.15	0.33	0.18
Er	0.58	0.47	0.79	1.01	0.30	0.38	0.91	0.48
Tm	0.08	0.06	0.10	0.16	0.04	0.04	0.13	0.07
Yb	0.48	0.41	0.77	0.90	0.32	0.31	0.80	0.43
Lu	0.06	0.06	0.09	0.12	0.04	0.05	0.10	0.06
Sc	95.27	81.43	106.72	118.84	81.26	82.24	117.92	88.25

Appendix 4-5						
Major and trace element compositions of selected minerals						
Rock Sample No 123187						
Plagioclase phenocrysts						
Major elements (in wt%) analysed by Electron Microprobe (EDS)						
Wt%	187pl-1	187pl-2	187pl-3	187pl2-1	187pl2-2	187pl2-3
SiO2	53.48	55.38	54.30	55.91	55.27	54.96
TiO2	<0.07	<0.07	<0.07	<0.07	<0.07	<0.07
Al2O3	29.16	28.11	29.19	27.53	28.21	28.54
Cr2O3	<0.07	<0.07	<0.07	<0.07	<0.07	<0.07
FeO	0.20	0.24	0.31	0.27	0.22	0.27
MnO	<0.07	<0.07	<0.07	<0.07	<0.07	<0.07
MgO	<0.07	<0.07	<0.07	<0.07	<0.07	<0.07
CaO	11.73	10.34	11.36	10.04	10.57	10.60
Na2O	5.04	5.80	5.33	6.12	5.71	5.71
K2O	0.12	0.12	0.09	0.16	0.14	0.11
Total	99.74	99.98	100.58	100.03	100.13	100.20
Trace elements (in ppm) analysed by Excimer Laser Ablation ICP-MS						
Ba	87.11	72.75	71.78	78.00	80.93	82.06
Th	n.a.	0.00	0.00	0.00	n.a.	0.00
U	0.00	0.00	n.a.	n.a.	n.a.	n.a.
La	3.48	2.83	3.07	3.18	3.19	3.29
Ce	5.09	4.16	4.51	4.57	4.78	4.65
Pr	0.44	0.34	0.36	0.41	0.35	0.43
Sr	723.43	687.03	645.32	659.09	672.54	712.00
Nd	1.15	1.10	1.03	0.84	1.10	1.04
Sm	0.13	0.11	0.16	0.12	0.07	0.08
Zr	n.a.	n.a.	0.03	n.a.	n.a.	0.17
Hf	0.01	0.00	n.a.	0.02	0.02	0.01
Eu	0.50	0.50	0.49	0.45	0.46	0.51
Gd	0.03	0.05	0.03	0.04	0.05	0.04
Tb	0.00	0.01	0.01	0.00	0.00	0.01
Dy	n.a.	0.04	0.01	0.03	0.02	0.03
Y	0.07	0.09	0.13	0.11	0.11	0.11
Ho	0.00	0.01	0.00	0.01	0.00	0.01
Er	0.01	n.a.	0.01	0.01	0.02	0.01
Tm	0.00	0.01	n.a.	0.00	n.a.	0.01
Yb	n.a.	0.00	0.01	0.01	0.00	0.01
Lu	0.00	0.00	0.00	n.a.	0.01	0.00
Sc	1.07	2.20	1.51	0.32	2.43	1.34
n.a. : not available						

Appendix 4-6									
Major and trace element compositions of selected minerals									
Rock Sample No 123187									
Groundmass									
Major elements (in wt%) analysed by Electron Microprobe (EDS)									
Wt%	187m1-1	187m1-2	187m1-3	187m2-1	187m2-2	187m2-3	187m3-1	187m3-2	187m3-3
SiO2	74.96	49.83	55.60	53.79	70.92	62.57	73.74	54.10	57.90
TiO2	0.15	0.54	0.21	0.07	0.66	0.20	0.12	<0.07	<0.07
Al2O3	12.46	4.34	22.00	24.63	16.07	21.60	15.46	27.91	25.26
Cr2O3	<0.07	0.12	<0.07	<0.07	<0.08	<0.07	<0.07	<0.07	<0.07
FeO	1.06	8.59	3.04	2.31	5.64	2.23	0.88	1.25	1.07
MnO	<0.07	0.12	<0.07	<0.07	<0.08	<0.07	<0.07	<0.07	<0.07
MgO	0.95	14.64	3.39	2.42	4.45	2.49	0.55	0.55	0.47
CaO	5.36	19.80	7.41	9.12	5.70	7.86	5.26	11.72	9.99
Na2O	2.70	0.26	3.84	4.56	2.83	4.43	3.52	4.14	4.40
K2O	0.93	<0.04	2.17	0.84	0.92	0.64	0.64	0.26	0.42
Total	98.59	98.24	97.66	97.75	107.19	102.02	100.17	99.93	99.51
Trace elements (in ppm) analysed by Excimer Laser Ablation ICP-MS									
Ba	403.44	1139.36		299.20	209.97		314.77	205.25	
Th	3.73	6.41		4.81	3.33		0.97	6.13	
U	2.70	2.17		2.28	1.40		0.18	2.00	
La	8.70	25.14		23.21	11.07		4.60	4.32	
Ce	20.90	49.06		44.26	22.90		8.31	12.35	
Pr	2.72	5.41		3.73	2.69		0.88	0.87	
Sr	555.25	667.14		547.23	554.80		551.16	458.23	
Nd	11.21	22.81		9.34	10.55		3.23	6.33	
Sm	2.65	5.07		1.28	2.07		1.01	0.72	
Zr	100.85	110.26		87.86	65.24		25.77	28.42	
Hf	3.09	3.14		2.24	1.89		0.90	1.88	
Eu	0.73	1.43		0.67	0.59		0.64	0.44	
Gd	2.82	4.50		1.27	1.89		0.78	0.62	
Tb	0.41	0.71		0.20	0.33		0.11	0.17	
Dy	3.09	4.00		1.81	2.36		0.78	6.91	
Y	17.00	23.08		10.09	13.35		3.55	3.44	
Ho	0.59	0.85		0.41	0.49		0.17	0.48	
Er	1.99	2.48		1.32	1.46		0.47	0.37	
Tm	0.26	0.36		0.21	0.21		0.07	0.38	
Yb	2.11	2.46		1.71	1.76		0.46	0.47	
Lu	0.31	0.39		0.30	0.25		0.08	0.08	
Sc	20.64	9.33		14.60	10.65		9.04	66.20	

APPENDIX 5				
The preferred set of values (ppm) for the standards used in this study				
	Standard Glass	Kilauea Basalt		
	NIST 612	**ANU 93-1489**	**C1 Chondrite**	**Primitive Mantle**
Reference	Pearce et al., 1997	Eggins et al., 1997	McDonough and Sun, 1995	Sun and McDonough, 1989
Ca43	115.10	104.885		
Ti	48.11	14362	440	1300
Cs	41.64	0.074	0.19	0.0079
Rb	31.63	7.15	2.3	0.635
Ba	37.74	99.9	2.41	6.989
Th	37.23	0.853	0.029	0.085
U	37.15	0.274	0.0074	0.021
Nb	38.06	13.24	0.24	0.713
Ta	39.77	0.82	0.0136	0.041
La	35.77	11.2	0.237	0.687
Ce	38.35	27.9	0.613	1.775
Pr	37.16	4.11	0.0928	0.276
Sr	76.15	317	7.25	21.1
Nd	35.24	19.21	0.457	1.354
Sm	36.72	5.21	0.148	0.444
Zr	35.99	147.2	3.82	11.2
Hf	34.77	3.58	0.103	0.309
Eu	34.44	1.783	0.0563	0.168
Gd	36.95	5.59	0.199	0.596
Tb	35.92	0.878	0.0361	0.108
Dy	35.97	4.96	0.246	0.737
Y	38.25	27	1.57	4.55
Ho	37.87	0.966	0.0546	0.164
Er	37.43	2.51	0.16	0.48
Tm	37.55		0.0247	0.074
Yb	39.95	1.974	0.161	0.493
Lu	37.71	0.279	0.0246	0.074
Sc	41.05	31.6	5.92	
Cr	39.88	471	2,650	
Tl	15.07	0.022	0.14	0.005
Pb	38.96	0.95	2.47	0.071
Bi	29.84		0.11	
V	39.22	301	56	
Cu	36.71	123	120	
Zn	37.92	104	310	
Ga	36.24	19.2	9.2	
As	37.33		1.85	
Mo	38.3	0.74	0.9	0.063
W	39.55		0.093	0.02

APPENDIX 6

Partition coefficients of trace elements between mineral and liquid in andesite

	Plagioclase (58% SiO2)	Plagioclase (64% SiO2)	Amphibole	Clinopyroxene	Orthopyroxene	Garnet	Apatite	Zircon	Allanite
La	0.247	0.687	1.507	0.033	0.26	0.076	14.5	5.25	2827
Ce	0.176	0.507	3.149	0.065	0.31	0.144	21.1	5.14	2494
Pr	0.143	0.450	5.637	0.127	0.39	0.188	26.95	5	2167
Nd	0.099	0.380	7.984	0.212	0.47	0.232	32.8	4.77	1840
Sm	0.052	0.240	11.523	0.380	0.46	1.25	46	5.16	977
Eu	0.644	1.834	8.830	0.382	0.34	1.52	25.5	4.23	122
Gd	0.030	0.181	15.906	0.557	0.58	5.2	43.9	6.41	404
Tb	0.020	0.148	14.987	0.535	0.69	7.1	40	18.9	235
Dy	0.015	0.143	14.240	0.378	0.40	15.45	34.8	31.4	150
Ho	0.012	0.131	12.131	0.473	0.52	23.8	30	48	125
Er	0.009	0.131	13.217	0.458	0.65	26.3	22.7	64.6	100
Tm	0.007	0.131	11.867	0.338					
Yb	0.006	0.144	10.615	0.368	0.77	53	15.4	128	37
Lu	0.005	0.167	9.962	0.307	0.71	57	13.8	196	44
Ba	0.184	0.360	0.050	0.0004	0.1	0.109			
Th	0.0004	0.052	0.017	0.002	0.14				420
U	0.002	0.173	0.017	0.001	0.023				14
Sr	1.230	2.820	0.202	0.067	0.01	0.04	1.3		1.8
Zr	0.001	0.982	0.806	0.053	0.11	0.4	0.636		0.29
Hf	0.005	0.578	1.301	0.090	0.11	0.570	0.730	997	9.8
Y	0.009	0.146	12.750	0.474	0.19	2.5			95.5
Sc	0.068	0.808	37.219	4.438	4.3	3.9			49.4

Reference:

Plagioclase, Amphibole, Clinopyroxene : this study; smoothed values for Dy, Ho, Er, Yb and Lu for Calcic Plagioclase	
Orthopyroxene :	Bacon and Druitt, 1988; Dunn and Sen, 1994 (Dy, Ho, Er, Y, U); smoothed values for Pr
Garnet :	Garnet : Irving and Frey, 1978; Shimizu, 1974 (Ce, Nd, Ba); Nicholls and Harris (Dy), 1980; Barth et al., 1997 (Er);
	Green et al., 1989 (Sr, Y, Zr); smoothed values for Pr
Apatite :	Fujimaki, 1986; Watson and Green, 1981 (Sr); smoothed values for Pr, Tb and Ho
Zircon :	Fujimaki, 1986; smoothed values for Pr
Allanite :	Mahood and Hildreth, 1983 (rhyolite); Ewart and Griffin, 1994 (Sr, Y, Zr); smoothed values for Pr, Gd, Ho and Er

APPENDIX 7-1

Summary of the U-Th-Pb zircon dates analysed by ELA-ICP-MS

Magerang-Imang andesite Sample No. 123158

Sample No.	P(ppm)	U(ppm)	$^{232}Th/^{238}U$	Uncorrected $^{206}Pb/^{238}U$ ratio	±	Uncorrected $^{207}Pb/^{235}U$ ratio	±	Uncorrected $^{208}Pb/^{232}Th$ ratio	±	f208	^{208}Pb corrected $^{206}Pb/^{238}U$ Date (Ma)	Observed Error (± 1s.e.)	f207	^{207}Pb corrected $^{206}Pb/^{238}U$ Date (Ma)	Observed Error (± 1s.e.)	Obs/Exp Error	Spot MSWD	Exclude?
158-01	137	37	0.472	0.003181	0.000034	0.032952	0.001465	0.001683	0.000061	0.047	19.41	0.22	0.031	19.83	0.22	1.2	1.38	
158-02	122	29	0.483	0.003267	0.000038	0.040776	0.001866	0.001758	0.000056	0.052	19.82	0.25	0.048	20.02	0.25	1.2	1.47	
158-03	144	49	0.496	0.003182	0.000031	0.028417	0.001259	0.001305	0.000040	0.023	19.95	0.20	0.020	20.07	0.20	1.2	1.28	
158-04	158	47	0.507	0.003030	0.000026	0.031850	0.001278	0.001337	0.000039	0.030	18.87	0.17	0.033	18.87	0.17	1.0	0.98	
158-05	146	59	0.762	0.003383	0.000055	0.067720	0.005523	0.001872	0.000106	0.091	19.71	0.40	0.108	19.43	0.42	2.2	2.63	yes; a
158-06	157	66	0.649	0.003100	0.000028	0.024964	0.001145	0.001154	0.000026	0.017	19.54	0.19	0.013	19.69	0.19	1.1	1.19	
158-07	93	27	0.494	0.003177	0.000055	0.041815	0.003320	0.001459	0.000070	0.035	19.69	0.36	0.054	19.36	0.37	1.2	1.36	
158-08	166	75	0.654	0.003119	0.000027	0.025952	0.001069	0.001119	0.000027	0.014	19.75	0.18	0.015	19.77	0.18	1.2	1.47	
158-09	192	80	0.617	0.003178	0.000030	0.025359	0.001369	0.001073	0.000036	0.006	20.28	0.20	0.012	20.20	0.20	1.4	1.43	
158-10	185	81	0.699	0.003157	0.000024	0.023397	0.000971	0.001085	0.000023	0.009	20.10	0.16	0.008	20.16	0.16	1.1	1.09	
158-11	190	112	0.725	0.003051	0.000022	0.023194	0.000825	0.001021	0.000021	0.007	19.47	0.16	0.010	19.45	0.15	1.2	1.38	
158-12	212	80	0.599	0.003122	0.000021	0.024532	0.000867	0.001080	0.000025	0.008	19.91	0.14	0.012	19.86	0.14	1.0	0.90	
158-13	314	60	0.603	0.003216	0.000030	0.028495	0.001430	0.001210	0.000037	0.018	20.30	0.20	0.019	20.30	0.20	1.1	1.18	
158-14	695	76	0.792	0.003159	0.000030	0.033932	0.001295	0.001342	0.000028	0.043	19.41	0.21	0.034	19.64	0.20	1.3	1.30	
158-15	118	55	0.643	0.003068	0.000031	0.028646	0.001418	0.001133	0.000031	0.017	19.41	0.21	0.023	19.29	0.21	1.1	1.18	
158-16	155	77	0.682	0.002986	0.000031	0.027150	0.001593	0.001135	0.000036	0.022	18.78	0.22	0.021	18.81	0.21	1.3	1.63	
158-17	125	47	0.572	0.003184	0.000031	0.025861	0.001612	0.001115	0.000037	0.011	20.26	0.22	0.014	20.22	0.21	1.0	0.93	
158-18	151	61	0.566	0.003234	0.000039	0.052899	0.003482	0.002083	0.000129	0.084	19.06	0.29	0.079	19.18	0.29	1.5	1.64	
158-19	162	65	0.657	0.003245	0.000033	0.026200	0.001245	0.001105	0.000037	0.008	20.72	0.23	0.013	20.61	0.22	1.2	1.25	
158-20	158	101	0.650	0.003110	0.000034	0.036315	0.002017	0.001379	0.000066	0.039	19.23	0.25	0.042	19.18	0.23	1.5	2.04	yes; a
158-21	158	75	0.562	0.003313	0.000050	0.056365	0.004352	0.002242	0.000166	0.089	19.42	0.36	0.084	19.53	0.37	2.1	3.08	yes; a
158-22	151	60	0.624	0.002995	0.000035	0.036514	0.002091	0.001323	0.000054	0.037	18.59	0.23	0.046	18.40	0.24	1.2	1.29	
158-23	260	91	0.684	0.003070	0.000027	0.023655	0.001025	0.001039	0.000027	0.007	19.63	0.18	0.010	19.56	0.18	1.0	0.97	
158-24	155	91	0.637	0.003991	0.000057	0.149993	0.004826	0.004514	0.000142	0.254	19.22	0.36	0.247	19.35	0.35	1.5	2.36	yes; a
158-25	132	76	0.571	0.003223	0.000040	0.043055	0.002096	0.001822	0.000069	0.067	19.37	0.26	0.055	19.60	0.26	1.3	1.64	
158-26	162	96	0.587	0.003067	0.000030	0.024714	0.000892	0.001083	0.000025	0.010	19.55	0.20	0.013	19.48	0.20	1.3	1.63	
158-27	123	64	0.670	0.003212	0.000038	0.039969	0.002437	0.001431	0.000066	0.041	19.84	0.27	0.048	19.69	0.26	1.1	1.09	
158-28	160	97	0.684	0.002943	0.000032	0.025816	0.001313	0.001015	0.000029	0.009	18.79	0.22	0.019	18.59	0.21	1.3	1.58	
158-29	132	59	0.667	0.003128	0.000047	0.025031	0.002245	0.001234	0.000062	0.025	19.65	0.33	0.013	19.88	0.32	1.2	1.35	
158-30	138	85	0.776	0.003122	0.000037	0.047000	0.001711	0.001582	0.000033	0.075	18.62	0.24	0.069	18.72	0.24	1.3	1.65	
158-31	129	65	0.589	0.003116	0.000043	0.028936	0.001889	0.001168	0.000070	0.015	19.78	0.29	0.023	19.60	0.28	1.4	1.74	
158-32	198	123	0.703	0.003104	0.000033	0.026703	0.001114	0.001051	0.000025	0.007	19.86	0.22	0.017	19.63	0.21	1.3	1.73	

Notes:

a : Date excluded based on the spot MSWD being larger than 2

b : Date excluded based on the ratio between the observed error to expected error being larger than 3

c : Date excluded based on the plot of probability distribution; inherited grain

d : Date excluded based on the plot of probability distribution; possibly due to Pb loss

APPENDIX 7-2

Summary of the U-Th-Pb zircon dates analysed by ELA-ICP-MS

Magerang-Imang Andesite Sample No. 123226-session1

Sample No.	P(ppm)	U(ppm)	$^{232}Th/^{238}U$	Uncorrected $^{206}Pb/^{238}U$ ratio	±	Uncorrected $^{207}Pb/^{235}U$ ratio	±	Uncorrected $^{208}Pb/^{232}Th$ ratio	±	f208	^{208}Pb corrected $^{206}Pb/^{238}U$ Date (Ma)	Observed Error (± 1s.e.)	f207	^{207}Pb corrected $^{206}Pb/^{238}U$ Date (Ma)	Observed Error (± 1s.e.)	Obs/Exp Error	Spot MSWD	Exclude?
226-1-01	160	55	0.643	0.003021	0.000038	0.021803	0.001402	0.000996	0.000033	0.004	19.42	0.25	0.006	19.32	0.25	1.2	1.42	
226-1-02	370	52	0.663	0.003147	0.000041	0.042784	0.003310	0.001455	0.000072	0.049	19.36	0.30	0.057	19.10	0.30	1.2	1.14	
226-1-03	183	83	0.766	0.002962	0.000033	0.019743	0.001174	0.000946	0.000028	0.001	19.04	0.23	0.002	19.03	0.22	1.2	1.32	
226-1-04	116	40	0.573	0.003071	0.000041	0.030992	0.002144	0.001102	0.000058	0.012	19.54	0.28	0.029	19.19	0.27	1.1	1.21	
226-1-05	130	50	0.532	0.002884	0.000040	0.021824	0.001739	0.000994	0.000044	0.008	18.40	0.27	0.009	18.40	0.27	1.1	1.16	
226-1-06	120	54	0.599	0.003106	0.000036	0.025324	0.001473	0.001114	0.000039	0.011	19.75	0.24	0.014	19.71	0.24	1.1	1.05	
226-1-07	118	44	0.614	0.003003	0.000041	0.025505	0.001873	0.000981	0.000039	0.002	19.27	0.27	0.017	19.01	0.28	1.1	1.11	
226-1-08	154	59	0.530	0.002980	0.000034	0.021644	0.001278	0.000922	0.000036	-0.002	19.20	0.23	0.007	19.05	0.23	1.1	1.16	
226-1-09	545	63	0.623	0.002992	0.000044	0.027746	0.002103	0.001160	0.000059	0.022	18.76	0.30	0.023	18.82	0.30	1.2	1.26	
226-1-10	192	126	0.970	0.002983	0.000037	0.020326	0.001225	0.000933	0.000026	-0.001	19.12	0.27	0.003	19.14	0.25	1.2	1.43	
226-1-11	322	74	0.707	0.002965	0.000039	0.029008	0.002292	0.001103	0.000043	0.018	18.66	0.26	0.027	18.57	0.27	1.3	1.20	
226-1-12	151	53	0.615	0.003097	0.000039	0.030249	0.001989	0.001158	0.000048	0.019	19.51	0.27	0.027	19.40	0.26	1.1	1.11	
226-1-13	193	127	0.664	0.003039	0.000044	0.020599	0.001228	0.000978	0.000036	0.000	19.45	0.29	0.003	19.50	0.29	1.3	1.61	
226-1-14	160	74	0.648	0.003434	0.000059	0.051430	0.005267	0.001826	0.000157	0.055	20.76	0.42	0.068	20.60	0.44	1.9	2.30	**yes; a**
226-1-15	193	48	0.698	0.003100	0.000056	0.034179	0.002817	0.001209	0.000050	0.027	19.32	0.37	0.037	19.22	0.37	1.2	1.43	
226-1-16	157	83	0.587	0.003048	0.000038	0.023679	0.001749	0.001122	0.000041	0.015	19.24	0.26	0.011	19.40	0.26	1.2	1.21	
226-1-17	136	74	0.690	0.003053	0.000038	0.020783	0.001425	0.000865	0.000035	-0.011	19.78	0.26	0.003	19.59	0.26	1.1	1.21	
226-1-18	141	82	0.656	0.002939	0.000079	0.022112	0.001940	0.000971	0.000049	0.003	18.79	0.52	0.009	18.75	0.51	1.9	2.44	**yes; a**
226-1-19	105	44	0.444	0.003092	0.000053	0.029593	0.002612	0.001098	0.000066	0.009	19.64	0.35	0.025	19.40	0.36	1.2	1.29	
226-1-20	146	87	0.701	0.003009	0.000055	0.032648	0.003357	0.001160	0.000079	0.022	18.77	0.38	0.035	18.69	0.38	1.6	1.70	
226-1-21	147	101	0.664	0.002967	0.000042	0.023554	0.001789	0.001039	0.000042	0.012	18.70	0.29	0.012	18.87	0.28	1.2	1.38	
226-1-22	307	108	0.662	0.003084	0.000035	0.024454	0.001552	0.000943	0.000032	-0.004	19.76	0.24	0.012	19.61	0.23	1.2	1.28	
226-1-23'	166	72	0.573	0.003053	0.000038	0.023081	0.001639	0.000935	0.000038	-0.003	19.58	0.25	0.009	19.47	0.25	1.1	1.01	
226-1-24	201	108	0.561	0.003055	0.000038	0.020086	0.001356	0.000894	0.000040	-0.007	19.67	0.26	0.001	19.64	0.25	1.1	1.13	
226-1-25	173	109	0.545	0.002937	0.000035	0.018980	0.001570	0.000963	0.000029	0.003	18.70	0.23	0.001	18.89	0.24	1.1	1.03	
226-1-26	147	79	0.561	0.003102	0.000039	0.024431	0.001523	0.000892	0.000035	-0.008	20.00	0.27	0.012	19.73	0.26	1.2	1.31	
226-1-27	213	76	0.647	0.003011	0.000044	0.027442	0.002147	0.001127	0.000050	0.019	18.83	0.30	0.022	18.97	0.30	1.0	0.92	
226-1-28	182	124	0.730	0.003004	0.000032	0.021537	0.001169	0.000911	0.000027	-0.004	19.22	0.22	0.006	19.22	0.21	1.1	1.18	
226-1-29	197	110	0.557	0.003032	0.000041	0.024439	0.001801	0.001001	0.000042	0.004	19.29	0.27	0.013	19.26	0.28	1.2	1.27	
226-1-30	135	52	0.483	0.003175	0.000054	0.033448	0.003144	0.001083	0.000076	0.004	20.20	0.36	0.033	19.76	0.37	1.1	1.01	
226-1-31	203	119	0.603	0.003216	0.000037	0.021703	0.001216	0.001090	0.000033	0.008	20.37	0.25	0.003	20.64	0.24	1.2	1.41	
226-1-32	228	70	0.644	0.003100	0.000040	0.025770	0.002314	0.001186	0.000053	0.020	19.35	0.27	0.015	19.65	0.28	1.2	1.12	

Notes:

a : Date excluded based on the spot MSWD being larger than 2

b : Date excluded based on the ratio between the observed error to expected error being larger than 3

c : Date excluded based on the plot of probability distribution; inherited grain

d : Date excluded based on the plot of probability distribution; possibly due to Pb loss

APPENDIX 7-3

Summary of the U-Th-Pb zircon dates analysed by ELA-ICP-MS

Magerang-Imang Andesite Sample No. 123226-session2

Sample No.	P(ppm)	U(ppm)	$^{232}Th/^{238}U$	Uncorrected $^{206}Pb/^{238}U$ ratio	±	Uncorrected $^{207}Pb/^{235}U$ ratio	±	Uncorrected $^{208}Pb/^{232}Th$ ratio	±	f208	^{208}Pb corrected $^{206}Pb/^{238}U$ Date (Ma)	Observed Error (± 1s.e.)	f207	^{207}Pb corrected $^{206}Pb/^{238}U$ Date (Ma)	Observed Error (± 1s.e.)	Obs/Exp Error	Spot MSWD	Exclude?
226-2-01	209.211	51.368	0.54	0.002991	0.000058	0.020653	0.002828	0.001024	0.000048	0.007	18.93	0.38	0.005	19.16	0.41	1.4	1.58	
226-2-02	239.636	72.471	0.58	0.003014	0.000028	0.021328	0.001260	0.000993	0.000027	0.002	19.16	0.19	0.006	19.28	0.19	1.3	1.42	
226-2-03	213.199	53.754	0.62	0.003283	0.000044	0.043050	0.003312	0.001717	0.000098	0.060	19.61	0.31	0.060	19.86	0.32	1.6	1.64	
226-2-04	195.817	51.254	0.67	0.003208	0.000036	0.034104	0.002281	0.001217	0.000053	0.021	19.95	0.26	0.038	19.87	0.26	1.4	1.60	
226-2-05	206.493	39.718	0.73	0.003691	0.000088	0.120417	0.017107	0.002331	0.000177	0.124	20.06	0.69	0.234	18.20	1.06	2.0	1.11	
226-2-06	215.562	61.672	0.56	0.002970	0.000049	0.023403	0.001733	0.001035	0.000058	0.010	18.73	0.34	0.013	18.87	0.33	1.4	1.60	
226-2-07	218.571	51.966	0.54	0.003098	0.000042	0.031963	0.002024	0.001193	0.000051	0.020	19.34	0.28	0.035	19.24	0.28	1.5	1.84	
226-2-08	299.614	114.520	0.80	0.003022	0.000029	0.027116	0.001806	0.001118	0.000030	0.023	18.78	0.23	0.023	19.01	0.21	1.1	1.03	
226-2-09	198.425	48.882	0.58	0.003069	0.000032	0.024206	0.001747	0.000929	0.000036	-0.006	19.73	0.22	0.013	19.49	0.23	1.2	1.14	
226-2-10	271.399	81.263	0.63	0.003154	0.000044	0.027903	0.002033	0.001064	0.000041	0.007	19.95	0.30	0.022	19.86	0.30	1.3	1.49	
226-2-11	236.964	64.602	0.51	0.003025	0.000034	0.021703	0.001585	0.001040	0.000034	0.007	19.18	0.23	0.007	19.34	0.23	1.3	1.48	
226-2-12	154.413	35.811	0.43	0.003300	0.000049	0.044033	0.003378	0.001628	0.000099	0.036	20.30	0.33	0.062	19.92	0.35	1.4	1.66	
226-2-13	259.455	101.095	0.46	0.003009	0.000022	0.024754	0.000950	0.001129	0.000027	0.015	18.97	0.15	0.016	19.05	0.15	1.2	1.27	
226-2-14	287.595	79.264	0.64	0.003092	0.000024	0.021297	0.001202	0.000991	0.000024	0.002	19.71	0.16	0.004	19.82	0.17	1.1	1.05	
226-2-15	341.507	324.334	0.54	0.009300	0.000037	0.065618	0.001232	0.003062	0.000041	0.003	59.00	0.25	0.005	59.38	0.25	1.0	0.97	**yes; c**
226-2-16	221.393	49.929	0.70	0.003028	0.000081	0.019742	0.002567	0.000993	0.000067	0.007	19.22	0.56	0.001	19.47	0.54	1.5	1.95	
226-2-17	267.526	68.467	0.62	0.003142	0.000049	0.034268	0.003562	0.001234	0.000074	0.025	19.51	0.36	0.040	19.41	0.37	1.2	1.07	
226-2-18	389.509	137.603	0.85	0.002963	0.000024	0.020830	0.000751	0.000982	0.000013	0.006	18.73	0.16	0.006	18.96	0.16	1.4	1.83	
226-2-19	132.252	783.882	0.13	0.016192	0.000080	0.107142	0.000873	0.005585	0.000068	0.002	103.10	0.51	0.000	103.56	0.51	1.1	1.16	**yes; c**
226-2-20	600.149	278.312	0.52	0.003033	0.000024	0.023394	0.001151	0.001055	0.000055	0.007	19.27	0.18	0.012	19.30	0.17	1.1	1.01	
226-2-21	238.559	60.708	0.50	0.003126	0.000035	0.019723	0.001083	0.000952	0.000032	-0.003	20.09	0.23	-0.001	20.14	0.23	1.3	1.79	
226-2-22	656.544	251.609	0.64	0.010541	0.000044	0.072819	0.001855	0.003413	0.000059	0.004	66.98	0.43	0.003	67.37	0.30	1.9	3.22	**yes; c**
226-2-23	306.198	115.871	0.83	0.003056	0.000026	0.018625	0.001251	0.000911	0.000023	-0.009	19.64	0.18	-0.003	19.72	0.18	1.2	1.13	
226-2-24	429.231	124.782	0.79	0.003138	0.000031	0.019823	0.000827	0.000976	0.000025	-0.003	20.06	0.22	-0.001	20.21	0.21	1.3	1.60	
226-2-25	253.035	71.544	0.60	0.003074	0.000033	0.021937	0.001101	0.000984	0.000026	0.001	19.66	0.22	0.007	19.66	0.22	1.4	1.79	
226-2-26	245.011	93.716	0.94	0.003043	0.000026	0.023824	0.001210	0.000942	0.000023	-0.005	19.52	0.22	0.013	19.34	0.18	1.3	1.48	

Notes:

a : Date excluded based on the spot MSWD being larger than 2

b : Date excluded based on the ratio between the observed error to expected error being larger than 3

c : Date excluded based on the plot of probability distribution; inherited grain

d : Date excluded based on the plot of probability distribution; possibly due to Pb loss

APPENDIX 7-4

Summary of the U-Th-Pb zircon dates analysed by ELA-ICP-MS

Nakan Andesite Sample No. 123187

Sample No.	P(ppm)	U(ppm)	$^{232}Th/^{238}U$	Uncorrected $^{206}Pb/^{238}U$ ratio	±	Uncorrected $^{207}Pb/^{235}U$ ratio	±	Uncorrected $^{208}Pb/^{232}Th$ ratio	±	f208	^{208}Pb corrected $^{206}Pb/^{238}U$ Date (Ma)	Observed Error (± 1s.e.)	f207	^{207}Pb corrected $^{206}Pb/^{238}U$ Date (Ma)	Observed Error (± 1s.e.)	Obs/Exp Error	Spot MSWD	Exclude?
187-01	237	114	0.669	0.003213	0.000024	0.025917	0.000580	0.001158	0.000017	0.014	20.29	0.15	0.013	20.41	0.15	1.5	2.14	yes; a
187-02	225	108	0.616	0.003111	0.000022	0.026458	0.000697	0.001138	0.000022	0.014	19.67	0.15	0.017	19.69	0.14	1.3	1.55	
187-03	178	76	0.520	0.003203	0.000033	0.026433	0.001133	0.001224	0.000037	0.015	20.24	0.22	0.015	20.32	0.22	1.5	1.73	
187-04	192	71	0.489	0.003240	0.000030	0.030234	0.001170	0.001277	0.000038	0.018	20.42	0.20	0.023	20.37	0.20	1.3	1.66	
187-05	178	122	0.741	0.003157	0.000021	0.027273	0.001017	0.001114	0.000030	0.012	19.99	0.15	0.018	19.96	0.14	1.2	1.43	
187-06	192	148	0.744	0.003035	0.000019	0.021411	0.000665	0.000942	0.000012	-0.003	19.54	0.13	0.005	19.44	0.13	1.2	1.39	
187-07	184	139	0.710	0.003067	0.000020	0.022630	0.000726	0.000972	0.000015	-0.001	19.71	0.14	0.008	19.59	0.13	1.3	1.48	
187-08	183	56	0.385	0.003192	0.000027	0.024956	0.001161	0.001158	0.000044	0.008	20.36	0.18	0.011	20.32	0.18	1.1	1.05	
187-09	167	52	0.362	0.003169	0.000033	0.025406	0.001397	0.001236	0.000053	0.012	20.13	0.22	0.013	20.14	0.22	1.2	1.37	
187-10	169	82	0.529	0.003117	0.000024	0.025132	0.001221	0.001041	0.000031	0.004	19.95	0.16	0.013	19.80	0.16	1.2	1.20	
187-11	187	84	0.566	0.003234	0.000029	0.024416	0.000985	0.001091	0.000027	0.005	20.68	0.19	0.009	20.62	0.19	1.3	1.61	
187-12	187	76	0.447	0.003151	0.000024	0.023210	0.001000	0.001113	0.000032	0.008	20.11	0.16	0.008	20.13	0.16	1.0	0.98	
187-13	174	60	0.424	0.003223	0.000032	0.023238	0.001212	0.001113	0.000046	0.005	20.62	0.21	0.006	20.61	0.21	1.2	1.25	
187-14	149	115	0.739	0.003127	0.000030	0.021842	0.000852	0.000996	0.000032	-0.002	20.13	0.25	0.005	20.03	0.20	1.6	2.45	yes; a
187-15	171	75	0.421	0.003110	0.000024	0.023607	0.001238	0.001070	0.000030	0.005	19.90	0.16	0.009	19.83	0.16	1.0	0.95	
187-16	171	90	0.525	0.003149	0.000035	0.023192	0.001303	0.001112	0.000040	0.009	20.08	0.24	0.008	20.12	0.23	1.3	1.49	
187-17	150	79	0.440	0.003249	0.000035	0.020923	0.001299	0.001167	0.000042	0.009	20.72	0.23	0.000	20.90	0.23	1.1	1.17	
187-18	212	81	0.401	0.003134	0.000031	0.022713	0.001022	0.001069	0.000037	0.004	20.08	0.20	0.007	20.04	0.20	1.2	1.30	
187-19	163	126	0.684	0.003108	0.000023	0.020681	0.000850	0.001013	0.000020	0.002	19.97	0.17	0.002	19.96	0.15	1.2	1.24	
187-20	276	200	0.771	0.003168	0.000024	0.021292	0.000759	0.001040	0.000016	0.004	20.32	0.16	0.003	20.34	0.16	1.4	1.78	
187-21	250	108	0.477	0.003126	0.000028	0.019114	0.000874	0.001068	0.000030	0.005	19.93	0.19	-0.002	20.16	0.19	1.3	1.47	
187-22	219	126	0.552	0.003132	0.000024	0.021746	0.000835	0.000953	0.000024	-0.003	20.24	0.16	0.004	20.07	0.16	1.1	1.20	
187-23	141	52	0.381	0.003131	0.000039	0.026802	0.001581	0.001081	0.000060	0.005	20.05	0.26	0.017	19.81	0.26	1.2	1.25	
187-24	150	64	0.414	0.003168	0.000029	0.025606	0.001573	0.001110	0.000050	0.006	20.27	0.20	0.013	20.12	0.20	1.0	0.91	
187-25	211	187	0.651	0.003032	0.000018	0.020439	0.000698	0.000960	0.000016	-0.001	19.55	0.12	0.003	19.46	0.12	1.1	1.05	
187-26	190	111	0.553	0.003128	0.000038	0.023503	0.001078	0.001052	0.000028	0.005	20.04	0.26	0.009	19.96	0.25	1.4	1.85	
187-27	205	182	0.627	0.003173	0.000022	0.021437	0.000657	0.001077	0.000018	0.007	20.30	0.15	0.003	20.37	0.14	1.2	1.21	
187-28	161	82	0.473	0.003256	0.000033	0.023452	0.001126	0.001108	0.000041	0.005	20.86	0.22	0.006	20.82	0.22	1.2	1.26	
187-29	157	146	0.558	0.003102	0.000022	0.022267	0.000769	0.001103	0.000028	0.010	19.78	0.15	0.006	19.84	0.14	1.1	1.22	
187-30	169	122	0.573	0.003141	0.000024	0.020842	0.000978	0.000993	0.000024	0.000	20.25	0.16	0.002	20.18	0.16	1.1	1.08	
187-31	227	175	0.787	0.003069	0.000023	0.023478	0.000964	0.000969	0.000026	-0.003	19.83	0.16	0.010	19.56	0.15	1.1	1.06	
187-32	166	80	0.476	0.003335	0.000038	0.026468	0.001353	0.001165	0.000056	0.007	21.33	0.26	0.012	21.20	0.25	1.1	1.19	

Notes:

a : Date excluded based on the spot MSWD being larger than 2

b : Date excluded based on the ratio between the observed error to expected error being larger than 3

c : Date excluded based on the plot of probability distribution; inherited grain

d : Date excluded based on the plot of probability distribution; possibly due to Pb loss

APPENDIX 7-5

Summary of the U-Th-Pb zircon dates analysed by ELA-ICP-MS

Kelian Central Andesite Sample No. 123200-session1

Sample No.	P(ppm)	U(ppm)	$^{232}Th/^{238}U$	Uncorrected $^{206}Pb/^{238}U$ ratio	±	Uncorrected $^{207}Pb/^{235}U$ ratio	±	Uncorrected $^{208}Pb/^{232}Th$ ratio	±	f208	^{208}Pb corrected $^{206}Pb/^{238}U$ Date (Ma)	Observed Error (± 1s.e.)	f207	^{207}Pb corrected $^{206}Pb/^{238}U$ Date (Ma)	Observed Error (± 1s.e.)	Obs/Exp Error	Spot MSWD	Population	exclude?
200-1-01	154	35	0.432	0.003596	0.000063	0.057413	0.003749	0.002428	0.000124	0.067	21.43	0.40	0.076	21.39	0.42	2.2	3.27		yes, a
200-1-02	153	43	0.383	0.003332	0.000029	0.036575	0.001503	0.001770	0.000051	0.039	20.50	0.19	0.036	20.67	0.20	1.2	1.33	3	
200-1-03	168	70	0.494	0.003347	0.000025	0.027070	0.000816	0.001294	0.000028	0.016	21.10	0.16	0.013	21.25	0.16	1.2	1.33	3	
200-1-04	158	92	0.621	0.003097	0.000020	0.025136	0.000690	0.001076	0.000019	0.009	19.68	0.13	0.014	19.66	0.13	1.1	1.13	1	
200-1-05	151	65	0.375	0.003344	0.000028	0.039762	0.001390	0.001858	0.000049	0.042	20.56	0.18	0.043	20.59	0.19	1.2	1.38	2	
200-1-06	135	61	0.526	0.003235	0.000028	0.025366	0.001117	0.001153	0.000031	0.011	20.56	0.19	0.011	20.58	0.19	1.2	1.36	2	
200-1-07	104	35	0.361	0.003317	0.000034	0.031466	0.001831	0.001219	0.000062	0.008	21.15	0.23	0.024	20.83	0.23	1.1	1.03	3	
200-1-08	171	119	0.760	0.003061	0.000022	0.024845	0.000716	0.001070	0.000019	0.012	19.40	0.15	0.014	19.44	0.14	1.4	1.71	1	
200-1-09	245	138	0.609	0.003201	0.000017	0.022731	0.000651	0.001015	0.000017	0.000	20.57	0.12	0.006	20.49	0.12	1.1	1.06	2	
200-1-10	111	41	0.395	0.003172	0.000045	0.035547	0.002416	0.001569	0.000097	0.033	19.72	0.30	0.038	19.64	0.30	1.4	1.64	1	
200-1-11	175	87	0.370	0.003218	0.000022	0.024414	0.000888	0.001233	0.000032	0.012	20.44	0.15	0.009	20.52	0.15	1.1	1.14	2	
200-1-12	154	76	0.453	0.003236	0.000024	0.027065	0.001055	0.001216	0.000032	0.013	20.54	0.16	0.016	20.50	0.16	1.1	0.99	2	
200-1-13	188	99	0.594	0.003103	0.000023	0.023385	0.000864	0.001017	0.000023	0.003	19.87	0.15	0.009	19.79	0.15	1.2	1.26	1	
200-1-14	173	112	0.531	0.003193	0.000025	0.022720	0.000756	0.001102	0.000027	0.007	20.39	0.16	0.006	20.44	0.16	1.3	1.58	2	
200-1-15	180	52	0.470	0.003296	0.000036	0.026547	0.001481	0.001193	0.000048	0.010	20.98	0.24	0.013	20.94	0.24	1.2	1.11	3	
200-1-16	175	68	0.513	0.003320	0.000036	0.040812	0.002724	0.001733	0.000114	0.043	20.43	0.26	0.047	20.37	0.26	1.6	1.66	2	
200-1-17	130	60	0.372	0.003206	0.000033	0.021067	0.001334	0.001201	0.000055	0.010	20.40	0.22	0.001	20.60	0.22	1.1	1.13	2	
200-1-18	138	67	0.390	0.003224	0.000034	0.024078	0.001519	0.001176	0.000043	0.009	20.56	0.22	0.008	20.57	0.23	1.1	1.12	2	
200-1-19	133	51	0.522	0.003298	0.000033	0.029179	0.001761	0.001123	0.000045	0.006	21.09	0.22	0.019	20.81	0.23	1.1	1.02	3	
200-1-20	134	58	0.557	0.003141	0.000033	0.024454	0.001195	0.001028	0.000037	0.003	20.15	0.22	0.011	20.00	0.22	1.2	1.32	1	
200-1-21	135	72	0.452	0.003208	0.000039	0.020160	0.001133	0.001026	0.000038	0.001	20.63	0.25	-0.001	20.67	0.26	1.4	1.68	3	
200-1-22	143	61	0.504	0.003135	0.000030	0.021390	0.001092	0.001016	0.000036	0.002	20.14	0.20	0.003	20.11	0.20	1.1	1.04	2	
200-1-23	157	99	0.500	0.003105	0.000027	0.021207	0.000918	0.000978	0.000027	0.000	20.00	0.18	0.003	19.92	0.18	1.1	1.24	1	
200-1-24	187	139	0.605	0.003193	0.000023	0.020366	0.000819	0.001079	0.000023	0.006	20.44	0.16	0.000	20.56	0.16	1.2	1.40	2	
200-1-25	153	70	0.540	0.003066	0.000037	0.023548	0.001428	0.000989	0.000039	0.002	19.70	0.25	0.010	19.53	0.25	1.3	1.48	1	
200-1-26	151	52	0.462	0.003162	0.000039	0.024460	0.001352	0.001308	0.000044	0.022	19.92	0.26	0.011	20.14	0.26	1.2	1.38	2	
200-1-27	205	174	0.661	0.003095	0.000020	0.021910	0.000633	0.000956	0.000018	-0.003	20.00	0.14	0.005	19.81	0.13	1.1	1.24	1	
200-1-28	154	100	0.515	0.003110	0.000025	0.026270	0.001245	0.001397	0.000052	0.030	19.45	0.17	0.016	19.70	0.17	1.0	1.02	1	
200-1-29	187	62	0.388	0.003161	0.000041	0.027424	0.001546	0.001147	0.000043	0.009	20.18	0.27	0.018	19.98	0.27	1.3	1.61	1	
200-1-30	150	72	0.407	0.003244	0.000036	0.025864	0.001435	0.001346	0.000050	0.019	20.50	0.24	0.012	20.62	0.24	1.2	1.42	2	
200-1-31	164	112	0.627	0.003249	0.000028	0.033203	0.001152	0.001414	0.000028	0.037	20.18	0.18	0.030	20.28	0.18	1.0	1.05	2	
200-1-32	125	57	0.554	0.003244	0.000041	0.025616	0.001833	0.001224	0.000050	0.017	20.56	0.28	0.012	20.63	0.28	1.1	1.12	2	

Notes:

a : Date excluded based on the spot MSWD being larger than 2

b : Date excluded based on the ratio between the observed error to expected error being larger than 3

c : Date excluded based on the plot of probability distribution; inherited grain

d : Date excluded based on the plot of probability distribution; possibly due to Pb loss

APPENDIX 7-6

Summary of the U-Th-Pb zircon dates analysed by ELA-ICP-MS

Kelian Central Andesite Sample No. 123200-session2

Sample No.	P(ppm)	U(ppm)	$^{232}Th/^{238}U$	Uncorrected $^{206}Pb/^{238}U$ ratio	±	Uncorrected $^{207}Pb/^{235}U$ ratio	±	Uncorrected $^{208}Pb/^{232}Th$ ratio	±	f208	^{208}Pb corrected $^{206}Pb/^{238}U$ Date (Ma)	Observed Error (± 1s.e.)	f207	^{207}Pb corrected $^{206}Pb/^{238}U$ Date (Ma)	Observed Error (± 1s.e.)	Obs/Exp Error	Spot MSWD	Population	exclude?
200-2-01	99	47	0.626	0.003183	0.000032	0.019761	0.001211	0.001074	0.000035	0.007	20.42	0.22	-0.002	20.52	0.22	1.1	1.11	2	
200-2-02	305	241	0.975	0.002980	0.000028	0.027633	0.002061	0.001051	0.000048	0.016	18.95	0.21	0.023	18.75	0.20	1.5	1.86		yes; d
200-2-03	144	80	0.567	0.003139	0.000041	0.027175	0.001323	0.001122	0.000029	0.011	19.99	0.27	0.018	19.85	0.27	1.7	1.95	1	
200-2-04	135	51	0.389	0.003118	0.000034	0.021734	0.001361	0.001103	0.000043	0.007	19.93	0.23	0.005	19.98	0.23	1.2	1.18	1	
200-2-05	133	48	0.462	0.003414	0.000044	0.031949	0.002256	0.001757	0.000083	0.042	21.04	0.29	0.023	21.46	0.30	1.2	1.36	3	
200-2-06	86	28	0.411	0.003244	0.000045	0.042610	0.002659	0.001935	0.000097	0.055	19.72	0.30	0.053	19.77	0.30	1.0	0.95	1	
200-2-07	146	54	0.455	0.003093	0.000032	0.025470	0.001690	0.001194	0.000051	0.016	19.57	0.22	0.015	19.62	0.22	1.0	0.97	1	
200-2-08	165	63	0.524	0.003285	0.000034	0.021163	0.001189	0.001124	0.000039	0.007	20.97	0.23	0.000	21.14	0.23	1.1	1.21	3	
200-2-09	134	60	0.562	0.003470	0.000048	0.058718	0.004599	0.002209	0.000137	0.089	20.30	0.37	0.083	20.47	0.36	1.6	1.91	2	
200-2-10	112	47	0.394	0.003213	0.000041	0.024065	0.001512	0.001054	0.000054	0.003	20.61	0.27	0.009	20.50	0.27	1.2	1.36	2	
200-2-11	123	34	0.379	0.003244	0.000054	0.034394	0.002591	0.001601	0.000109	0.032	20.17	0.36	0.033	20.19	0.36	1.2	1.32	2	
200-2-12	140	71	0.415	0.003224	0.000031	0.025775	0.001426	0.001102	0.000044	0.006	20.61	0.21	0.013	20.49	0.21	1.1	1.10	2	
200-2-13	141	60	0.566	0.003132	0.000048	0.029531	0.001733	0.001147	0.000052	0.014	19.81	0.32	0.024	19.68	0.31	1.3	1.69	1	
200-2-14	119	47	0.437	0.003417	0.000051	0.031263	0.002402	0.001364	0.000069	0.018	21.54	0.34	0.022	21.52	0.34	1.1	1.23	3	
200-2-15	151	91	0.520	0.003344	0.000030	0.025471	0.001042	0.001239	0.000040	0.012	21.18	0.20	0.010	21.31	0.19	1.1	1.11	3	
200-2-16	151	55	0.461	0.003286	0.000034	0.023169	0.001280	0.001110	0.000046	0.006	20.97	0.23	0.005	21.04	0.23	1.0	1.02	3	
200-2-17	166	62	0.421	0.003197	0.000033	0.024610	0.001808	0.001160	0.000051	0.010	20.31	0.23	0.010	20.37	0.23	1.1	1.10	2	
200-2-18	160	101	0.619	0.003031	0.000024	0.022312	0.001231	0.000971	0.000026	0.001	19.42	0.16	0.008	19.36	0.16	1.0	0.90	1	
200-2-19	130	68	0.343	0.003093	0.000037	0.024270	0.001421	0.001070	0.000056	0.005	19.76	0.25	0.011	19.68	0.25	1.1	1.16	1	
200-2-20	177	108	0.584	0.003351	0.000056	0.040272	0.003370	0.001823	0.000151	0.052	20.40	0.38	0.044	20.61	0.38	2.1	3.20		yes; a
200-2-21	138	53	0.364	0.003157	0.000044	0.027623	0.001930	0.000937	0.000055	-0.003	20.34	0.29	0.019	19.95	0.29	1.1	1.38	1	
200-2-22	133	65	0.466	0.003068	0.000039	0.023023	0.001416	0.001033	0.000048	0.004	19.61	0.26	0.009	19.58	0.26	1.2	1.31	1	
200-2-23	92	47	0.384	0.003095	0.000047	0.029542	0.002309	0.001303	0.000082	0.020	19.40	0.31	0.025	19.43	0.32	1.1	1.17	1	
200-2-24	202	162	0.644	0.003179	0.000028	0.021700	0.000830	0.001068	0.000024	0.006	20.17	0.18	0.003	20.39	0.18	1.2	1.35	2	
200-2-25	148	79	0.431	0.003224	0.000038	0.026717	0.001860	0.001069	0.000041	0.004	20.54	0.25	0.015	20.44	0.26	1.1	1.10	2	
200-2-26	125	54	0.351	0.003417	0.000104	0.037575	0.004060	0.001083	0.000148	0.000	21.86	0.68	0.036	21.19	0.67	1.2	1.50	3	
200-2-27	231	291	0.893	0.003304	0.000031	0.028414	0.001209	0.001126	0.000021	0.011	20.73	0.21	0.017	20.89	0.21	1.2	1.42	3	
200-2-28	212	193	0.607	0.002934	0.000024	0.023988	0.000990	0.000975	0.000025	0.004	18.65	0.16	0.014	18.62	0.16	1.1	1.14		yes; d
200-2-29	141	100	0.400	0.003127	0.000039	0.023577	0.001370	0.001140	0.000047	0.008	19.84	0.25	0.009	19.95	0.26	1.3	1.50	1	
200-2-30	144	59	0.313	0.003129	0.000043	0.030762	0.002122	0.001215	0.000063	0.011	19.82	0.28	0.027	19.59	0.29	1.1	1.12	1	
200-2-31	184	184	0.662	0.003022	0.000035	0.021717	0.001327	0.000974	0.000029	0.002	19.24	0.24	0.006	19.33	0.23	1.2	1.28	1	
200-2-32	151	82	0.424	0.003263	0.000032	0.025047	0.001462	0.001085	0.000042	0.003	20.82	0.21	0.010	20.79	0.21	1.0	0.88	3	

Notes:

- **a :** Date excluded based on the spot MSWD being larger than 2
- **b :** Date excluded based on the ratio between the observed error to expected error being larger than 3
- **c :** Date excluded based on the plot of probability distribution; inherited grain
- **d :** Date excluded based on the plot of probability distribution; possibly due to Pb loss

APPENDIX 7.7

Summary of the U-Th-Pb zircon dates analysed by ELA-ICP-MS

Kelian Runcing Rhyolite Sample No. 123218

Sample No.	P(ppm)	U(ppm)	$^{232}Th/^{238}U$	Uncorrected $^{206}Pb/^{238}U$ ratio	±	Uncorrected $^{207}Pb/^{235}U$ ratio	±	Uncorrected $^{208}Pb/^{232}Th$ ratio	±	f208	^{208}Pb corrected $^{206}Pb/^{238}U$ Date (Ma)	Observed Error (± 1s.e.)	f207	^{207}Pb corrected $^{206}Pb/^{238}U$ Date (Ma)	Observed Error (± 1s.e.)	Obs/Exp Error	Spot MSWD	Population	exclude?
218-01	599	188	0.787	0.003298	0.000015	0.024695	0.000471	0.001139	0.000016	0.010	20.88	0.11	0.009	21.04	0.10	1.2	1.45	3	
218-02	888	219	0.442	0.003266	0.000017	0.025396	0.000536	0.001184	0.000022	0.009	20.75	0.11	0.011	20.79	0.11	1.1	1.31	3	
218-03	858	215	0.544	0.003047	0.000017	0.023066	0.000501	0.001025	0.000012	0.005	19.46	0.12	0.009	19.43	0.11	1.1	1.23	1	
218-04	304	69	0.680	0.003366	0.000032	0.033321	0.001480	0.001330	0.000036	0.026	21.01	0.22	0.028	21.06	0.22	1.4	1.86	3	
218-05	357	65	0.504	0.003862	0.000075	0.039120	0.002406	0.001669	0.000116	0.023	24.21	0.48	0.029	24.12	0.48	2.1	2.89		yes; c
218-06	758	146	0.551	0.003655	0.000025	0.035798	0.001476	0.001412	0.000039	0.019	23.01	0.19	0.027	22.89	0.17	1.3	1.34		yes; c
218-07	1151	387	0.887	0.003017	0.000014	0.022201	0.000456	0.000967	0.000010	0.001	19.34	0.15	0.008	19.27	0.09	1.4	1.89	1	
218-08	1036	325	0.766	0.003003	0.000013	0.021988	0.000383	0.000969	0.000010	0.001	19.26	0.11	0.007	19.19	0.08	1.2	1.43	1	
218-09	1162	362	0.696	0.003109	0.000020	0.024460	0.000580	0.001064	0.000013	0.007	19.83	0.14	0.012	19.78	0.13	1.5	2.37	2	
218-10	1026	247	0.426	0.003196	0.000018	0.022407	0.000504	0.001100	0.000016	0.005	20.45	0.13	0.005	20.47	0.12	1.5	1.90		yes; c
218-11	635	271	0.829	0.003259	0.000019	0.024121	0.000557	0.001045	0.000025	0.001	20.93	0.14	0.008	20.81	0.12	1.4	1.75	3	
218-12	1136	414	1.364	0.003053	0.000014	0.021787	0.000391	0.000973	0.000007	0.000	19.59	0.10	0.006	19.54	0.09	1.3	1.71	1	
218-13	1085	396	1.362	0.003016	0.000015	0.021605	0.000385	0.000938	0.000008	-0.005	19.48	0.11	0.006	19.30	0.10	1.4	1.94	1	
218-14	1132	406	1.373	0.003021	0.000023	0.021694	0.000528	0.000978	0.000008	0.004	19.32	0.15	0.006	19.32	0.15	1.7	2.88	1	
218-15	655	263	0.936	0.003283	0.000028	0.023242	0.000577	0.001109	0.000020	0.008	20.90	0.20	0.005	21.01	0.18	2.1	3.79	3	
218-16	792	312	0.914	0.003119	0.000014	0.021675	0.000452	0.000984	0.000009	-0.001	20.08	0.10	0.004	19.99	0.09	1.2	1.17	2	
218-17	897	204	0.297	0.003304	0.000019	0.022016	0.000605	0.001043	0.000023	0.000	21.26	0.12	0.002	21.22	0.13	1.3	1.61	3	
218-18	492	119	0.412	0.003664	0.000036	0.057486	0.002779	0.002962	0.000149	0.086	21.53	0.25	0.074	21.84	0.25	1.7	2.42		yes; c
218-19	494	114	0.804	0.003356	0.000027	0.026838	0.001116	0.001120	0.000022	0.006	21.46	0.19	0.013	21.32	0.18	1.2	1.30	3	
218-20	324	86	0.909	0.003492	0.000028	0.064849	0.002279	0.001789	0.000042	0.092	20.34	0.22	0.096	20.31	0.20	1.2	1.26	2	
218-21	155	39	0.660	0.003173	0.000049	0.025201	0.002230	0.001170	0.000057	0.019	20.03	0.34	0.012	20.17	0.33	1.1	1.13	2	
218-22	1392	440	0.344	0.003212	0.000015	0.022630	0.000439	0.001076	0.000021	0.003	20.62	0.10	0.005	20.57	0.10	1.3	1.73		yes; c
218-23	523	207	0.655	0.003268	0.000025	0.023701	0.000659	0.001103	0.000019	0.006	20.90	0.17	0.007	20.89	0.16	1.4	1.96	3	
218-24	1084	493	1.668	0.003126	0.000012	0.020793	0.000384	0.000972	0.000005	-0.007	20.27	0.10	0.002	20.08	0.08	1.2	1.38	2	
218-25	45738	218	0.147	0.056679	0.002518	2.715317	0.121482	0.350732	0.022332	0.312	36.40	2.51	0.325	241.89	10.57	6.4	93.08		yes; c
218-26	977	289	0.805	0.003102	0.000026	0.029738	0.000943	0.001190	0.000030	0.020	19.59	0.21	0.025	19.46	0.17	1.9	3.57	1	
218-27	936	285	0.638	0.003052	0.000024	0.027829	0.000760	0.001127	0.000018	0.016	19.35	0.16	0.022	19.22	0.15	1.5	1.97	1	
218-28	322	116	0.541	0.003808	0.000043	0.035299	0.001173	0.001615	0.000036	0.028	23.84	0.28	0.023	23.95	0.28	1.6	2.52		yes; c
218-29	1242	486	1.233	0.003154	0.000019	0.028432	0.000717	0.001018	0.000011	0.003	20.28	0.16	0.021	19.88	0.12	1.3	1.55	2	
218-30	1372	579	1.540	0.003035	0.000021	0.025243	0.000594	0.000970	0.000009	0.001	19.57	0.16	0.015	19.24	0.13	1.5	2.21	1	
218-31	937	322	0.507	0.003085	0.000021	0.027480	0.000818	0.001175	0.000021	0.015	19.58	0.14	0.020	19.47	0.14	1.3	1.41	1	
218-32	1427	677	0.270	0.069414	0.002950	7.678004	0.349709	0.533978	0.032711	0.829	40.65	8.04	0.825	77.71	7.16	2.0	20.50		yes; c
218-33	856	311	0.425	0.003105	0.000023	0.021770	0.000605	0.001044	0.000018	0.003	19.93	0.16	0.005	19.89	0.15	1.7	2.19	2	

Notes:

- **a :** Date excluded based on the spot MSWD being larger than 4
- **b :** Date excluded based on the ratio between the observed error to expected error being larger than 3
- **c :** Date excluded based on the plot of probability distribution; inherited grain
- **d :** Date excluded based on the plot of probability distribution; possibly due to Pb loss

APPENDIX 7.8

Summary of the U-Th-Pb zircon dates analysed by ELA-ICP-MS

Kelian Mine Tuff Sample No. 123366

Sample No.	P(ppm)	U(ppm)	$^{232}Th/^{238}U$	Uncorrected $^{206}Pb/^{238}U$ ratio	±	Uncorrected $^{207}Pb/^{235}U$ ratio	±	Uncorrected $^{208}Pb/^{232}Th$ ratio	±	f208	^{208}Pb corrected $^{206}Pb/^{238}U$ Date (Ma)	Observed Error (± 1s.e.)	f207	^{207}Pb corrected $^{206}Pb/^{238}U$ Date (Ma)	Observed Error (± 1s.e.)	Obs/Exp Error	Spot MSWD	Population	exclude?
366-01	1145	1119	0.512	0.011017	0.000073	0.068802	0.000734	0.003408	0.000035	-0.002	70.41	0.47	-0.003	70.82	0.47	1.0	0.99	1	
366-02	295	259	0.636	0.011309	0.000056	0.130138	0.002762	0.004922	0.000054	0.040	68.41	0.37	0.044	69.30	0.38	1.5	2.07	1	
366-03	746	309	0.380	0.011097	0.000055	0.106211	0.002488	0.005279	0.000097	0.030	68.72	0.44	0.027	69.23	0.37	1.8	3.25	1	
366-04	359	88	0.861	0.013282	0.000166	0.220071	0.015121	0.006195	0.000360	0.073	76.69	1.40	0.089	77.52	1.28	2.4	3.87	2	
366-05	460	212	0.225	0.012003	0.000070	0.081144	0.001973	0.004061	0.000073	0.002	76.42	0.45	0.002	76.78	0.46	1.4	1.90	2	
366-06	564	972	0.706	0.010662	0.000059	0.072726	0.000843	0.003508	0.000022	0.005	67.19	0.38	0.003	68.20	0.38	1.1	1.16	1	
366-07	365	355	0.694	0.013517	0.000240	0.375515	0.017910	0.012535	0.000813	0.196	68.20	2.00	0.189	70.26	1.56	2.1	2.56	1	
366-08	174	218	0.859	0.069639	0.000176	0.537074	0.003730	0.021180	0.000110	-0.004	430.01	1.12	0.000	433.78	1.07	1.9	3.59		yes; c
366-09	232	184	0.648	0.011857	0.000037	0.081165	0.000987	0.003729	0.000032	-0.001	75.34	0.25	0.003	75.79	0.24	1.3	1.35	2	
366-10	284	118	0.728	0.011168	0.000046	0.069726	0.001843	0.003192	0.000054	-0.012	71.82	0.41	-0.003	71.78	0.31	0.9	0.64	1	
366-11	329	97	1.106	0.018488	0.000169	0.702194	0.022783	0.013414	0.000259	0.248	86.27	1.11	0.279	85.31	1.46	1.9	1.60		yes; c
366-12	144	301	0.383	0.297684	0.000643	4.235285	0.011502	0.087706	0.000239	0.001	1672.32	3.33	0.000	1679.57	3.20	4.0	8.83		yes; c
366-13	1312	780	0.649	0.011113	0.000069	0.099943	0.001515	0.004398	0.000056	0.027	68.84	0.44	0.022	69.69	0.44	1.3	1.73	1	
366-14	301	210	1.190	0.013487	0.000061	0.092070	0.001051	0.004211	0.000035	-0.004	84.89	0.44	0.002	86.17	0.39	1.6	2.62		yes; c
366-15	702	791	0.467	0.011188	0.000071	0.095764	0.001379	0.004405	0.000053	0.018	69.95	0.45	0.018	70.44	0.45	1.1	1.25	1	
366-16	446	602	0.424	0.010924	0.000075	0.073041	0.000819	0.003530	0.000027	0.001	69.57	0.48	0.001	69.95	0.48	1.2	1.38	1	
366-17	698	153	0.869	0.012209	0.000072	0.093287	0.002094	0.004035	0.000051	0.006	76.83	0.47	0.010	77.48	0.47	2.0	3.86	2	
366-18	427	304	0.599	0.011866	0.000115	0.187640	0.006415	0.006751	0.000198	0.079	68.96	0.76	0.083	69.79	0.76	1.2	1.44	1	
366-19	1064	1107	0.770	0.011055	0.000058	0.088717	0.001401	0.004157	0.000039	0.024	68.34	0.37	0.013	69.94	0.37	1.4	1.90	1	
366-20	203	157	0.328	0.068708	0.000277	0.521356	0.004274	0.019810	0.000184	-0.004	428.23	1.70	0.000	428.55	1.68	1.8	3.19		yes; c
366-21	518	334	0.523	0.017606	0.000290	0.761654	0.022624	0.027923	0.000764	0.343	72.78	1.64	0.327	75.94	1.64	1.2	1.55	2	
366-22	1608	246	0.556	0.013951	0.000092	0.316231	0.010086	0.011408	0.000367	0.146	75.19	0.74	0.143	76.57	0.75	2.6	3.89	2	
366-23	942	1074	1.523	0.010850	0.000068	0.072113	0.000875	0.003400	0.000023	-0.004	68.60	0.47	0.001	69.50	0.44	1.3	1.52	1	
366-24	645	675	0.612	0.011437	0.000165	0.104627	0.002482	0.004343	0.000075	0.020	71.92	1.05	0.023	71.62	1.03	1.4	1.89	1	
366-25	227	266	0.691	0.012376	0.000082	0.099021	0.002995	0.004067	0.000055	-0.003	79.09	0.60	0.013	78.28	0.54	1.9	3.51	2	
366-26	649	315	0.784	0.012438	0.000071	0.098758	0.002427	0.003991	0.000059	0.001	78.70	0.51	0.012	78.71	0.47	1.7	2.76	2	

Notes:

a : Date excluded based on the spot MSWD being larger than 4

b : Date excluded based on the ratio between the observed error to expected error being larger than 3

c : Date excluded based on the plot of probability distribution; inherited grain

d : Date excluded based on the plot of probability distribution; possibly due to Pb loss

APPENDIX 7-9

Summary of the U-Th-Pb zircon dates analysed by ELA-ICP-MS

Han Andesite Sample No. 1103

Sample No.	P(ppm)	U(ppm)	$^{232}Th/^{238}U$	Uncorrected $^{206}Pb/^{238}U$ ratio	±	Uncorrected $^{207}Pb/^{235}U$ ratio	±	Uncorrected $^{208}Pb/^{232}Th$ ratio	±	f208	^{208}Pb corrected $^{206}Pb/^{238}U$ Date (Ma)	Observed Error (± 1s.e.)	f207	^{207}Pb corrected $^{206}Pb/^{238}U$ Date (Ma)	Observed Error (± 1s.e.)	Obs/Exp Error	Spot MSWD	Exclude?
1103-01	557.438	142.702	0.598	0.003003	0.000019	0.021502	0.000804	0.000991	0.000024	0.003	19.11	0.14	0.007	19.20	0.13	1.2	1.12	
1103-02	477.708	89.632	0.423	0.002957	0.000023	0.019860	0.001179	0.001219	0.000044	0.020	18.53	0.16	0.003	18.98	0.16	1.1	1.00	
1103-03	390.498	65.714	0.479	0.003071	0.000041	0.024796	0.001854	0.001082	0.000051	0.009	19.43	0.27	0.015	19.47	0.28	1.3	1.49	
1103-04	390.343	100.925	0.468	0.003087	0.000021	0.027901	0.000725	0.001221	0.000031	0.019	19.33	0.14	0.024	19.40	0.14	1.1	1.15	
1103-05	360.891	70.600	0.412	0.003239	0.000035	0.038416	0.002669	0.001673	0.000098	0.042	19.78	0.25	0.049	19.83	0.26	1.4	1.39	
1103-06	457.743	130.441	0.582	0.003284	0.000029	0.053169	0.001880	0.002058	0.000058	0.095	18.88	0.21	0.087	19.29	0.20	1.3	1.47	
1103-07	456.870	94.425	0.497	0.003505	0.000040	0.079357	0.002249	0.002868	0.000075	0.129	19.35	0.25	0.145	19.29	0.25	1.3	1.99	
1103-08	391.727	112.231	0.619	0.003264	0.000031	0.050116	0.001845	0.001794	0.000049	0.076	19.18	0.21	0.080	19.33	0.21	1.3	1.57	
1103-09	452.306	87.445	0.455	0.003156	0.000025	0.041683	0.001578	0.001858	0.000057	0.063	18.86	0.17	0.061	19.08	0.17	1.2	1.22	
1103-10	454.020	85.335	0.460	0.003143	0.000028	0.025969	0.001283	0.001231	0.000037	0.017	19.72	0.19	0.017	19.90	0.19	1.3	1.49	
1103-11	410.010	122.835	0.557	0.002958	0.000017	0.022440	0.000892	0.000980	0.000019	0.003	18.84	0.12	0.011	18.84	0.12	1.0	0.91	
1103-12	411.477	86.078	0.487	0.003162	0.000035	0.039072	0.002407	0.001461	0.000083	0.036	19.39	0.26	0.053	19.27	0.25	1.5	1.73	
1103-13	478.836	78.396	0.591	0.003423	0.000056	0.060966	0.004930	0.002376	0.000131	0.117	19.24	0.40	0.102	19.79	0.43	1.5	1.73	
1103-14	506.150	136.808	0.505	0.003154	0.000019	0.023074	0.000844	0.001093	0.000021	0.007	20.01	0.13	0.008	20.13	0.13	1.2	1.20	
1103-15	514.589	104.889	0.511	0.003084	0.000026	0.027365	0.001501	0.001129	0.000034	0.013	19.44	0.18	0.022	19.41	0.19	1.2	1.15	
1103-16	441.485	99.020	0.478	0.003080	0.000026	0.037622	0.001974	0.001511	0.000055	0.042	18.80	0.18	0.052	18.79	0.19	1.3	1.31	
1103-17	432.292	99.674	0.472	0.003019	0.000028	0.026762	0.001384	0.001194	0.000039	0.019	18.91	0.19	0.022	19.00	0.19	1.3	1.50	
1103-18	407.069	81.916	0.463	0.003276	0.000031	0.057686	0.001782	0.002232	0.000045	0.088	18.98	0.20	0.100	18.98	0.20	1.2	1.49	
1103-19	452.368	81.260	0.416	0.003187	0.000028	0.036608	0.001846	0.001549	0.000057	0.036	19.63	0.19	0.045	19.58	0.20	1.2	1.06	
1103-20	585.799	84.038	0.514	0.003125	0.000029	0.021502	0.001440	0.001146	0.000045	0.013	19.72	0.21	0.004	20.03	0.21	1.2	1.36	
1103-21	822.240	127.543	0.708	0.003026	0.000025	0.020997	0.000975	0.000956	0.000020	-0.001	19.34	0.17	0.005	19.39	0.17	1.2	1.18	
1103-22	384.469	100.416	0.588	0.003926	0.000077	0.118440	0.004832	0.004225	0.000220	0.233	19.26	0.48	0.212	19.90	0.46	1.6	2.86	**yes, a**
1103-23	419.244	75.710	0.400	0.003278	0.000035	0.044530	0.003178	0.001898	0.000105	0.053	19.82	0.25	0.064	19.75	0.28	1.6	1.63	
1103-24	277.830	58.604	0.522	0.003343	0.000036	0.062849	0.002230	0.002221	0.000048	0.095	19.33	0.23	0.111	19.13	0.24	1.2	1.34	
1103-25	621.219	80.888	0.488	0.003766	0.000039	0.110059	0.003162	0.004398	0.000102	0.215	18.88	0.24	0.204	19.30	0.26	1.4	1.83	
1103-26	430.095	115.067	0.525	0.002973	0.000026	0.028364	0.001056	0.001124	0.000031	0.016	18.73	0.17	0.028	18.60	0.17	1.3	1.55	

Notes:

a : Date excluded based on the spot MSWD being larger than 2

b : Date excluded based on the ratio between the observed error to expected error being larger than 3

c : Date excluded based on the plot of probability distribution; inherited grain

d : Date excluded based on the plot of probability distribution; possibly due to Pb loss

APPENDIX 7-10

Summary of the U-Th-Pb zircon dates analysed by ELA-ICP-MS

Plata Dacite Sample No. 1121

Sample No.	P(ppm)	U(ppm)	$^{232}Th/^{238}U$	Uncorrected $^{206}Pb/^{238}U$ ratio	±	Uncorrected $^{207}Pb/^{235}U$ ratio	±	Uncorrected $^{208}Pb/^{232}Th$ ratio	±	f208	^{208}Pb corrected $^{206}Pb/^{238}U$ Date (Ma)	Observed Error (±1s.e.)	f207	^{207}Pb corrected $^{206}Pb/^{238}U$ Date (Ma)	Observed Error (±1s.e.)	Obs/Exp Error	Spot MSWD	Exclude?
1121-01	246	510	0.935	0.002869	0.000017	0.018371	0.000313	0.001000	0.000009	0.015	17.88	0.11	5.6E-05	18.46	0.11	1.0	0.98	
1121-02	210	339	0.628	0.002894	0.000018	0.020315	0.000616	0.000996	0.000015	0.009	18.25	0.12	0.006	18.53	0.12	1.3	1.54	
1121-03	280	303	0.874	0.002909	0.000023	0.019539	0.000628	0.000973	0.000017	0.008	18.29	0.18	0.003	18.67	0.15	1.4	1.78	
1121-04	279	393	0.985	0.002904	0.000019	0.023307	0.001129	0.001029	0.000015	0.020	17.95	0.13	0.015	18.42	0.14	1.2	1.12	
1121-05	270	341	0.914	0.002888	0.000017	0.022807	0.000554	0.000944	0.000018	0.002	18.29	0.12	0.013	18.34	0.11	1.2	1.23	
1121-06	505	1285	2.457	0.002871	0.000021	0.018678	0.000327	0.000934	0.000008	0.012	17.15	0.43	0.001	18.46	0.14	1.3	1.58	
1121-07	214	303	0.809	0.002886	0.000019	0.018081	0.000712	0.000873	0.000017	-0.007	18.51	0.14	-0.001	18.60	0.13	1.3	1.56	
1121-08	289	384	1.103	0.002952	0.000019	0.027718	0.000706	0.001081	0.000022	0.030	18.07	0.15	0.027	18.49	0.12	1.1	1.14	
1121-09	344	102	1.046	0.003151	0.000027	0.023930	0.001144	0.001059	0.000019	0.009	19.78	0.21	0.011	20.06	0.18	1.3	1.46	**yes; c**
1121-10	274	431	1.069	0.002867	0.000026	0.019149	0.000593	0.001008	0.000009	0.020	17.69	0.17	0.003	18.41	0.17	1.0	0.89	
1121-11	239	306	0.943	0.002847	0.000015	0.018906	0.000439	0.000892	0.000012	-0.003	18.17	0.11	0.002	18.29	0.10	1.4	1.63	
1121-12	209	328	1.061	0.002925	0.000027	0.019829	0.001258	0.000880	0.000017	-0.011	18.76	0.19	0.003	18.77	0.19	1.3	1.40	
1121-13	768	371	0.862	0.002873	0.000020	0.019839	0.000413	0.000951	0.000010	0.005	18.18	0.14	0.005	18.41	0.13	1.0	0.99	
1121-14	229	348	0.930	0.002857	0.000012	0.018105	0.000433	0.000858	0.000008	-0.010	18.34	0.09	-0.001	18.40	0.08	1.3	1.38	
1121-15	354	296	0.901	0.002925	0.000014	0.021536	0.000535	0.000960	0.000013	0.005	18.55	0.10	0.009	18.67	0.09	1.3	1.49	
1121-16	224	281	0.801	0.002933	0.000016	0.020503	0.000858	0.000945	0.000017	0.000	18.66	0.13	0.005	18.78	0.12	0.9	0.67	
1121-17	217	404	0.933	0.002881	0.000021	0.019068	0.000427	0.000970	0.000008	0.010	18.09	0.13	0.002	18.51	0.13	1.1	1.19	
1121-18	244	316	0.796	0.002950	0.000047	0.021123	0.000719	0.000968	0.000017	0.005	18.67	0.31	0.007	18.86	0.30	1.3	1.54	
1121-19	226	410	1.055	0.002870	0.000014	0.019314	0.000432	0.000940	0.000008	0.005	18.09	0.10	0.003	18.42	0.10	1.3	1.63	
1121-20	384	909	1.561	0.002922	0.000019	0.021274	0.000456	0.000996	0.000010	0.020	17.98	0.20	0.008	18.66	0.12	1.2	1.33	
1121-21	445	374	0.900	0.002873	0.000022	0.021004	0.000809	0.000966	0.000020	0.010	18.12	0.16	0.008	18.35	0.15	1.3	1.57	
1121-22	282	398	1.073	0.002902	0.000016	0.020095	0.000606	0.000938	0.000010	0.003	18.32	0.11	0.005	18.60	0.11	1.2	1.33	
1121-23	283	86	0.908	0.003033	0.000047	0.024584	0.001985	0.001116	0.000129	0.026	18.80	0.54	0.015	19.23	0.32	1.4	1.79	**yes; c**
1121-24	241	325	0.939	0.002929	0.000025	0.021290	0.000807	0.000910	0.000011	-0.004	18.69	0.16	0.008	18.71	0.17	1.4	1.91	
1121-25	316	795	1.544	0.003151	0.000024	0.021708	0.000572	0.001122	0.000009	0.037	19.09	0.16	0.004	20.19	0.16	1.4	1.98	**yes; c**
1121-26	209	297	0.861	0.002919	0.000013	0.020233	0.000554	0.000907	0.000012	-0.004	18.72	0.09	0.005	18.70	0.09	1.2	1.20	

Notes:

a : Date excluded based on the spot MSWD being larger than 2

b : Date excluded based on the ratio between the observed error to expected error being larger than 3

c : Date excluded based on the plot of probability distribution; inherited grain

d : Date excluded based on the plot of probability distribution; possibly due to Pb loss

APPENDIX 8-1

Summary of the U-Th-Pb zircon dates analysed by ELA-ICP-MS

Kelian River Detrital Zircon Sample No. 123230

Sample No.	$^{232}Th/^{238}U$	Uncorrected $^{206}Pb/^{238}U$ ratio	±	Uncorrected $^{207}Pb/^{235}U$ ratio	±	f207	^{207}Pb corrected $^{206}Pb/^{238}U$ Date (Ma)	Observed Error (±1s.e.)	Obs/Exp Error	Exclude?
230-01	0.867	0.016294	0.000081	0.095937	0.004252	-0.0010	104.19	0.51	1.41	
230-02	1.059	0.015867	0.000052	0.109415	0.002538	-0.0010	101.48	0.33	1.58	
230-03	1.443	0.010157	0.000037	0.068298	0.003460	0.0010	65.15	0.24	1.41	
230-04	0.885	0.018074	0.000060	0.118825	0.003709	-0.0001	115.47	0.38	1.33	
230-05	1.180	0.016602	0.000056	0.114081	0.002800	0.0004	106.15	0.36	1.30	
230-06	0.566	0.016122	0.000105	0.106657	0.003304	0.0014	103.10	0.67	1.51	
230-07	0.401	0.003188	0.000038	0.021009	0.001788	0.0126	20.52	0.24	1.15	
230-08	0.703	0.018979	0.000141	0.121286	0.004755	-0.0002	121.20	0.89	1.57	
230-09	0.938	0.016384	0.001013	0.010681	0.088965	0.6696	104.77	6.42	4.36	yes *
230-10	0.809	0.018370	0.000101	0.122913	0.004863	0.0097	117.34	0.64	1.46	
230-11	0.571	0.016595	0.000066	0.102012	0.002599	0.0007	106.10	0.42	1.55	
230-12	0.701	0.016497	0.000078	0.096575	0.003031	0.0017	105.48	0.50	1.46	
230-13	0.932	0.017869	0.000091	0.104566	0.004733	0.0022	114.18	0.58	1.34	
230-14	0.959	0.017944	0.000078	0.111013	0.004034	-0.0003	114.65	0.49	1.19	
230-15	0.534	0.018703	0.000081	0.122338	0.003215	-0.0004	119.45	0.51	1.31	
230-16	1.035	0.002538	0.000026	0.018322	0.001347	0.0074	16.34	0.17	1.31	
230-17	1.206	0.016946	0.000072	0.106474	0.005144	0.0008	108.33	0.46	1.41	
230-18	1.107	0.016719	0.000063	0.106773	0.002541	-0.0013	106.89	0.40	1.52	
230-19	0.890	0.002448	0.000013	0.014575	0.000702	0.0054	15.76	0.09	1.21	
230-20	0.741	0.016198	0.000080	0.103378	0.003121	-0.0005	103.59	0.50	1.43	
230-21	0.701	0.019273	0.000062	0.120353	0.002167	0.0007	123.06	0.39	1.60	
230-22	0.631	0.019082	0.000085	0.124384	0.003350	-0.0006	121.85	0.54	1.30	
230-23	0.248	0.041619	0.000134	0.297828	0.006940	-0.0003	262.86	0.83	2.00	
230-24	1.119	0.013662	0.000084	0.089404	0.004251	0.0023	87.47	0.53	1.44	
230-25	0.837	0.016877	0.000073	0.097310	0.006222	0.0009	107.89	0.47	1.21	
230-26	0.385	0.057002	0.000181	0.398940	0.010448	0.0001	357.37	1.11	1.79	
230-27	0.737	0.019317	0.000077	0.116992	0.003722	-0.0011	123.34	0.49	1.49	
230-28	0.667	0.017184	0.000062	0.109645	0.002785	0.0009	109.84	0.39	1.12	
230-29	1.289	0.012258	0.000057	0.072689	0.003156	0.0010	78.54	0.36	1.47	
230-30	0.928	0.019792	0.000071	0.122290	0.004206	0.0000	126.34	0.45	1.18	
230-31	0.459	0.003253	0.000039	0.019704	0.001799	-0.0006	20.94	0.25	1.23	
230-32	0.820	0.012482	0.000078	0.078060	0.004201	0.0025	79.97	0.50	1.23	
230-33	1.359	0.016291	0.000058	0.098514	0.005327	0.0009	104.17	0.37	1.40	
230-34	0.852	0.016925	0.000063	-0.003338	0.002154	-0.0008	108.19	0.40	1.05	
230-35	0.965	0.034838	0.000129	-0.005806	0.001543	-0.0019	220.76	0.80	1.57	
230-36	0.988	0.016965	0.000083	-0.010265	0.001777	-0.0007	108.44	0.53	1.55	
230-37	0.630	0.000263	0.000008	0.061381	0.012636	0.0979	1.69	0.05	1.39	
230-38	0.355	0.003138	0.000057	0.007426	0.003728	0.0108	20.20	0.37	1.33	
230-39	0.798	0.017280	0.000441	0.212051	0.014039	0.2138	110.44	2.79	6.38	yes *
230-40	0.700	0.017083	0.000077	-0.001585	0.001145	-0.0001	109.19	0.49	1.28	
230-41	1.066	0.016631	0.000081	-0.008833	0.001966	-0.0012	106.33	0.51	1.30	
230-42	0.654	0.016531	0.000081	-0.002460	0.001117	-0.0017	105.69	0.51	1.26	
230-43	1.233	0.016353	0.000075	-0.007933	0.004434	-0.0010	104.57	0.48	1.85	
230-44	0.902	0.015892	0.000084	-0.002450	0.002109	-0.0003	101.64	0.54	1.50	
230-45	0.820	0.018614	0.000101	0.000416	0.002048	0.0001	118.89	0.64	1.63	
230-46	0.871	0.016101	0.000062	-0.002856	0.001117	-0.0017	102.97	0.40	1.41	
230-47	0.833	0.017354	0.000062	-0.001149	0.002149	-0.0002	110.91	0.40	1.23	
230-48	1.522	0.016570	0.000069	-0.000718	0.003081	-0.0003	105.94	0.44	1.47	
230-49	0.823	0.016449	0.000061	-0.001541	0.001084	-0.0008	105.17	0.39	1.10	
230-50	0.584	0.000435	0.000019	0.060661	0.013205	0.0448	2.80	0.12	1.67	
230-51	0.666	0.050041	0.000265	-0.004444	0.001174	0.0016	314.78	1.63	1.45	
230-52	0.607	0.018571	0.000086	-0.002778	0.000971	-0.0027	118.62	0.54	1.44	
230-53	1.312	0.016093	0.000052	-0.005227	0.002190	-0.0009	102.92	0.33	1.64	

APPENDIX 8-1

Summary of the U-Th-Pb zircon dates analysed by ELA-ICP-MS

Kelian River Detrital Zircon Sample No. 123230

Sample No.	$^{232}Th/^{238}U$	Uncorrected $^{206}Pb/^{238}U$ ratio	±	Uncorrected $^{207}Pb/^{235}U$ ratio	±	f207	^{207}Pb corrected $^{206}Pb/^{238}U$ Date (Ma)	Observed Error (±1s.e.)	Obs/Exp Error	Exclude?
230-54	1.078	0.016627	0.000073	-0.000060	0.001684	-0.0008	106.30	0.46	1.34	
230-55	0.842	0.016222	0.000081	-0.005212	0.001322	-0.0012	103.74	0.51	1.32	
230-56	1.275	0.016576	0.000066	-0.004035	0.002339	0.0004	105.98	0.42	1.40	
230-57	0.626	0.018127	0.000086	-0.000933	0.001252	-0.0005	115.81	0.55	1.14	
230-58	0.889	0.011851	0.000052	-0.003182	0.001728	-0.0013	75.95	0.33	1.07	
230-59	0.988	0.016168	0.000075	-0.004337	0.001975	-0.0005	103.39	0.47	1.36	
230-60	0.903	0.038961	0.000176	-0.008248	0.001383	-0.0012	246.39	1.09	1.21	
230-61	0.691	0.017108	0.000060	0.000892	0.002009	-0.0012	109.35	0.38	1.15	
230-62	0.433	0.003122	0.000029	0.001114	0.002268	0.0064	20.10	0.19	1.08	
230-63	0.586	0.039543	0.000160	-0.002418	0.000993	-0.0014	250.00	0.99	1.39	
230-64	0.679	0.014953	0.000130	-0.000403	0.002933	-0.0005	95.68	0.82	1.52	
230-65	0.444	0.003094	0.000030	0.004249	0.002542	0.0000	19.91	0.19	1.13	
230-66	0.961	0.015993	0.000063	-0.001048	0.002669	0.0007	102.28	0.40	1.35	
230-67	0.867	0.016428	0.000092	0.022066	0.003342	0.0201	105.04	0.58	1.26	
230-68	1.271	0.000273	0.000006	0.074528	0.009949	0.0759	1.76	0.04	1.43	
230-69	1.080	0.016355	0.000058	-0.003528	0.001368	-0.0002	104.58	0.37	1.22	
230-70	0.993	0.016452	0.000061	-0.003948	0.001326	-0.0013	105.20	0.39	1.31	
230-71	0.665	0.019139	0.000068	0.000593	0.001017	-0.0007	122.21	0.43	1.68	
230-72	0.467	0.058466	0.000252	-0.000851	0.000546	-0.0011	366.29	1.53	1.95	
230-73	0.586	0.016444	0.000062	-0.000908	0.001359	-0.0006	105.15	0.39	1.48	
230-74	1.018	0.016574	0.000097	0.004312	0.001761	0.0013	105.97	0.62	1.45	
230-75	0.900	0.015263	0.000082	0.002308	0.003535	0.0023	97.65	0.52	1.56	
230-76	0.928	0.016873	0.000092	0.000185	0.001201	-0.0019	107.86	0.58	1.78	
230-77	0.407	0.015767	0.000080	0.001035	0.005082	0.0013	100.84	0.51	1.16	
230-78	0.593	0.011307	0.000055	-0.003065	0.001361	0.0002	72.48	0.35	1.76	
230-79	0.410	0.002958	0.000023	-0.004277	0.001238	-0.0004	19.04	0.15	1.82	
230-80	0.433	0.003833	0.000062	0.013081	0.003241	0.0081	24.66	0.40	1.53	
230-81	1.124	0.013021	0.000071	-0.002818	0.001903	0.0007	83.40	0.45	1.29	
230-82	0.068	0.002492	0.000025	0.004590	0.000851	0.0048	16.05	0.16	1.62	
230-83	0.570	0.013971	0.000120	0.016684	0.002221	0.0014	89.44	0.76	1.99	
230-84	0.792	0.015607	0.000135	0.015001	0.001673	0.0002	99.83	0.86	2.45	
230-85	0.497	0.011272	0.000046	0.007474	0.001865	0.0003	72.26	0.30	2.01	
230-86	1.058	0.002840	0.000035	-0.001690	0.004375	-0.0025	18.28	0.23	1.37	
230-87	0.399	0.018119	0.000094	0.000416	0.001099	0.0023	115.76	0.60	1.20	
230-88	3.550	0.009355	0.000044	-0.027632	0.014923	0.0089	60.02	0.28	1.38	
230-89	0.199	0.010546	0.000041	0.000922	0.000373	-0.0003	67.62	0.26	1.89	
230-90	1.124	0.016145	0.000082	0.001702	0.001716	0.0017	103.24	0.52	1.60	
230-91	0.452	0.059605	0.000277	-0.002236	0.001879	-0.0013	373.22	1.69	1.52	
230-92	0.888	0.018344	0.000070	-0.003286	0.001184	0.0000	117.18	0.44	1.38	
230-93	0.464	0.013715	0.001229	0.098017	0.018144	0.2046	87.81	7.82	2.00	
230-94	0.686	0.016870	0.000081	-0.000955	0.001113	0.0007	107.85	0.51	1.36	
230-95	0.787	0.024292	0.000071	-0.002863	0.001390	-0.0004	154.72	0.45	1.47	
230-96	1.045	0.016609	0.000067	-0.003185	0.001289	0.0005	106.19	0.43	1.55	
230-97	1.278	0.016813	0.000077	-0.001284	0.002093	0.0018	107.48	0.49	1.44	
230-98	0.768	0.000263	0.000007	0.016941	0.009757	0.0647	1.70	0.04	1.21	
230-99	1.149	0.016820	0.000070	0.001584	0.001985	0.0016	107.53	0.45	1.44	
230-100	0.489	0.003211	0.000031	0.007962	0.002531	-0.0033	20.67	0.20	1.07	
230-101	0.452	0.010965	0.000054	0.001672	0.000929	0.0014	70.30	0.35	1.44	
230-102	0.601	0.010805	0.000091	0.026674	0.002619	0.0205	69.28	0.58	1.12	
230-103	0.998	0.016331	0.000075	-0.003357	0.002444	0.0014	104.42	0.47	1.26	
230-104	0.674	0.000270	0.000007	0.022813	0.010192	0.0686	1.74	0.05	1.25	
230-105	0.750	0.017291	0.000100	-0.003322	0.001558	0.0012	110.51	0.63	1.44	
230-106	0.942	0.016342	0.000131	0.000497	0.002643	0.0058	104.50	0.83	1.38	

APPENDIX 8-1

Summary of the U-Th-Pb zircon dates analysed by ELA-ICP-MS

Kelian River Detrital Zircon Sample No. 123230

Sample No.	$^{232}Th/^{238}U$	Uncorrected $^{206}Pb/^{238}U$ ratio	±	Uncorrected $^{207}Pb/^{235}U$ ratio	±	f207	^{207}Pb corrected $^{206}Pb/^{238}U$ Date (Ma)	Observed Error (±1s.e.)	Obs/Exp Error	Exclude?
230-107	0.736	0.016826	0.000065	0.001000	0.001239	0.0002	107.56	0.42	1.09	
230-108	0.440	0.013820	0.000060	-0.000066	0.000907	0.0008	88.48	0.38	1.35	
230-109	0.668	0.016572	0.000063	0.000061	0.000988	0.0021	105.95	0.40	1.18	
230-110	0.978	0.016756	0.000068	-0.005338	0.002806	0.0015	107.12	0.43	1.40	
230-111	1.036	0.016503	0.000067	-0.004918	0.004011	0.0009	105.52	0.43	1.33	
230-112	1.005	0.016804	0.000061	-0.006945	0.001132	0.0001	107.43	0.38	1.23	
230-113	0.821	0.016906	0.000077	0.000140	0.001485	0.0002	108.07	0.49	1.29	
230-114	0.809	0.017332	0.000091	0.003828	0.001366	0.0001	110.77	0.58	1.46	
230-115	0.393	0.036738	0.000186	-0.000907	0.000952	0.0013	232.58	1.16	1.38	
230-116	0.527	0.003372	0.000047	-0.005049	0.004173	0.0088	21.70	0.30	1.04	
230-117	1.155	0.016802	0.000080	-0.004167	0.002254	-0.0005	107.41	0.51	1.40	
230-118	0.439	0.003257	0.000029	0.025971	0.002504	0.0183	20.96	0.19	1.20	
230-119	1.177	0.016380	0.000061	-0.004872	0.003337	0.0004	104.74	0.39	1.27	
230-120	1.079	0.016958	0.000094	0.001095	0.001876	0.0002	108.40	0.60	1.47	
230-121	0.734	0.016963	0.000090	0.006055	0.002079	0.0044	108.43	0.57	1.43	
230-122	0.427	0.038547	0.000294	0.001751	0.001568	0.0034	243.82	1.82	1.20	
230-123	0.877	0.015874	0.000064	0.005589	0.002823	0.0015	101.53	0.41	1.63	
230-124	0.838	0.017265	0.000086	0.004596	0.001755	-0.0002	110.35	0.54	1.21	
230-125	0.698	0.017009	0.000139	0.005328	0.002423	0.0005	108.72	0.88	1.17	
230-126	0.705	0.015808	0.000053	0.002921	0.002025	0.0011	101.11	0.33	1.59	
230-127	0.861	0.000362	0.000015	0.005220	0.010641	0.0612	2.33	0.10	1.70	

Notes: * : Date excluded based on the ratio between the observed error to expected error being larger than 4

APPENDIX 8-1

Summary of the U-Th-Pb zircon dates analysed by ELA-ICP-MS

Kelian River Detrital Zircon Sample No. 123230

Sample No.	$^{232}Th/^{238}U$	Uncorrected $^{206}Pb/^{238}U$ ratio	±	Uncorrected $^{207}Pb/^{235}U$ ratio	±	f207	^{207}Pb corrected $^{206}Pb/^{238}U$ Date (Ma)	Observed Error (±1s.e.)	Obs/Exp Error	Exclude?
230-54	1.078	0.016627	0.000073	-0.000060	0.001684	-0.0008	106.30	0.46	1.34	
230-55	0.842	0.016222	0.000081	-0.005212	0.001322	-0.0012	103.74	0.51	1.32	
230-56	1.275	0.016576	0.000066	-0.004035	0.002339	0.0004	105.98	0.42	1.40	
230-57	0.626	0.018127	0.000086	-0.000933	0.001252	-0.0005	115.81	0.55	1.14	
230-58	0.889	0.011851	0.000052	-0.003182	0.001728	-0.0013	75.95	0.33	1.07	
230-59	0.988	0.016168	0.000075	-0.004337	0.001975	-0.0005	103.39	0.47	1.36	
230-60	0.903	0.038961	0.000176	-0.008248	0.001383	-0.0012	246.39	1.09	1.21	
230-61	0.691	0.017108	0.000060	0.000892	0.002009	-0.0012	109.35	0.38	1.15	
230-62	0.433	0.003122	0.000029	0.001114	0.002268	0.0064	20.10	0.19	1.08	
230-63	0.586	0.039543	0.000160	-0.002418	0.000993	-0.0014	250.00	0.99	1.39	
230-64	0.679	0.014953	0.000130	-0.000403	0.002933	-0.0005	95.68	0.82	1.52	
230-65	0.444	0.003094	0.000030	0.004249	0.002542	0.0000	19.91	0.19	1.13	
230-66	0.961	0.015993	0.000063	-0.001048	0.002669	0.0007	102.28	0.40	1.35	
230-67	0.867	0.016428	0.000092	0.022066	0.003342	0.0201	105.04	0.58	1.26	
230-68	1.271	0.000273	0.000006	0.074528	0.009949	0.0759	1.76	0.04	1.43	
230-69	1.080	0.016355	0.000058	-0.003528	0.001368	-0.0002	104.58	0.37	1.22	
230-70	0.993	0.016452	0.000061	-0.003948	0.001326	-0.0013	105.20	0.39	1.31	
230-71	0.665	0.019139	0.000068	0.000593	0.001017	-0.0007	122.21	0.43	1.68	
230-72	0.467	0.058466	0.000252	-0.000851	0.000546	-0.0011	366.29	1.53	1.95	
230-73	0.586	0.016444	0.000062	-0.000908	0.001359	-0.0006	105.15	0.39	1.48	
230-74	1.018	0.016574	0.000097	0.004312	0.001761	0.0013	105.97	0.62	1.45	
230-75	0.900	0.015263	0.000082	0.002308	0.003535	0.0023	97.65	0.52	1.56	
230-76	0.928	0.016873	0.000092	0.000185	0.001201	-0.0019	107.86	0.58	1.78	
230-77	0.407	0.015767	0.000080	0.001035	0.005082	0.0013	100.84	0.51	1.16	
230-78	0.593	0.011307	0.000055	-0.003065	0.001361	0.0002	72.48	0.35	1.76	
230-79	0.410	0.002958	0.000023	-0.004277	0.001238	-0.0004	19.04	0.15	1.82	
230-80	0.433	0.003833	0.000062	0.013081	0.003241	0.0081	24.66	0.40	1.53	
230-81	1.124	0.013021	0.000071	-0.002818	0.001903	0.0007	83.40	0.45	1.29	
230-82	0.068	0.002492	0.000025	0.004590	0.000851	0.0048	16.05	0.16	1.62	
230-83	0.570	0.013971	0.000120	0.016684	0.002221	0.0014	89.44	0.76	1.99	
230-84	0.792	0.015607	0.000135	0.015001	0.001673	0.0002	99.83	0.86	2.45	
230-85	0.497	0.011272	0.000046	0.007474	0.001865	0.0003	72.26	0.30	2.01	
230-86	1.058	0.002840	0.000035	-0.001690	0.004375	-0.0025	18.28	0.23	1.37	
230-87	0.399	0.018119	0.000094	0.000416	0.001099	0.0023	115.76	0.60	1.20	
230-88	3.550	0.009355	0.000044	-0.027632	0.014923	0.0089	60.02	0.28	1.38	
230-89	0.199	0.010546	0.000041	0.000922	0.000373	-0.0003	67.62	0.26	1.89	
230-90	1.124	0.016145	0.000082	0.001702	0.001716	0.0017	103.24	0.52	1.60	
230-91	0.452	0.059605	0.000277	-0.002236	0.001879	-0.0013	373.22	1.69	1.52	
230-92	0.888	0.018344	0.000070	-0.003286	0.001184	0.0000	117.18	0.44	1.38	
230-93	0.464	0.013715	0.001229	0.098017	0.018144	0.2046	87.81	7.82	2.00	
230-94	0.686	0.016870	0.000081	-0.000955	0.001113	0.0007	107.85	0.51	1.36	
230-95	0.787	0.024292	0.000071	-0.002863	0.001390	-0.0004	154.72	0.45	1.47	
230-96	1.045	0.016609	0.000067	-0.003185	0.001289	0.0005	106.19	0.43	1.55	
230-97	1.278	0.016813	0.000077	-0.001284	0.002093	0.0018	107.48	0.49	1.44	
230-98	0.768	0.000263	0.000007	0.016941	0.009757	0.0647	1.70	0.04	1.21	
230-99	1.149	0.016820	0.000070	0.001584	0.001985	0.0016	107.53	0.45	1.44	
230-100	0.489	0.003211	0.000031	0.007962	0.002531	-0.0033	20.67	0.20	1.07	
230-101	0.452	0.010965	0.000054	0.001672	0.000929	0.0014	70.30	0.35	1.44	
230-102	0.601	0.010805	0.000091	0.026674	0.002619	0.0205	69.28	0.58	1.12	
230-103	0.998	0.016331	0.000075	-0.003357	0.002444	0.0014	104.42	0.47	1.26	
230-104	0.674	0.000270	0.000007	0.022813	0.010192	0.0686	1.74	0.05	1.25	
230-105	0.750	0.017291	0.000100	-0.003322	0.001558	0.0012	110.51	0.63	1.44	
230-106	0.942	0.016342	0.000131	0.000497	0.002643	0.0058	104.50	0.83	1.38	

APPENDIX 8-1

Summary of the U-Th-Pb zircon dates analysed by ELA-ICP-MS

Kelian River Detrital Zircon Sample No. 123230

Sample No.	$^{232}Th/^{238}U$	Uncorrected $^{206}Pb/^{238}U$ ratio	±	Uncorrected $^{207}Pb/^{235}U$ ratio	±	f207	^{207}Pb corrected $^{206}Pb/^{238}U$ Date (Ma)	Observed Error (±1s.e.)	Obs/Exp Error	Exclude?
230-107	0.736	0.016826	0.000065	0.001000	0.001239	0.0002	107.56	0.42	1.09	
230-108	0.440	0.013820	0.000060	-0.000066	0.000907	0.0008	88.48	0.38	1.35	
230-109	0.668	0.016572	0.000063	0.000061	0.000988	0.0021	105.95	0.40	1.18	
230-110	0.978	0.016756	0.000068	-0.005338	0.002806	0.0015	107.12	0.43	1.40	
230-111	1.036	0.016503	0.000067	-0.004918	0.004011	0.0009	105.52	0.43	1.33	
230-112	1.005	0.016804	0.000061	-0.006945	0.001132	0.0001	107.43	0.38	1.23	
230-113	0.821	0.016906	0.000077	0.000140	0.001485	0.0002	108.07	0.49	1.29	
230-114	0.809	0.017332	0.000091	0.003828	0.001366	0.0001	110.77	0.58	1.46	
230-115	0.393	0.036738	0.000186	-0.000907	0.000952	0.0013	232.58	1.16	1.38	
230-116	0.527	0.003372	0.000047	-0.005049	0.004173	0.0088	21.70	0.30	1.04	
230-117	1.155	0.016802	0.000080	-0.004167	0.002254	-0.0005	107.41	0.51	1.40	
230-118	0.439	0.003257	0.000029	0.025971	0.002504	0.0183	20.96	0.19	1.20	
230-119	1.177	0.016380	0.000061	-0.004872	0.003337	0.0004	104.74	0.39	1.27	
230-120	1.079	0.016958	0.000094	0.001095	0.001876	0.0002	108.40	0.60	1.47	
230-121	0.734	0.016963	0.000090	0.006055	0.002079	0.0044	108.43	0.57	1.43	
230-122	0.427	0.038547	0.000294	0.001751	0.001568	0.0034	243.82	1.82	1.20	
230-123	0.877	0.015874	0.000064	0.005589	0.002823	0.0015	101.53	0.41	1.63	
230-124	0.838	0.017265	0.000086	0.004596	0.001755	-0.0002	110.35	0.54	1.21	
230-125	0.698	0.017009	0.000139	0.005328	0.002423	0.0005	108.72	0.88	1.17	
230-126	0.705	0.015808	0.000053	0.002921	0.002025	0.0011	101.11	0.33	1.59	
230-127	0.861	0.000362	0.000015	0.005220	0.010641	0.0612	2.33	0.10	1.70	

Notes: * : Date excluded based on the ratio between the observed error to expected error being larger than 4

APPENDIX 8-2

Summary of the U-Th-Pb zircon dates analysed by ELA-ICP-MS

Mahakam River Detrital Zircon Sample No. 123231

Sample No.	$^{232}Th/^{238}U$	Uncorrected $^{206}Pb/^{238}U$ ratio	±	Uncorrected $^{207}Pb/^{235}U$ ratio	±	f207	^{207}Pb corrected $^{206}Pb/^{238}U$ Date (Ma)	Observed Error (± 1s.e.)	Obs/Exp Error	Exclude?
231-01	1.133	0.015977	0.000058	0.102598	0.003026	0.0008	102.18	0.37	1.46	
231-02	1.237	0.016129	0.000063	0.110518	0.002949	-0.0003	103.15	0.40	1.52	
231-03	0.393	0.030345	0.000073	0.204179	0.002320	-0.0002	192.70	0.45	1.64	
231-04	0.541	0.002587	0.000023	0.016652	0.000918	0.0052	16.65	0.15	1.51	
231-05	0.799	0.054464	0.000199	0.380328	0.007564	-0.0004	341.87	1.22	1.43	
231-06	1.018	0.014180	0.000065	0.087076	0.004424	-0.0009	90.77	0.41	1.48	
231-07	0.490	0.019240	0.000125	0.125365	0.004000	0.0005	122.85	0.79	1.47	
231-08	0.864	0.012369	0.000084	0.076904	0.003578	0.0003	79.25	0.54	1.53	
231-09	0.551	0.001013	0.000015	0.006391	0.000794	0.0075	6.53	0.10	1.27	
231-10	1.014	0.016076	0.000063	0.092998	0.003334	-0.0002	102.81	0.40	1.62	
231-11	0.259	0.002394	0.000014	0.015205	0.000345	0.0025	15.42	0.09	1.53	
231-12	0.249	0.002367	0.000011	0.014689	0.000410	0.0016	15.24	0.07	1.21	
231-13	0.816	0.016216	0.000081	0.099787	0.003027	0.0009	103.70	0.51	1.41	
231-14	1.105	0.016169	0.000058	0.098664	0.004094	0.0006	103.40	0.36	1.22	
231-15	1.244	0.012189	0.000060	0.075626	0.003557	0.0010	78.10	0.38	1.30	
231-16	0.490	0.002787	0.000161	0.015345	0.002541	0.0243	17.94	1.04	8.81	yes *
231-17	1.174	0.016927	0.000064	0.102960	0.002692	-0.0003	108.21	0.40	1.58	
231-18	0.860	0.000301	0.000007	0.000932	0.000376	0.0128	1.94	0.04	1.43	
231-19	1.694	0.013881	0.000039	0.076458	0.006472	0.0003	88.87	0.25	1.48	
231-20	0.931	0.018229	0.000076	0.119893	0.003514	0.0011	116.45	0.48	1.37	
231-21	0.140	0.000522	0.000008	0.003837	0.000383	0.0231	3.36	0.05	1.23	
231-22	0.525	0.017087	0.000093	0.095816	0.003281	0.0014	109.22	0.59	1.48	
231-23	0.777	0.017529	0.000092	0.104002	0.006782	-0.0001	112.02	0.58	1.32	
231-24	0.474	0.039083	0.000150	0.268675	0.005319	0.0007	247.15	0.93	1.34	
231-25	0.829	0.018024	0.000086	0.105992	0.004223	0.0006	115.16	0.55	1.30	
231-26	0.903	0.016336	0.000065	0.102982	0.002412	-0.0002	104.46	0.41	1.55	
231-27	0.579	0.017569	0.000102	0.108480	0.004792	-0.0003	112.27	0.65	1.41	
231-28	0.707	0.014505	0.000079	0.089428	0.005632	0.0012	92.83	0.50	1.14	
231-29	0.179	0.002494	0.000021	0.015154	0.000817	0.0036	16.06	0.14	1.33	
231-30	0.807	0.019260	0.000068	0.128181	0.002937	0.0010	122.98	0.43	1.36	
231-31	0.835	0.040259	0.000206	0.285272	0.011426	0.0001	254.44	1.28	1.37	
231-32	0.311	0.002476	0.000012	0.015247	0.000496	0.0013	15.94	0.08	1.10	
231-33	1.011	0.013298	0.000038	0.081040	0.002830	0.0000	85.16	0.24	1.45	
231-34	2.049	0.002732	0.000025	0.015732	0.002623	-0.0014	17.59	0.16	1.64	
231-35	0.268	0.018520	0.000146	0.138741	0.005668	0.0005	118.29	0.92	1.28	
231-36	0.524	0.017710	0.000102	0.120872	0.004050	-0.0001	113.17	0.64	1.36	
231-37	0.589	0.013849	0.000054	0.097425	0.001824	-0.0020	88.66	0.34	1.40	
231-38	0.509	0.017392	0.000080	0.122070	0.003548	0.0036	111.15	0.51	1.35	
231-39	1.158	0.012428	0.000054	0.092522	0.003331	-0.0020	79.62	0.35	1.18	
231-40	1.166	0.014376	0.000061	0.111294	0.003655	-0.0009	92.01	0.39	1.31	
231-41	0.827	0.017433	0.000092	0.130663	0.004658	0.0005	111.41	0.58	1.43	
231-42	0.509	0.000271	0.000011	0.001729	0.001151	0.1098	1.75	0.07	1.59	
231-43	0.739	0.000747	0.000011	0.005739	0.000819	0.0045	4.82	0.07	1.41	
231-44	0.723	0.232258	0.002454	3.508584	0.057037	0.0210	1346.32	12.84	3.64	
231-45	0.429	0.019439	0.000175	0.126514	0.003975	0.0039	124.11	1.11	2.60	
231-46	0.495	0.018683	0.000131	0.121367	0.004310	-0.0003	119.33	0.83	1.46	
231-47	0.494	0.039708	0.000161	0.286325	0.005420	-0.0006	251.02	1.00	1.41	
231-48	0.279	0.002792	0.000035	0.018289	0.001082	0.0020	17.97	0.23	1.41	
231-49	0.618	0.018627	0.000102	0.122782	0.005943	0.0101	118.97	0.65	1.64	
231-50	0.811	0.016983	0.000108	0.117765	0.004788	-0.0014	108.56	0.68	2.24	
231-51	0.827	0.014317	0.000087	0.099569	0.003446	0.0003	91.64	0.55	1.76	
231-52	0.342	0.015975	0.000116	0.095489	0.003520	0.0005	102.17	0.74	1.70	
231-53	0.715	0.014008	0.000272	0.102706	0.009422	0.0034	89.68	1.73	1.93	

APPENDIX 8-2

Summary of the U-Th-Pb zircon dates analysed by ELA-ICP-MS

Mahakam River Detrital Zircon Sample No. 123231

Sample No.	$^{232}Th/^{238}U$	Uncorrected $^{206}Pb/^{238}U$ ratio	±	Uncorrected $^{207}Pb/^{235}U$ ratio	±	f207	^{207}Pb corrected $^{206}Pb/^{238}U$ Date (Ma)	Observed Error (± 1s.e.)	Obs/Exp Error	Exclude?
231-54	0.506	0.000773	0.000009	0.005905	0.000465	0.0157	4.98	0.06	1.27	
231-55	0.867	0.031745	0.000218	0.178783	0.005894	0.0006	201.46	1.36	2.50	
231-56	0.198	0.017496	0.000075	0.115303	0.004889	-0.0017	111.81	0.47	1.33	
231-57	0.349	0.001413	0.000042	0.006459	0.000895	0.0061	9.10	0.27	2.45	
231-58	0.513	0.015149	0.000212	0.080815	0.006556	0.0042	96.92	1.35	1.92	
231-59	0.717	0.015875	0.000172	0.094171	0.009929	0.0274	101.53	1.09	2.58	
231-60	0.794	0.015626	0.000091	0.106049	0.005285	0.0228	99.96	0.58	1.33	
231-61	0.363	0.013773	0.000055	0.089564	0.001612	-0.0004	88.18	0.35	1.42	
231-62	0.647	0.000791	0.000008	0.005636	0.000343	0.0070	5.10	0.05	1.37	
231-63	0.768	0.000260	0.000009	0.002012	0.000848	0.0968	1.68	0.06	1.34	
231-64	0.679	0.032641	0.000104	0.235477	0.003652	0.0000	207.05	0.65	1.73	
231-65	0.339	0.002500	0.000043	0.015883	0.001379	0.0117	16.09	0.28	2.03	
231-66	0.443	0.026051	0.000542	0.114184	0.007156	0.0007	165.78	3.41	4.37	yes *
231-67	0.819	0.014045	0.000128	0.097606	0.006119	0.0009	89.91	0.81	1.48	
231-68	0.897	0.014261	0.000081	0.102924	0.003872	0.0027	91.29	0.52	1.48	
231-69	0.644	0.015791	0.000095	0.097654	0.003302	-0.0013	101.00	0.60	1.46	
231-70	0.491	0.024147	0.000117	0.165723	0.003739	-0.0006	153.81	0.74	1.41	
231-71	0.732	0.016784	0.000149	0.095675	0.004379	-0.0015	107.30	0.94	2.14	
231-72	0.909	0.001690	0.000067	0.013968	0.002795	-0.0037	10.89	0.43	2.27	
231-73	0.876	0.018845	0.000079	0.123418	0.004104	-0.0014	120.35	0.50	1.71	
231-74	0.625	0.014498	0.000060	0.096043	0.002203	-0.0007	92.79	0.38	1.35	
231-75	0.380	0.017126	0.000094	0.119532	0.003137	0.0034	109.46	0.59	1.32	
231-76	0.873	0.017326	0.000087	0.129572	0.004153	0.0012	110.73	0.55	1.12	
231-77	0.942	0.018695	0.000106	0.143551	0.007079	0.0009	119.40	0.67	1.54	
231-78	0.872	0.019566	0.000114	0.131961	0.006488	0.0009	124.91	0.72	1.57	
231-79	0.781	0.017140	0.000073	0.123833	0.003355	-0.0001	109.56	0.46	1.32	
231-80	1.046	0.016390	0.000075	0.116192	0.003926	0.0002	104.80	0.48	1.48	
231-81	0.588	0.011658	0.000083	0.066999	0.003491	0.0094	74.72	0.53	1.30	
231-82	0.539	0.024427	0.000142	0.172456	0.007884	0.0003	155.58	0.89	1.22	
231-83	0.404	0.014273	0.000130	0.066820	0.004845	0.0002	91.36	0.83	1.36	
231-84	0.946	0.001047	0.000022	0.007538	0.001683	0.0236	6.75	0.14	1.22	
231-85	1.228	0.011697	0.000050	0.084354	0.003234	-0.0011	74.97	0.32	1.40	
231-86	0.468	0.036544	0.000427	0.279196	0.014416	0.0046	231.38	2.65	1.47	
231-87	0.925	0.002755	0.000031	0.021573	0.002254	0.0060	17.73	0.20	1.10	
231-88	0.753	0.039084	0.000248	0.255831	0.009308	-0.0012	247.15	1.54	1.79	
231-89	0.546	0.011402	0.000087	0.069491	0.007051	0.0102	73.09	0.56	1.14	
231-90	0.428	0.027476	0.000142	0.182071	0.006036	0.0015	174.73	0.89	1.48	
231-91	0.730	0.033779	0.000167	0.249278	0.006670	0.0009	214.16	1.04	1.42	
231-92	0.725	0.002505	0.000029	0.019382	0.001536	0.0013	16.13	0.19	1.17	
231-93	0.478	0.018725	0.000095	0.125709	0.002967	-0.0001	119.59	0.60	1.29	
231-94	0.731	0.016079	0.000095	0.112063	0.004950	0.0008	102.83	0.60	1.32	
231-95	0.645	0.013085	0.000094	0.086173	0.003408	0.0012	83.81	0.60	1.43	
231-96	0.777	0.166095	0.000547	1.710969	0.019286	0.0020	990.56	3.02	1.55	
231-97	0.657	0.018779	0.000106	0.128622	0.004376	0.0003	119.94	0.67	1.23	
231-98	0.538	0.048349	0.000306	0.343467	0.008808	0.0034	304.38	1.88	1.48	
231-99	0.337	0.038063	0.000166	0.273114	0.006255	-0.0011	240.81	1.03	1.15	
231-100	1.185	0.013446	0.000110	0.109337	0.004456	0.0022	86.10	0.70	1.87	
231-101	0.899	0.087609	0.000355	0.756550	0.016306	-0.0001	541.38	2.11	1.49	
231-102	0.398	0.036696	0.000238	0.258401	0.010796	0.0002	232.32	1.48	1.06	
231-103	0.568	0.037817	0.000211	0.278725	0.007723	0.0006	239.29	1.31	1.23	
231-104	0.553	0.068441	0.000253	0.486804	0.019257	0.0063	426.76	1.53	2.36	
231-105	0.854	0.014573	0.000070	0.100815	0.003630	-0.0013	93.26	0.44	1.11	
231-106	0.924	0.014707	0.000062	0.098212	0.004675	-0.0005	94.11	0.40	1.14	

APPENDIX 8-2

Summary of the U-Th-Pb zircon dates analysed by ELA-ICP-MS

Mahakam River Detrital Zircon Sample No. 123231

Sample No.	$^{232}Th/^{238}U$	Uncorrected $^{206}Pb/^{238}U$ ratio	±	Uncorrected $^{207}Pb/^{235}U$ ratio	±	f207	^{207}Pb corrected $^{206}Pb/^{238}U$ Date (Ma)	Observed Error (± 1s.e.)	Obs/Exp Error	Exclude?
231-107	0.496	0.005697	0.000056	0.030838	0.002701	-0.0027	36.62	0.36	1.14	
231-108	0.833	0.016025	0.000051	0.109627	0.001641	0.0006	102.48	0.32	1.97	
231-109	0.713	0.016063	0.000109	0.112473	0.003772	0.0008	102.72	0.69	1.68	
231-110	0.672	0.033828	0.000113	0.241097	0.005242	-0.0001	214.46	0.71	1.27	
231-111	0.561	0.000780	0.000014	0.002851	0.001624	0.0703	5.02	0.09	1.79	
231-112	0.705	0.033684	0.000173	0.243396	0.006712	0.0009	213.56	1.08	1.32	
231-113	0.592	0.014241	0.000194	0.086812	0.005760	0.0028	91.16	1.24	1.44	
231-114	0.590	0.010518	0.000051	0.075285	0.002315	0.0012	67.45	0.33	1.29	
231-115	0.671	0.018610	0.000105	0.134611	0.005361	0.0002	118.87	0.67	1.10	
231-116	0.387	0.021567	0.000133	0.148727	0.004656	0.0003	137.55	0.84	1.20	
231-117	0.469	0.024897	0.000220	0.199631	0.007023	-0.0012	158.53	1.38	1.57	
231-118	0.656	0.019241	0.000088	0.131649	0.004294	0.0021	122.86	0.56	1.15	
231-119	0.402	0.037680	0.000228	0.265799	0.009368	0.0031	238.44	1.42	1.20	
231-120	0.907	0.018609	0.000090	0.137225	0.004666	0.0000	118.86	0.57	1.38	
231-121	0.351	0.039032	0.000401	0.282921	0.012211	0.0000	246.83	2.49	1.48	
231-122	0.597	0.018345	0.000095	0.125667	0.005445	0.0017	117.19	0.60	1.20	
231-123	0.705	0.047796	0.000237	0.337838	0.007825	0.0000	300.98	1.46	1.53	
231-124	0.522	0.020603	0.000101	0.140604	0.004890	0.0009	131.47	0.64	1.06	
231-125	0.619	0.002552	0.000022	0.016580	0.000928	0.0052	16.43	0.14	1.29	
231-126	0.884	0.018500	0.000078	0.105648	0.012816	0.0008	118.17	0.50	1.36	
231-127	0.539	0.002540	0.000023	0.016569	0.001573	0.0096	16.35	0.15	0.88	
231-128	0.748	0.017583	0.000072	0.118155	0.003439	0.0000	112.36	0.46	1.59	
231-129	0.469	0.037020	0.000178	0.265700	0.007175	0.0010	234.34	1.10	2.33	
231-130	0.633	0.034313	0.000168	0.237921	0.005679	0.0011	217.49	1.05	1.65	
231-131	0.691	0.001198	0.000020	0.005538	0.000590	-0.0044	7.72	0.13	1.85	
231-132	0.438	0.017477	0.000123	0.120362	0.003799	0.0033	111.69	0.78	1.58	
231-133	0.776	0.057941	0.000239	0.442476	0.007856	0.0005	363.09	1.46	1.66	
231-134	1.149	0.013616	0.000069	0.100737	0.005227	0.0025	87.18	0.44	1.31	
231-135	1.015	0.018120	0.000142	0.138435	0.011315	0.0004	115.77	0.90	2.67	
231-136	0.651	0.037765	0.000180	0.268495	0.008626	0.0029	238.96	1.12	1.06	
231-137	0.666	0.050228	0.000200	0.397286	0.021545	0.0014	315.92	1.23	1.54	
231-138	0.797	0.014451	0.000069	0.100576	0.002735	-0.0002	92.49	0.44	1.37	
231-139	0.794	0.152349	0.000576	1.491882	0.018283	0.0001	914.12	3.22	3.51	
231-140	0.505	0.000830	0.000010	0.005276	0.000417	0.0027	5.35	0.07	1.30	
231-141	0.525	0.036473	0.000201	0.262340	0.008282	0.0016	230.93	1.25	1.41	
231-142	0.916	0.000645	0.000022	0.007022	0.001252	0.0272	4.16	0.14	1.53	
231-143	1.222	0.599323	0.002123	21.758117	0.113777	0.0360	3027.11	8.56	2.12	
231-144	0.485	0.038575	0.000296	0.291850	0.011193	0.0100	244.00	1.84	1.51	
231-145	0.624	0.000289	0.000007	0.003806	0.000575	0.0657	1.86	0.04	1.12	
231-146	1.169	0.010824	0.000118	0.075680	0.007216	0.0035	69.40	0.75	1.43	
231-147	1.352	0.012988	0.000080	0.085920	0.011739	0.0010	83.19	0.51	1.89	
231-148	1.030	0.012173	0.000190	0.104687	0.015727	0.2508	78.00	1.21	1.35	
231-149	0.434	0.000817	0.000015	0.005819	0.000683	0.0082	5.26	0.10	1.39	
231-150	1.022	0.013236	0.000187	0.094676	0.007744	0.0077	84.77	1.19	1.88	
231-151	2.415	0.181296	0.001280	1.757385	0.154279	0.0191	1074.05	6.99	1.99	
231-152	0.631	0.018709	0.000134	0.120430	0.007411	0.0127	119.49	0.85	1.45	
231-153	0.635	0.009903	0.000098	0.047107	0.007727	0.0239	63.53	0.62	1.58	

APPENDIX 9-1

Table 5.1 : Instrumental operating conditions

Instrument	:	Agilent 7500 Series ICP-MS
RF Power	:	1200 W
RF Matching	:	1.7 V
Nebuliser	:	Concentric Nebulizer
Carrier gas flow rate	:	0.86 L / minute
Make up gas flow rate	:	0.1 L / minute
Peripump1	:	0.1 rps
Spray Chamber	:	Scott Spray Chamber
Spray Chamber Temp	:	0°C
Electron multiplier	:	ETP model AF 220, a discrete dynode type

Analog mode used at > 400000 cps. Pulse to analog conversion factors are measured at the start of each analytical session.

Sensitivity	:	350000 cps/ppm for ^{115}In and 220000 cps/ppm for ^{238}U
Ion collection	:	peak hopping
Dwell time and points/peak	:	0.33 seconds, 3 points per peak
Analysis time	:	33.2 seconds acquisition , 5 repeats

Table 5.2 : Interference elements and correction factors

Main Isotopes	Interference Elements	Type	Interference Correction Factor
197Au	181Ta	oxide	0.00169 – 0.00338
195Pt	181Ta	nitride	0 – 0.00002
108Pd	92Zr	oxide	0.00307 – 0.00408
106Pd	90Zr	oxide	0.00291 – 0.00378
106Pd	66Zn	argide	0.00003 – 0.00028
105Pd	89Y	oxide	0.00171 – 0.00203
105Pd	65Cu	argide	0.00005 – 0.00028
105Pd	67Zn	argide	0 – 0.00201
103Rh	63Cu	argide	0.00004 – 0.00015
103Rh	89Y	nitride	0
102Ru	62Ni	argide	0.00004 – 0.00009
102Ru	64Zn	argide	0 – 0.00023
101Ru	61Ni	argide	0.00004 – 0.00010
101Ru	63Cu	argide	0 – 0.00001
99Ru	59Co	argide	0.00002 – 0.00004
99Ru	61Ni	argide	0.00002 – 0.00005

APPENDIX 9-2

Table 5.3 : The PGE, Au and Cu abundances in the intrusive andesite of the Kelian area.

Magerang-Imang hornblende andesite				Concentration in ppb			
Rhenium	**Gold**	**Palladium**	**Platinum**	**Rhodium**	**Ruthenium**	**Iridium**	**Osmium**
0.31189	0.03031	1.96281	1.35374	0.11536	0.12894	0.09977	0.09843
0.38513	0.07464	1.60800	1.10856	0.08917	0.06046	0.06093	0.07410
0.33771	0.07667	1.55507	2.28478	0.10468	0.09177	0.10219	0.35065
0.09383	0.01974	1.17937	1.41749	0.06674	0.05085	0.05855	0.03101
0.03600	0.01231	1.09482	0.59424	0.03515	0.04404	0.03671	0.02621
0.09285	0.01445	0.42364	0.23111	0.01635	0.02389	0.01249	0.06398
0.04634	0.01285	0.25408	0.12318	0.00644	0.00569	0.01445	0.00898
0.05336	0.00340	0.18886	0.11302	0.00874	0.00487	0.00348	0.00658
Nakan pyroxene andesite							
Rhenium	**Gold**	**Palladium**	**Platinum**	**Rhodium**	**Ruthenium**	**Iridium**	**Osmium**
0.02981	0.03975	1.91621	1.15147	0.07521	0.07504	0.01814	0.01306
0.02815	0.01448	1.69341	1.40663	0.06010	0.05463	0.01821	0.01784
0.09336	0.07003	2.85392	1.84565	0.12115	0.07676	0.02824	0.01193
0.02264	0.01342	1.65053	0.87799	0.04898	0.03767	0.01276	u.d.l
0.02733	0.00408	0.99628	0.48053	0.02730	0.02217	0.00795	u.d.l
0.02820	0.00461	0.96152	0.57654	0.03878	0.02101	0.01611	0.00630
Kelian Mine altered andesite							
Rhenium	**Gold**	**Palladium**	**Platinum**	**Rhodium**	**Ruthenium**	**Iridium**	**Osmium**
0.12549	0.89488	1.37616	0.87772	0.04195	0.11848	0.00791	0.00262
0.03376	0.00720	0.18080	4.07184	0.03613	u.d.l	0.00792	u.d.l
0.05441	4.45709	0.15086	0.06096	0.00370	u.d.l	0.01163	0.01358
0.05551	0.03086	0.11898	0.04704	0.00343	0.00418	0.06075	0.02856
1.13109	11.46116	0.34994	0.06011	0.08538	u.d.l	0.01197	0.08665
Fusion Blank (average values)							
Rhenium	**Gold**	**Palladium**	**Platinum**	**Rhodium**	**Ruthenium**	**Iridium**	**Osmium**
0.03233	0.01518	0.06247	0.02372	0.00257	0.00235	0.00277	0.01917
Mantle values (Barnes et al., 1988)							
Rhenium	**Gold**	**Palladium**	**Platinum**	**Rhodium**	**Ruthenium**	**Iridium**	**Osmium**
0.35	1.2	4.4	8.3	1.6	5.6	4.4	4.2

u.d.l. : under detection limit